10-5-2016 12:00 AM

The Sudbury Impact Structure - New Insights Into the Origin and Emplacement of the Basal Onaping Intrusion and the Parkin, Trill and Foy Offset Dykes of the North Range

Denise Anders
The University of Western Ontario

Supervisor
Gordon Osinski
The University of Western Ontario

Graduate Program in Geology
A thesis submitted in partial fulfillment of the requirements for the degree in Doctor of Philosophy

Abstract

The 1.85 Ga Sudbury impact structure is considered a remnant of a multi-ring basin with an estimated original diameter of 150-200 km. The so-called “Basal Onaping Intrusion” form discontinuous sheets between the Granophyre of the Sudbury Igneous Complex (SIC) and the Sandcherry Member of the Onaping Formation and had been considered part of the complex breccia series of the Onaping Formation. Based on the investigation of core and field samples from the North Range we conclude that the Basal Onaping Intrusion, in fact, are the roof rocks of the SIC and, thus, may represent the initial bulk composition of the SIC. It should no longer be considered part of the Onaping Formation, but rather the uppermost member of the SIC, and we recommend “Upper Contact Unit” as a new name. The Offset Dykes are radial and concentric dykes around the SIC and are composed of the so-called Inclusion-rich Quartz Diorite (IQD) and Inclusion-poor Quartz Diorite (QD). Metabreccia (MTBX), an enigmatic and overlooked lithology observed within some dykes in the North Range had been sparsely studied in detail. This investigation of MTBX from the Parkin, Trill and Foy Offset Dykes indicates that MTBX originates from Footwall Breccia (FWBX) that was ripped off during the outward emplacement of the Offset Dykes, which is in contrast to previous studies. The fragments, clasts and blocks were included into the dyke melt and subsequently thermally metamorphosed resulting in an intensive recrystallized fabric within MTBX. A genetic relationship between MTBX and FWBX is supported by whole rock geochemical analyses and similarities in Ni-Cu-PGE mineralization. Oscillatory, compositionally zoned pyrites containing traces of Platinum-Group-Elements (PGEs) are observed within MTBX but not in QD or IQD. Additional PGEs are hosted within Pt-Pd-bismuthotellurides, with MTBX containing a higher amount of Te and Pt than QD/IQD. This study provides new insights into the field relationships, petrology, geochemistry and Ni-Cu-PGE sulfide mineralization of MTBX from the Parkin, Trill and Foy Offset Dykes in the North Range of the Sudbury impact structure compared to QD, IQD and FWBX.

Keywords

Sudbury, Impact Cratering, Offset Dykes, Metabreccia, Ore Deposits, PGEs, Geochemistry

Co-Authorship Statement

Chapter 1 represents a literature review and compilation of previous studies and was written by the candidate with comments and edits by Gordon R. Osinski and Richard A. F. Grieve.

Chapter 2 was published in Meteoritics and Planetary Science. Initial field work at the Joe Lake area, sampling, sample preparation and data interpretation of the field samples was conducted by Derek T. M. Brillinger, who also contributed to the writing of the manuscript. Peter Lightfoot from Vale provided the core samples. Sample preparation, analyses and data interpretation of the core samples was carried out by the candidate. The manuscript was written by the candidate and Gordon R. Osinski and Richard A. F. Grieve provided comments and edits. Balz Kamber and Paul Sylvester provided reviewer comments during the submission process.

Sample collection, preparation and analyses of the samples investigated in Chapter 3, 4 and 5 was carried out by the candidate. Two samples (SUD-NB-113 and SUD-NB-56) from the Parkin and Trill Offset Dykes and all samples collected from the Whistle Offset Dyke were kindly provided by Nicola Barry. The candidate led the data collection, interpretation and writing of the manuscript. Gordon R. Osinski and Richard A. F. Grieve contributed to the data interpretation and provided comments and suggestions to the final manuscripts. Part of Chapter 3 was presented at the conference "Bridging the Gap III" in 2015 in Freiburg, Germany. Gordon R. Osinski, Richard A. F. Grieve, and Attila Péntek contributed to editing the abstract.

Acknowledgments

I wish to express my gratitude and appreciation to my supervisors Dr. Gordon Osinski and Dr. Richard Grieve for their scientific guidance, constructive criticism, inspirations and valuable contribution during the course of this research. I feel very lucky to have been given the opportunity to conduct research under the supervision of such great and dedicated scientists.

I would like to thank Wallbridge Mining Limited for their guidance, support, and cooperation, for providing access to the properties at the Parkin and Trill Offset Dyke, core samples and a large dataset of geochemical analyses.

I want to acknowledge the research funding provided by the Mitacs Accelerate Internship, the Centre for Excellence and Mining, the Barringer Travel Award, NSERC, CSA, and MDA through their Industrial Research Chair support to GRO.

I would also like to thank Peter Lightfoot from Vale for his support and providing the core samples for the investigation in Chapter 2, Doreen Ames for assistance with initial fieldwork at Joe Lake and Balz Kamber and Paul Sylvester for their constructive and useful reviews in the process of publishing the manuscript in Chapter 2.

A special thanks goes to Anna, Matt and B. for their friendship, inspiration, motivation, and emotional support, throughout the PhD journey, in particular during the last days of the final writing phase.

I also want to acknowledge Dr. Astrid Holzheid and Dr. Philip Kegler, who engaged my interest in Planetary Science in the first place, and David Kring, Martin Schmieder, and Elmar Buchner who taught me the very first things about impact crater.

Last, but not least, I would like to thank my family. The completion of this thesis could not have been possible without the constant support and help, encouragement and love from my parents Ute und Harri, my siblings Haike and Michael, my brother in law Mike and my niece Franziska with Niclas. Thanks for never giving up on me.

Table of Contents

List of Tables

List of Figures

List of Appendices

List of Abbreviations

An	Anorthite
Bism	Bismuthides
Bn	Bornite
BSE	Backscattered Electron
XPL	Crossed polarized light
PPL	Plane polarized light
Cbn	Cubanite
Ccp	Chalcopyrite
Co	Cobalt
Cu	Copper
Fro	Froodite
FW	Footwall
FWBX	Footwall Breccia
IQD	Inclusion-rich Quartz Diorite
Ktsk	Kosulskite
LOI	Loss of ignition
Mcnr	Michenerite
Mlr	Millerite
Mnch	Moncheite
Mrsk	Merenskyite
Mslv	Maslovite
MTBX	Metabreccia
Ni	Nickel
OD	Offset Dykes
OF	Onaping Formation
Pbpl	Plumbopalladinite
PDFs	Planar deformation features
PFs	Planar fractures
PGE	Platinum-Group-Elements
PGM	Platinum-Group-Mineralization
Pn	Pentlandite
Po	Pyrrhotite
Py	Pyrite
QD	Quartz Diorite
SDBX	Sudbury Breccia
SIC	Sudbury Igneous Complex
Sprl	Sperrylite
SRBB	South Range Breccia Belt
SRSZ	South Range Shear Zone

Tel	Tellurides
Px	Pyroxene
Qtz	Quartz
ICP-MS	Inductively coupled mass spectrometry
ICP-AES	Inductively coupled plasma atomic emission spectroscopy
WDS	Wavelength-dispersive spectroscopy
EDS	Energy-dispersive spectroscopy
LILE	Large-ion lithophile elements
LREE	Light-group rare-earth element
HREE	Heavy-group rare-earth element
Ab	Albite
Chl	Chlorite
Fsp	Feldspar
Qtz	Quartz
As	Arsenic
S	Sulfur
Fe	Iron
Pt	Platinum
Pd	Palladium
Os	Osmium
Ir	Iridium
Bi	Bismuth
Te	Tellurium
Ag	Silver
Rh	Rhodium
Ru	Ruthenium
nA	Nano Ampere

1 Introduction

1.1 Geological setting of the Sudbury impact structure

The target rocks of the Sudbury impact structure are composed of rocks of the Huronian Supergroup of the Southern Province in the south and rocks of the Archean Superior Province in the north and east (Dressler 1984a) (Fig. 1.1). An overview of the geologic pre-impact history of the Sudbury area is provided in Table 1.1. Archean basement rocks are composed of rocks of the Levack Gneiss Complex (Langford 1960), Cartier Batholith, and the Benny Greenstone Belt, formed and metamorphic overprinted during the 2.72–2.68 Ga Kenoran Orogeny (Krogh et al. 1984; James et al. 1991; Card 1994; Percival 2004). The Archean Levack Gneiss Complex (~2.71 Ga, Krogh et al. 1984) forms most of the Archean basement beneath the Sudbury Igneous Complex (SIC). It consists of tonalitic, granodioritic, and dioritic gneisses, as well as mafic, ultramafic, and anorthositic intrusions (Card et al. 1984). The Levack gneisses were subjected to repeated metamorphic events: high-grade granulite facies metamorphism at 2.65 Ga, followed by amphibolite facies metamorphism accompanied by uplifting during the formation of the Cartier batholith (Krogh et al. 1984; James et al. 1991; Card 1994; Wodicka and Card 1995). The rocks of the Archean Benny Greenstone Belt consist of calc-alkalic and tholeiitic mafic, intermediate, and felsic units (Card and Innes 1981), which have been metamorphosed under greenschist to amphibolite facies conditions. The Cartier batholith is a late Archean granitic intrusion in the North Range of the SIC dominated by monzogranites and granodiorites (Card and Innes 1981; Krogh et al. 1984; Meldrum et al. 1997). It was formed by partial melting of rocks of the Levack Gneiss Complex and emplaced at 2.64 Ga (Meldrum et al. 1997). The Levack Gneiss and the Cartier Batholith are intruded by northwest-trending mafic dykes of the 2.45 Ga (Card 1994) Matachewan Diabase, an anhedral porphyry that contains large white plagioclase inclusions (Heaman 1997). The intrusion of the Matachewan dykes continued into the deposition of the early Huronian sediments of the Elsie Mountain and Stobie Formation.

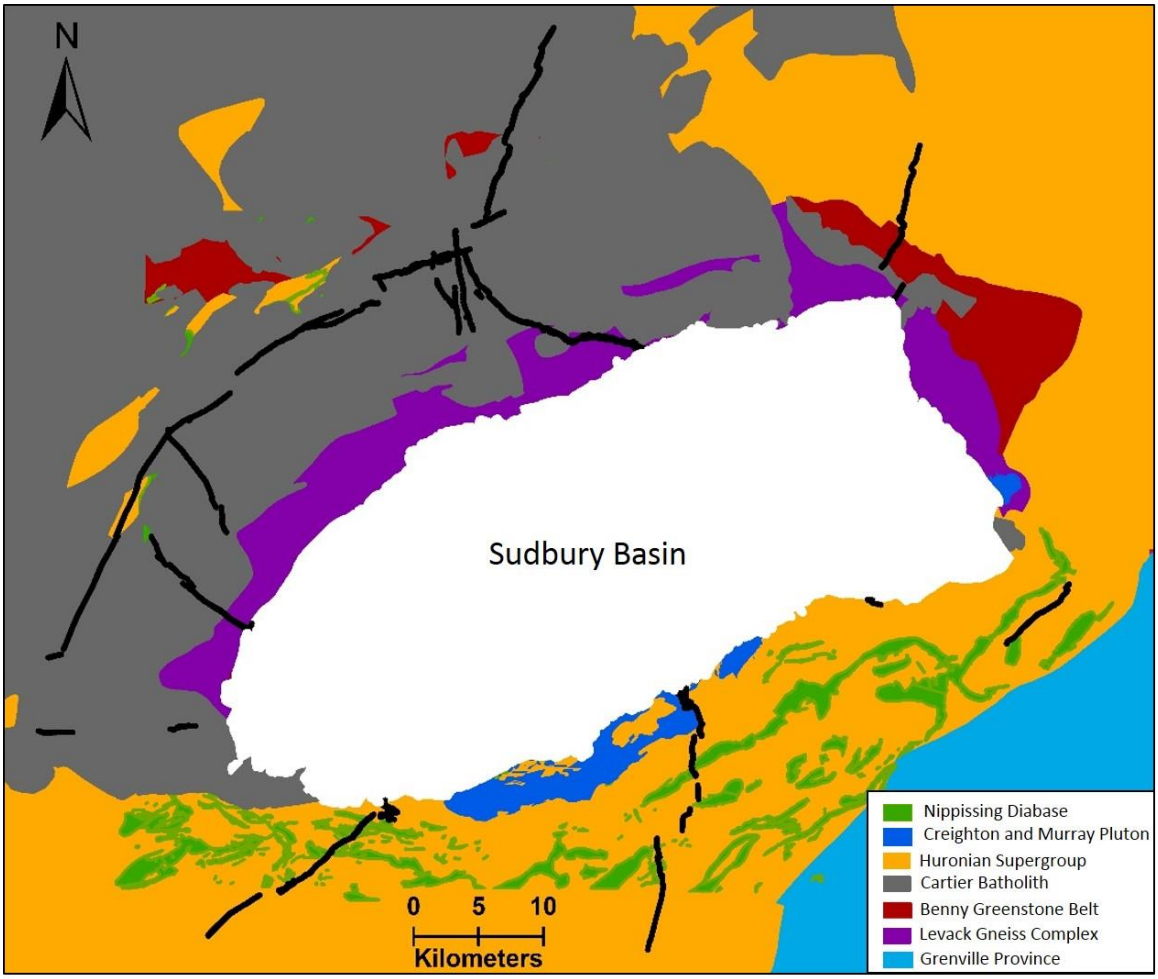

Figure 1.1. Simplified geologic map showing country rocks of the Sudbury area (map modified after Ames and Gibson (2004)).

The southern part of the SIC footwall rocks are composed of mafic intrusive rocks of the East Bull Lake suite (2.49 – 2.47 Ga, James et al. 2002), metasedimentary and metavolcanic rocks of the Paleoproterozoic Huronian Supergroup deposited between 2.40–2.20 Ga (Young et al. 2001). The Huronian Supergroup can be divided into four units from oldest to youngest: the Elliot Lake, Hough Lake, Quirke Lake, and Cobalt Groups. This Supergroup mainly consist of metasedimentary rocks, except for the Elliot Lake Group, which contains mafic and felsic volcanic and pyroclastic rocks (Dressler 1984a). Granitic plutons intrude the Huronion metasedimentary rocks in the South: Murray at 2.38 Ga and Creighton plutons at 2.30 Ga (Frarey et al. 1982; Dressler 1984a; Krogh et al. 1984, 1996).

Table 1.1. Pre-impact geologic history of the Sudbury area in chronological order.

Proterozoic Southern Province	Huronian Supergroup	2.22 Ga (13, 14, 15)	Nipissing Diabase		Gabbroic sills	2.40–2.20 Ga Blezardian Orogeny (10)
		2.30 Ga (12)	Creighton pluton		Granites	
		2.38 Ga (11)	Murray pluton		Granites	
		2.40 – 2.20 Ga (8)	Cobalt (9)	Lorrain	Arkose, wacke, arenite, conglomerate	
				Gowganda	Conglomerate, wacke, mudstone,	
			Quirke Lake (9)	Serpent	Quartzite, arkose	
				Espanola	Carbonates, wacke	
				Bruce	Wacke, conglomerate	
			Hough Lake (9)	Mississagi	Quartzite, arkose, wacke, conglomerate	
				Pecors	Wacke, arenite	
				Ramsey Lake	Conglomerate and sandstone	
			Elliot Lake (9)	McKim	Wacke, mudstone	
				Matinenda	Quartzite, wacke, conglomerate,	
				Copper Cliff	Felsic flows, pyroclastic rocks	
				Stobie	Mafic flows, pyroclastic rocks	
				Elsie Mountain	Mafic flows	
		2.45 Ga (2)	Matachewan Diabase		Anhedral porphyry (7)	
		2.49 – 2.47 (6)	East Bull Lake suite		Mafic intrusive rocks	
Archean Superior Province	Archean basement rocks	2.65 Ga (5)	Cartier Batholith		Monzogranites, granodiorites (1, 4, 5)	
		2.71 Ga (1)	Benny Greenstone Belt		Mafic, intermediate, felsic volcanics (4)	2.72–2.68 Ga Kenoran Orogeny (3)
			Levack Gneiss		Gneisses, mafic, ultramafic, anorthositic intrusions (2)	

(1) Krogh et al. (1984), (2) Card (1994), (3) Percival (2004), (4) Card and Innes (1981), (5) Meldrum et al. (1997), (6) James et al. (2002), (7) Heaman (1997), (8) Young et al. (2001) (9) Card et al. (1984), (10) Riller and Schwerdtner (1997), (11) Krogh et al. (1996), (12) Frarey et al. (1982), (13) Corfu and Andrews (1986), (14) Krogh et al. (1987), (15) Noble and Lightfoot (1992).

During the Blezardian Orogeny 2.4–2.2 Ga, the Huronion sediments were subject of deformation and amphibolite facies metamorphism resulting in a NW-SE folding of the rocks of the Southern Province (Riller and Schwerdtner 1997). The gabbroic dykes of the Nipissing Diabase are dated at approximately 2.22 Ga and intrude Huronion metasedimentary rocks in the South (Van Schmus 1965; Fairbairn et al. 1969; Corfu and Andrews 1986; Krogh et al. 1987; Noble and Lightfoot 1992).

1.2 The Sudbury Impact Structure

The 1.85 Ga (Krogh et al. 1984) Sudbury impact structure is located currently at the contact of the Superior Province and Southern Province of the Canadian Shield bordered to the South by the Grenville Province (Fig. 1.1). The Sudbury structure is generally considered a remnant of a complex crater with a multi-ring basin (Stöffler et al. 1989, 1992; Deutsch and Grieve 1994; Deutsch et al. 1995; Spray and Thompson 1995). With an estimated original diameter of approximately 200 km (Stöffler et al. 1992; Deutsch and Grieve 1994; Grieve 1994; Deutsch et al. 1995; Grieve et al. 2008), it counts among the largest impact structures on Earth. The elliptical outline of the so-called Sudbury Basin with a length of ~60 km and a width of ~30 km (Deutsch and Grieve 1994), is a result of post-impact deformation (Shanks and Schwerdtner 1990, 1991; Grieve et al. 1991; Milkereit and Green 1992; Deutsch and Grieve 1994; Wu et al. 1994; Deutsch et al. 1995). The origin of the Sudbury structure had been controversial and the impact structure was formerly interpreted as a result of volcanic processes (Burrows and Rickaby 1930; Stevenson 1960, 1963). Since the detection of shatter cones (Fig. 1.2a) by Dietz (1964) and planar deformation features (French 1967) (Fig. 1.2b), as clear markers for an impact origin, followed by further evidence listed in Table 1.2, the Sudbury structure has been widely accepted as an impact structure.

The Sudbury area is known for its world-class Ni-Cu-PGE mineralization, and with an estimated pre-mining resource at more than 1,648 million metric tons of ~1.2 % Ni and ~1.0 percent Cu (Naldrett and Lightfoot 1993), it counts among the largest and most productive mining camps in the world (Ames et al. 2008). The impact basin had been topic of intensive research for decades; however, several unanswered questions still remain. In

the sub-sections that follow, the various main impact-produced rock types pertinent to this study are described.

Table 1.2. Evidence for an impact origin of the Sudbury structure.

Evidence	References
Shatter cones up to distance of 20 km from the centre of the Sudbury Igneous Complex	Dietz (1964); Dietz and Butler (1964); Dressler (1984b); Peredery and Morrison (1984); Müller-Mohr (1992)
PDFs in quartz and feldspar within the Onaping Intrusion, FWBX and SDBX	French (1967); Peredery (1972a); Deutsch and Grieve (1994); Dressler et al. (1996)
Footwall Breccia	(Dietz 1962, 1964))
Sudbury Breccia (Pseudotachylite)	Dressler (1984b)
Shock features in zircon	Bohor et al. (1993); Krogh et al. (1996)
Impact Melt Sheet	Grieve et al. (1991); Grieve (1994); Deutsch et al. (1995); Warner et al. (1998); Dickin et al. (1999); Therriault et al. (2002)
Impact diamonds	Masaitis (1999)
Iridium anomaly	Mungall et al. (2004); Ames et al. (2005, 2008)

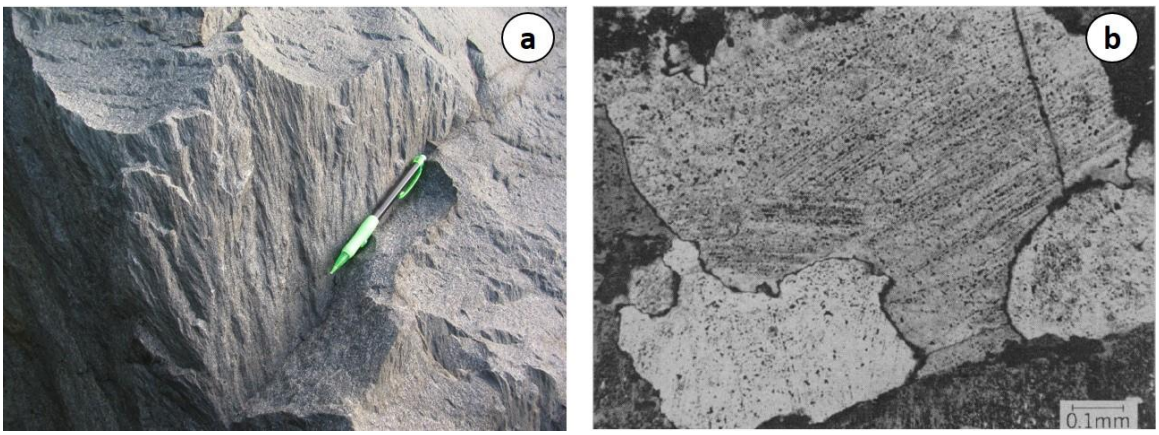

Figure 1.2. a) Field photograph of shatter cones from the Sudbury impact structure (pen ~15 cm in length). b) Planar deformation features (PDFs) within quartz in the Onaping Formation (French 1967).

1.2.1 Sudbury Breccia

Sudbury Breccia (SDBX) (Fig. 1.3) is defined as a heterolithic (Dressler 1984a), polymict (Müller-Mohr 1992), pseudotachylitic breccia, composed of country rock clasts within an

aphanitic, grey to black, massive groundmass. The matrix of SDBX (Müller-Mohr 1992; Dressler and Reimold 2004) is characterized by the presence of glass, flow features, fine-grained igneous textures, vesicles and amygdules (Dressler 1984b; Maghloughlin and Spray 1992; Reimold and Colliston 1994; Thompson and Spray 1996; Rousell et al. 2003). SDBX occurs within the footwall in the form of mm wide veins and large zones many kilometres in size up to 80 km away from the SIC (Dressler 1984b; Dressler et al. 1991; Rousell et al. 2003). It is more frequent in the southern footwall rocks of the Sudbury structure, where it also forms the South Range Breccia Belt, a 45 km long and up to one kilometre thick zone of Sudbury Breccia (Scott and Spray 2000), that is host to the concentric Frood-Stobie, McConnell, Kirkwood, Manchester, and Vermilion Offset Dykes (Grant and Bite 1984; O'Connor and Spray 1997). Large zones of SDBX within footwall rocks around the Sudbury basin have been associated with possible multi-ring features of the Sudbury structure (Dressler 1984b; Spray and Thompson 1995).

Pseudotachylites are not restricted to impact structures, but also form at faults and shear zones within tectonic settings, thus the formation of SDBX as a pseudotachylite is complex and still a topic of intensive research and discussion. It has been suggested to have formed due to comminution and cataclasis during the excavation and modification stages of the impact event (Dietz and Butler 1964; Card 1978; Dressler 1984b; Müller-Mohr 1992; Spray and Thompson 1995; Thompson and Spray 1996; Spray 1997; Scott and Benn 2002; Legault et al. 2003; Rousell et al. 2003; Riller 2005; Lafrance et al. 2008); while others implied that frictional melting also played a role in the formation of SDBX (Card 1978; Dressler 1984b; Lakomy 1990; Müller-Mohr 1992; Spray 1992; Spray and Thompson 1995; Scott and Spray 2000). Some scientists proceeded on the assumption that decompression melting played an important role and SDBX was formed due to the release of pressure during the modification stage (Shand 1916; Reimold and Gibson 2005). Other authors assumed a formation by shock melting (Fiske et al. 1995), a combination of frictional and shock melting (Kenkmann et al. 2000), or an origin from the impact melt sheet (Lieger et al. 2009; Riller et al. 2010). Spray (1998) divided the SDBX into two types, based on their origin: the endogenic (E)-type pseudotachylites formed by friction and shock melting during the compression phase, and the shock (S)-type pseudotachylites formed during crater modification by processes that are similar to

the formation of tectonic pseudotachylites. SDBX is an important host Cu–(Ni)–PGE mineralization (Farrow 1994; Fedorowich et al. 1999; Hanley and Mungall 2003) and seems to have played an important role in the transportation of metal-bearing fluids (Farrow 1994; Morrison et al. 1994; Hanley and Mungall 2003) and has acted as structural traps to sulfide veining ((Farrow 1994; Fedorowich et al. 1999).

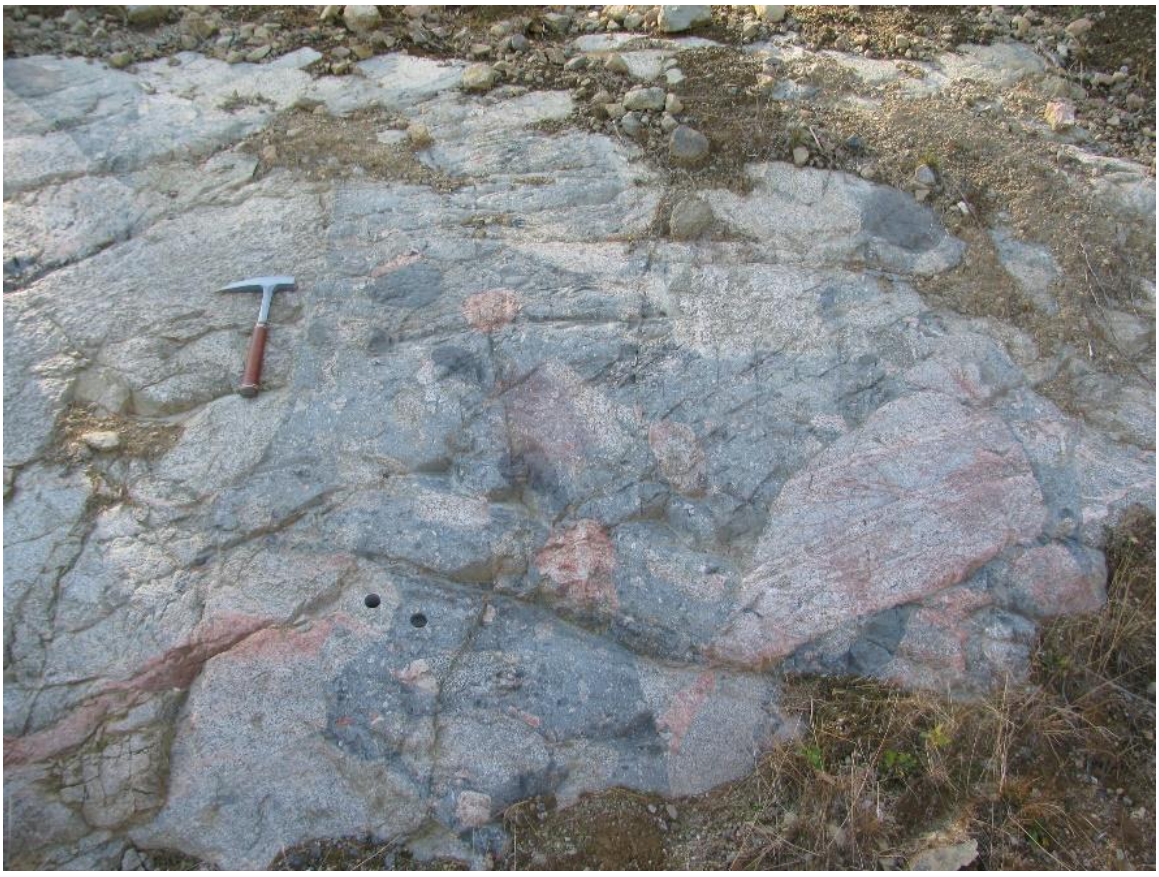

Figure 1.3. Field image of SDBX from the Sudbury impact structure (32 cm hammer for scale).

1.2.2 Footwall Breccia (Leucocratic Breccia, Late Granite Breccia)

Footwall Breccia (FWBX) (Figs. 1.4a and b) mainly exists in the northern, western and eastern footwall (Grant and Bite 1984; Deutsch et al. 1995; McCormick 2002), however, has also been reported in the South Range from the 120 zone in the Copper Cliff Offset Dyke (Cochrane 1984) and the Little Stobie Mine (Davis 1984). It forms discontinuous

kilometre-long layers of up to 200 m thick underlying the SIC (Coats and Snajdr 1984; Dressler 1984b; Lakomy 1990; Dressler and Reimold 2004), and locally extending up to 250 m into the footwall rocks (McCormick 2002; Dressler and Reimold 2004). The heterolithic polymict, matrix-supported breccia (Lakomy 1990; Dressler and Reimold 2004) is composed of a fine to medium-grained, igneous to metamorphic, poikilitic matrix (Pattison 1979; Deutsch et al. 1989) (Fig. 1.4b) and displays locally granophyric intergrowth and flow textures, as a result of partial melting (Dressler and Reimold 2004).

Clasts included within the matrix are up to several metres in size (McCormick 2002; Naldrett 2004), angular to subrounded and originate from adjacent country rocks (Dressler and Reimold 2004), main mass Norite, Sudbury Breccia (Dressler 1984b; Lakomy 1990; Dressler and Reimold 2004), of the Sublayer (Pattison 1979; McCormick 2002), and rarely exotic fragments (Dressler and Reimold 2004). They locally show features of recrystallization, partial melting, and relicts of planar deformation features (PDFs) (Dressler and Reimold 2004).

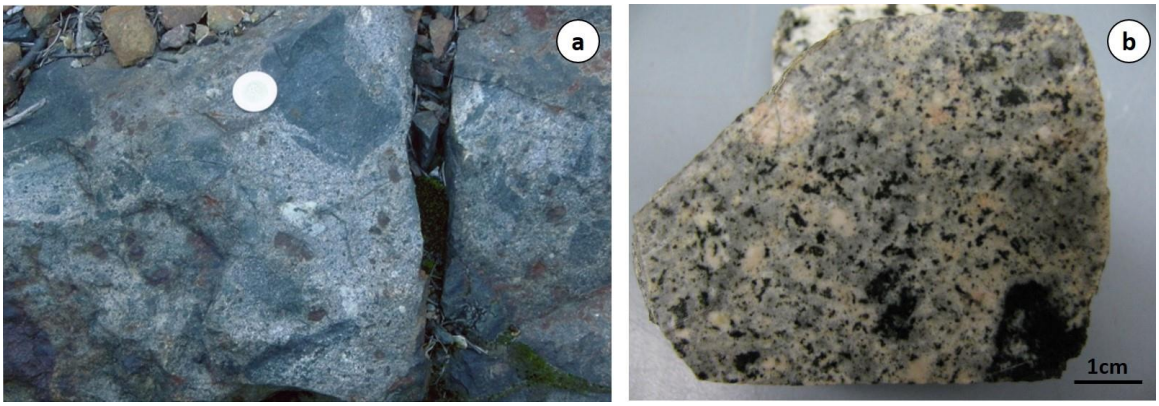

Figure 1.4. a) Field photograph of FWBX at Longvack pit (coin for scale (Rousell and Brown 2009)). b) Hand sample of FWBX from the Coleman Mine (FWBX I).

FWBX was formed by crushing and brecciation of crater floor rocks at shock pressures exceeding 10 GPa (Lakomy 1990), during the first stages of the impact event (Deutsch et al. 1989; Lakomy 1990; Lightfoot et al. 1997b; Farrow and Lightfoot 2002; McCormick 2002; Dressler and Reimold 2004; Carter et al. 2009) and subsequent thermal

metamorphism and partial melting (Dressler 1984b; Deutsch et al. 1995) by the SIC at temperatures above 1000°C (Deutsch et al. 1989; Lakomy 1990; Prevec and Cawthorn 2002).

The FWBX matrix has a granitic to quartz-dioritic composition (Deutsch et al. 1989) and geochemical signatures indicate that the breccia solely originated from adjacent footwall rocks (Deutsch et al. 1989; Lakomy 1990) which points to a parautochthonous origin of the breccia.

McCormick (2002) defined three phases of FWBX: i) the Sublayer-footwall breccia transition which she interpreted as an impact melt-rich, partially molten breccia, ii) a middle FWBX phase formed by *in situ* fragmentation, plastic deformation, and partial melting of footwall rocks, and iii) a later phase in which FWBX forms small dykes and veins within lower units of the SIC and fractured country rock beneath the breccia (Dressler and Reimold 2004). As host for Ni-Cu-PGE mineralization (McCormick 2002), FWBX has economically importance.

1.2.3 Sudbury Igneous Complex (SIC)

The Sudbury basin is delineated by the elliptical Sudbury Igneous Complex (SIC), a layered impact melt sheet from bottom to top composed of the so-called Sublayer, Norite, Quartz Gabbro, and Granophyre (Dressler et al. 1992) (Fig. 1.5). The names of the SIC units are misleading, as they do not represent the composition they are named after. The Sublayer, in fact, is noritic to gabbroic (Naldrett 1984b; Hecht et al. 2008); while the Norite shows the composition of quartz monzo-gabbro to quartz gabbro (Therriault et al. 2002; Darling et al. 2010a). The granitic Granophyre received its name based on its dominant texture, the granophyric intergrowth of quartz and feldspar. To avoid confusion and misunderstanding Therriault et al. (2002) introduced a more appropriate terminology for the SIC units: Upper Unit for the Granophyre, Middle Unit corresponds to the Quartz Gabbro, and Lower Unit represents the Norite. The thickness of the SIC varies from about 2 km in the North and East Ranges to about ~2.5 km in the South Range (Naldrett and Hewins 1984; Hecht et al. 2008).

Until the 1960s, it was assumed that the SIC (formerly called the Sudbury or Nickel Irruptive) formed during an intrusive, magmatic process after the formation of the Onaping Formation and the deposition of post-impact sediments (Burrows and Rickaby 1930; Stevenson 1960, 1963). Dietz (1964) suggested that the SIC is the result of an impact triggered magmatic process and Krogh et al. (1984) isotopically dated the SIC at 1.850 Ga and provided evidence for an impact-induced formation.

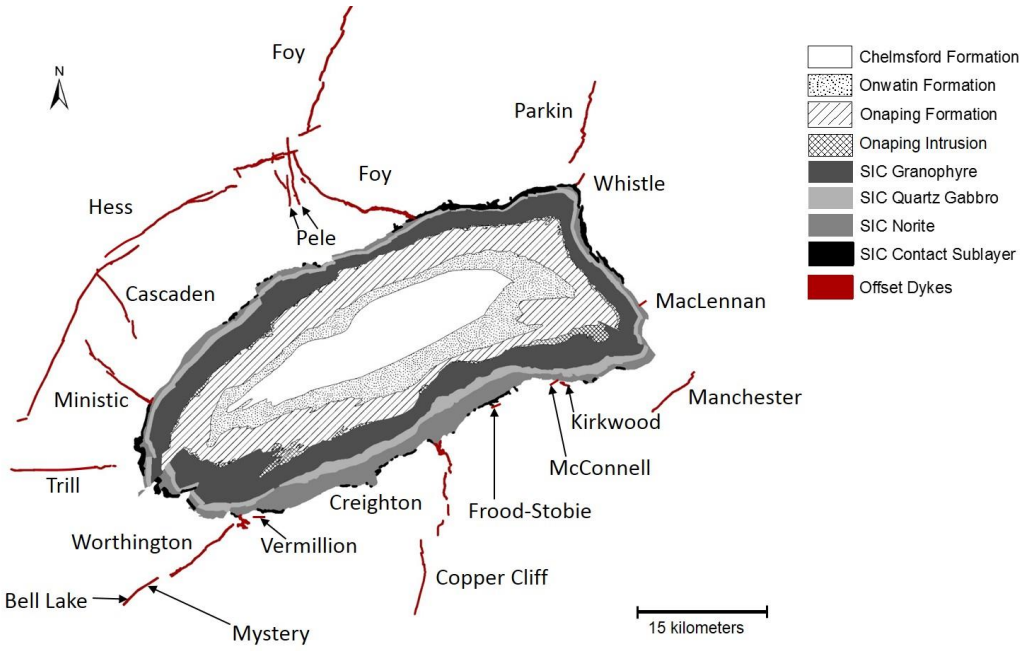

Figure 1.5. Simplified map of the Sudbury impact structure showing the main impact melt-related units.

Today it is generally accepted that the SIC was formed by impact melting and subsequent fractional crystallization and differentiation of a single superheated melt sheet (Grieve et al. 1991; Grieve 1994; Deutsch et al. 1995; Ostermann et al. 1996; Warner et al. 1998; Dickin et al. 1999; Therriault et al. 2002). Isotopic studies indicate that the impact melt sheet originated from a mix of crustal target rocks of the Superior Province and Huronian metasedimentary rocks (Gibbins and McNutt 1975; Hurst and Farhat 1977; Kuo and Crocket 1979; Faggart et al. 1985; Walker et al. 1991; Dickin et al. 1992, 1996, 1999; Golightly 1994; Grieve 1994; Ostermann et al. 1996; Morgan et al. 2002). This assumption is supported by Rare Earth Element (REE) patterns that are enriched in Light REEs

(LREEs) and point to upper continental crust (Kuo and Crocket 1979; Naldrett 1984a; Naldrett and Hewins 1984; Faggart et al. 1985). Thus, to explain the composition of the SIC, there is no need for a mantle contamination, as it had been suggested by some authors (Chai and Eckstrand 1993, 1994; Lightfoot et al. 1997b; Lightfoot 2001). However, there is still discussion if the SIC originated from a homogenized, coherent single magma (Lakomy 1990; Grieve et al. 1991; Lightfoot et al. 1997c; Therriault et al. 2002; Lavrenchuk et al. 2010), or if the magma separated into two melts, with a mafic portion at the bottom, differentiating into Quartz Gabbro and Norite, and a felsic melt on top forming the Granophyre (Golightly 1994; Ariskin et al. 1999; Prevec 2000; Zieg and Marsh 2005). A reason for this disagreement are the unusual proportions of the SIC subunits, which are approximately 30:10:60 for Norite, Quartz Gabbro and Granophyre (Darling et al. 2010b). The initial temperature of the SIC has been estimated in the range of 1700°C (Ivanov and Deutsch 1999; Zieg and Marsh 2005) to 2000°C and higher (Grieve 1977, 1994).

Assuming an initial temperature of at least 1800°C and a cooling process involving conductive and convective heat transfer, the melt sheet cooled down to the liquidus within approximately 10,000 years (Prevec and Cawthorn 2002; Zieg and Marsh 2005), during which it may have partially melted the target rocks to a depth of about 500 m below the SIC (Prevec and Cawthorn 2002). The country rocks up to a distance of 1 km from the SIC reached temperatures of above 500°C (Prevec and Cawthorn 2002), leading to the formation of a 1 to 2 km-wide contact metamorphic aureole around the Sudbury basin (Coats and Snajdr 1984; Dressler 1984b; Hanley and Mungall 2003; Boast and Spray 2006).

1.2.4 The Offset Dykes

The Offset Dykes (Fig. 1.5) play an important role in the Ni-Cu-PGE exploration at the Sudbury impact structure. To-date 19 radial and concentric Offset Dykes are known around the Sudbury impact structure, which are listed with their important characteristics in Table 1.3. Most radial Offset Dykes emanate from embayments of the SIC, composed of main mass Norite and Sublayer (Grant and Bite 1984; Morrison 1984), and extend into the country rocks, while concentric Offset Dyke do not have a known direct connection to the SIC and are located sub-concentric around the SIC.

Table 1.3. Overview of the main characteristics of the Offset Dykes.

	Offset Dyke	Geometry	Mines	Length/ thickness	Strike/Dip	Lithologies	Host Rock
East	McLennan	radial	/	<1 km/n.a. (3,18)	E/n.a.	QD (3, 18)	Huronian Sediments
North	Cascaden	radial	/	9 km/10-20 m (1)	NW/n.a. (1)	n.a.	Cartier Batholith (1)
	Foy	radial	Ni Offset	30 km/50-400 m (2)	NW and NE/70-80°NE (2)	QD, IQD (2), FWBX (3), MTBX (17)	Levack Gneiss, Benny Greenstone Belt, Cartier Batholith (2)
	Hess	concentric	/	41 km/10-80 m (4)	SW/≤70°NW (4)	QD, IQD, MTBX (4)	Huronian Sediments (4)
	Ministic	radial	/	8 km/10-30 m (1, 18)	NW/subvertical (1, 18)	QD (1)	Cartier Batholith (1)
	Parkin	radial	Milnet	9 km/1-30 m (5)	NE/80° (6)	QD, IQD, MTBX (6)	Benny Greenstone Belt, Huronian Supergroup
	Pele	radial	/	4.5 km/10-30 m (1)	NW/vertical (18)	n.a.	Cartier Batholith (1)
	Trill	radial	/	W/1-5 m (18)	W/n.a.	QD, IQD (7), MTBX (17)	Cartier Batholith and SDBX
	Whistle	radial	Whistle, Podolsky	2 km/30 m (6, 8)	NE/vertical (6, 8, 18)	QD, IQD, MTBX (6, 8)	Levack Gneiss (6, 8)
South	Bell Lake	radial	/	1.1 km/n.a. (9)	SW/subvertical (3)	QD (9)	Huronian Sediments
	Copper Cliff	radial	Copper Cliff North, Clarabelle	19 km/40-100 m (10)	SW/subvertical (3)	QD and IQD (10)	Huronian Sediments (11)
	Creighton	radial	Creighton	3 km/n.a. (1)	SE/n.a.	Norite, Sublayer (1)	Huronian Sediments
	Frood-Stobie	concentric	Frood-Stobie	3 km/1-7 m (3, 12, 18)	NE/60°N (16)	QD	SDBX (12)
	Kirkwood	concentric	Kirkwood	1.5 km/up to 60 m (12)	NW/n.a.	n.a.	SDBX (12)

	Offset Dyke	Geometry	Mines	Length/ thickness	Strike/Dip	Lithologies	Host Rock
	Manchester	concentric	/	5 km/12-30 m (5)	NE/60°SE (5)	QD (5)	SDBX (13)
	McConnell	concentric	/	1.2 km/60 m (10)	E/n.a.	n.a.	SDBX (10)
	Mystery	radial	/	0.8 km/15–30 m (14)	SW/subvertical (3)	QD (13)	Huronian Sediments
	Vermilion	concentric	Vermilion	200 m /n.a. (12)	NW/	QD, IQD (3)	SDBX (12)
	Worthington	radial	Victoria, Totten, McIntyr, Rosen, Robinson, Howland Worthington	15 km/30-100 m (5, 15)	SW/60°-80°SE (3, 5)	QD, IQD (15)	Huronian Sediments, Creighton pluton, Nipissing Diabase (15)

(1) Wallbridge Mining, (2) Tuchscherer and Spray (2002), (3) Grant and Bite (1984), (4) Wood and Spray (1998), (5) Lightfoot et al. (1997), (6) Murphy and Spray (2002), (7) Klimesch (2009), (8) Lafrance and Bygnes (2014), (9) North American Nickel, (10) Clayton Capes (2001), (11) Cochrane (1984), (12) Scott and Spray (2000), (13) O'Connor and Spray (1997), (14) CaNickel Mining, (15) Lightfoot and Farrow (2002), (16) Zurbrigg (1957), (17) This thesis. (18) Lightfoot (2016) Abbreviations: n.a. not available

The dykes consist of the so-called Quartz Diorite (QD) (Fig. 1.6a), an inclusion-rich version of Quartz Diorite (IQD) and Metabreccia (Fig. 1.6b). IQD has been described as a light-coloured, fine to medium-grained igneous rock (Scott and Benn 2002) that contains host rock and QD inclusions and sulfides (Lightfoot and Farrow 2002; Hecht et al. 2008), while QD is darker in colour, coarse-grained and contains less inclusions and sulfides (Scott and Benn 2002) (Fig. 1.6a). QD is usually detected at the margins of the dyke surrounding IQD (Grant and Bite 1984; Hecht et al. 2008), which led to the assumption of a two stage dyke emplacement with QD being the first phase followed by the intrusion of IQD (Morris and Pay 1981; Lightfoot et al. 1997b; Lightfoot and Farrow 2002; Murphy and Spray 2002; Hecht et al. 2008; Lafrance and Bygnes 2014).

The proto-SIC melt is generally considered to be the source of the radial dykes (Stöffler et al. 1992; Deutsch et al. 1995; Lightfoot et al. 1997a; Hecht et al. 2008); however, it is still unclear at what evolutionary stage of the SIC the Offset Dykes formed. It has been suggested that the dykes derived from the proto-SIC before differentiation (Pattison 1979; Grant and Bite 1984; Dressler et al. 1996; Lightfoot et al. 1997a; Ames et al. 2002; Tuchscherer and Spray 2002), or from intermediate stages of fractional crystallization of the main mass (Chai and Eckstrand 1993, 1994; Wood and Spray 1998; Prevec 2000; Therriault et al. 2002). Different theories of the emplacement of the radial Offset Dykes have been proposed and include the injection of the Offset Dyke melts into fractures within the cater floor and surrounding footwall rocks during i) the formation of the transient cavity (Grant and Bite 1984; Lightfoot and Farrow 2002; Murphy and Spray 2002) ii) the formation of a central uplift structure (Wood and Spray 1998; Tuchscherer and Spray 2002) or iii) the modification of the transient crater cavity (Scott and Spray 1999; Scott and Benn 2002).Other theories proceed on the assumption that the formation of the Offset Dykes took place after the impact event i.e. during post-impact isostatic readjustment of the crust (Wichman and Schultz 1993), post-impact cooling and subsequent contraction of the host rocks around the main mass (Riller 2005), or post-impact tectonism (Therriault et al. 2002). Concentric Offset Dykes have been suggested to have formed along concentric fractures during the crater modification stage (Wood and Spray, 1998).

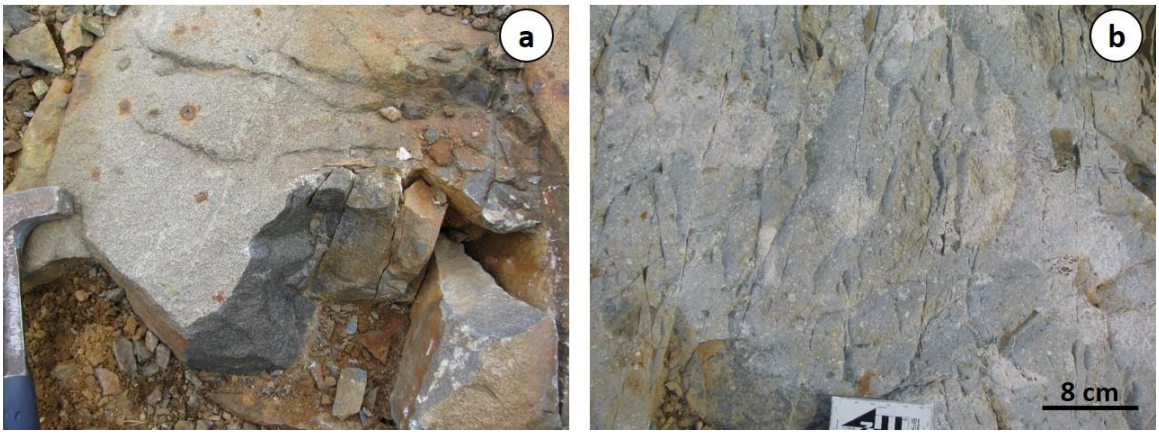

Figure 1.6. Field photographs from the Parkin Offset Dyke of a) QD containing some gossanized sulfide patches (hammer for scale), and b) MTBX.

A third Offset Dyke lithology is the so-called Metabreccia (MTBX) (Fig. 1.6b), which received its name according to its assumed origin as a result of thermal metamorphism of FWBX during the cooling of the SIC and/or the Offset Dykes (Farrow et al. 2005). Other authors suggested that the breccia formed in situ along the offset fractures (Dressler 1984b; Wood and Spray 1998). More recent studies suggested that the formation of MTBX was similar to that of QD and IQD, i.e., the injection of a melt originating from the proto-SIC into offset faults around the Sudbury structure during excavation and modification stage (Lightfoot et al. 1997c; Murphy and Spray 2002; Giroux and Benn 2005; Lafrance and Bygnes 2014). Based on research at the Whistle Offset Dyke Lafrance and Bygnes (2014) suggested that MTBX was the first melt phase before QD and IQD to intrude the Offset Dyke fractures. MTBX is usually associated with the North Range Offset Dykes and has been reported from the Parkin (Murphy and Spray 2002) and Whistle Offset Dykes (Farrow and Lightfoot 2002; Carter et al. 2009; Lafrance and Bygnes 2014) in the North Range; and at the Ministic and Foy Offset Dykes (Grant and Bite 1984). At the Whistle Offset Dyke, MTBX is associated with the Podolsky and Whistle sulfide deposits (Farrow and Lightfoot 2002; Lafrance and Bygnes 2014). Despite its economic importance, as host for Platinum-Group-Element (PGE) mineralization, little is known about MTBX and it is one of the major overlooked factors in Offset Dyke research.

1.2.5 The Onaping Formation

The Onaping Formation forms the lowest unit of the Whitewater Group and appears as an elliptical ring with a thickness of 1.4 to 1.6 km (Ames et al. 1998; Grieve et al. 2010) overlying the SIC. It consists of a complex series of breccias (Grieve et al. 2010) divided from bottom to top into Basal Onaping Intrusion, Sandcherry Member, and Dowling Member (Gibbins 1994; Ames et al. 2002). Until mid of the 19th century the Onaping Formation was thought to be a volcanic deposits (Bonney 1888; Burrows and Rickaby 1930; Thomson 1957; Williams 1957; Stevenson 1990). An impact origin for the Onaping Formation was first suggested by Dietz (1964) and later confirmed by the detection of planar deformation features (PDFs) in quartz and feldspar (French 1967; Peredery 1972a; Dressler et al. 1996), shock features in zircon (Bohor et al. 1993; Krogh et al. 1996), and impact diamonds (Masaitis 1999).

The Basal Onaping Intrusion (formerly the Basal Member) forms discontinuous, up to 300 m thick sheets between the SIC and the Sandcherry. Some authors suggested including the Basal Onaping Intrusion into the SIC (Deutsch et al. 1990; Avermann and Brockmeyer 1992; Grieve et al. 2010) and this is the focus of Chapter 2. The Sandcherry Member (Fig. 1.7a) has a thickness of up to 500 m (Ames et al. 2002; Grieve et al. 2010) and is composed of cored bombs and equant or fluidal vitric clasts within a microcrystalline matrix (Ames et al. 2002).

The Dowling Member (Fig. 1.7b) is characterized by a higher amount of matrix that contains smaller equant shards compared to the Sandcherry Member (Grieve et al. 2010). It can be divided into 4 stratigraphic subunits: Contact (35 to 300 m thick), Lower (up to 300 m thick), Middle (600 to 780 m thick) and Upper Dowling (140 to 220 m thick) (Ames et al. 2002). The Contact zone is not existent over the entire Onaping Formation and is composed of a very fine-grained, grey to black groundmass containing chloritic shards, blocky shards, and andesitic clasts (Grieve et al. 2010). The Lower Dowling is characterized by a heterogeneous breccia dominated by vitric fragments at the base that change morphology with increasing heights to lenticular clasts on the top (Ames et al. 2002). The Middle Dowling is described as a tuff- and lapillistone sized breccia with chloritic shards and sparse blocks and bombs (Grieve et al. 2010). The Upper Dowling is

characterized by a fine-grained breccia that contains a small amount of sedimentary fragments and is interpreted as a reworked and redeposited breccia unit (Ames et al. 2002). All units contain igneous or aphanitic textured intrusive rocks, formerly called melt bodies (Peredery 1972b; Stevenson 1990; Dressler et al. 1996; Ames et al. 2002; Grieve et al. 2010), which mainly occur in the lower parts of the Onaping Formation.

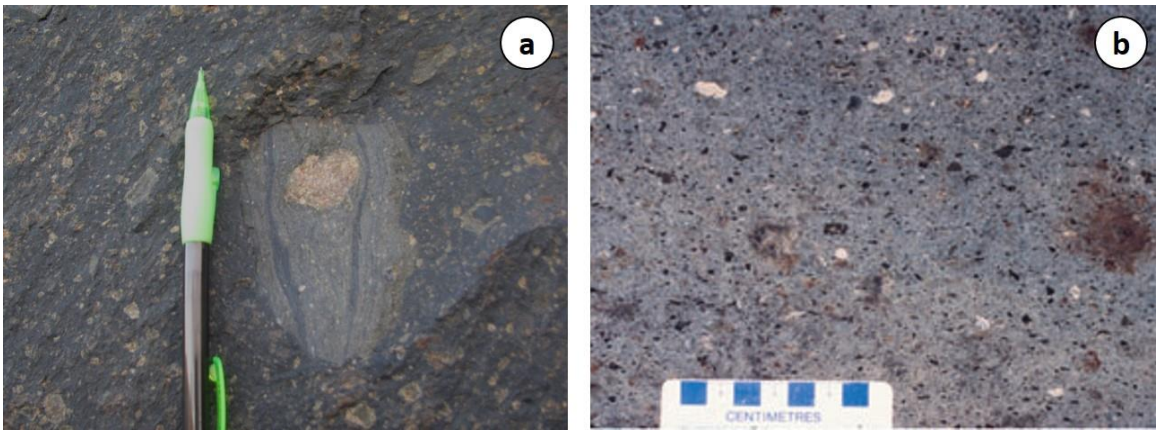

Figure 1.7. Field photographs of a) Sandcherry Member of the Onaping Formation (pen ~15 cm in length) and b) of the Dowling Member (Grieve et al. 2010).

Based on similarities with the so-called suevite from the Ries crater, Germany, the Onaping Formation had been interpreted as a suevitic breccia (French 1967, 1970; Dence 1972; Peredery 1972a; Stöffler 1977; Peredery and Morrison 1984; Avermann and Brockmeyer 1992). Generally, the origin of the entire Onaping Formation had been attributed to the ejection of material due to the impact and subsequent deposition on top of the proto-SIC forming fall-back breccias (French 1967, 1970; Peredery 1972a, 1972b; Avermann and Brockmeyer 1992). However, Grieve et al. (2010) noted that the Onaping Formation differs from the Ries suevite and pointed out that the thickness ratio of Onaping Formation to SIC would be approximately 1:2, which is not consistent with fallback breccia-impact melt ratios from other impact structures. Based on the general textures of the Onaping Formation and its complexity, the difference to typical fallback breccias, and the existence of different breccias types and breccias-in-breccias, the authors concluded an origin for the Onaping Formation that involved phreatomagmatic explosions. The Sudbury impact event occurred in a shallow marine environment, where sea water reacted with the superheated impact

melt sheet resulting in phreatomagmatic explosions, which led to mixing of proto-SIC with fallback material, and thus, to the formation of the complex Onaping Formation on top of the SIC.

1.3 Mineralization and Ore deposits

With pre-mining resources of over 1,648 million metric tons at ~1.2 percent Ni and ~1.0 percent Cu (Naldrett and Lightfoot 1993), the Sudbury structure represents one of the world's largest and most productive mining camps in the world (Ames et al. 2008). Ni-Cu-platinum-group element (Ni-Cu-PGE) deposits in the Sudbury area were discovered in 1883 (Giblin 1984; Farrow et al. 2005) and, since then, possesses the largest economic concentration of Ni in the world (Lightfoot and Naldrett 1996).

Three main different deposit types are existent at the Sudbury structure: i) progenetic deposits already existed before and were only modified and redistributed due to the impact (e.g. Ni-Cu-PGE sulfide deposits in the East Bull Lake gabbros; Ames and Farrow 2007); ii) syngenetic deposits formed during or immediately after the impact due to phase changes and melting (e.g., 1.85 Ga magmatic-hydrothermal Ni-Cu-PGE; Ames and Farrow 2007); ii) epigenetic deposits formed after the impact and are associated with fluids (e.g., minor Zn-Pb-Cu-Ag sulfide deposits within the Whitewater Group, as the result post-impact hydrothermal alteration; Ames et al. 1998; Ames and Farrow 2007). Syngenetic Ni-Cu-PGE deposits from the Sudbury structure can be divided based on their location: i) mineralization within the Sublayer and FWBX are called contact deposits and represent about half of the resources (Ames et al. 2008), ii) deposits within the Offset Dykes are referred to as offset-type deposits and make up about 25% of the resources (Ames et al. 2008), iii) the South Range Breccia Belt with 15% of the resources (Ames and Farrow 2007), and iii) footwall-type deposits within footwall rocks represent less than 10% of the Ni-Cu-PGE resources (Ames and Farrow 2007). Farrow et al. (2005) furthermore divided the footwall-type deposits based on the amount of sulfide. The Sudbury deposit types and their main characteristics are summarized in Table 1.4. All Sudbury deposit types contain PGEs, however, main hosts for PGEs are sulfide and silicate minerals within the footwall, Offset Dykes, and South Range Breccia Belt (Farrow and Lightfoot 2002; Farrow et al. 2005).

Table 1.4. Comparison the most common ore deposit types at the Sudbury impact structure.

Deposit Type	Contact-type deposits		Offset-type deposits		Footwall-type deposits (1)			South Range Breccia Belt
	North Range	South Range	Radial	Concentric	Sharp-walled vein systems	Low-sulfide mineralization	Hybrid Cu-PGE mineralization	
Location	Embayments and the base of the SIC (2, 3, 4, 5, 6, 7)		Radial Offset Dykes	Sub-parallel to the base of the SIC (1)	Footwall		Contact of SIC, embayments (1)	SDBX belt sub-concentric to the SIC
Host rock	Sublayer and FWBX (2, 3, 4, 5, 6, 6, 7), factures in FW below Sublayer (8)		IQD, MTBX	Brecciated rocks in FW (1)	SDBX (1)	SDBX (1)	Sublayer, IQD, MTBX (1)	IQD, FWBX, SDBX (17, 19)
Cu-Ni-Minerals	+ Po, - Pn (9, 13)		+ Po, - Pn, - Ccp (1, 10)		+ Ccp, - Cbn - Po, - Pn, - Mlr, - Bn (1)	+ Ccp (1)	+ Ccp, + Mlr (1)	+ Po, + Ni-mineralization (1)
Cu/Ni ratio	~0.7 (9)		1.5 to 2 (9)		>6 (1)			
Cu-Ni contents in wt %	Ni 3.9 - 6.1 Cu 1.3 - 5.5 (9,11)	Ni 4.0 - 5.9 Cu 2.4 - 7.1 (9, 11)	Ni 3.2 - 6.5 Cu 2.6 - 12.8 (9)		Cu>Ni (8)	Cu>Ni (8) <1% sulfide (1)	Cu>Ni (8)	
PGMs					Bism, Tel, Mnch, Mcnr, Mrsk, Ktsk, Fro (1)	Mnch, Mslv, Mrsk, Sprl, Mcnr, - Fro Pbpl (1)	Mnch, Mslv, Mrsk, Ktsk, Mcnr, Fro, Sprl (1)	

Deposit Type	Contact-type deposits		Offset-type deposits		Footwall-type deposits (1)			South Range Breccia Belt
Pt+Pd+Au contents in g/t (ppm)	<1 (7, 9) Pt 0.4 - 1.6 Pd 0.3 - 1.4 (9, 11)	<1 (7, 9) Pt 0.6 - 2.6 Pd 0.3 - 3.0 (9, 11)	>2.5 (1) Pt 1.7 - 13.8 Pd 0.6 - 15.0 (9)		>7 (1)			
Examples	Craig, Hardy McCreedy East, Victor Broken Hammer	Murray, Creighton, Lindsley, Lockerby, Crean Hill	Copper Cliff, Worthington, Parkin, Whistle, Trill, Foy, Ministic, Cascaden, Pele	Hess, Kirkwood, McConnell, Garson Mine, Manchester	Coleman, Strathcona, Deep Copper Ore, Fraser, (4, 12, 13, 14, 15, 16),	McCreedy (1), Levack mine, Victor, Nickel Rim, Broken Hammer, Crean Hill, Little Stobie (18)	Whistle and Podolsky Mine (1, 9), Whistle Open Pit (1)	Frood Stobie
Occurrence of the sulfides	Disseminated to massive stringers	Massive in the FW to disseminated in Sublayer (8)	Pods, disseminated sulfides (8), pipe-shaped massive bodies, complex sulfide vein stockworks (10)			Veins, stockworks, disseminated		massive sulfides on the base and disseminated sulfides on top (8)

(1) Farrow et al. (2005), (2) Souch et al. (1969), (3) Pattison (1979), (4) Coats and Snajdr (1984), (5) Davis (1984), (6) Morrison (1984), (7) Naldrett (1984b), (8) Naldrett (2004), (9) Farrow and Lightfoot (2002), (10) Grant and Bite (1984), (11) Naldrett (1999), (12) Abel et al. (1979), (13) Naldrett (1984a), (14) Li et al. (1992), (15) Morrison et al. (1994), (16) Farrow and Watkinson (1997), (17) Scott and Spray (2000), (18) Ames et al. (2008), (19) Ames and Farrow (2007). Abbreviations: Ccp Chalcopyrite, Py Pyrite, Pn Pentlandite, Po Pyrrhotite, Tel Tellurides, Bism Bismuthides, Pbpl Plumbopalladinite, Fro Froodite, Bn Bornite, Mlr Millerite, Cbn Cubanite, Mrsk Merenskyite, Mslv Maslovite, Ktsk Kosulskite, Sprl Sperrylite, Mnch Moncheite, Mcnr Michenerite, FW Footwall, + dominant, - minor.

Farrow and Lightfoot (2002) observed differences in the PGM occurrence between the North and South Range, with PGEs usually associated with arsenic in the form of sperrylite ($PtAs_2$) in the South, and moncheite $(Pt,Pd)(Te,Bi)_2$ as the dominant Pt mineral in the North (Li and Naldrett 1992; Farrow and Watkinson 1997).

The origin of the Sudbury sulfides was topic of discussion since their detection. Magmatic (e.g. Bell 1893; Coleman 1905; Collins 1934; Hawley 1962) and hydrothermal processes were suggested. Most authors today proceed on the assumption that the sulfide deposits at the Sudbury structure formed by a combination of magmatic and hydrothermal processes (Farrow and Lightfoot 2002; Naldrett 2004; Ames and Farrow 2007; Ames et al. 2008; Carter et al. 2009). Magmatic sulfides were formed during cooling of the SIC by sulfide segregation, resulting in contact and offset-type deposits (Hawley 1962; Keays and Crocket 1970; Naldrett et al. 1979; Naldrett 1984b; Farrow and Watkinson 1997; Farrow and Lightfoot 2002). With further cooling of the SIC and the development of a hydrothermal system, the sulfides were mobilized and redistributed (Farrow and Watkinson 1997; Naldrett 2004). The low-sulfide- mineralization of the footwall-type deposits, for example, was a result of this hydrothermal mobilization and redistribution of the initial magmatic sulfides (Farrow et al. 2005; Ames and Farrow 2007; Ames et al. 2008). The genesis of Cu-rich footwall-type deposits has also been associated with magmatic processes and seems to be the result of a Cu-rich residuum after the fractionation of the Ni-bearing Fe monosulfide solid-solution that formed the contact ores (Li et al. 1992, 1993; Ebel and Naldrett 1996).

1.4 Post-impact geologic and tectonic history

A chronologic overview about the major post-impact events is provided in Table 1.5. The Onaping Formation is overlain by post-impact sediments of the Vermilion, Onwatin and Chelmsford Formation (1.72 Ga) (Fairbairn et al. 1969). Onaping Formation, Vermilion, Onwatin and Chelmsford Formation form the 2.9 km thick Whitewater Group. During and after its formation, the Sudbury structure was affected by the Penokean orogeny, dated between 1.70–1.90 Ga, which led to tectonic shortening, thrusting and folding of the SIC

resulting in the elliptical shape of the Sudbury basin (Shanks and Schwerdtner 1990, 1991; Grieve et al. 1991; Milkereit and Green 1992; Deutsch and Grieve 1994; Wu et al. 1994; Deutsch et al. 1995). The impact structure including host rocks experienced metamorphism under greenschist- to amphibolite-facies (Card 1978; Thomson et al. 1985; Fleet et al. 1987; Riller and Schwerdtner 1997; Riller 2005), with the metamorphic grade decreasing to the north.

Table 1.5. Overview about the major post-impact events.

<table>
<tr><td>Paleogene</td><td>37 Ma (7)</td><td colspan="3">Wanapitei Impact Event</td><td></td></tr>
<tr><td rowspan="5">Proterozoic</td><td>1.20–0.90 Ga (6)</td><td colspan="3">Grenville Orogeny</td><td></td></tr>
<tr><td>1.23 Ga (5)</td><td colspan="3">Sudbury Diabase Swarm</td><td></td></tr>
<tr><td>1.70–1.60 Ga (4)</td><td colspan="3">Mazatzal Orogeny</td><td></td></tr>
<tr><td rowspan="3">1.72 Ga (2)</td><td rowspan="3">Whitewater Group</td><td>Chelmsford</td><td>Wacke, argillite, siltstone</td><td rowspan="3">Penokean orogeny 1.9–1.7</td></tr>
<tr><td>Onwatin</td><td>Argillite, siltstone</td></tr>
<tr><td>Vermilion</td><td>Carbonate chert</td></tr>
</table>

(1) Krogh et al. (1984), (2) Fairbairn et al. (1969), (3) Van Schmus (1976), (4) Bailey et al. (2004), (5) Dudas et al. (1994), (6) Lumbers (1975), (7) Winzer et al. (1976).

The South Range Shear Zone (SRSZ) (Burrows and Rickaby 1930; Shanks and Schwerdtner 1990), approximately 64 km long and 1 to 5 km wide, is a northeast-trending, south-dipping major zone of reverse ductile shear, which displaced the South Range of the SIC and its underlying Huronian country rocks towards northwest (Card 1994). The SRSZ is most likely associated with the Penokean Orogeny (Riller and Schwerdtner 1997) or the Mazatzal Orogeny, which dates at 1.70–1.60 Ga (Bailey et al. 2004). Olivine diabase dykes of the Sudbury Dyke Swarm (1.23 Ga, (Dudas et al. 1994)) intrude the rocks of the Superior and Southern Province (Dressler 1984a). Further modification of the Sudbury impact structure may have occurred during the Grenville Orogeny between 1.20–0.90 Ga (Lumbers 1975), however, the effects would have been slight and cannot be distinguished from preceding tectonic events. Approximately 37 Ma ago the Sudbury-Wanapitei area experienced another impact, the Wanapitei impact structure that today is contained entirely

in Wanapitei Lake, northeast of the Sudbury structure. This structure did not, however, cause any deformation of the rocks exposed around Wanapitei Lake and part of the Sudbury impact structure.

1.5 Thesis Structure

The main aim of this research project is to investigate the formation of the Offset Dykes, and their relationship to the SIC, and the Basal Onaping Intrusion. To accomplish this, the first part of this research focused on the Basal Onaping Intrusion (Chapter 2). The Basal Onaping Intrusion are located at the contact between Granophyre of the SIC and the Sandcherry Member of the Onaping Formation. The study consisted of an analytical based investigation of drill cores and field samples of the Basal Onaping Intrusion in the eastern North Range of the SIC with a focus on details of the contact relations between the Granophyre of the SIC, the Basal Onaping Intrusion, and the Sandcherry Member of the Onaping Formation. In Chapter 2 we show that the Onaping Formation are the roof rocks of the SIC, and not as suggested, part of the complex breccia series of the Onaping Formation.

The remainder of this research focused on the origin and emplacement of the Parkin, Trill and Foy Offset Dykes in the North Range based on the detailed investigation of MTBX. Understanding the formation of the Offset Dykes is important for understanding the process of the crater formation and, particularly for Sudbury, the formation of the SIC, which is unique on Earth. The results of this part of the thesis are presented in three chapters. Chapter 3 provides the results of a basic petrographic and geochemical study of MTBX from the Parkin Offset Dyke. Samples of different dyke lithologies and country rocks were collected from all accessible trenches. Detailed investigation of the different lithologies, contacts between them, and as well as between the dyke and the county rocks was of great importance as changes in textures and grain size, and the presence of possible interaction features provide information about the emplacement of the dykes and the timing. In this Chapter, it is suggested that MTBX is a recrystallized impact breccia that shares more similarities with FWBX rather than IQD and QD.

Chapter 4 extends the investigation of MTBX to the Trill and Foy Offset Dykes, and provides basic petrographic and geochemical results from those dykes in comparison to the Parkin MTBX. Furthermore, this chapter expands on the timing and mode of emplacement and evolution of the Offset Dykes. Determining the origin and formation of the MTBX and its relationship to the other dyke phases is important for reconstructing the mode and timing of emplacement and the factors that have contributed to the formation of the North Range Trill, Foy and Parkin Offset Dyke.

Chapter 5 focuses on mineralization within MTBX and the economic potential of MTBX with respect to PGE deposits. MTBX is very often associated with mineralization; it contains disseminated and blebby sulfides and is often directly in contact with gossanized pods. Zoning of ore minerals was investigated by quantitative analyses and element mapping using a field emission electron microprobe. Changes in mineralogy within one mineral can reflect formation conditions and approximate compositions during the crystallization of the mineral and will help to investigate the mineralization process. Answering those questions is an important step further to understand the formation of mineral deposits with the Offset Dykes and their economic significance, which could provide necessary information for exploration strategies.

Finally, Chapter 6 reviews and synthesizes the results of the entire thesis and Chapter 7 provides recommendations for future work.

1.6 References

Ames, D.E., Davidson, A., Buckle, J., Card, K.D., 2005. Sudbury bedrock compilation; Geology. Geol. Surv. Canada Open File 4570, 2 maps.

Ames, D.E., Davidson, A., Wodicka, N., 2008. Geology of the giant Sudbury polymetallic mining camp, Ontario, Canada. Econ. Geol. 103, 1057–1077.

Ames, D.E., Farrow, C.E.G., 2007. Metallogeny of the Sudbury mining camp, Ontario, in: Goodfellow, W.D. (Ed.), Mineral Deposits of Canada: A Synthesis of Major Deposit-Types, District Metallogeny, the Evolution of Geological Provinces, and Exploration

Methods. Geological Association of Canada, Mineral Deposits Division, Special Publication 5. pp. 329–350.

Ames, D.E., Gibson, H.L., 2004. Geology, alteration and mineralization of the Onaping Formation, Morgan Township, Sudbury Structure, Ontario. Geol. Surv. Canada Open File 3717, 2 maps.

Ames, D.E., Golightly, J.P., Lightfoot, P.C., Gibson, R.L., 2002. Vitric compositions in the Onaping Formation and their relationship to the Sudbury Igneous Complex, Sudbury structure. Econ. Geol. 97, 1541–1562.

Ames, D.E., Watkinson, D.H., Parrish, R.R., 1998. Dating of a regional hydrothermal system induced by the 1850 Ma Sudbury impact event. Geology 26, 447–450.

Ariskin, A.A., Deutsch, A., Ostermann, M., 1999. Sudbury Igneous Complex: Simulating phase equilibria and in situ differentiation for two proposed parental magmas, in: Dressler, B.O., Sharpton, V. (Eds.), Large Meteorite Impacts and Planetary Evolution II, GSA Special Paper 339. pp. 373–387.

Avermann, M., Brockmeyer, P., 1992. The Onaping Formation of the Sudbury Structure (Canada) - an example of of allochthonous impact breccias. Tectonophysics 216, 227–234.

Bailey, J., Lafrance, B., McDonald, A.M., Fedorowich, J.S., Kamo, S., Archibald, D.A., 2004. Mazatzal-Labradorian age (1.7– 1.6 Ga) ductile deformation of the South Range Sudbury impact structure at the Thayer Lindsley mine, Ontario. Can. J. Earth Sci. 41, 1491–1505.

Bell, R., 1893. On the Sudbury Mining District. Geol. Surv. Canada Annu. Rep. 5, 1–95.

Boast, M., Spray, J.G., 2006. Superimposition of a thrust-transfer fault system on a large impact structure: Implications for Ni-Cu-PGE exploration at Sudbury. Econ. Geol. 101, 1583–1594.

Bohor, B.F., Betterton, W.J., Krogh, T.E., 1993. Impact shocked zircons: Discovery of shock-induced textures reflecting increasing degrees of shock metamorphism. Earth Planet. Sci. Lett. 119, 419–424.

Bonney, T.G., 1888. Notes on a part of the Huronian series in the neighborhood of Sudbury (Canada). Q. J. Geol. Soc. London 44, 32–45.

Burrows, A.G., Rickaby, H.C., 1930. Sudbury Basin Area. Ontario Dep. Mines Annu. Rep. 38, 55 pp.

Card, K.D., 1978. Metamorphism of the middle Precambrian (Aphebian) rocks of the Eastern Southern Province, in: Fraser, J.A., Heywood, W.W. (Eds.), Metamorphism in the Canadian Shield, Geological Survey of Canada, 78, 10. pp. 269–282.

Card, K.D., 1994. Geology of the Levack gneiss complex, the northern footwall of the Sudbury structure, Ontario. Geol. Surv. Canada Curr. Res. 1994-C, 269–278.

Card, K.D., Gupta, V.K., McGrath, P.H., Grant, F.S., 1984. The Sudbury Structure: Its Regional Geological and Geophysical Setting, in: Pye, E.G., Naldrett, A.J., Giblin, P.E. (Eds.), The Geology and Ore Deposits of the Sudbury Structure. pp. 25–44.

Card, K.D., Innes, D.G., 1981. Geology of the Benny Area, District of Sudbury. Ontario Geol. Surv. Open File 206, 117 pp.

Carter, W.M., Watkinson, D.H., Ames, D.E., Jones, P.C., 2009. Quartz Diorite Magmas and Cu-(Ni)-PGE Mineralization, Podolsky Deposit, Whistle Offset Structures, Sudbury, Ontario. Geol. Surv. Canada Open File 6134, 58 pp.

Chai, G., Eckstrand, R., 1993. Origin of the Sudbury Igneous Complex, Ontario - differentiate of two separate magmas. Geol. Surv. Canada Open File 93-1E, 219–230.

Chai, G., Eckstrand, R., 1994. Rare-earth element characteristics and origin of the Sudbury Igneous Complex, Ontario, Canada. Chem. Geol. 113, 221–244.

Clayton Capes, P., 2001. A Petrological Investigation of the Copper Cliff Embayment

Structure Sudbury, Ontario. University of Toronto Copyright.

Coats, C.J.A., Snajdr, P., 1984. Ore deposits of the North Range, Onaping–Levack area, Sudbury, in: Pye, E.G., Naldrett, A.J., Giblin, P.E. (Eds.), The Geology and Ore Deposits of the Sudbury Structure. pp. 327–346.

Cochrane, L.B., 1984. Ore Deposits of the Copper Cliff Offset, in: Pye, E.G., Naldrett, A.J., Giblin, P.E. (Eds.), The Geology and Ore Deposits of the Sudbury Structure. pp. 347–360.

Coleman, A.P., 1905. The Sudbury Nickel Region. Ontario Dep. Mines Annu. Rep. 14, 1–188.

Collins, W.H., 1934. Life history of the Sudbury nickel irruptive. I. Petrogenesis. R. Soc. Canada Trans. 28, 123–177.

Corfu, F., Andrews, A.J., 1986. A U–Pb age for mineralized Nipissing diabase, Gowganda. Can. J. Earth Sci. 23, 107–109.

Darling, J.R., Hawkesworth, C.J., Lightfoot, P.C., Storey, C.D., Tremblay, E., 2010a. Isotopic heterogeneity in the Sudbury impact melt sheet. Earth Planet. Sci. Lett. 289, 347–356.

Darling, J.R., Hawkesworth, C.J., Storey, C.D., Lightfoot, P.C., 2010b. Shallow impact: Isotopic insights into crustal contributions to the Sudbury impact melt sheet. Geochim. Cosmochim. Acta 74, 5680–5696.

Davis, G.C., 1984. Little Stobie Mine: A South Range Contact Deposit, in: Pye, E.G., Naldrett, A.J., Giblin, P.E. (Eds.), The Geology and Ore Deposits of the Sudbury Structure. pp. 361–370.

Dence, M.R., 1972. Meteorite impact craters and the structure of the Sudbury Basin, in: Guy-Bray, J.V. (Ed.), New Developments in Sudbury Geology. Geological Association of Canada Special Paper 10, Toronto, pp. 7–18.

Deutsch, A., Brockmeyer, P., Buhl, D., 1990. Sudbury again: New and old isotope data, in: 21st Lunar and Planetary Science Conference. pp. 282–283.

Deutsch, A., Grieve, R.A.F., 1994. The Sudbury Structure: Constraints on its genesis from Lithoprobe results. Geophys. Res. Lett. 21, 963–966.

Deutsch, A., Grieve, R.A.F., Avermann, M., Bischoff, L., Brockmeyer, P., Buhl, D., Lakomy, R., Müller-Mohr, V., Ostermann, M., Stöffler, D., 1995. The Sudbury Structure (Ontario, Canada): a tectonically deformed multi-ring impact basin. Geol. Rundschau 84, 697–709.

Deutsch, A., Lakomy, R., Buhl, D., 1989. Strontium-and neodymium-isotopic characteristics of a heterolithic breccia in the basement of the Sudbury impact structure, Canada. Earth Planet. Sci. Lett. 93, 359–370.

Dickin, A.P., Artan, M.A., Crocket, J.H., 1996. Isotopic evidence for distinct crustal sources of North and South Range ores, Sudbury Igneous Complex. Geochim. Cosmochim. Acta 60, 1605 – 1613.

Dickin, A.P., Nguyen, T., Crocket, J.H., 1999. Isotopic evidence for a single impact melting origin of the Sudbury Igneous Complex, in: Dressler, B.O., Sharpton, V.L. (Eds.), Large Meteorite Impacts and Planetary Evolution II, GSA Special Paper 339. pp. 361–371.

Dickin, A.P., Richardson, J.M., Crocket, J.H., McNutt, R.H., Peredery, W. V., 1992. Osmium isotope evidence for a crustal origin of platinum group elements in the Sudbury nickel ore, Ontario, Canada. Geochim. Cosmochim. Acta 56, 3531 – 3537.

Dietz, R.S., 1962. The Vredefort Ring Structure: A Reply. J. Geol. 70, 502–504.

Dietz, R.S., 1964. Sudbury structure as an astrobleme. Trans. - Am. Geophys. Union 43, 445– 446.

Dietz, R.S., Butler, L.W., 1964. Shatter-cone orientation at Sudbury Canada. Nature 204,

280–281.

Dressler, B.O., 1984a. General geology of the Sudbury area, in: Pye, E.G., Naldrett, A.J., Giblin, P.E. (Eds.), The Geology and Ore Deposits of the Sudbury Structure. pp. 57–82.

Dressler, B.O., 1984b. The effects of the Sudbury event and the intrusion of the Sudbury Igneous Complex on the footwall rocks of the Sudbury structure, in: Pye, E.G., Naldrett, A.J., Giblin, P.E. (Eds.), The Geology and Ore Deposits of the Sudbury Structure. pp. 97–138.

Dressler, B.O., Gupta, V.K., Muir, T.L., 1991. The Sudbury structure. Geol. Ontario, OGS Spec. Vol. 4, 593–626.

Dressler, B.O., Peredery, W. V., Muir, T.L., 1992. Geology and Mineral Deposits of the Sudbury Structure. Ontario Geological Survey Guidebook 8.

Dressler, B.O., Reimold, W.U., 2004. Order or chaos? Origin and mode of emplacement of breccias in floors of large impact structures. Earth-Science Rev. 67, 1–54.

Dressler, B.O., Weiser, T., Brockmeyer, P., 1996. Recrystallized impact glasses of the Onaping formation and the Sudbury igneous Complex, Sudbury Structure, Ontario, Canada. Geochim. Cosmochim. Acta 60, 2019 – 2036.

Dudas, F.O., Davidson, A., Bethune, K.M., 1994. Age of the Sudbury diabase dykes and their metamorphism in the Grenville Province, Ontario. Radiogenic Age Isot. Stud. Geol. Surv. Canada Rep. 8, 97–106.

Ebel, D.S., Naldrett, A.J., 1996. Fractional crystallization of sulfide ore liquids at high temperature. Econ. Geol. 91, 607–621.

Faggart, B.E., Basu, A.R., Tatsumoto, M., 1985. Origin of the Sudbury complex by meteoritic impact: Neodymium isotopic evidence. Science (80-.). 230, 436–439.

Fairbairn, H.W., Hurley, P.M., Card, K.D., Knight, C.J., 1969. Correlation of Radiometric

Ages of Nipissing Diabase and Huronian Metasediments with Proterozoic Orogenic Events in Ontario. Can. J. Earth Sci. 6, 489–497.

Farrow, C.E.G., 1994. Geology, alteration, and the role of fluids in Cu–Ni–PGE mineralization of the footwall rocks to the Sudbury Igneous Complex, Levack and Morgan Townships, Sudbury District, Ontario. Carleton University.

Farrow, C.E.G., Everest, J.O., King, D.M., Jolette, C., 2005. Sudbury Cu-(Ni)-PGE-Systems: Refining the classification: Using McCreedy West Mine, and Podolski project case studies, in: Mungall, J.E. (Ed.), Exploration for Platinum- Group Elements Deposits. Mineralogical Association of Canada, Short Course Series Volume 35, pp. 163–180.

Farrow, C.E.G., Lightfoot, P.C., 2002. Sudbury PGE Revisited: Towards an Integrated Model, in: Cabri, L.J. (Ed.), Geology, Geochemistry, Mineralogy and Mineral Beneficiation of Platinum-Group Elements. Canadian Institute of Mining, Metallurgy and Petroleum, Special Volume 54, pp. 273–297.

Farrow, C.E.G., Watkinson, D.H., 1997. Diversity of precious-metal mineralization in footwall Cu-Ni-PGE deposits, Sudbury, Ontario; implications for hydrothermal models of formation. Can. Mineral. 35, 817–839.

Fedorowich, J.S., Rousell, D.H., Peredery, W. V., 1999. Sudbury breccia distribution and orientation in a embayment environment. Geol. Soc. Am. Spec. Pap. 339, 305–315.

Fiske, P.S., Nellis, W.J., Lipp, M., Lorenzana, H., Kikuchi, M., Syono, Y., 1995. Pseudotachylites generated in shock experiments: implications for impact cratering products and processes. Science (80-.). 270, 281–283.

Fleet, M.E., Barnett, R.L., Morris, W.A., 1987. Prograde metamorphism of the Sudbury Igneous Complex. Can. Mineral. 25, 499–514.

Frarey, M.J., Loveridge, W.D., Sullivan, R.W., 1982. A U-Pb zircon age for the Creighton granite, Ontario. Geol. Surv. Canada Pap. 81-1C, 129–132.

French, B.M., 1967. Sudbury structure, Ontario: Some petrographic evidence for an origin by meteorite impact, in: French, B.M., Short, N.M. (Eds.), Shock Metamorphism of Natural Materials. Mono Book Corporation, Baltimore, pp. 383–412.

French, B.M., 1970. Possible Relations Between Meteorite Impact and Igneous Petrogenesis, as Indicated by the Sudbury Structure, Ontario, Canada. Bull. Volcanol. 34, 466–517.

Gibbins, S.F.M., 1994. Geology, geochemistry, stratigraphy and mechanisms of emplacement of the Onaping Formation, Dowling area, Sudbury structure, Ontario, Canada. M.Sc. Thesis, Laurentian University.

Gibbins, W.A., McNutt, R.H., 1975. The Age of the Sudbury Nickel Irruptive and the Murray Granite. Can. J. Earth Sci. 12, 1970–1989.

Giblin, P.E., 1984. History of Exploration and Development, of Geological Studies and Development of Geological Concepts, in: Pye, E.G., Naldrett, A.J., Giblin, P.E. (Eds.), The Geology and Ore Deposits of the Sudbury Structure. pp. 3–23.

Giroux, L.A., Benn, K., 2005. Emplacement of the Whistle dike, the Whistle embayment and hosted sulfides, Sudbury Impact Structure, based on anisotropies of magnetic susceptibility and. Econ. Geol. 100, 1207–1227.

Golightly, J.P., 1994. The Sudbury Igneous Complex as an impact melt: evolution and ore genesis, in: Lightfoot, P.C., Naldrett, A.J. (Eds.), Proceedings of the Sudbury-Noril'sk Symposium. Ontario Geological Survey Special Volume 5, pp. 105–118.

Grant, R.W., Bite, A., 1984. Sudbury Quartz Diorite Offset Dikes, in: Pye, E.G., Naldrett, A.J., Giblin, P.E. (Eds.), The Geology and Ore Deposits of the Sudbury Structure. pp. 275–300.

Grieve, R.A.F., 1977. Cratering processes-As interpreted from the occurrence of impact melts, in: Roddy, D.J., Pepin, R.O., Merrill, R.B. (Eds.), Impact and Explosion Cratering. Pergamon Press, New York, pp. 791–814.

Grieve, R.A.F., 1994. An Impact Model of the Sudbury Structure, in: Lightfoot, P.C., Naldrett, A.J. (Eds.), Proceedings of the Sudbury-Noril'sk Symposium. Ontario Geological Survey Special Volume 5, pp. 119–132.

Grieve, R.A.F., Ames, D.E., Morgan, J. V., Artemieva, N.A., 2010. The evolution of the Onaping Formation at the Sudbury impact structure. Meteorit. Planet. Sci. 45, 759–782.

Grieve, R.A.F., Reimold, W.U., Morgan, J., Riller, U., Pilkington, M., 2008. Observations and interpretations at Vredefort, Sudbury, and Chicxulub; towards an empirical model of terrestrial impact basin formation. Meteorit. Planet. Sci. 43, 855–882.

Grieve, R.A.F., Stöffler, D., Deutsch, A., 1991. The Sudbury structure: Controversial or misunderstood? J. Geophys. Res. 96, 753–764.

Hanley, J.J., Mungall, J.E., 2003. Chlorine enrichment and hydrous alteration of Sudbury Breccia hosting footwall Cu–Ni–PGE mineralization at the Fraser Mine, Sudbury, Ontario, Canada. Can. Mineral. 41, 857–881.

Hawley, J.E., 1962. The Sudbury ores, their mineralogy and origin; Part 3, Interpretations; The history and origin of the Sudbury ores. Can. Mineral. 7, 146–207.

Heaman, L.M., 1997. Global mafic magmatism at 2.45 Ga: remnants of an ancient large igneous province? Geology 25, 299.

Hecht, L., Wittek, A., Riller, U., Mohr, T., Schmitt, R.T., Grieve, R.A.F., 2008. Differentiation and emplacement of the Worthington Offset Dike of the Sudbury impact structure, Ontario. Meteorit. Planet. Sci. 43, 1659–1679.

Hurst, R.W., Farhat, J., 1977. Geochronologic investigations of the Sudbury Nickel Irruptive and the Superior Province granites north of Sudbury. Geochim. Cosmochim. Acta 41, 1803–1815.

Ivanov, B.A., Deutsch, A., 1999. Sudbury impact event: Cratering mechanics and thermal

history, in: Dressler, B.O., Sharpton, V.L. (Eds.), Large Meteorite Impacts and Planetary Evolution II, GSA Special Paper 339. pp. 389–398.

James, R.S., Easton, R.M., Peck, D.C., Hrominchuk, J.L., 2002. The East Bull Lake Intrusive Suite: Remnants of a ~2.48 Ga Large Igneous and Metallogenic Province in the Sudbury Area of the Canadian Shield. Econ. Geol. 92, 1577–1606.

James, R.S., Sweeny, J.M., Peredery, W. V., 1991. Thermobaromehy of the Levack Gneisses-Footwall rocks to the Sudbury Igneous Complex, in: Lithoprobe, Abitibi-Grenville Project, Abitibi Grenville Transect, Report 32. pp. 179– 182.

Keays, R.R., Crocket, J.H., 1970. A study of precious metals in the Sudbury nickel irruptive ores. Econ. Geol. 65, 438–450.

Kenkmann, T., Hornemann, U., Stöffler, D., 2000. Experimental generation of shock-induced pseudotachylites along lithological interfaces. Meteorit. Planet. Sci. 35, 1275–1290.

Klimesch, L., 2009. Mapping Project: Creighton Pluton at Graham Fault, Sudbury, Canada. and Emplacement, Differentiation and Mineralisation of the Trill Offset Dike, Sudbury, Canada. Freie Universität Berlin.

Krogh, T.E., Corfu, F., Davis, D.W., Dunning, G.R., Heaman, L.M., Kamo, S.L., Machado, N., Greenough, J.D., Nakamura, E., 1987. Precise U-Pb isotopic ages of diabase dykes and mafic to ultramafic rocks using trace amounts of baddeleyite and zircon, in: Halls, H.C., Fahrig, W.F. (Eds.), Mafic Dyke Swarms, Geological Association of Canada Special Paper 34. pp. 147–152.

Krogh, T.E., Davis, D.W., Corfu, F., 1984. Precise U–Pb zircon and baddeleyite ages for the Sudbury area, in: Pye, E.G., Naldrett, A.J., Giblin, P.E. (Eds.), The Geology and Ore Deposits of the Sudbury Structure. pp. 431–447.

Krogh, T.E., Kamo, S.L., Bohor, B.F., 1996. Shock metamorphosed zircons with correlated U-Pb discordance and melt rocks with concordant protolith ages indicate an impact

origin for the Sudbury structure, in: Hart, S., Basu, A. (Eds.), Earth Processes: Reading the Isotopic Code. American Geophysical Union Monograph 95, pp. 343–353.

Kuo, H.Y., Crocket, J.H., 1979. Rare earth elements in the Sudbury Nickel Irruptive; comparison with layered gabbros and implications for nickel irruptive petrogenesis. Econ. Geol. 74, 590–605.

Lafrance, B., Bygnes, L.C., 2014. Emplacement of metabreccia along the Whistle offset dike, Sudbury: implications for post-impact modification of the Sudbury impact structure. Can. J. Earth Sci. 19, 1–19.

Lafrance, B., Legault, D., Ames, D.E., 2008. The formation of the Sudbury breccia in the North Range of the Sudbury impact structure. Precambrian Res. 165, 107–119.

Lakomy, R., 1990. Implications for cratering mechanics from a study of the Footwall Breccia of the Sudbury impact structure, Canada. Meteorit. Planet. Sci. 25, 195–207.

Langford, F.F., 1960. Geology of Levack Township, District of Sudbury, Ontario Department of Mines, Preliminary Report 1960-5.

Lavrenchuk, A., Latypov, R., Lightfoot, P.C., 2010. The Sudbury Igneous Complex, Canada: Numerical Modeling Confirms Fractionation of a Single Parental Magma, in: 11th International Platinum Symposium. Ontario Geological Survey.

Legault, D., Lafrance, B., Ames, D.E., 2003. Structural study of Sudbury breccia and sulphide veins, Levack embayment, North Range of the Sudbury structure, Ontario. Geol. Surv. Canada Curr. Res. 2003-C1, 11 pp.

Li, C., Naldrett, A.J., 1992. PGE Studies in the Footwall at Sudbury. Ontario Geol. Surv. Open File 5830, 138 pp.

Li, C., Naldrett, A.J., Coats, C.J.A., Johannessen, P., 1992. Platinum, palladium, gold, copper-rich stringers at the Strathcona Mine, Sudbury; their enrichment by

fractionation of a sulfide liquid. Econ. Geol. 87, 1584–1598.

Li, C., Naldrett, A.J., Rucklidge, J.C., Kilius, L.R., 1993. Concentrations of Platinum-Group Elements and gold in sulfides from the Strathcona deposit, Sudbury, Ontario. Can. Mineral. 30, 523–531.

Lieger, D., Riller, U., Gibson, R.L., 2009. Generation of fragment-rich pseudotachylite bodies during central uplift formation in the Vredefort impact structure, South Africa. Earth Planet. Sci. Lett. 279, 53–64.

Lightfoot, P.C., 2001. Chemical Evolution and Origin of Nickel Sulfide Mineralization in the Sudbury Igneous Complex, Ontario, Canada. Econ. Geol. 96, 1855–1875.

Lightfoot, P.C., 2016. Nickel Sulfide Ores and Impact Melts: Origin of the Sudbury Igneous Complex. Elsevier.

Lightfoot, P.C., Doherty, W., Farrell, K.P., Keays, R.R., Pedeski, D., 1997a. Geochemistry of the main mass, sublayer, offset dikes, and inclusions from the Sudbury Igneous Complex. Ontario Geol. Surv. Open File 5959, 231 pp.

Lightfoot, P.C., Farrow, C.E.G., 2002. Geology, geochemistry, and mineralogy of the Worthington offset dike: A genetic model for offset dike mineralization in the Sudbury Igneous Complex. Econ. Geol. 97, 1419–1446.

Lightfoot, P.C., Keays, R.R., Morrison, G.G., Bite, A., Farrell, K.P., 1997b. Geologic and geochemical relationships between the contact sublayer, inclusions, and the main mass of the sudbury igneous complex: A Case study of the whistle mine embayment. Econ. Geol. 92, 647–673.

Lightfoot, P.C., Keays, R.R., Morrison, G.G., Bite, A., Farrell, K.P., 1997c. Geochemical relationships in the Sudbury igneous complex; origin of the main mass and offset dikes. Econ. Geol. 92, 289–307.

Lightfoot, P.C., Naldrett, A.J., 1996. Petrology and geochemistry of the Nipissing Gabbro:

Exploration strategies for nickel, copper, and platinum group elements in a large igneous province. Ontario Geol. Surv. Study 58, 92 pp.

Lumbers, S.B., 1975. Geology of the Burwash Area. Districts of Nipissing, Parry Sound, and Sudbury; Ontario Div. Mines, Geol. Rep. 116, 160.

Maghloughlin, J.F., Spray, J.G., 1992. Frictional melting process and products in geological materials: introduction and discussion. Tectonophysics 115, 197–206.

Masaitis, V.L., 1999. Impact structures of northeastern Eurasia; The territories of Russia and adjacent countries. Meteorit. Planet. Sci. 34, 691–711.

McCormick, K.A., 2002. A textural, mineralogical, and statistical study of the footwall breccia within the Strathcona embayment of the Sudbury structure. Econ. Geol. 97, 125–143.

Meldrum, A., Abdel-Rahman, A.F.M., Martin, R.F., Wodicka, N., 1997. The nature, age and petrogenesis of the Cartier Batholith, northern flank of the Sudbury Structure, Ontario, Canada. Precambrian Res. 82, 265–285.

Milkereit, B., Green, A., 1992. Deep geometry of the Sudbury structure from seismic reflection profiling. Geology 20, 807–8011.

Morgan, J.W., Walker, R.J., Horan, M.F., Beary, E.S., Naldrett, A.J., 2002. 190Pt – 186Os and 187Re – 187Os systematics of the Sudbury Igneous Complex, Ontario. Geochim. Cosmochim. Acta 66, 273–290.

Morris, W.A., Pay, R., 1981. Genesis of the Foy (?) offset and its sulfide ores; the paleomagnetic evidence from a study in Hess Township, Sudbury, Ontario. Econ. Geol. 76, 1895–1905.

Morrison, G.G., 1984. Morphological features of the Sudbury Structure in relation to an impact origin, in: Pye, E.G., Naldrett, A.J., Giblin, P.E. (Eds.), The Geology and Ore Deposits of the Sudbury Structure. pp. 513–522.

Morrison, G.G., Jago, B.C., White, T.L., 1994. Footwall mineralization of the Sudbury Igneous Complex, in: Lightfoot, P.C., Naldrett, A.J. (Eds.), Proceedings of the Sudbury-Noril'sk Symposium. Ontario Geological Survey Special Volume 5, pp. 57–64.

Müller-Mohr, V., 1992. Breccias in the basement of a deeply eroded impact structure, Sudbury, Canada. Tectonophysics 216, 219–226.

Mungall, J.E., Ames, D.E., Hanley, J.J., 2004. Geochemical evidence from the Sudbury Structure for crustal redistribution by large bolide impacts. Nature 429, 546–548.

Murphy, A.J., Spray, J.G., 2002. Geology, mineralization and emplacement of the Whistle–Parkin offset dike, Sudbury impact structure. Econ. Geol. 97, 1369–1389.

Naldrett, A.J., 1984a. Ni–Cu ores of the Sudbury Igneous Complex –Introduction, in: Pye, E.G., Naldrett, A.J., Giblin, P.E. (Eds.), The Geology and Ore Deposits of the Sudbury Structure. pp. 302–307.

Naldrett, A.J., 1984b. Mineralogy and composition of the Sudbury ores, in: Pye, E.G., Naldrett, A.J., Giblin, P.E. (Eds.), The Geology and Ore Deposits of the Sudbury Structure. pp. 309–325.

Naldrett, A.J., 2004. Magmatic Sulfide Deposits: Geology, Geochemistry and Exploration. Springer Verlag, Heidelberg, Berlin.

Naldrett, A.J., Hewins, R.H., 1984. The Main Mass of the Sudbury Igneous Complex, in: Pye, E.G., Naldrett, A.J., Giblin, P.E. (Eds.), The Geology and Ore Deposits of the Sudbury Structure. pp. 235–252.

Naldrett, A.J., Hoffman, E.L., Green, A.H., Chou, C., Naldrett, S.R., 1979. The composition of Ni-Sulfide ores, with particular reference to their content of PGE and Au. Can. Mineral. 17, 403–415.

Naldrett, A.J., Lightfoot, P.C., 1993. Ni-Cu-PGE ores of the Noril'sk region Siberia: A

model for giant magmatic ore deposits associated with flood basalt. Soc. Econ. Geol. Spec. Publ. 2, 81–123.

Noble, S.R., Lightfoot, P.C., 1992. U–Pb baddeleyite ages for the Kerns and Triangle Mountain intrusions, Nipissing diabase, Ontario. Can. J. Earth Sci. 29, 1124–1129.

O'Connor, J.P., Spray, J.G., 1997. Geological setting of the Manchester offset dike within the South Range of the Sudbury impact structure, in: Conference on Large Meteorite Impacts and Planetary Evolution (Sudbury 1997). p. 38.

Ostermann, M., Schärer, U., Deutsch, A., 1996. Impact melt dikes in the Sudbury multi-ring basin (Canada): Implications from uranium-lead geochronology on the Foy Offset Dike. Meteorit. Planet. Sci. 31, 494–501.

Pattison, E.F., 1979. The Sudbury Sublayer. Can. Mineral. 17, 257–274.

Percival, J.A. and Western Superior NATMAP working group, 2004. Orogenic framework for the Superior Province: Dissection of the "Kenoran Orogeny," in: The Lithoprobe Celebratory Conference: From Parameters to Processes - Revealing the Evolution of a Continent. Toronto, Canada.

Peredery, W. V., 1972a. Chemistry of fluidal glasses and melt bodies in the Onaping Formation, in: Guy-Bray, J. V. (Ed.), New Developments in Sudbury Geology. Geological Association of Canada.

Peredery, W. V., 1972b. The Origin of Rocks at the Base of the Onaping Formation, Sudbury, Ontario. University of Toronto, Toronto, Ontario, Canada.

Peredery, W. V., Morrison, R.S., 1984. Discussion of the origin of the Sudbury structure, in: Pye, E.G., Naldrett, A.J., Giblin, P.E. (Eds.), The Geology and Ore Deposits of the Sudbury Structure.

Prevec, S.A., 2000. An examination of modal variation mechanisms in the contact sublayer of the Sudbury Igneous Complex, Canada. Mineral. Petrol. 68, 141–157.

Prevec, S.A., Cawthorn, R.G., 2002. Thermal evolution and interaction between impact melt sheet and footwall: A genetic model for the contact sublayer of the Sudbury Igneous Complex, Canada. J. Geophys. Res. 107, 1–14.

Reimold, W.U., Colliston, W.P., 1994. Pseudotachylites of the Vredefort Dome and the surrounding Witwatersrand Basin, South Africa, in: Dressler, B.O., Grieve, R.A.F., Sharpton, V.L. (Eds.), Large Meteorite Impacts and Planetary Evolution I, GSA Special Paper 293. pp. 177–196.

Reimold, W.U., Gibson, R.L., 2005. "Pseudotachylites" in large impact structures, in: Koeberl, C., Henkel, H. (Eds.), Impact Tectonics. Springer, Berlin, pp. 1 – 51.

Riller, U., 2005. Structural characteristics of the Sudbury impact structure, Canada: Impact-induced versus orogenic deformation-A review. Meteorit. Planet. Sci. 40, 1723–1740.

Riller, U., Lieger, D., Gibson, R.L., Grieve, R.A.F., Stöffler, D., 2010. Origin of large-volume pseudotachylite in terrestrial impact structures. Geology 38, 619–622.

Riller, U., Schwerdtner, W.M., 1997. Mid-crustal deformation at the southern flank of the Sudbury Basin, central Ontario, Canada. Geol. Soc. Am. Bull. 109, 841–854.

Rousell, D.H., Brown, G.H. (Eds.), 2009. A Field Guide to the Geology of Sudbury, Ontario. Ontario Geol. Surv. Open File 6243, 200 pp.

Rousell, D.H., Fedorowich, J.S., Dressler, B.O., 2003. Sudbury Breccia (Canada): a product of the 1850 Ma Sudbury Event and host to footwall Cu–Ni–PGE deposits. Earth-Science Rev. 60, 147–174.

Scott, R.G., Benn, K., 2002. Emplacement of Sulfide Deposits in the Copper Cliff Offset Dike during Collapse of the Sudbury Crater Rim: Evidence from Magnetic Fabric Studies. Econ. Geol. 97, 1447–1458.

Scott, R.G., Spray, J.G., 1999. Magnetic fabric constraints on friction melt flow regimes

and ore emplacement direction within the South Range Breccia Belt, Sudbury Impact Structure. Tectonophysics 307, 163–189.

Scott, R.G., Spray, J.G., 2000. The South Range Breccia Belt of the Sudbury Impact Structure : Meteorit. Planet. Sci. 505–520.

Shand, S.J., 1916. The pseudotachylyte of Parijs (Orange Free State), and its relation to "trap- schotten gneiss" and "flinty crush-rock." Q. J. Geol. Soc. London 72, 198–221.

Shanks, W.S., Schwerdtner, W.M., 1990. Structural analysis of the central and southwestern Sudbury Structure, Southern Province, Canadian Shield. Can. J. Earth Sci. 28, 411–430.

Shanks, W.S., Schwerdtner, W.M., 1991. Crude quantitative estimates of the original northwest-southeast dimension of the Sudbury Structure, south-central Canadian Shield. Can. J. Earth Sci. 28, 1677–1686.

Spray, J.G., 1992. A physical basis for the frictional melting of some rock-forming minerals. Tectonophysics 204, 205–221.

Spray, J.G., 1997. Superfaults. Geology 25, 579–582.

Spray, J.G., Thompson, L.M., 1995. Friction melt distribution in a multi-ring impact basin. Nature 373, 130–132.

Stevenson, J.S., 1960. Origin of quartzite at the base of the Whitewater series, Sudbury basin, Ontario. Internat. Geol. Congr. 21st Sess. Nord. 32–41.

Stevenson, J.S., 1963. The upper contact phase of the Sudbury micropegmatite. Can. Mineral. 7, 413–419.

Stevenson, J.S., 1990. The volcanic origin of the Onaping Formation, Sudbury, Canada. Tectonophysics 171, 249–257.

Stöffler, D., 1977. Research drilling, Nördlingen 1973: polymict breccias, crater basement

and cratering model of the Ries impact structure. Geol. Bavarica 75, 443–458.

Stöffler, D., Avermann, M., Bischoff, L., Brockmeyer, P., Deutsch, A., Dressler, B.O., Lakomy, R., Müller-Mohr, V., 1989. Sudbury, Canada: Remnant of the only multi-ring (?) impact basin on Earth. Meteoritics 24, 328.

Stöffler, D., Deutsch, A., Avermann, M., Bischoff, L., Brockmeyer, P., Buhl, D., Lakomy, R., Müller-Mohr, V., 1992. The formation of the Sudbury structure, Canada, Toward a unified impact model. Geol. Soc. Am. Spec. Pap. 293, 303–318.

Therriault, A.M., Fowler, A.D., Grieve, R.A.F., 2002. The Sudbury Igneous Complex: A differentiated impact melt sheet. Econ. Geol. 97, 1521–1540.

Thompson, L.M., Spray, J.G., 1996. Pseudotachylyte petrogenesis: constraints from the Sudbury impact structure. Contrib. to Mineral. Petrol. 125, 359–374.

Thomson, J.E., 1957. Geology of the Sudbury Basin. Ontario Dep. Mines Annu. Rep. 65, 1–56.

Thomson, M.L., Barnett, R.L., Fleet, M.E., Kerrich, R., 1985. Metamorphic assemblages in the South-Range norite and footwall mafic rocks near the Kirkwood Mine, Sudbury, Ontario. Can. Mineral. 23, 173–186.

Tuchscherer, M.G., Spray, J.G., 2002. Geology, mineralization, and emplacement of the Foy Offset Dike, Sudbury impact structure. Econ. Geol. 97, 1377–1397.

Van Schmus, W.R., 1965. Early and middle Proterozoic history of the Great Lakes area, North America. R. Soc. London Philos. Trans. 280, 606–628.

Van Schmus, W.R., 1976. Early and middle Proterozoic history of the Great Lakes area, North America. R. Soc. London Philos. Trans. 280, 606–628.

Walker, R.J., Morgan, J.W., Naldrett, A.J., 1991. Re-Os isotope systematics of Ni-Cu sulfide ores, Sudbury Igneous Complex, Ontario: evidence for a major crustal component. Earth Planet. Sci. Lett. 105, 416–429.

Warner, S., Martin, R.F., Abdel-Rahman, A.F.M., Doig, R., 1998. Apatite as a monitor of fractionation, degassing, and metamorphism in the Sudbury igneous complex, Ontario. Can. Mineral. 36, 981–999.

Wichman, R.W., Schultz, P.H., 1993. Floor-fractured crater models of the Sudbury Structure, Canada: implications for initial crater size and crater modification. Meteoritics 28, 222–231.

Williams, H., 1957. Glowing Avalanche Deposits of the Sudbury Basin. Ontario Dep. Mines Annu. Rep. 65, 57–89.

Winzer, S.R., Lum, R.K.L., Schuhmann, S., 1976. Rb-Sr and Strontium Isotopic Composition, K/Ar Age and Large Ion Lithophile Trace Element Abun dance in Rocks and Glasses from the Wanapitei Lake Impact Structure. Geochim. Cosmochim. Acta 44, 51–57.

Wodicka, N., Card, K.D., 1995. Late Archean history of the Levack Gneiss Complex, southern Superior Province, Sudbury, Ontario, new evidence from U -Pb geochronology, in: Precambrian`95. p. 1991.

Wood, C.R., Spray, J.G., 1998. Origin and emplacement of Offset Dykes in the Sudbury impact structure: Constraints from Hess. Meteorit. Planet. Sci. 33, 337–347.

Wu, J., Milkereit, B., Boerner, D.E., 1994. Timing constraints on deformation history of the Sudbury Impact Structure. Can. J. Earth Sci. 31, 1654–1660.

Young, G.M., Long, D.G.F., Fedo, C.M., Nesbitt, H.W., 2001. Paleoproterozoic Huronian basin: product of a Wilson cycle punctuated by glaciations and a meteorite impact. Sediment. Geol. 141-142, 233–254.

Zieg, M.J., Marsh, B.D., 2005. The Sudbury Igneous Complex: Viscous emulsion differentiation of a superheated impact melt sheet. Geol. Soc. Am. Bull. 117, 1427–1450.

Zurbrigg, H.F., 1957. The Frood-Stobie Mine. Struct. Geol. Can. ore Depos. Vol. 2 341–350.

2 The Basal Onaping Intrusion in the North Range: Roof rocks of the Sudbury Igneous Complex[1]

Denise Anders, Gordon R. Osinski, Richard A. F. Grieve, and Derek T. M. Brillinger

2.1 Introduction

The Sudbury impact structure, Ontario, Canada (Fig. 2.1a), was formed at ~1.85 Ga (Krogh et al. 1984) and, with an estimated original diameter on the order of ~200 km (Grieve et al. 2010), ranks among the largest impact structures on Earth. As a result of post-impact tectonic deformation (Riller and Schwerdtner 1997; Riller et al. 1999; Riller 2005), the most evident feature of the structure – namely the outcrop pattern of the Sudbury Igneous Complex (SIC) – exhibits an elliptical shape (Deutsch and Grieve 1994) and can be divided into North, South and East Ranges. At the present exposure, the target rocks are composed of Huronian meta-volcanics and meta-sedimentary rocks in the south and east and Archean gneisses, granites, meta-volcanic and meta-sedimentary rocks in the north and west (Dressler 1984a). The SIC is what remains of the coherent impact melt sheet at the Sudbury impact structure (Faggart et al. 1985; Grieve et al. 1991; Dickin et al. 1992, 1996; Deutsch 1994; Johns and Dressler 1995; Lightfoot et al. 1997a, 1997b) and comprises from bottom to top: the so-called Contact Sublayer, Norite, Quartz Gabbro, and Granophyre (Dressler et al. 1992; Therriault et al. 2002) (Fig. 2.1b). Grieve (1994) estimated an original volume of 8,000 to 14,000 km3 for the now 27 x 60 km impact melt sheet and it is distinguished from other terrestrial impact melt sheets by its thickness and large-scale differentiation. The SIC is overlain by rocks of the ~3 km thick Whitewater Group composed of the breccias of the Onaping Formation and post-impact sedimentary rocks of the Vermilion, Onwatin and Chelmsford Formations (Coleman 1905; Rousell 1984) (Fig. 2.1b).

---

[1] This chapter was published in Meteoritics and Planetary Science in 2015. Anders, D., Osinski, G.R., Grieve, R.A.F. (2015) Meteoritics & Planetary Science 50, Nr 9, 1577–1594.

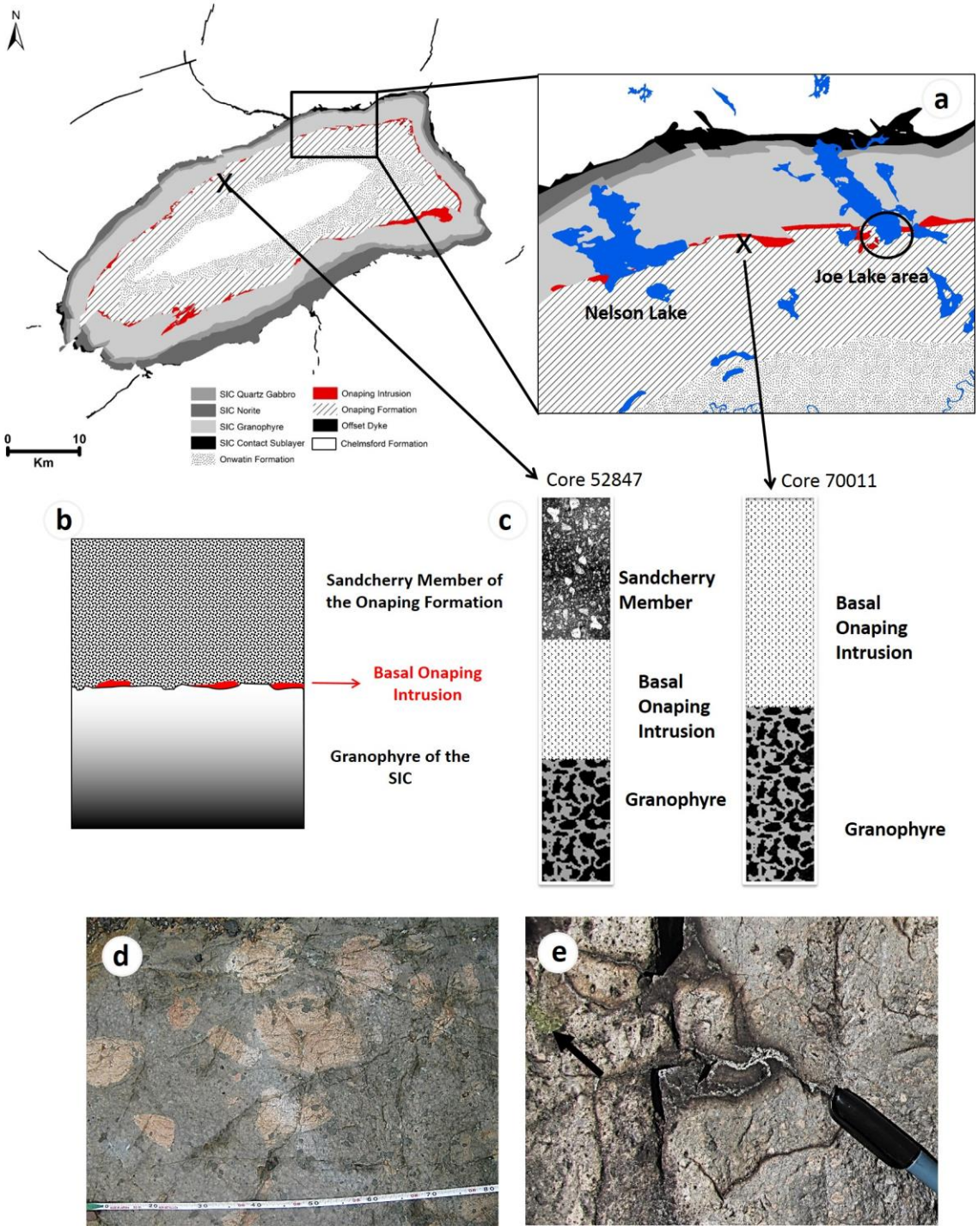

Figure 2.1. a) Simplified map (modified from Ames and Gibson (2004) of the elliptically-shaped SIC and the units of the Onaping Formation (left) and a close up of the Joe Lake area (right). The locations of both cores are marked by a black X and the Joe Lake area. b) Schematic cross section of the Granophyre of the SIC and the overlying Sandcherry Member of the Onaping Formation. Marked in red is the Basal Onaping Intrusion. c) Schematic illustration of the lithologies of core 70011 and

52847. d) Field photograph of the Basal Onaping Intrusion at Joe Lake showing reddish granitic clasts in a grey matrix. Measuring tape is in cm. e) Field photograph of the weathered and fissured surface of the Basal Onaping Intrusion at Joe Lake. The arrow points to an aggregate of secondary epidote as a result of alteration at the rim of a granitic clast.

One of the unusual and generally overlooked aspects of the SIC is that it is apparently missing roof rocks that are characteristic at the top of coherent impact melt sheets at other impact structures (Grieve et al. 2010). Such roof rocks have an igneous texture and are finer-grained than the main mass of the underlying coherent melt sheet and exhibit increasing grain size with increasing depth and contain target rock clasts, which decrease in amount and size with increasing depth (Grieve et al. 2010). They originate from the same melt pool as the melt sheet and, thus, could represent the initial bulk composition of the melt sheet. Their formation is the consequence of the relatively rapid cooling of the upper parts of the melt sheet, as a result of heat transfer between the upper portion of the melt and the surrounding environment, and cooling due to thermal equilibrium between a relatively higher percentage of incorporated cold lithic clasts and the melt (Onorato et al. 1978). The heat gradient within the cooling roof rocks leads to the increasing grain size and decreasing clast size and clast amount with increasing depth. The apparent lack of roof rocks to the SIC provided motivation for this study and led to a focus on the units immediately overlying the SIC.

The Onaping Formation, the lowest unit of the Whitewater Group (Fig. 2.1b), appears as an elliptical ring with a width of 2.4 to 4.8 km and a thickness of 1.4 km to 1.6 km (Ames et al. 1998, 2002; Grieve et al. 2010), and is composed of a complex series of breccias (Ames et al. 2002). Based on a revision of the nomenclature by Ames et al. (2002), the Onaping Formation has been divided into three units; namely, the Garson, Sandcherry and Dowling Members. The Garson Member is only present in a small region stratigraphically above the southeast lobe of the SIC. Enigmatic igneous textured bodies (Stevenson 1963; Brockmeyer and Deutsch 1989; Stöffler et al. 1989; Ames et al. 1998; Ames 1999; Grieve et al. 2010), the so called “Basal Onaping Intrusion”, form up to 300 m thick discontinuous,

semi-conformable sheets at the contact between the SIC and the Sandcherry Member of the overlying Onaping Formation (Muir and Peredery 1984; Ames et al. 1998; Ames 1999; Grieve et al. 2010) (Fig. 2.1b). The Basal Onaping Intrusion occupies approximately 50% of this contact zone (Grieve et al. 2010). Where the Basal Onaping Intrusion is absent, the Granophyre of the SIC is in direct and sharp contact with the Sandcherry Member (Muir and Peredery 1984).

First documented by Bell (1893), the Basal Onaping Intrusion was initially interpreted as a quartzite conglomerate. The enigmatic nature of the Basal Onaping Intrusion is mirrored by the various names and interpretations given to this unit over time (Table 2.1).

Table 2.1. Overview of the various nomenclature of the Basal Onaping Intrusion.

Name	Authors
Basal Onaping Intrusion	Ames et al. 2005, 2008; Grieve et al. 2010
Basal Intrusion	Ames et al. 1998; Ames and Gibson 2004
Basal Intrusion (= Basal Member + Melt bodies)	Gibbins 1994
Basal Member	Muir 1981, 1983; Muir and Peredery 1984
Basal Breccia	Peredery 1972a, 1972b
Tectonic Quartzite Breccia	Stevenson 1961, 1963, 1972
Rhyolite Breccia, Rhyolite	Thomson 1957; Williams 1957
Rhyolite, Agglomerate	Burrows and Rickaby 1930
Trout Lake Conglomerate	Coleman 1905
Quartzite Conglomerate	Bell 1893

Although the Basal Onaping Intrusion has generally been classified as breccia (Stevenson 1963; Peredery and Naldrett 1975; Brockmeyer and Deutsch 1989; Dressler et al. 1992) and considered part of the Onaping Formation (Peredery and Naldrett 1975; Muir and Peredery 1984; Ames et al. 1998; Ames 1999), some workers also noticed similarities between the Basal Onaping Intrusion and the Granophyre (Stevenson 1963; Brockmeyer and Deutsch 1989; Deutsch et al. 1995) or suggested the Basal Onaping Intrusion to be part of the SIC (Brockmeyer and Deutsch 1989; Stöffler et al. 1989; Deutsch et al. 1990, 1995; Grieve et al. 2010). Brockmeyer and Deutsch (1989) first suggested the Basal Onaping

Intrusion might be an early phase of the SIC, which has been quenched by assimilation of clasts. Here, we present the results of a field and drill core study of the Basal Onaping Intrusion along a strike length of ~30 km in the eastern North Range of the SIC (Fig. 2.1) and details of the contact relations between the Granophyre of the SIC, the Basal Onaping Intrusion and the Sandcherry Member of the Onaping Formation.

2.2 Samples and Techniques

This study focuses on two drill cores, provided by Vale, and field samples collected in the Joe Lake area of Wisner Township (Fig. 2.1a). A total of 65 samples were taken from the field, from which 35 thin sections were made. Core 70011 was drilled in 1981 in the North Range (Fig. 2.1a) of the SIC (Northing 495439.00, Easting 5174637.62). Core 52847 (Fig. 2.1a) was drilled in 1978 also in the North Range (Northing 485139.76, Easting 5169948.90). Twenty-two samples of core 52847 and 28 samples of 70011 from various depths were selected for polished thin sections, which were examined by optical microscopy. Thin sections of six samples of core 70011 were chosen to carry out point counting in order to determine modal analyses. Approximately 1,850 to 2,250 points were counted and examined for mineralogical identification, grain size and grain shape. For the field samples, modal percentages were determined by estimation and grain size was analyzed by measurements of minimum 15 clasts or grains within all of 13 thin sections. For each field sample, the distance on the surface from the Granophyre contact was measured and taken as an indicator of general stratigraphic position. The vertical distances from the Granophyre have been calculated by using a dip in the Joe Lake area of 35° (Riller 2005). Ten thin sections of the 70011 core and five thin sections of the field samples were studied using backscattered electron (BSE) imagery on a Hitachi SU6600 FEG Scanning Electron Microscope (SEM), in order to characterize microstructures and textures (ZAPLab, University of Western Ontario), along with EDS semi-quantitative analyses. Quantitative analyses of feldspars from 8 thin sections of core 70011 were carried out using a JXA JEOL-8900L Electron Microprobe (McGill University). X-Ray Fluorescence (XRF) whole rock analyses was conducted to determine the major and trace element abundances of 9 samples of core 70011 and 19 field samples (University of Western Ontario). All

samples were carefully chosen to avoid clasts. Based on the presence of quartz clasts, thirty-two thin sections of the field samples were selected and examined for planar deformation features (PDFs). Measurements of the crystallographic orientations of the quartz grain c-axis and the orientation of PDFs in six of the selected thin sections were carried out using an X–Y universal stage microscope (University of Western Ontario).

2.3 Observations

2.3.1 Field Work

Pod-like outcrops of the Basal Onaping Intrusion, Sandcherry Member of the Onaping Formation, and Granophyre, can be found in the area at Joe Lake (Fig. 2.1). Exact field relationships and contacts are difficult to deduce in the field because of the typically smooth, glaciated, and heavily weathered nature of the outcrops. Detailed sampling of the Basal Onaping Intrusion and the Granophyre was performed to obtain an accurate representation of both units and to conduct comparative analyses. The rocks of the Basal Onaping Intrusion around Joe Lake are composed of a grey to black fine-grained groundmass that contains various clasts. The dominating clast population are rounded to sub-rounded pink-reddish granite clasts (Fig. 2.1d). The clasts are characterized by a sharp contact with the surrounding matrix and a size range from several mm up to 1 m. In places, the rocks are cut by veins of quartz, chlorite and epidote (Fig. 2.1e).

2.3.2 Petrology

The core 70011 is composed of Basal Onaping Intrusion at depths of 15 m to 91 m, followed by Granophyre of the SIC (Fig. 2.1c), while core 52847 consists of Sandcherry Member until approximately 314 m, underlain by 21 m of Basal Onaping Intrusion and Granophyre beginning at 335 m (Fig. 2.1c). The Basal Onaping Intrusion can be described as a dark aphanitic assemblage that contains clasts of variable size, shape, and composition. Veins filled with an assemblage of chlorite, epidote and hornblende are present in some thin sections.

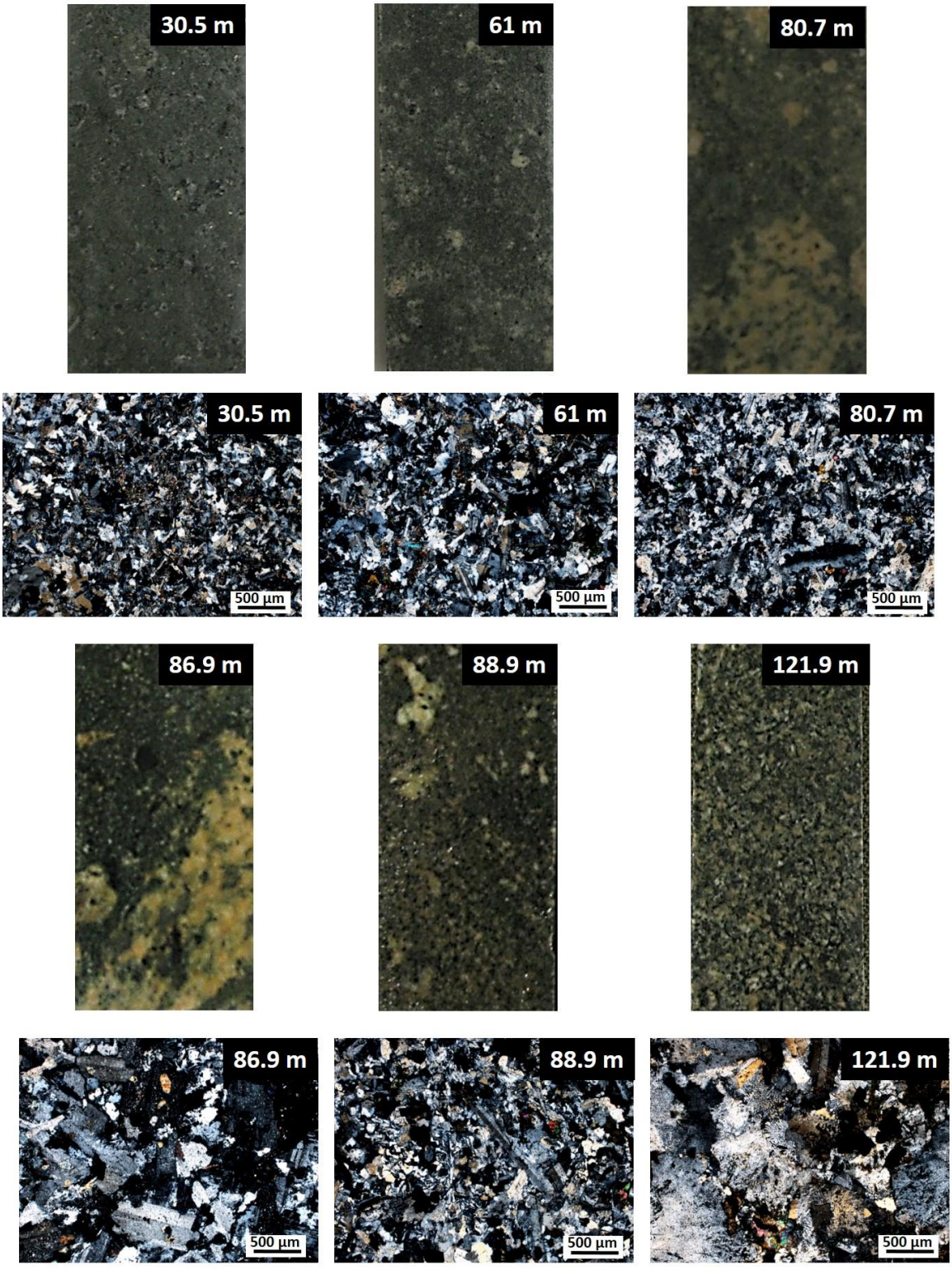

Figure 2.2. Scanned polished core sections and optical photomicrographs of samples of core 70011 (core width is 3.5 cm) arranged in order of increasing depth (number

in top right gives depth of sample in metres). Corresponding microscopic pictures show an increase.

2.3.2.1 Groundmass

The groundmass of the Basal Onaping Intrusion of core 70011 is characterized by an interlocking intergrowth of feldspar and quartz (Fig. 2.2). With increasing depth, the groundmass gets brighter and reddish-pink, reflecting an increasing amount of alkali feldspar. Feldspar is the most abundant mineral (Table 2.2) and typically occurs as alkali feldspar with tartan twinning (microcline), euhedral orthoclase with simple twinning and isolated, small plagioclase showing multiple twinning.

Quartz occurs as euhedral crystals with typical undulose extinction and locally contains inclusions. The groundmass also contains mafic minerals; in particular, amphibole and pyroxene, which occur as small laths distributed within the groundmass and are often decomposed at the edges and replaced by chlorite and epidote. Additional chlorite can appear in the form of small needles and laths distributed within the matrix; however, sometimes they also can be arranged in clustered aggregates. Epidote, another major mineral (Table 2.2), forms small crystals, at greater depths larger grains and aggregates, within the igneous groundmass and is sometimes accompanied by opaque minerals, such as magnetite, pyrite, ilmenite, titanite, and apatite, which are common minor phases. Additional minor phases, which have not been detected within the field samples, are calcite and some phosphates. Biotite is a very rare mineral in the core samples (Table 2.2) but comprises ~5–10% of the field samples, which might be associated to increased alteration of the field samples.

The field samples, which are further from the Granophyre contact than the core samples, show a similar mineralogy. They are, however, characterized by a higher amount of plagioclase (15–30%), amphibole (10–20%), but only 5 to 15% of alkali feldspar. Two types of textures dominate in these samples. The most evident texture is an interlocking intergrowth of plagioclase and quartz, the second, less evident, involves the skeletal-shaped

intergrowth of alkali feldspar and quartz. Indeed, point counting confirms this qualitative observation in particular for feldspar and quartz (Table 2.2; Fig. 2.3).

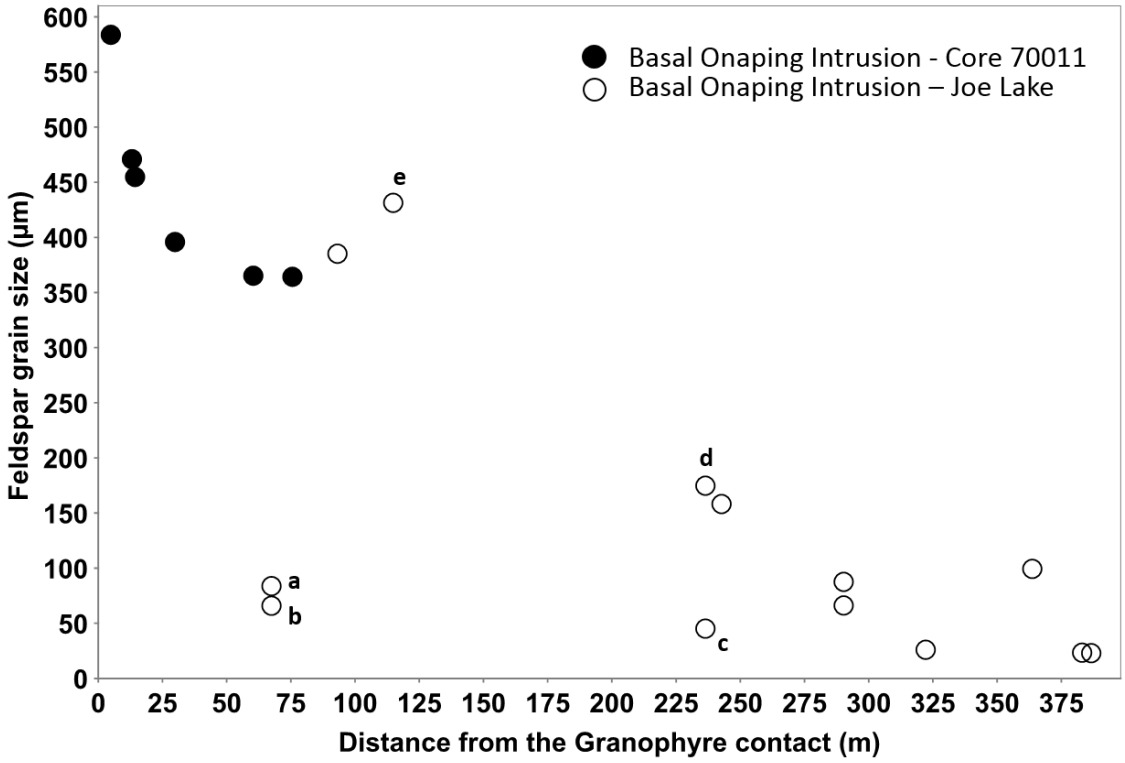

Figure 2.3. Grain size plotted versus distance from the Granophyre contact. The grain size of feldspar in the Basal Onaping Intrusion of core 70011 (filled circles) and from Joe Lake (open circles) tends to increase as the Granophyre contact is approached. Similar trends are observed for the amphiboles within the Basal Onaping Intrusion at Joe Lake and quartz in the Basal Onaping Intrusion of the core samples. Data points labelled a, b and c correspond to outliers with high amounts of clasts, while outlier can be explained by an anomalously low number of clasts. Data point d is not an outlier in grain size; however, it shows a small amount of clasts in Figure 2.4.

A similar relation is seen in the field samples from Joe Lake, where the grain size can be correlated to the distance from the Granophyre contact, as demonstrated for feldspar (Fig. 2.3). In general, the core samples of 70011 show larger mineral grains ranging from 350 to 550 µm for feldspar, while in the field samples the grain size of feldspar varies from 25 to 425 µm (Fig. 2.3).

Table 2.2. Modal Percentages of 6 thin sections of core 70011 determined by point counting.

Sample		50-3	100-3	200-3	241-2	255-2	282-2
Depth (m)		15.2	30.5	61.0	73.5	77.7	85.9
Points		2028	1911	2240	1945	1869	1867
Onaping Intrusion		100.0	100.0	100.0	100.0	100.0	98.1
Granophyre		n.d.	n.d.	n.d.	n.d.	n.d.	1.9
Groundmass		91.4	93.8	95.7	97.9	98.1	99.6
Clasts		8.6	6.3	4.3	2.1	1.9	0.4
Feldspar		31.3	32.5	32.9	38.6	38.9	45.3
	Alkali Feldspar (inclusive Albite)	24.7	27.8	26.1	34.2	35.7	36.6
	Plagioclase	6.6	4.7	6.8	4.4	3.2	8.7
Quartz		29.0	26.4	30.7	36.4	46.2	14.7
Chlorite		14.8	15.7	15.4	19.3	5.6	18.0
Biotite		0.3	n.d.	0.4	0.2	n.d.	0.2
Hornblende		4.1	7.0	4.3	n.d.	n.d.	n.d.
Epidote		7.9	8.1	8.2	1.5	4.1	17.5
Orthopyroxene		1.0	0.6	1.1	1.0	0.5	n.d.
Clinopyroxene		0.7	0.5	0.7	1.4	1.6	1.1
Opaque		2.1	3.1	2.1	1.5	1.1	2.3
Calcite		n.d.	n.d.	n.d.	0.3	0.1	0.4
Chlorite clast without rim		2.8	0.9	0.4	0.5	0.1	0.2
Mafic clast with felsic rim		1.0	1.1	0.7	n.d.	n.d.	n.d.
Qtz clast with mafic and felsic rim		n.d.	0.3	n.d.	n.d.	n.d.	n.d.
Felsic clast without rim		2.1	0.3	1.4	0.3	1.1	n.d.
Qtz clast, fine-grained without rim		n.d.	0.5	n.d.	n.d.	0.3	n.d.
Mafic clast without rim		1.0	0.9	0.4	n.d.	n.d.	n.d.
Qtz clast coarse-grained, without rim		1.7	2.0	1.4	0.3	0.3	0.3
Mafic clast with Qtz and mafic rim		n.d.	0.2	n.d.	n.d.	n.d.	n.d.
Qtz clast, fine and coarse-grained		n.d.	n.d.	n.d.	0.5	0.1	n.d.
Qtz clast, fine and coarse-grained with mafic rim		n.d.	n.d.	n.d.	0.5	n.d.	n.d.
		100.0	100.0	100.0	100.0	100.0	100.0

2.3.2.2 Clasts

As mentioned above, lithic clasts of different composition and size are encountered within the matrix (Fig. 2.4). Samples of the Basal Onaping Intrusion from Joe Lake demonstrate a range in clast content (5–50%) that is typically higher than in the samples of the core 70011, which are below 10%.

Mineral clasts of core 70011 are characterized by a rounded to sub-rounded shape, show a sharp contact, and usually display one or two reaction rims (Figs. 2.4a–d). The rims are composed of mafic minerals altered to chlorite and epidote (Fig. 2.4a) or felsic minerals (Figs. 2.4c and d). Similar observations have been reported by Muir and Peredery (1984), who described quartz inclusions surrounded by alkali feldspar. Clasts can be divided into several groups. Fine-grained quartz clasts are composed of recrystallized quartz grains smaller than 0.02 mm (Fig. 2.4d). Coarse-grained quartz clasts are equigranular and characterized by a small number (> 6) of large quartz crystals showing none or slight signs of recrystallization (Fig. 2.4a). The quartz minerals are sometimes characterized by a grainy, brownish surface appearance and contain numerous inclusions.

Mixed quartz clasts contain non-equigranular quartz, where grain sizes range from several 100 µm to tiny grains of 10 µm. Felsic clasts (Fig. 2.4b) are composed of fine-grained, recrystallized feldspar and quartz. Chlorite clasts occur usually as green particles, which either contain small needles or grain free aggregates and, sometimes, relicts of pyroxene and hornblende. Mafic clasts contain hornblende, pyroxene and also chlorite and epidote, and are, sometimes, surrounded by a rim of feldspar and quartz (Fig. 2.4c).

Clast phases of the Joe Lake samples vary in both size and composition and are similar to the clasts observed in core 70011. Within coarse-grained, non-equigranular quartz clasts, grain sizes range from 0.01–0.8 mm, while the grains within fine-grained quartz clasts are generally less than 0.02 mm. Felsic clasts include quartz, plagioclase laths, minor clinopyroxene and pyrite.

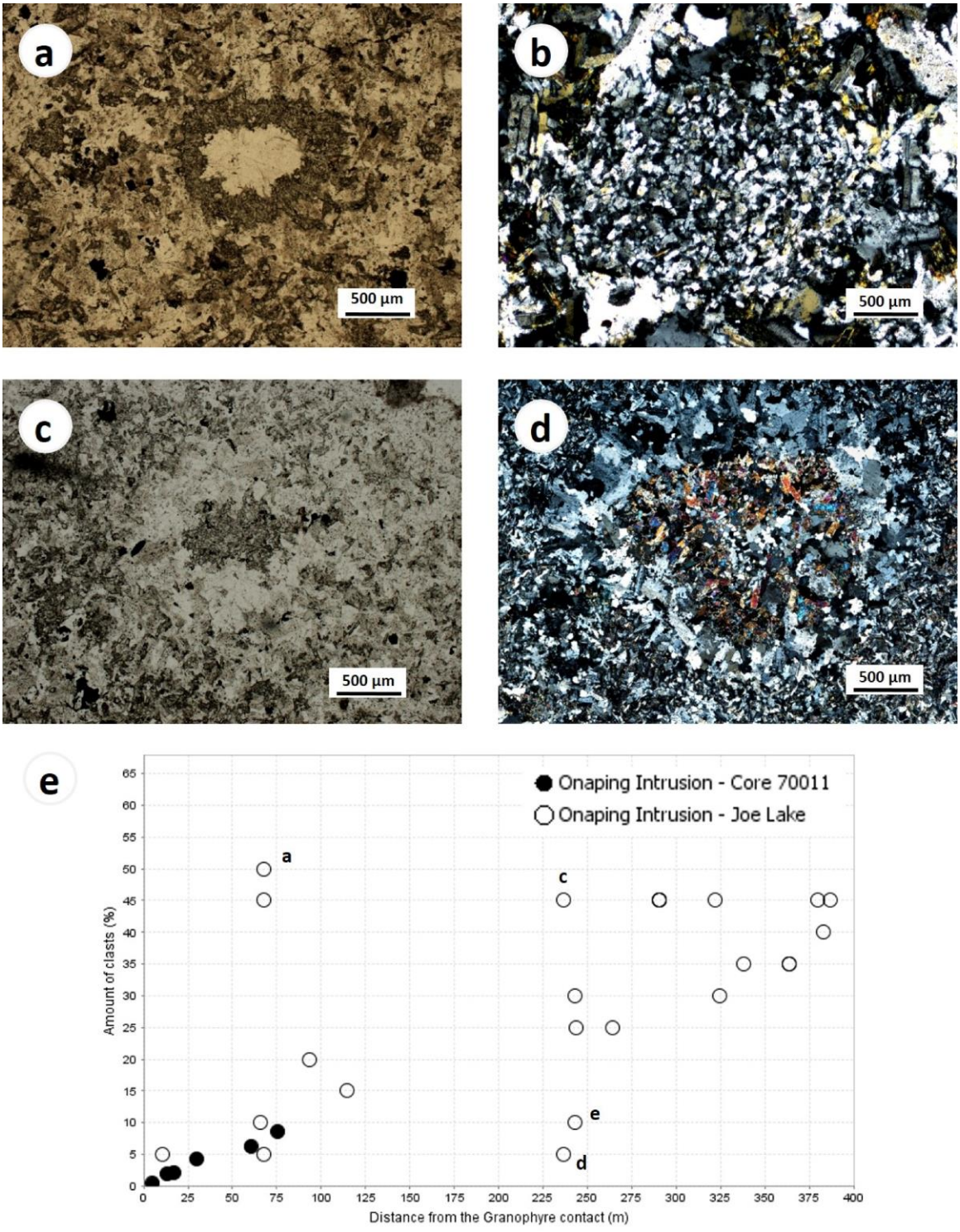

Figure 2.4. Photomicrographs of various clasts within the Basal Onaping Intrusion. a) Sample 50-1 (depth ~15 m): Coarse-grained quartz clast surrounded by a rim of mafic minerals (PPL). b) Sample 241-2 (depth ~73 m): Recrystallized felsic clast without rim (XPL). c) Sample 100-2 (depth ~30 m): Mafic clast with a felsic rim (PPL).

d) Sample 100-2 (depth ~30 m): Fine-grained recrystallized quartz clast surrounded by a mafic and a felsic rim (XPL). e) Modal percentages of clasts versus distance from the Granophyre contact of core 70011 (filled circles) and for the field samples (open circles). The amount of clasts increases with increasing distance from the Granophyre contact. Major outliers, marked with small letters, displaying high and low amounts of clasts also exhibit anomalies in grain size (Fig. 2.3). Outlier d shows a grain size that fit the pattern in Figure 2.3 and, thus, cannot be explained by a large grain size.

Clasts with an intermediate igneous composition contain quartz grains, hornblende, plagioclase laths, grains of clinopyroxene, chlorite grains and grains of epidote. Some clasts demonstrate reaction textures at boundaries with the matrix phase. The most evident reaction texture is observed at the boundary of clasts composed of non-equigranular quartz. In many cases, a distinct corona of amphibole and clinopyroxene occur between the clast and matrix phase. Both minerals are commonly altered to chlorite. Rarely, apatite is found associated with rimmed clast. A much less distinct reaction texture is seen with felsic igneous clasts, which demonstrate an irregular and sometimes undistinguishable boundary with the matrix. Point counting of 70011 core samples revealed a decrease in the number of clasts with increasing depth (Table 2.2; Fig. 2.4e). A similar trend is observed within the field samples, but generally with higher clast abundances (Fig. 2.4e).

2.3.2.3 Contact relationships between the Sandcherry Member, Basal Onaping Intrusion, and Granophyre

The contact between the Granophyre and Basal Onaping Intrusion is gradational over a distance of approximately 5 m, i.e., there is no sharp contact between the two lithological units. The first isolated patches of micrographic intergrowth of quartz and feldspar (i.e., granophyric texture) appear at a depth of 86 m within the groundmass of the Basal Onaping Intrusion, in core 70011 (Fig. 2.5). Over the next 5 m, the granophyric content increases gradationally until a depth of 91 m, where the lithology is classed as Granophyre (Fig. 2.5).

The contact between Basal Onaping Intrusion and Granophyre in core 52847 is similar to that in core 70011; i.e., the Basal Onaping Intrusion merges into the Granophyre; although the thickness of the Basal Onaping Intrusion is much less than in core 70011. The Basal

Onaping Intrusion in core 52847 spans over only a depth of approximately 21 m; starting at 314 m until 335 m, where it is logged as Granophyre; however, the first patches of micrographic intergrowth occur at 322 m. Core 52847 is similar to the Basal Onaping Intrusion of core 70011, exhibits an igneous texture, with interlocking intergrowth of feldspar and quartz; however, it is coarser-grained than in 70011 and contains less clasts (Fig. 2.6a).

In contrast to the Granophyre – Basal Onaping Intrusion contact, the contact area between Sandcherry Member and Basal Onaping Intrusion in core 52847 appears sharp. Although the actual contact between Basal Onaping Intrusion and overlying Sandcherry Member was not recognizable, it was possible to narrow its location to within <2 m in which no features of transition or merging were observed. Until depths of 244 m, the Sandcherry Member in core 52847 is characterized by ~80% angular equant shard clasts, without any reaction rims, within a brown, clastic fine-grained groundmass (Fig. 2.6b). With increasing depths, the clasts and shards decrease in size and finally disappear completely at 305 m (Fig. 2.6a), while the fine-grained clastic groundmass becomes increasingly coarse-grained and paler. The Granophyre in both cores (Figs. 2.5a, b and 2.6c) is characterized by characteristic vermicular-wormy, micrographic intergrowth of quartz and feldspar. The mineralogy of the Granophyre is generally similar to the Basal Onaping Intrusion. In addition to coarser-grained quartz and feldspar, which form the micrographic intergrowth, the Granophyre contains pyroxene and hornblende, which are altered to epidote and chlorite. The micrographic intergrowth starts from albite with simple twinning (Fig. 2.5b) and radiates outwards.

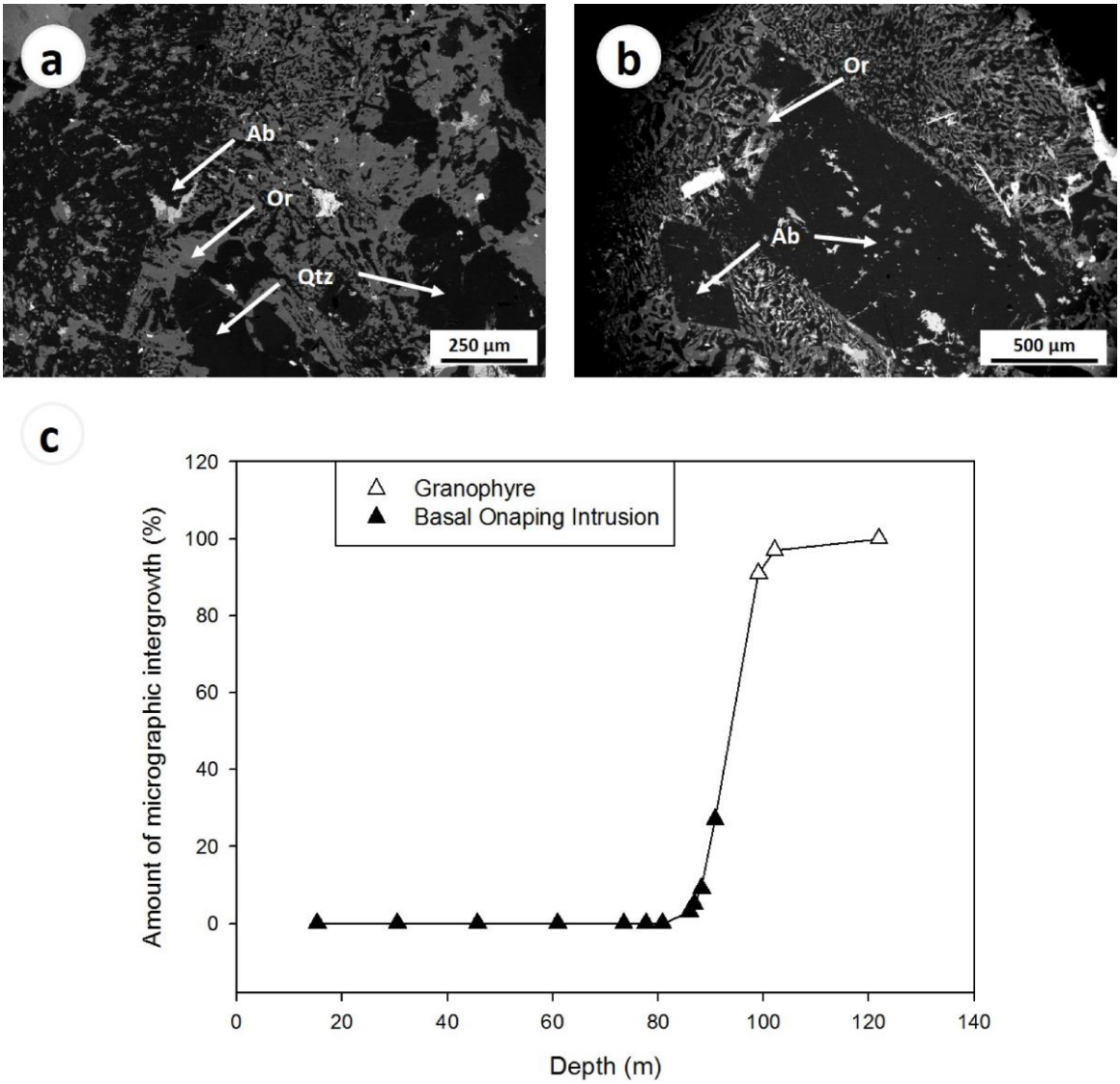

Figure 2.5. Backscattered electron (BSE) images of: a) first patches of micrographic intergrowth within the Basal Onaping Intrusion at 86 m and b) distinctive micrographic intergrowth in the Granophyre at a depth of 96 m of core 70011. Ab = Albite, Or = Orthoclase, Qtz = Quartz. c) Diagram showing the variation in the amount of micrographic/granophyric intergrowth within the Basal Onaping Intrusion of core 70011. The first micrographic intergrowth within the Basal Onaping Intrusion occurs at 86 m, increases with increasing depth and at 91 m the Basal Onaping Intrusion transitions into Granophyre.

2.3.2.4 Shock features

Shock features are present in the form of planar deformation features (PDFs) in quartz grains within specific samples of the Basal Onaping Formation in core 70011 and the field samples. Planar deformation features are single or multiple sets of parallel and narrow (spacing of 2–10 µm) lamellae, composed of amorphous silica glass (Stöffler and Langenhorst 1994), and provide diagnostic criteria for shock metamorphic events.

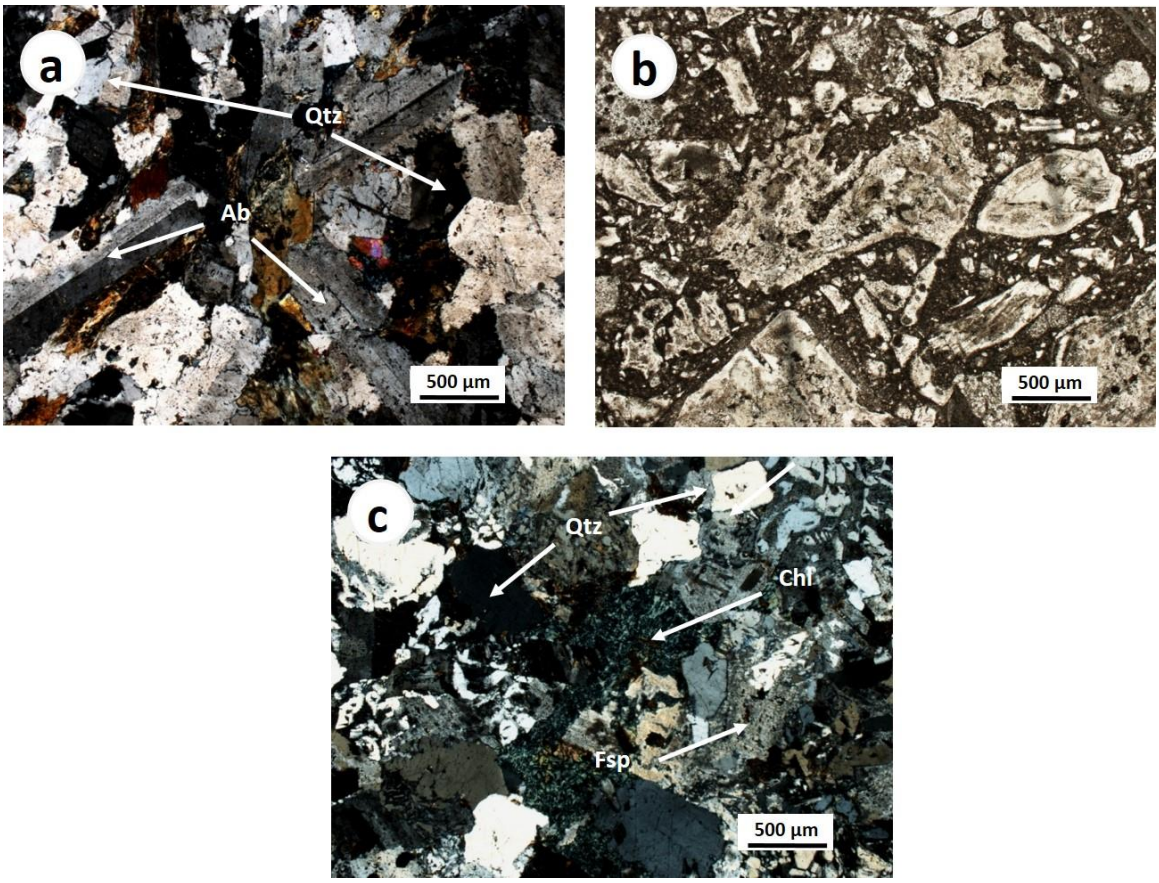

Figure 2.6. Microscopic pictures of core 52847 of: a) the coarse-grained igneous texture of the Basal Onaping Intrusion at ~320 m (XPL). b) Sandcherry Member at ~76 m, which is characterized by a dark brown clastic microcrystalline groundmass with vitric shards. c) Granophyre at a depth of ~335 m (XPL). Ab = Albite, Chl = Chlorite, Fsp = Feldspar, Qtz = Quartz

Planar deformation features in quartz within granitic lithic clasts in the Onaping Formation were first discovered by French (1968), who, thus, suggested an impact origin for this

lithology and, by extension, the Sudbury structure. We have documented PDFs in the deeper parts of the Basal Onaping Intrusion of core 70011 starting at 79.2 m, where they occur in quartz grains, mostly larger than 500 µm, of coarse-grained quartzite clasts.

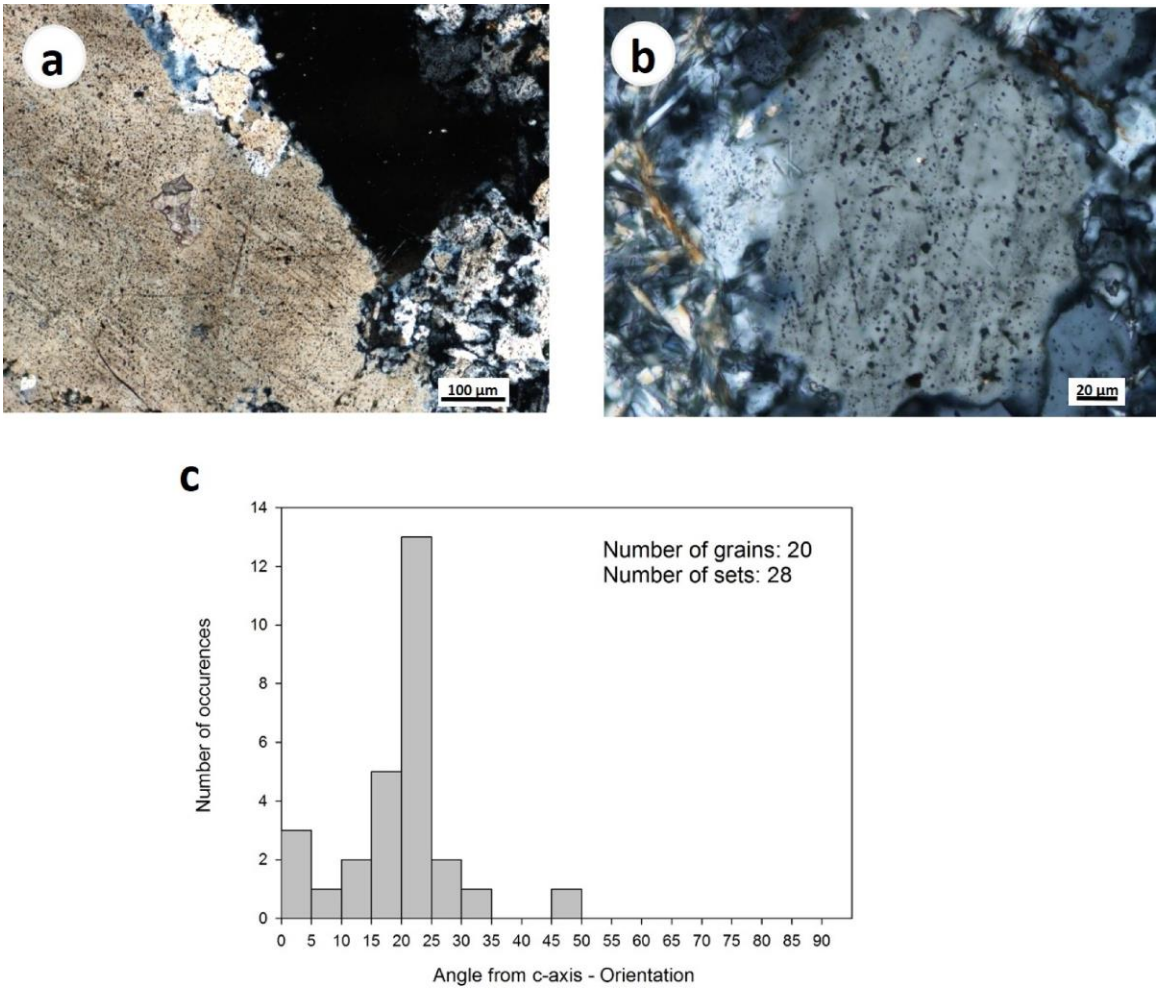

Figure 2.7. Microscopic pictures of a) two sets of decorated and annealed PDFs at ~79 m of the core 70011 (XPL) and b) 2 sets of decorated and heavily annealed PDFs in the field sample SBD-054. c) Histogram showing the number of PDF sets for a specific range of angles between the c-axis and the poles for the field samples.

No PDFs in quartz grains forming the igneous groundmass of the Basal Onaping Intrusion were detected. The PDFs in the field samples are weakly to moderate preserved, strongly decorated, and annealed (Figs. 2.7a and b). Planar deformation feature-containing grains

range in size 0.05–0.3 mm and are found both within larger clasts and within individual quartz clasts dispersed in the matrix. The orientation of twenty eight PDFs within 20 grains were measured using the universal stage microscope. The histograms show dominant angles between 21 and 25°, with ~13% of frequency (Fig. 2.7c); however, no grain contained more than three sets of PDFs and most grains typically only had one set and, thus, could not be uniquely indexed.

2.3.3 Geochemistry

Whole rock major element analyses (Table 2.3) demonstrate the relatively high SiO_2 content of the Basal Onaping Intrusion in the core 70011 (63.6 wt % to 70.4 wt %) and the field samples (60.6 to 71.0 wt % SiO_2). These values are slightly lower than the SiO_2 content of the Granophyre (70.8 wt % to 72.8 wt %) of core 70011 in this study. Electron microprobe analyses of feldspars (Fig. 2.8a) within the groundmass of the Basal Onaping Intrusion and the upper part of the Granophyre samples revealed only Ca-depleted plagioclase (An < 4 %) and orthoclase with Na < 6 %. No Ca-rich plagioclase was detected, which confirms the low modal percentages of plagioclase in the thin sections. Figures 2.8b–d show spider plots of selected trace elements for Granophyre, Quartz Gabbro, Norite, and Basal Onaping Intrusion normalized to the average Felsic Norite (Lightfoot et al. 1997a). Compared to the Felsic Norite, the Granophyre is, apart from Sr, enriched in incompatible and depleted in compatible elements. The Basal Onaping Intrusion shows a slight enrichment in the incompatible elements U, Nb, Zr, and Y, but a depletion in all other incompatible and compatible trace elements (Fig. 2.8b). The Quartz Gabbro and Basal Onaping Intrusion display similar concentrations in the majority of the trace elements and have comparable patterns, with respect to incompatible elements, but show differences in compatible elements (Fig. 2.8c). It is interesting to note that the trace element pattern of the Basal Onaping Intrusion shares more similarities with the Norite (Fig. 2.8c) than any other SIC unit. Aside from the small negative Sr anomaly, as well as the positive U and Co anomalies, both units show similar trace element patterns.

Table 2.3. Whole rock X-ray fluorescence analyses of core 70011 and Joe Lake field samples.

	Core 70011								Joe Lake field samples				
Sample Nr.	**50-3**	**100-3**	**200-3**	**241-3**	**265-6**	**298-2**	**335-1**	**400-1**	**SBD-001**	**SBD-002**	**SBD-003**	**SBD-005**	**SBD-011**
Latitude									**46.7259**	**46.7259**	**46.7259**	**46.72791**	**46.7279**
Longitude									**-81.00014**	**-81.00014**	**-81.00014**	**-81.009**	**-81.00933**
Depth in m	**15.2**	**30.5**	**61.0**	**73.5**	**80.8**	**90.8**	**102.1**	**121.9**					
Distance to Granophyre in m	**75.6**	**60.4**	**29.9**	**17.4**	**10.1**				**414.5**	**414.5**	**414.5**	**347.6**	**346.6**
Lithology	**Basal Onaping Intrusion**					**Granophyre**			**Basal Onaping Intrusion**				
SiO_2	65.3	63.6	67.5	66.0	70.4	72.8	70.9	70.5	62.8	62.2	66.6	69.5	65.6
TiO_2	0.5	0.5	0.5	0.5	0.4	0.6	0.8	0.7	0.5	0.5	0.5	0.4	0.6
Al_2O_3	12.2	12.5	12.9	13.0	13.8	12.1	12.2	12.1	11.4	11.5	12.8	12.0	12.9
Fe_2O_3	5.9	7.1	4.9	5.8	2.7	3.2	4.8	5.1	8.8	8.6	2.8	5.3	3.6
MnO	0.1	0.1	0.1	0.1	n.d.	0.1	0.1	0.1	0.2	0.2	0.1	0.1	0.1
MgO	4.4	5.0	3.8	4.1	2.2	1.1	0.7	0.8	4.9	5.1	3.4	2.9	4.6
CaO	3.8	3.6	2.2	2.1	2.1	1.1	2.6	2.1	3.6	3.6	5.2	2.0	2.4
K_2O	1.2	0.8	1.8	3.1	0.5	4.5	3.1	3.8	2.0	2.3	0.1	2.2	0.3
Na_2O	4.7	4.8	4.8	3.3	6.6	3.1	3.7	3.0	4.1	4.0	7.7	3.4	6.5
P_2O_5	0.1	0.1	0.1	0.1	0.1	0.1	0.2	0.1	0.1	0.1	n.d.	0.1	0.1
Cr_2O_3	0.2	n.d.	n.d.	0.1	0.2	n.d.	n.d.	n.d.	n.d.	n.d.	n.d.	n.d.	n.d.
LOI.	1.7	1.9	1.5	2.3	1.2	1.0	0.9	1.1	1.5	1.6	0.9	1.4	1.4
Total	100.2	100.2	100.2	100.3	100.3	99.7	99.9	99.4	100.0	99.6	100.0	99.1	98.1
Nb	6.6		5.5		3.0	7.0	9.2	12.1		10.8			12.3
Zr	148.4		163.6		160.5	111.7	100.1	156.0		151.1			162.6
Y	36.7		36.2		36.6	28.6	27.3	39.3		22.3			15.2
Sr	216.9		124.1		192.7	201.4	229.8	195.0		120.1			126.6
Rb	38.8		58.1		11.3	121.0	91.1	109.3		66.6			8.0
Pb	< 5		10.1		13.2	3.6	12.6	< 5		5.6			5.0
Ga	10.2		15.0		12.3	15.6	15.0	14.2		17.4			17.3
Zn	23.7		15.6		18.7	22.2	25.3	26.5		45.9			27.7
Cu	94.0		4.6		< 5	8.4	4.6	9.6		67.0			14.1
Ni	98.3		64.1		18.7	< 5	< 5	< 5		45.2			83.5
Co	29.3		16.5		10.5	12.4	8.3	5.8		25.6			8.3
Mn	579.7		523.2		264.3	272.6	470.1	496.4		1251.4			689.5
Cr	186.0		144.2		86.0	15.3	< 5	24.0		101.8			141.5
V	114.3		92.3		51.2	26.0	59.0	53.6		148.4			112.9
Ba	444.3		649.7		259.1	1601.9	900.8	1107.2		810.2			100.3
U	< 2		2.1		< 2	5.1	3.7	4.3					
Th	3.9		7.4		< 2	15.8	12.2	15.1					
As	< 2		< 2		2.3	1.7	< 2	< 2					

	Joe Lake Samples											
Sample Nr.	**SBD-012**	**SBD-016**	**SDB-020**	**SBD-024**	**SBD-031**	**SBD-034**	**SBD-037**	**SBD-039**	**SBD-050**	**SBD-054**	**SBD-055**	**SBD-058**
Easting	**46.7279**	**46.72642**	**46.72642**	**46.72625**	**46.72799**	**46.72799**	**46.72992**	**46.72992**	**46.72954**	**46.72598**	**46.72588**	**46.72665**
Northing	**-81.00933**	**-81.01064**	**-81.01064**	**-81.01226**	**-81.00824**	**-81.00824**	**-81.0167**	**-81.0167**	**-81.0101**	**-81.01243**	**-81.01281**	**-81.01253**
Depth in m												
Distance to Granophyre in m	**346.6**	**509.8**	**509.8**	**519.4**	**337.6**	**337.6**	**96.3**	**96.3**	**164**	**547.1**	**552.2**	**463.1**
Lithology	**Basal Onaping Intrusion**											
SiO_2	70.1	71	68.8	69.9	64.3	67.7	60.6	62	69	69.5	69.8	67.7
TiO_2	0.5	0.2	0.3	0.3	0.5	0.5	0.5	0.5	0.5	0.5	0.4	0.5
Al_2O_3	12.5	12.9	12.9	13.4	11.5	12.4	11.7	11.6	12.3	10.8	10.7	12.7
Fe_2O_3	2.2	3.2	2.7	3.5	6.4	5.6	8.2	8.6	5.5	4.7	4.9	4.6
MnO	0.1	n.d.	n.d.	0.1	0.1	0.1	0.2	0.2	0.1	0.1	0.1	0.1
MgO	3.6	1.6	2.1	1.6	5.9	2.9	5.2	4.8	3.3	4.6	4	3.5
CaO	2.7	0.9	1	0.7	3.4	1.8	4.8	4.2	2	2.4	1.9	2
K_2O	0.6	4	0.4	4.7	0.1	2.9	1	2.1	1.8	0.7	0.6	1.6
Na2O	7	4.5	6.9	4.1	5	4.7	5.1	3.8	3.8	4.9	4.8	5.2
P_2O_5	n.d.	0.1	0.1	0.1	n.d.	0.1	0.2	0.1	0.1	0.1	0.1	0.2
Cr_2O_3	n.d.	n.d.	n.d.	n.d.	n.d.	n.d.	n.d.	n.d.	n.d.	n.d.	n.d.	n.d.
LOI	0.9	0.7	0.9	1	1.8	1	0.8	1.7	1.7	1.4	1.5	1.4
Total	100	99.2	96	99.3	99.1	99.7	98.3	99.6	100.1	99.8	98.8	99.4
Nb	9.7	5.5	10.4	3.2	11.8		11.4			14.4	12.5	6.6
Zr	139.5	117.1	143.4	145.8	144.8		150.2			137.4	133.3	165.7
Y	9.2	11.7	10.8	11.9	19.5		20.8			18.8	18.8	20.1
Sr	127.2	91.1	74.3	122.4	133		139.1			47.5	50.1	224.8
Rb	15.8	96.3	15.3	107	4		38.3			18.4	17.2	50
Pb	5	8.6	4.8	7.8	7.7		13.6			5	5	4.6
Ga	12.5	15.4	15.7	17	16.5		16.1			13	13.5	17
Zn	27.4	34.6	21.2	23.9	20.8		30.9			27.2	28	32.9
Cu	11.1	25.5	7.5	15.8	5		11.9			9.5	5	8.3
Ni	18.5	32.4	30.5	37.1	20.2		64.3			41	48.2	43.8
Co	5	6.8	5.7	8.7	17.2		22.4			14.9	15.9	15.3
Mn	596	327.3	307.1	358.8	1097.7		1488.3			771	689.8	554.5
Cr	127.9	47.6	54.1	55.3	159.8		103.5			89.2	99.3	124.5
V	60.2	41.5	50.1	47.1	174.2		137.3			114.5	98.4	108
Ba	191.9	982.5	126.7	1343.4	49.9		325.6			108.6	121.4	773.8
U												
Th												
As												

LOI = Loss of ignition

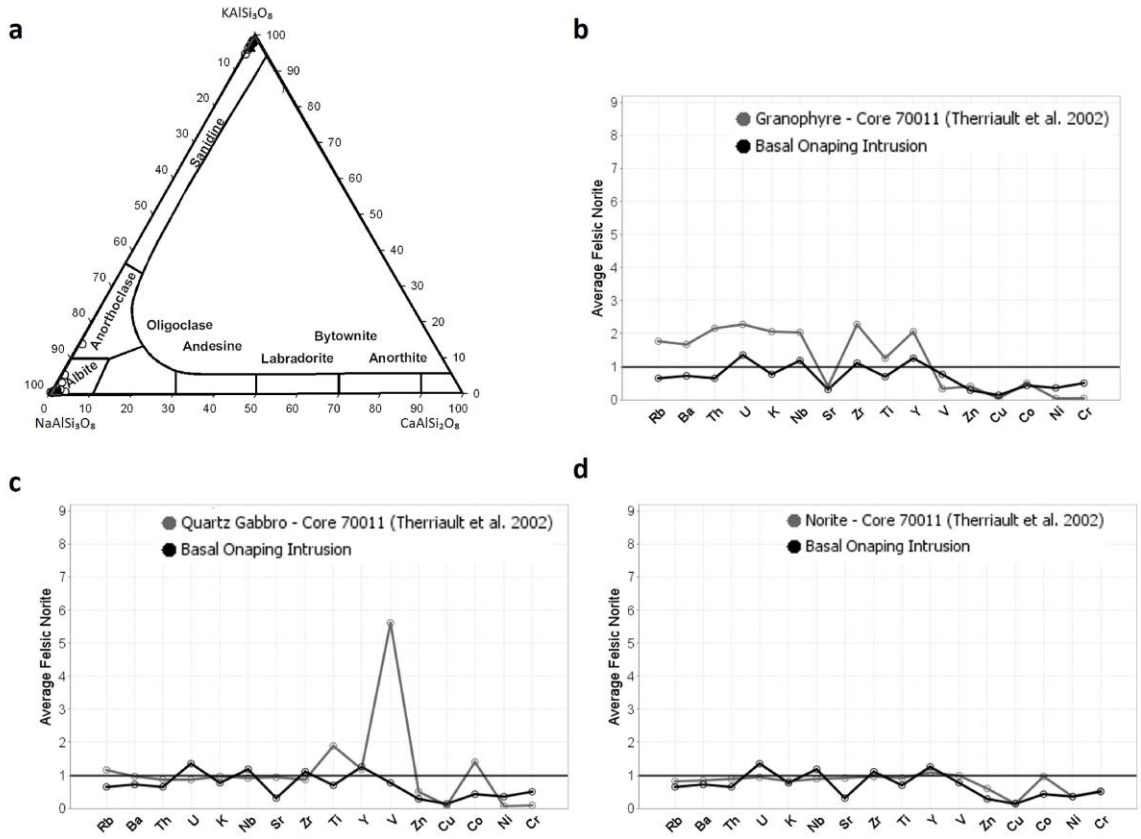

Figure 2.8. a) Feldspar ternary plot showing the composition of feldspars in the Basal Onaping Intrusion (white dots) and the Granophyre (black dots) of samples of the core 70011. They have similar composition, mostly albite and orthoclase, and no Ca-rich plagioclase. b), c), and d) Average trace elements composition normalized to Felsic Norite (Lightfoot et al. 1997a) in the order from incompatible to compatible behaviour of Basal Onaping Intrusion compared to b) Granophyre, c) Quartz Gabbro, and d) Norite (Therriault et al. 2002).

2.4 Interpretations and Discussion

2.4.1 Nature of the Basal Onaping Intrusion

As shown in Table 2.1, the unit we have referred to here as the Basal Onaping Intrusion has had various different names and various explanations as to its origin over the past century. The interlocking intergrowth of feldspar and quartz in the Basal Onaping Intrusion clearly demonstrates the igneous nature and points to rapid and simultaneous crystallization

from a melt (Brockmeyer and Deutsch 1989; Stöffler et al. 1989; Avermann and Brockmeyer 1992) (Fig. 2.2). Within a quickly cooling melt, time is insufficient to form large crystals with distinct boundaries; instead the assemblage is composed of small, interlocking feldspar and quartz crystals that often does not exhibit grain boundaries. With increasing distance from the Granophyre, the feldspar crystals within the Basal Onaping Intrusion of core and field samples decrease in size (Fig. 2.3) and grain boundaries become invisible. Together with this evidence for an igneous groundmass and the detection of PDFs within quartz clasts in the Basal Onaping Intrusion (Fig. 2.7), which demonstrates that this unit contains shocked material, the general nature of the Basal Onaping Intrusion conforms to the definition of an impact melt rock.

The presence of exclusively decorated PDFs points to post-impact alteration processes. Decorated PDFs are secondary features formed as a result of post-impact annealing and alteration of fresh, non-decorated PDFs (Stöffler and Langenhorst 1994; Grieve et al. 1996). Therriault et al. (2002) detected two sets of PDFs in one grain within the Basal Onaping Intrusion of core 70011, parallel to the crystallographic orientation of 23°, which is consistent with our data.

2.4.2 Comparison of the Basal Onaping Intrusion, Sandcherry Member and Granophyre

The mineralogy of the Granophyre in this study is equivalent to previous studies, where it has been described as a micrographic and granophyric intergrowth of coarse-grained alkali feldspars (perthite and microcline) quartz, albite with An <5%, epidote, biotite and amphibole as well as minor minerals like apatite, calcite and chlorite (Therriault et al. 2002). Interestingly, Peredery and Naldrett (1975) and Therriault et al. (2002) have reported that the upper parts of the Granophyre are sometimes more plagioclase-rich, including in the same core (70011) that we studied. The analyzed feldspars within the Basal Onaping Intrusion and the upper parts of the Granophyre show identical compositions; orthoclase and plagioclase with An < 4% (Fig. 2.8b). Primary igneous feldspar end members are not common in layered igneous complexes; however, similar observations have been described from the SIC (Therriault et al. 2002), and also from the Manicouagan

impact melt sheet (Floran and Grieve 1978). Both authors interpreted the observed feldspars as xenocrysts which is also most likely true for the feldspars of the Basal Onaping Intrusion. Epidote, chlorite and calcite are secondary minerals that have been formed by alteration of hornblende, pyroxene and biotite due to post-impact hydrothermal activities. Extensive hydrothermal alteration been described throughout the Sudbury region (Ames et al. 1998, 2002; Ames 1999).

In contrast, the Sandcherry Member does not show any similarities to the Basal Onaping Intrusion or the Granophyre (Fig. 2.6b). Instead of shocked country rock clasts seen in the Basal Onaping Intrusion, the Sandcherry Member contains equant-shaped shards of altered glass and lithic clasts (Ames et al. 1998). Such shard clasts (Fig. 2.6b), which have not been detected within the Basal Onaping Intrusion, are angular to sub-angular, show a complex structure, and do not display any reaction rims. The groundmass of the Sandcherry Member is clastic, fine-grained while the groundmass of the Basal Onaping Intrusion and Granophyre is igneous. In terms of geochemistry, whole rock major element analyses reveal the relatively high SiO_2 contents for the Basal Onaping Intrusion and the Granophyre. Compositional variations within the groundmass of the Basal Onaping Intrusion suggest that equilibrium was not reached and homogenization was incomplete between matrix and clasts. Impact melt rocks can be texturally heterogeneous over distances from millimetres to metres, mostly due to incomplete melting of clasts (Engelhardt 1984; Grieve et al. 1987a).

2.4.3 Origin of the Basal Onaping Intrusion

As outlined above, the Basal Onaping Intrusion is an impact melt rock and not a post-impact intrusive body. Critically, the gradational transition between Basal Onaping Intrusion and Granophyre implies a relationship between these two units – an observation which is consistent with other studies (Stevenson 1963; Brockmeyer and Deutsch 1989; Avermann and Brockmeyer 1992; Gibbins 1994). We, therefore, suggest that the Basal Onaping Intrusion represents the fine-grained roof rocks to the SIC.

Therriault et al. (2002) reported granophyric intergrowth within the Quartz Gabbro and Norite members of the SIC. They explained the formation of Granophyre by the sudden decrease in water pressure leading to a simultaneous and rapid under cooling of the crystallizing and differentiating melt phase and subsequent formation of the Granophyre. Residual melt within the Quartz Gabbro and Norite members of the SIC also crystallized as granophyric texture due to this sudden decrease in water pressure. A similar process might account for the presence of granophyric textures in the contact area of Basal Onaping Intrusion and Granophyre. Although at this stage, the Basal Onaping Intrusion was potentially already partially solidified, the heat of the fractionating SIC led locally to partial re-melting of the Basal Onaping Intrusion at the contact to the Granophyre, which would explain the features of thermal metamorphism reported from the lower Onaping Formation (Stevenson 1984). This interstitial melt might have undergone rapid cooling when the water pressure decreased and formed the isolated patches of micrographic intergrowth within the Basal Onaping Intrusion, resulting in the transitional contact to the Granophyre.

Decreasing grain size with increasing distance from the Granophyre contact in the Basal Onaping Intrusion points to the existence of a temperature gradient during crystallization, which resembles previous studies (Muir and Peredery 1984; Grieve et al. 2010). This is consistent with the upper part of the Basal Onaping Intrusion losing its energy to the overlying Onaping Formation, while the lower part obtained heat from the underlying pre-differentiated SIC. This led to slower cooling in proximity to the proto-SIC and, thus, to longer crystallization times. Another influencing factor was the clasts within the melt of the Basal Onaping Intrusion, which promoted cooling and inhibited the matrix crystals from growing in the upper parts of the Basal Onaping Intrusion. The varying amount of clasts with increasing depth can also be explained by this temperature gradient. Similar relationships of clast content and grain size have already been noted by Grieve et al. (2010) and also have been observed from other impact melt sheets, such as at the Manicouagan (Floran and Grieve 1978), West Clearwater (Simonds et al. 1978), Boltysh (Grieve et al. 1987b), and Mistastin Lake impact structures (Grieve 1975). Close to the SIC, temperatures remained high over a longer period of time enabling assimilation of clasts and leading to the smaller amount of residual clasts. At shallower depths, temperatures were not sufficient

for assimilation, resulting in quenching of the melt before clasts could have been digested. The rounded shape of lithic clasts is an indicator of resorption and melting processes (Fig. 2.4). Partial melting of incorporated clasts from the country rocks led to the formation of rims around clasts (Figs. 2.4a, c and d) and can be interpreted as a result of reactions between liquid melt and entrained target rock clasts (Taylor and Dence 1969; Fudali 1974).

In terms of trace element it is apparent that the Basal Onaping Formation shares similarities with all three units of the SIC; however, it most resembles the Norite. Geochemical relationships between the Basal Onaping Intrusion and units of the SIC have been recognized by various authors in the past (Dressler et al. 1996; Zieg and Marsh 2005). However, a more extensive and detailed geochemical investigation of the Basal Onaping Formation, including more trace elements and rare earth elements is needed, as the formation process of the SIC was complex.

The Basal Onaping Intrusion has been described as intrusive into the Sandcherry Member (Dressler et al. 1992; Ames et al. 1998); however, no intrusive, discordant contact relationships and no signs of interaction, melting or assimilation at the contact between these two units have been found in this study. Moreover, the sharp contact between the Basal Onaping Intrusion and Sandcherry Member is consistent with previous observations (Brockmeyer and Deutsch 1989; Dressler et al. 1992), and speaks to a time gap and suggests that the Basal Onaping Intrusion was already, in part, cooled and solidified, when the Sandcherry Member formed. Some workers (Dressler et al. 1992) have reported inclusions of Basal Onaping Intrusion-like materials within the Granophyre, leading to the assumption that parts of the partially solid Basal Onaping Intrusion were dislodged and sank into the SIC, where they were preserved as clasts within the Granophyre. Based on the above, we present the following working hypothesis for the origin of the Basal Onaping Intrusion:

i. Melting of a large volume of crustal target rocks resulted in the formation of the proto-SIC;
ii. Fallback of clasts into the top of the ponded but still hot and fluid proto-SIC occurred, with the subsequent downward settling of the clasts;

iii. The incorporation of cold clasts led to faster cooling and crystallization of the upper part of the proto-SIC;
iv. A temperature gradient formed with lower temperatures at the upper surface and increasing temperature with increasing depth, leading to the increasing grain size and the decreasing clast content;
v. The clast-bearing, more rapidly cooled upper part of the proto-SIC formed the roof rocks to the SIC, which is now manifested as the Basal Onaping Intrusion;
vi. The proto-SIC, covered and thermally protected by those roof rocks, cooled relatively slowly, differentiated and crystallized to finally form the present SIC.

In this working hypothesis, the Basal Onaping Intrusion is not part of the Onaping Formation, but is rather the uppermost member of the SIC, which is consistent with previous suggestions (Stevenson 1963; Brockmeyer and Deutsch 1989; Stöffler et al. 1989). An important complicating environmental factor is the suggested water-rich environment at the time of, and after, the impact event (French 1970; Ames et al. 1998; Grieve et al. 2010). As proposed by Grieve et al. (2010), this provides the simplest explanation for the origin of the Onaping Formation. In their working hypothesis, sea water flowing into the crater depression interacts with the hot, undifferentiated and melt sheet of the proto-SIC leading to phreatomagmatic-like or melt-fuel-coolant interaction (MFCI) explosions in the upper parts of the proto-SIC and resulting in the deposition of a series of overlying breccias. This provides a simple and elegant explanation as to why the Basal Onaping Intrusion is not present throughout the whole crater and to why it varies in thickness. Namely, where it is absent represents regions where water infiltration and MFCI explosions occurred, thereby removing the roof rocks, and where present represents zones where the underlying SIC was protected. Those powerful phreatomagmatic eruptions could also have led to the rupture of already solid parts of the SIC and thus to the injection of still liquid Onaping Intrusion into the Onaping Formation, which would explain the discordant, intrusive relationships observed by other authors (Stevenson 1963; Ames et al. 1998; Ames 1999; Grieve et al. 2010).

If our working hypothesis is correct, it has also implications for estimating the original composition of the SIC, which remains elusive. It has been suggested, that the so-called Offset Dykes around the Sudbury structure have been injected from the SIC in an early stage of the SIC formation and, thus, could preserve a composition representing the proto-SIC (Lightfoot et al. 1997a), but the vitric compositions of the Onaping Formation have also been suggested as an estimate for the composition of the proto-SIC (Ames et al. 2002). If the Basal Onaping Intrusion are the roof rocks of the SIC, they may represent a composition close to the bulk initial composition of the SIC. This is consistent with previous work by Brockmeyer and Deutsch (1989), who suggested, based on neodymium isotope data, that the Basal Onaping Intrusion was formed by an early phase of the SIC.

2.4.4 The Basal Onaping Intrusion as part of the SIC

We have shown above that the Basal Onaping Intrusion is SiO_2-rich (Table 2.3); however, the values are not quite as high as the Granophyre of the SIC. Collins (1934) first suggested an overall granodioritic composition for the SIC, which has since been confirmed (e.g., Therriault et al. 2002) and coincides with the observations made in this study. The amount of SiO_2 varies throughout the Basal Onaping Intrusion (Table 2.3), which is potentially related to the encountering, assimilation and partial melting of clasts. Assimilation of clasts, most likely of felsic composition, could have led to an enrichment of SiO2, K2O and Na_2O. Another possible explanation could be the contamination of the matrix composition of the Basal Onaping Intrusion by included clasts. Although the samples have been carefully chosen and visible clasts have been removed, it is still possible that small clasts changed the composition of the Basal Onaping Intrusion matrix.

The overall trends, seen in Figure 2.8, might point to a cogenetic relationship between the Basal Onaping Intrusion and the SIC. Based on the trace element distribution of the Basal Onaping Intrusion compared to the SIC, it is clear that there is a relationship between the units of the SIC and the Basal Onaping Intrusion and the Basal Onaping Intrusion may, therefore, qualify as parental melt for the SIC. As a result of melting of Archean and Huronian crust, the SIC shows a distinctive crustal isotopic signature, which was first observed from Sm-Nd isotope data (Faggart et al. 1985) and later confirmed using other

isotopic methods (Walker et al. 1991; Deutsch 1994; Dickin et al. 1996). It was, thus, concluded that all the units of the SIC were produced by fractional crystallization and differentiation from a single SiO_2-enriched impact melt sheet. The Basal Onaping Intrusion did not undergo fractionation and differentiation as it is too thin and was quenched too quickly. Changes in major and trace element abundances are, thus, not related to crystallization and fractionation of minerals but either related to post-impact alteration or due to the greater assimilation of silicate and felsic clasts in the lower parts of the Basal Onaping Intrusion.

2.5 Concluding Remarks

Our observations indicate the igneous nature of the groundmass of the Basal Onaping Intrusion. Skeletal intergrowth of feldspar and quartz points to simultaneous cooling of those components; rims around clasts are a result of interaction processes between liquid melt and target rock clasts. The presence of PDFs further indicates that the Basal Onaping Intrusion is an impact melt rock. Increasing grain size, decreasing amounts of clasts with increasing depth and an transitional contact between Granophyre of the SIC and the Basal Onaping Intrusion are consistent with general features of roof rocks at coherent impact melt sheets leading to the hypothesis that the Basal Onaping Intrusion represents the roof rock of the SIC. Therefore, the Basal Onaping Intrusion should no longer be considered as part of the Onaping Formation, but rather the uppermost member of the SIC. Based on the analogy with layered igneous intrusions, such as Skargaard and Bushveld, we recommend "Upper Contact Unit" of the SIC as a new name for the Basal Onaping Intrusion.

2.6 References

Ames, D.E., 1999. Geology and regional hydrothermal alteration of the crater-fill, Onaping Formation: Association with Zn-Pb-Cu mineralization, Sudbury structure, Canada. PhD. Thesis, Dep. Earth Sci. Carlet. Univ. Ottawa, Ontario, Canada 460.

Ames, D.E., Davidson, A., Buckle, J., Card, K.D., 2005. Sudbury bedrock compilation; Geology. Geol. Surv. Canada Open File 4570, 2 maps.

Ames, D.E., Davidson, A., Wodicka, N., 2008. Geology of the giant Sudbury polymetallic mining camp, Ontario, Canada. Econ. Geol. 103, 1057–1077.

Ames, D.E., Gibson, H.L., 2004. Geology, alteration and mineralization of the Onaping Formation, Morgan Township, Sudbury Structure, Ontario. Geol. Surv. Canada Open File 3717, 2 maps.

Ames, D.E., Golightly, J.P., Lightfoot, P.C., Gibson, R.L., 2002. Vitric compositions in the Onaping Formation and their relationship to the Sudbury Igneous Complex, Sudbury structure. Econ. Geol. 97, 1541–1562.

Ames, D.E., Watkinson, D.H., Parrish, R.R., 1998. Dating of a regional hydrothermal system induced by the 1850 Ma Sudbury impact event. Geology 26, 447–450.

Avermann, M., Brockmeyer, P., 1992. The Onaping Formation of the Sudbury Structure (Canada) - an example of of allochthonous impact breccias. Tectonophysics 216, 227–234.

Bell, R., 1893. On the Sudbury Mining District. Geol. Surv. Canada Annu. Rep. 5, 1–95.

Brockmeyer, P., Deutsch, A., 1989. The origin of the breccias in the lower Onaping Formation, Sudbuy Structure, Canada: Evidence from petrographic observations and Sr-Nd isotope data, in: 20th Lunar and Planetary Science Conference. p. 113.

Burrows, A.G., Rickaby, H.C., 1930. Sudbury Basin Area. Ontario Dep. Mines Annu. Rep. 38, 55 pp.

Coleman, A.P., 1905. The Sudbury Nickel Region. Ontario Dep. Mines Annu. Rep. 14, 1–188.

Collins, W.H., 1934. Life history of the Sudbury nickel irruptive. I. Petrogenesis. R. Soc. Canada Trans. 28, 123–177.

Deutsch, A., 1994. Isotope systematics support the impact origin of the Sudbury Structure (Ontario, Canada), in: Dressler, B.O., Grieve, R.A.F., Sharpton, V.L. (Eds.), Large

Meteorite Impacts and Planetary Evolution I, GSA Special Paper 293. pp. 289–302.

Deutsch, A., Brockmeyer, P., Buhl, D., 1990. Sudbury again: New and old isotope data, in: 21st Lunar and Planetary Science Conference. pp. 282–283.

Deutsch, A., Grieve, R.A.F., 1994. The Sudbury Structure: Constraints on its genesis from Lithoprobe results. Geophys. Res. Lett. 21, 963–966.

Deutsch, A., Grieve, R.A.F., Avermann, M., Bischoff, L., Brockmeyer, P., Buhl, D., Lakomy, R., Müller-Mohr, V., Ostermann, M., Stöffler, D., 1995. The Sudbury Structure (Ontario, Canada): a tectonically deformed multi-ring impact basin. Geol. Rundschau 84, 697–709.

Dickin, A.P., Artan, M.A., Crocket, J.H., 1996. Isotopic evidence for distinct crustal sources of North and South Range ores, Sudbury Igneous Complex. Geochim. Cosmochim. Acta 60, 1605 – 1613.

Dickin, A.P., Richardson, J.M., Crocket, J.H., McNutt, R.H., Peredery, W. V., 1992. Osmium isotope evidence for a crustal origin of platinum group elements in the Sudbury nickel ore, Ontario, Canada. Geochim. Cosmochim. Acta 56, 3531 – 3537.

Dressler, B.O., 1984. General geology of the Sudbury area, in: Pye, E.G., Naldrett, A.J., Giblin, P.E. (Eds.), The Geology and Ore Deposits of the Sudbury Structure. pp. 57–82.

Dressler, B.O., Peredery, W. V., Muir, T.L., 1992. Geology and Mineral Deposits of the Sudbury Structure. Ontario Geological Survey Guidebook 8.

Dressler, B.O., Weiser, T., Brockmeyer, P., 1996. Recrystallized impact glasses of the Onaping formation and the Sudbury igneous Complex, Sudbury Structure, Ontario, Canada. Geochim. Cosmochim. Acta 60, 2019 – 2036.

Engelhardt, W., 1984. Melt products from terrestrial impact structures, in: 27th International Geological Congress. pp. 149–163.

Faggart, B.E., Basu, A.R., Tatsumoto, M., 1985. Origin of the Sudbury complex by meteoritic impact: Neodymium isotopic evidence. Science (80-.). 230, 436–439.

Floran, R.J., Grieve, R.A.F., 1978. Manicouagan impact melt, Quebec, 1, Stratigraphy, petrology, and chemistry. J. Geophys. Res. 83, 2737–2758.

French, B.M., 1967. Sudbury structure, Ontario: Some petrographic evidence for an origin by meteorite impact, in: French, B.M., Short, N.M. (Eds.), Shock Metamorphism of Natural Materials. Mono Book Corporation, Baltimore, pp. 383–412.

French, B.M., 1970. Possible Relations Between Meteorite Impact and Igneous Petrogenesis, as Indicated by the Sudbury Structure, Ontario, Canada. Bull. Volcanol. 34, 466–517.

Fudali, R.F., 1974. Genesis of the melt rocks at Tenoumer crater, Mauritania. J. Geophys. Res. 79, 2115–2121.

Gibbins, S.F.M., 1994. Geology, geochemistry, stratigraphy and mechanisms of emplacement of the Onaping Formation, Dowling area, Sudbury structure, Ontario, Canada. M.Sc. Thesis, Laurentian University.

Grieve, R.A.F., 1975. Petrology and chemistry of the impact melt at Mistastin Lake crater, Labrador. Geol. Soc. Am. Bull. 86, 1617–1629.

Grieve, R.A.F., 1994. An Impact Model of the Sudbury Structure, in: Lightfoot, P.C., Naldrett, A.J. (Eds.), Proceedings of the Sudbury-Noril'sk Symposium. Ontario Geological Survey Special Volume 5, pp. 119–132.

Grieve, R.A.F., Ames, D.E., Morgan, J. V., Artemieva, N.A., 2010. The evolution of the Onaping Formation at the Sudbury impact structure. Meteorit. Planet. Sci. 45, 759–782.

Grieve, R.A.F., Langenhorst, F., Stöffler, D., 1996. Shock metamorphism of quartz in nature and experiment: II. Significance in geoscience. Meteorit. Planet. Sci. 31, 6–35.

Grieve, R.A.F., Reny, G., Gurov, E.P., Ryabenko, V.A., 1987a. The melt rocks of the Boltysch impact crater, Ukraine, USSR. Contrib. to Mineral. Petrol. 96, 56–62.

Grieve, R.A.F., Reny, G., Gurov, E.P., Ryabenko, V.A., 1987b. The melt rocks of the Boltysh impact crater, Ukraina, USSR. Contrib. to Mineral. Petrol. 96, 56–62.

Grieve, R.A.F., Stöffler, D., Deutsch, A., 1991. The Sudbury structure: Controversial or misunderstood? J. Geophys. Res. 96, 753–764.

Johns, G.W., Dressler, B.O., 1995. The Sudbury Igneous Complex - an impact melt sheet?, in: 42nd Lunar and Planetary Science Conference. p. abstract 1340.

Krogh, T.E., Davis, D.W., Corfu, F., 1984. Precise U–Pb zircon and baddeleyite ages for the Sudbury area, in: Pye, E.G., Naldrett, A.J., Giblin, P.E. (Eds.), The Geology and Ore Deposits of the Sudbury Structure. pp. 431–447.

Lightfoot, P.C., Keays, R.R., Morrison, G.G., Bite, A., Farrell, K.P., 1997a. Geochemical relationships in the Sudbury igneous complex; origin of the main mass and offset dikes. Econ. Geol. 92, 289–307.

Lightfoot, P.C., Keays, R.R., Morrison, G.G., Bite, A., Farrell, K.P., 1997b. Geologic and geochemical relationships between the contact sublayer, inclusions, and the main mass of the sudbury igneous complex: A Case study of the whistle mine embayment. Econ. Geol. 92, 647–673.

Muir, T.L., 1981. Geology of the Capreol Area, District of Sudbury; Ontario. Geol. Surv. Canada Open File 5344, 215 pp.

Muir, T.L., 1983. Geology of the Morgan Lake – Nelson Lake area, District of Sudbury, Ontario. Ontario Geol. Surv. Open File 5426, 245 pp.

Muir, T.L., Peredery, W. V., 1984. The Onaping Formation, in: Pye, E.G., Naldrett, A.J., Giblin, P.E. (Eds.), The Geology and Ore Deposits of the Sudbury Structure. pp. 139–210.

Onorato, P.I.K., Uhlmann, D.R., Simonds, C.H., 1978. The thermal history of the Manicouagan impact melt sheet, Quebec. J. Geophys. Res. 83, 2789–2798.

Peredery, W. V., 1972a. Chemistry of fluidal glasses and melt bodies in the Onaping Formation, in: Guy-Bray, J. V. (Ed.), New Developments in Sudbury Geology. Geological Association of Canada.

Peredery, W. V., 1972b. The Origin of Rocks at the Base of the Onaping Formation, Sudbury, Ontario. University of Toronto, Toronto, Ontario, Canada.

Peredery, W. V., Naldrett, A.J., 1975. Petrology of the upper irruptive rocks, Sudbury, Ontario. Econ. Geol. 70, 164–175.

Riller, U., 2005. Structural characteristics of the Sudbury impact structure, Canada: Impact-induced versus orogenic deformation-A review. Meteorit. Planet. Sci. 40, 1723–1740.

Riller, U., Schwerdtner, W.M., 1997. Mid-crustal deformation at the southern flank of the Sudbury Basin, central Ontario, Canada. Geol. Soc. Am. Bull. 109, 841–854.

Riller, U., Schwerdtner, W.M., Halls, H.C., Card, K.D., 1999. Transpressive tectonism in the eastern Penokean orogen, Canada: Consequences for Proterozoic crustal kinematics and continental fragmentation. Precambrian Res. 93, 51–70.

Rousell, D.H., 1984. Onwatin and Chelmsford Formations, in: Pye, E.G., Naldrett, A.J., Giblin, P.E. (Eds.), The Geology and Ore Deposits of the Sudbury Structure. pp. 57–82.

Simonds, C.H., Phinney, W.C., McGee, P.E., Cochran, A., 1978. West Clearwater, Quebec impact Structure, Part 1: Field geology, structure and bulk chemistry, in: 9th Lunar and Planetary Science Conference. pp. 2633–2658.

Stevenson, J.S., 1961. Recognition of the Quartzite Breccia in the Whitewater Series, Sudbury Basin, Ontario. Trans. R. Soc. Canada 60, 57–66.

Stevenson, J.S., 1963. The upper contact phase of the Sudbury micropegmatite. Can. Mineral. 7, 413–419.

Stevenson, J.S., 1972. The Onaping Ash–Flow Sheet, Sudbury, Ontario, in: Guy–Bray, J. V. (Ed.), New Developments in Sudbury Geology. Geological Association of Canada Special Paper 10, pp. 41–48.

Stevenson, J.S., 1984. Sudbury Problems and Suggestions for Further Research, in: Pye, E., Naldrett, A.J., Giblin, P.E. (Eds.), The Geology and Ore Deposits of the Sudbury Structure.

Stöffler, D., Avermann, M., Bischoff, L., Brockmeyer, P., Deutsch, A., Dressler, B.O., Lakomy, R., Müller-Mohr, V., 1989. Sudbury, Canada: Remnant of the only multi-ring (?) impact basin on Earth. Meteoritics 24, 328.

Stöffler, D., Langenhorst, F., 1994. Shock metamorphism of quartz in nature and experiment: Basic observation and theory. Meteoritcs 29, 155–181.

Taylor, F.C., Dence, M.R., 1969. A probable meteorite origin for Mistastin Lake. Can. J. Earth Sci. 6, 39 – 45.

Therriault, A.M., Fowler, A.D., Grieve, R.A.F., 2002. The Sudbury Igneous Complex: A differentiated impact melt sheet. Econ. Geol. 97, 1521–1540.

Thomson, J.E., 1957. Geology of the Sudbury Basin. Ontario Dep. Mines Annu. Rep. 65, 1–56.

Walker, R.J., Morgan, J.W., Naldrett, A.J., 1991. Re-Os isotope systematics of Ni-Cu sulfide ores, Sudbury Igneous Complex, Ontario: evidence for a major crustal component. Earth Planet. Sci. Lett. 105, 416–429.

Williams, H., 1957. Glowing Avalanche Deposits of the Sudbury Basin. Ontario Dep. Mines Annu. Rep. 65, 57–89.

Zieg, M.J., Marsh, B.D., 2005. The Sudbury Igneous Complex: Viscous emulsion

differentiation of a superheated impact melt sheet. Geol. Soc. Am. Bull. 117, 1427–1450.

3 Origin and formation of Metabreccia in the Parkin Offset Dyke, Sudbury impact structure, Canada[2]

Denise Anders, Gordon R. Osinski, and Richard A. F. Grieve

3.1 Introduction

The 1.85 Ga (Krogh et al. 1984) Sudbury structure (Fig. 3.1), located in Ontario, Canada, is the remnant of a peak-ring or multi-ring basin (Stöffler et al. 1992; Deutsch and Grieve 1994; Deutsch et al. 1995), and with an estimated original diameter in the range of 150–200 km (Stöffler et al. 1992; Deutsch and Grieve 1994; Grieve 1994; Deutsch et al. 1995; Spray et al. 2004) counts as one of the largest impact structures on Earth. A unique feature of the Sudbury structure is the Sudbury Igneous Complex (SIC), an extensively differentiated impact melt sheet (Faggart et al. 1985; Grieve 1991; Dickin et al. 1992, 1996; Deutsch 1994; Lightfoot et al. 1997a, 1997b); composed from bottom to top of the so-called Sublayer, Norite, Transition Zone, Quartz Gabbro, Granophyre (Dressler et al. 1992; Therriault et al. 2002) and Upper Contact Unit (former Basal Member or Onaping Intrusion, Anders et al. (2015)). The so-called Offset Dykes (Fig. 3.1) are concentric and radial dykes, the latter originating from embayments of the main mass of the SIC and the Sublayer (Grant and Bite 1984). The dykes are composed of two major lithologies: the fine-grained and mineralized so-called ‘Inclusion-rich Quartz Diorite’ (IQD), which typically occurs in the middle of the dyke, and the coarser-grained ‘Inclusion-free Quartz Diorite’ (QD), which is usually located at the margins and contains less clasts and mineralization (Lightfoot et al. 1997a, 1997c; Lightfoot and Farrow 2002; Hecht et al. 2008). A third lithology, so-called Metabreccia (MTBX) has not received much attention to date and is not well documented around the Sudbury Basin.

[2] This chapter will be submitted to the Canadian Journal of Earth Sciences.

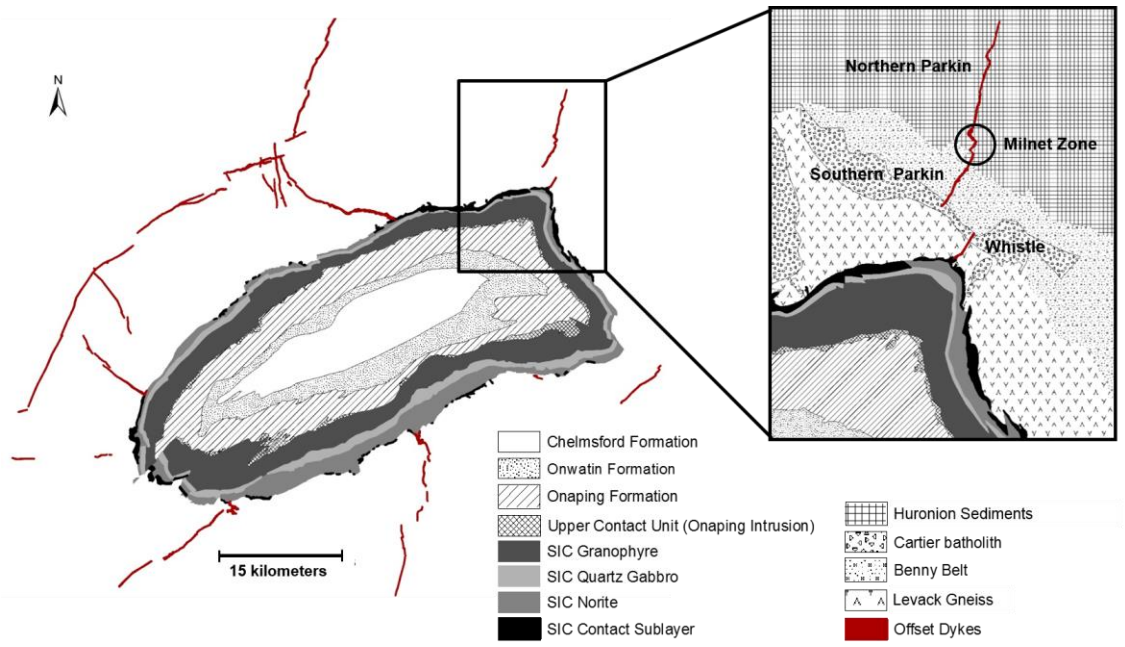

Figure 3.1. Simplified geological map of the Sudbury impact structure and the location of the Offset Dykes in red. Inset shows the regional geology of the Whistle-Parkin area.

Notable exceptions include reports of MTBX on the Parkin (Murphy and Spray 2002) and Whistle Offset Dykes (Lafrance and Bygnes 2014) in the North Range; and in the embayments of Ministic and Foy Offset Dykes (Grant and Bite 1984) (Fig. 3.1). Souch et al. (1969) first noticed that North Range Offset Dykes hosted by Archean rocks tend to be associated with intensely brecciated and melted crustal rocks. Grant and Bite (1984) reported a siliceous, recrystallized breccia, which they interpreted had formed from Footwall Breccia (FWBX) at the Whistle Offset Dyke. This was later termed MTBX (Farrow et al. 2005), based on its assumed formation as a result of thermal metamorphism of FWBX during the cooling of the SIC and/or the Offset Dykes. In contrast, more recent studies have suggested that the formation of MTBX was similar to that of QD and IQD, i.e., the injection of a melt originating from the proto-SIC into fractures around the Sudbury structure during or after the impact (Murphy and Spray 2002; Lafrance and Bygnes 2014). All workers agree that MTBX is characterized by an igneous assemblage mainly composed of feldspar and quartz (Murphy and Spray 2002; Bygnes 2011). As host for Ni-Cu-

Platinum-Group-Element mineralization (Ni-Cu-PGE), it has economic importance, however, little is known about MTBX and it is one of the major overlooked rock types in Offset Dyke research. Understanding the formation of MTBX and, thus, the Offset Dykes is a crucial detail in understanding the process of crater formation at Sudbury.

3.2 Regional Geology

The Parkin Offset Dyke has a length of ~9.5 km and starts ~3 km north of the northeastern corner of the SIC. It can be divided into three parts: the southern Parkin, Milnet zone and the northern Parkin (Fig. 3.1). The southern part of the dyke, extending up to the Milnet Mine, intrudes mafic and felsic metavolcanics of the Cartier Batholith and Benny Greenstone Belt of the Archean Superior Province, while the northern part of the dyke is hosted by Early Proterozoic Huronian sediments of the Mississagi, Bruce, Espanola, Serpent, Gowganda, and Lorrain Formation overlying the Archean basement (Card et al. 1984; Dressler et al. 1992). Both, Archean and Huronian country rocks, are intruded by late Proterozoic dykes of the Nipissing Diabase. The basement rocks and the Sudbury impact structure have been subjected to repeated post-impact deformation of the Paleoproterozoic Penokean orogeny (Brocoum and Dalziel 1974; Sims et al. 1989; Dressler et al. 1992). The Milnet zone, located ~3 km from the beginning of the dyke, marks the contact between the Archean basement rocks and the sediments of the Huronian Supergroup and is host to the Milnet 1500 zone, which was discovered in 2009 and the historical Milnet Mine, which was active from 1952 to 1954 (Wallbridge report 2013). There, the dyke changes its direction to the northwest for ~250 m and then continues trending to the northeast for ~6 km. This fault system has been associated with the sulfide mineralization of the Milnet mine and the 1500 zone.

The almost vertical dipping dyke (Grant and Bite 1984) has a width of 45 to 135 m in the southern part and pinches out to a width of 30 to 90 m in the northern part. Historically, the southern Parkin Dyke was poorly exposed at the surface of 6 trenches, strongly overgrown by vegetation, as well as gossanized and altered by weathering processes. Field relationships were, thus, in some places difficult to establish. In 2015, Wallbridge Mining stripped, re-trenched and, thus, exposed a large part of the southern Parkin Offset Dyke.

The Parkin Offset Dyke displays no known connection to the SIC and it was, thus, suggested to be the extension of the Whistle Dyke that was displaced by 2 km to the northwest by the Post Creek Fault (Grant and Bite 1984; Murphy and Spray 2002). This is why the dykes have been referred to as the Whistle-Parkin-Offset Dyke. The Whistle Offset Dyke originates at the Whistle embayment and extends to the northeast through tonalitic–granodioritic gneisses of the Archean Levack Gneiss Complex (Krogh et al. 1984), monzonitic to granodioritic units of the Cartier Batholith (Meldrum et al. 1997) intruded by late Proterozoic Matachewan dykes (Heaman 1997). The funnel-shaped Whistle embayment consists of Sublayer, underlain by FWBX and Archean basement rocks (Pattison 1979; Lightfoot et al. 1997c). FWBX is composed of fragments of granitic target rocks, diabase, amphibolite, and norite, in a fine-grained granitic matrix with a fragmental metamorphic (Lightfoot et al. 1997c) to “mosaic granoblastic metamorphic" texture (Pattison 1979). Ni-Cu-Sulfide mineralization within the Offset Dykes is usually associated with the inclusion bearing phase of quartz diorite (IQD); however, the economic important sulfide deposit with elevated PGEs at the Podolsky and Whistle Mine is mainly hosted by MTBX (Farrow and Lightfoot 2002; Lightfoot and Farrow 2002; Farrow et al. 2005).

3.3 Methodology

Fieldwork was conducted in the summers of 2013, 2014 and 2015 predominantly at the 6 main trenches of the southern Parkin. Polished thin sections of samples collected from the Parkin Offset Dyke were examined by optical microscopy, in order to characterize mineralogy, microstructures and textures. Whole rock analyses of powdered samples were carried out by the ALS laboratory in Sudbury. Major oxides were analyzed by inductively coupled plasma atomic emission spectroscopy (ICP-AES), and lithium borate fusion inductively coupled plasma mass spectrometry (ICP-MS) provided trace element analyses with the exception of base metals (Co, Cu, Ni, Sc, Zn), which were analyzed by 4-acid digestion ICP-AES. Clasts within IQD and MTBX were avoided prior to crushing and pulverizing.

3.4 Field Observations

Detailed field investigation of different dyke lithologies and contact relationships was carried out at all of the Parkin trenches. Special focus was given to the MTBX-bearing southern Parkin and the Milnet zone. The northern Parkin is completely free of MTBX being solely composed of QD and IQD. The quartz diorite phases at the Southern Parkin are mainly inclusion-free or inclusion-poor and only in rare cases inclusion-rich. MTBX was observed as clasts within an inclusion-poor phase of QD (Fig. 3.2a), but, more frequently, as pods within the dyke, in a complex intermingling relationship with QD (Fig. 3.2b). In several instances, MTBX was observed within QD, similar to the crosscutting relationships reported by Murphy and Spray (2002).

The contacts between the units are sharp and the phases do not mix, but rather intermingle, and fingers of QD/IQD were seen to intrude MTBX (Figs. 3.2a–c). Contact relationships between MTBX and IQD are difficult to establish; the contacts are usually gradational; the two phases merge into each other and can only be identified by a change in amount of clasts and/or spherulitic amphiboles within the IQD matrix, if present. There are no chilled or baked contacts between QD/IQD and MTBX.

MTBX is composed of clasts set in an aphanitic, grey to black, locally milky, matrix that usually weathers light grey, sometimes with a bluish tint (Fig. 3.2d). It typically contains 50 to 75% clasts, occasionally more, of different size and shape, which often merge into the matrix, creating diffuse and gradational contacts. This makes it locally very difficult to distinguish between matrix and clasts. The dominant clast population is felsic, composed of only quartz, or quartz and feldspar, and rare alkali feldspar inclusions. Green to black mafic clasts are locally abundant within MTBX, and produce small surficial pits and depressions when removed by weathering processes (Fig. 3.1e). Where mafic clasts predominate, MTBX has been referred to as “mafic, sulfide bearing breccia” (Murphy and Spray 2002). The majority of clasts are cm-sized, rarely m-sized; however, an approximately 60 x 25 m gneiss clast was reported within the Parkin Dyke (Murphy and Spray 2002), which was confirmed during the field visits in this study.

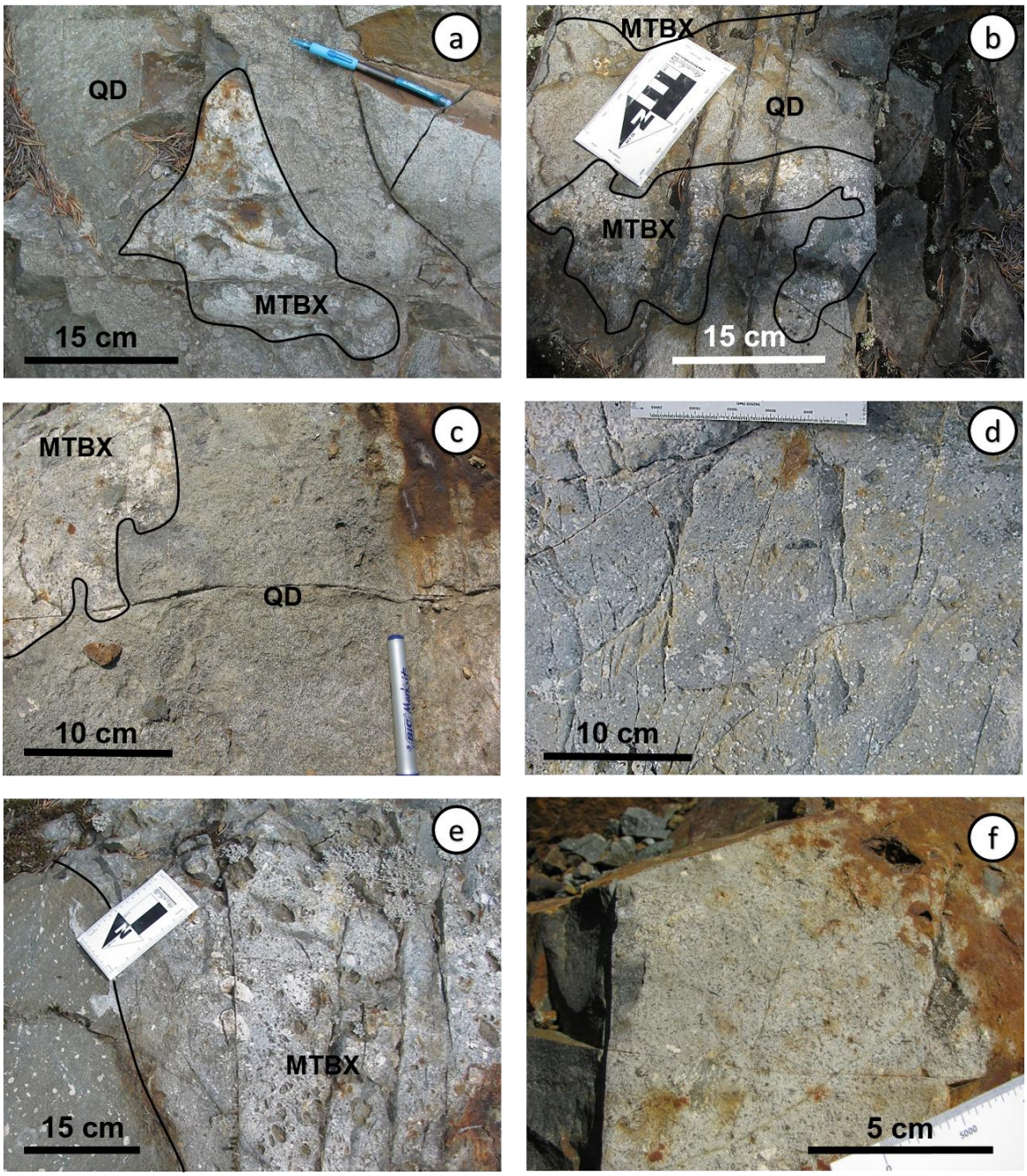

Figure 3.2. Field photographs from the Parkin Offset Dyke. a) Clast of MTBX within inclusion-poor QD. b) Intermingling relationship of MTBX and QD. c) MTBX in a sharp contact with QD. d) Smooth MTBX surface. The dominant clast population is white and felsic. e) MTBX in contact with Matachewan Diabase. The surface is rough and has pits and depressions, where mafic clasts have been removed by weathering. f) Typical inclusion-poor QD, displaying large, green amphiboles.

An important characteristic of MTBX is that it is associated with mineralization; it contains disseminated to blebby sulfides and is very often directly in contact with gossanized pods or mineralized mafic clasts (Figs. 3.1a, b and d). Compared to IQD (Fig. 3.1f), MTBX typically has a higher amount of clasts, smaller grain size and rarely contains the large spherulitic amphiboles typical of IQD. In most cases, however, it is difficult to distinguish between MTBX and IQD, based solely on outcrop observations. MTBX is characterized by a higher amount of K-feldspar, visible in hand samples as pink to salmon-coloured aggregates, while QD and IQD show a black and white, dioritic texture, often referred to as salt and pepper texture. The clast population in both, MTBX and QD/IQD, is similar. As a result of the predominantly felsic composition of recrystallized quartz and feldspar, MTBX displays on a fresh surface the typical milky-white, flaky fracture of quartz-rich metamorphic rocks; whereas IQD and QD, in contrast, usually break into smooth blocks with sharp edges.

3.5 Petrography

MTBX is composed of a quartzo-feldspatic matrix with minor biotite, amphibole and pyroxene which are locally replaced by secondary chlorite, epidote and calcite. The matrix is characterized by an intergrowth of quartz and feldspar with merging, interlocking grain boundaries and other features indicative of intensive recrystallization (Fig. 3.3a). New, smaller grains replacing the old fabric, are very common throughout the MTBX matrix and show irregular to amoeboid, serrated grain boundaries with dark rims (Fig. 3.3b). Commonly, the grain boundary forms bulges that migrate into an adjacent grain (Fig. 3.3c). Larger quartz grains are usually divided into sub-areas, so-called subgrains, which show slightly different orientations than the adjacent area or the host grain (Fig. 3.3c and d). The felsic MTBX groundmass is aphanitic but, locally, shows a variation in grain size from 10 μm to 100 μm (Fig. 3.3d). It appears strain free and ductile deformation features, such as preferred grain orientation, elongated or ribbon-shaped minerals, have not been detected. Relicts of poikilitic textures, defined by smaller grains included in a larger, different mineral, have been observed (Fig. 3.3e). Embayed and indented quartz xenocrysts are distributed within the MTBX matrix (Fig. 3.3a).

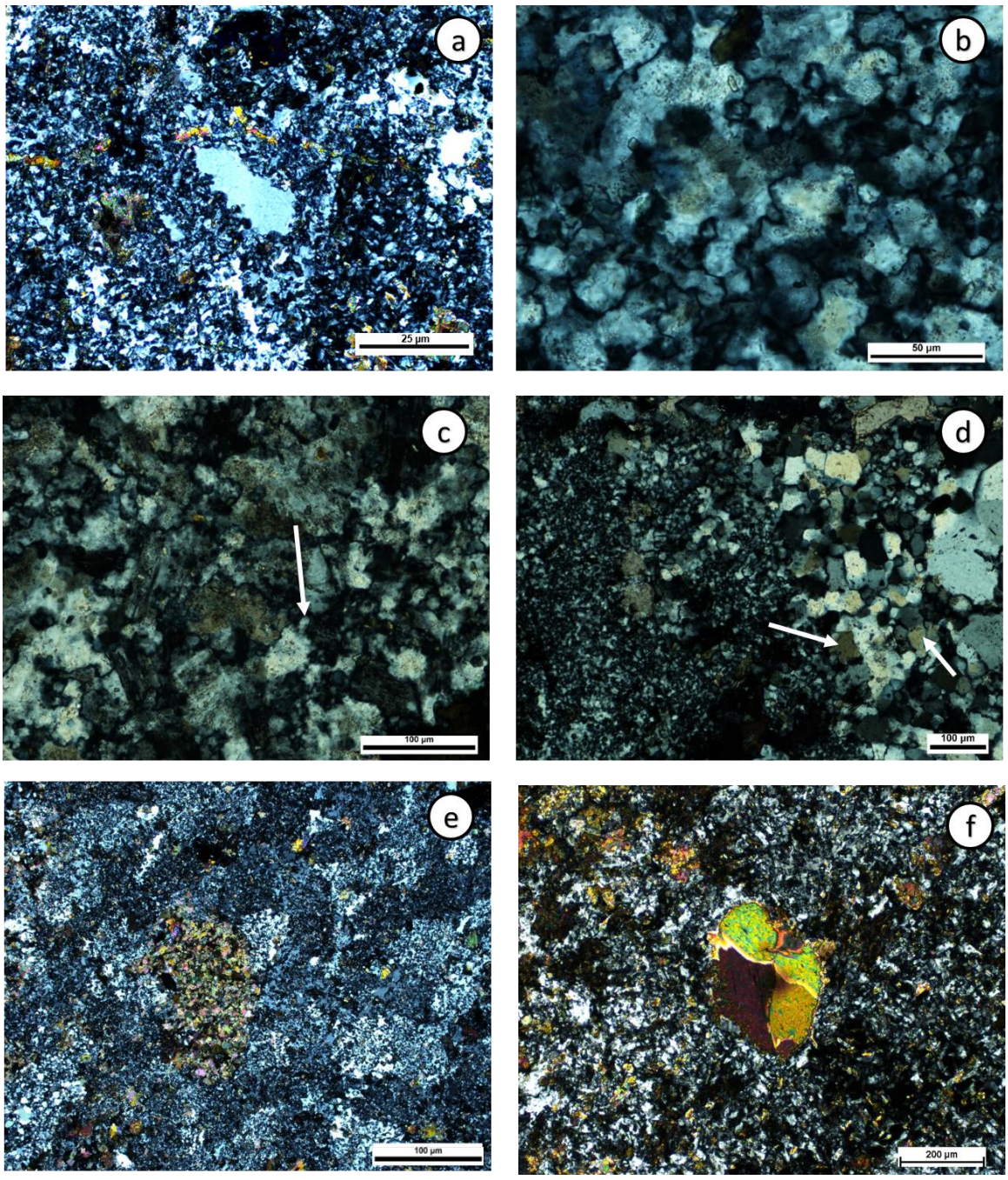

Figure 3.3. Photomicrographs (XPL) of a) MTBX groundmass characterized by an intergrowth of quartz and feldspar. The quartz xenocryst in the middle of the picture represents a relic of the original igneous texture. b) Amoeboid and interlocking grain boundaries with dark rims. c) Formation of a subgrain within the MTBX groundmass (white arrow). d) Two subgrains (white arrows) showing different orientations than host grain. e) Relicts of poikilitic texture within MTBX. f) Biotite xenocryst with subgrains and beginning marginal recrystallization.

More rarely, biotite xenocrysts within the matrix are also characterized by subgrains and beginning recrystallization at the margins (Fig. 3.3f). Feldspar within MTBX is characterized by brittle fracturing, undulose extinction, micrographic intergrowth and subgrains with diffuse boundaries.

Clasts within MTBX are usually rounded to subrounded and embayed and display signs of partial melting and digestion (Fig 3.4a). The dominant clast population are pure quartz aggregates (Fig. 3.4b), followed by felsic clasts composed of quartz and feldspar, and mafic clasts (Fig. 3.4a) that usually are altered to chlorite and epidote. It is sometimes difficult to establish the origin of the clasts based on their size, but larger clasts originate from felsic and mafic gneiss, granitic rocks, and amphibolite.

Recrystallization features have also been detected in clasts within MTBX. Chessboard texture (Fig. 3.4b), which is defined by polygonal subgrains with different orientations (Stipp et al. 2002a), is common in quarzitic clasts, but also locally within in the MTBX matrix. Figure 3.4c shows a microphotograph of an approximately 1 cm-sized embayed clast, composed of large quartz grains surrounded by new smaller grains at the grain boundaries, so-called necklace structures. A few quartz grains in larger clasts show impact-induced deformation features, such as planar fractures (PFs) and in rare occasion relicts of decorated and annealed planar deformation features (PDFs) (Fig. 3.4d). Some clasts display so-called core-and mantle features (Fig. 3.4e), representing relicts of old grains or aggregates that are surrounded by sheets of recrystallized grains.

The contact between MTBX and QD in thin section is semi-sharp and characterized by a change in texture and a difference in and grain size. However, no chilled or baked areas or reaction rims have been detected. QD and IQD are composed of a coarse-grained assemblage of euhedral quartz, feldspar and mafic minerals, usually acicular and spherulitic amphibole, rarely biotite. The amount of interstitial micrographic intergrowth within the matrix of IQD/QD is higher than within MTBX.

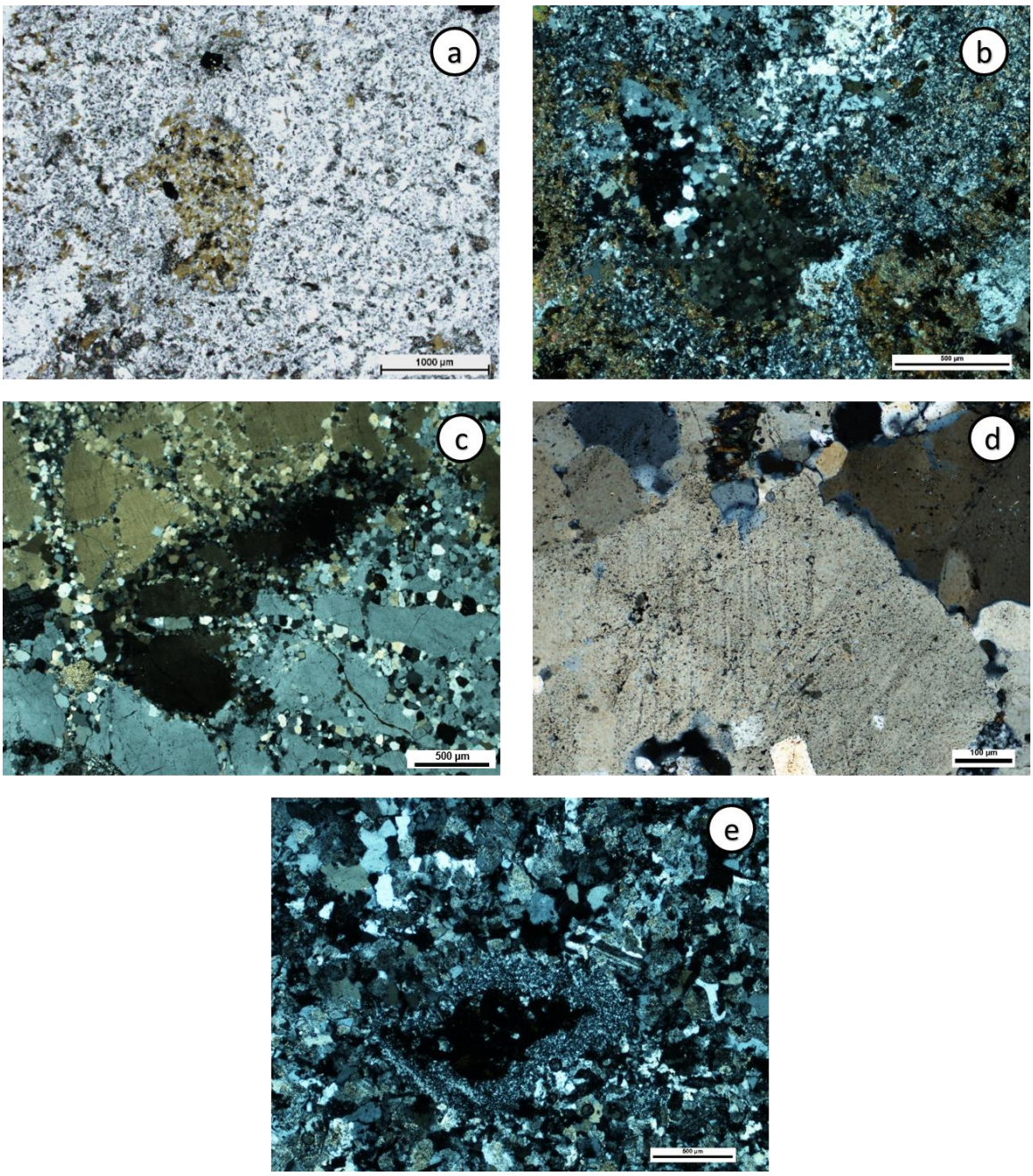

Figure 3.4. Photomicrographs of a) Rounded, embayed mafic clast within MTBX (PPL). b) Felsic clast with a mafic rim showing chessboard texture (XPL). c) Large clast with recrystallization at the grain boundaries (PPL). d) Two sets of decorated and annealed PDFs within a clast of MTBX (XPL). e) Core-and mantle feature within MTBX. Relicts of old quartz grains are surrounded by small recrystallized quartz grains.

3.6 Geochemistry

Average major and trace element compositions of QD/IQD, MTBX, FWBX and country rocks from Parkin and Whistle are presented in Table 3.1. MTBX from Parkin shows a wide range of SiO_2 than QD/IQD containing 54.6–75.1 wt % (average 62.8 wt %), which agrees with the reported compositions of MTBX from Whistle (Lightfoot et al. 1997b, 1997d; Carter et al. 2009; Lafrance and Bygnes 2014); the majority of QD and IQD samples from the Parkin Offset Dyke have > 60 wt % SiO_2 (average 59.2 wt % for IQD and 59.3 wt % for QD) and are, thus, slightly less siliceous and more mafic than MTBX. FWBX has an average of 60.5 wt % SiO_2. Generally, however, the major oxides are similar for QD/IQD, MTBX, FWBX and county rocks. Trace element spider plots (Fig. 3.5) normalized to the average Felsic Norite of the SIC (Lightfoot et al. 1997b) show little geochemical variation between IQD and QD (Fig. 3.5a). They display a very close compositional relationship with a similar trace element pattern and resembling absolute abundances, often close to the absolute abundances of the Felsic Norite (Fig. 3.6). They are characterized by small negative Sr and Eu anomalies and a slightly positive K anomaly, but otherwise, the pattern is relatively flat without pronounced anomalies.

Large-Ion-Lithophile-Elements (LILE) such as K, Rb, Sr and Ba are similar in MTBX and QD/IQD. While FWBX (Fig. 3.5b) does not show any pronounced anomaly in Sr and a positive anomaly in Th, MTBX displays a negative Sr, a negative Th and a more pronounced negative U anomaly. Otherwise, the trace element patterns and the absolute values of MTBX and FWBX are markedly similar.

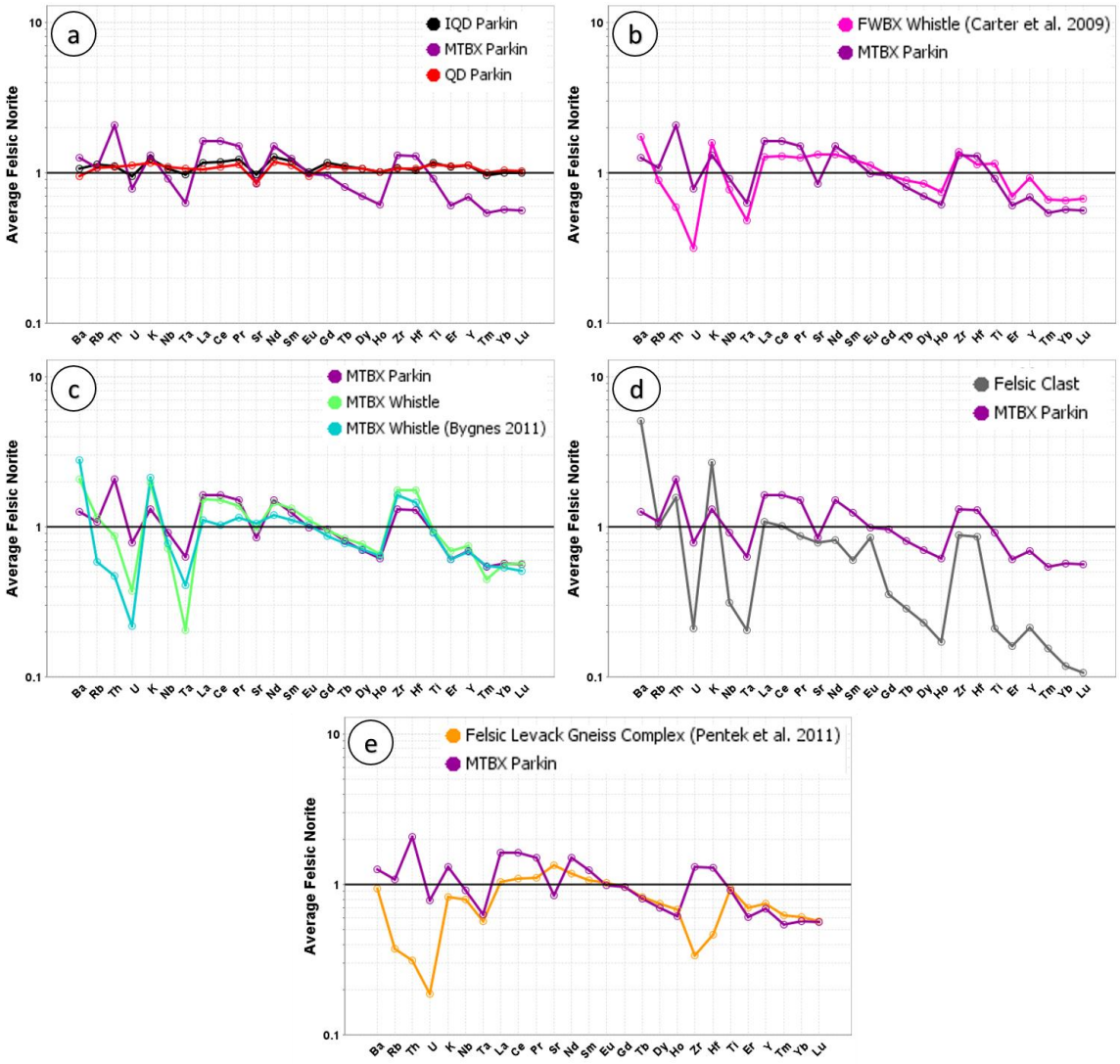

Figure 3.5. Trace element spider plots normalized to the Felsic Norite (Lightfoot et al. 1997b) of a) MTBX (this study) compared to QD and IQD. b) FWBX (Carter et al. 2009) and MTBX (this study), which show, apart from the Th anomaly, a similar pattern and absolute abundances. c) MTBX from Whistle (Bygnes 2011) and Parkin (this study). d) Felsic clasts within MTBX and MTBX (this study). e) MTBX (this study) in comparison the Felsic Levack Gneiss from Windy Lake (Péntek et al. 2011).

Table 3.1. Average major and trace element composition of MTBX and FWBX from Parkin and Whistle, with representative county rock lithologies.

	MTBX P Avg. n=14	MTBX WH WH-001 n=1	Clast Avg. n=2	IQD P Avg. n=112	QD P Avg. n=108	FWBX W Avg. n=16	MTBX W Avg. n=10	MTBX WP Avg. n=5	MBX WP Avg. n=3	FLG Avg. n=8	FWGN W 93PCL-202 n=1	FWMD W 92PCL-57 n=1
SiO_2 wt %	62.82	61.00	71.80	59.45	60.07	60.51	61.09	64.98	57.60	64.26	66.12	68.38
Al_2O_3 wt %	14.76	16.10	14.25	14.34	14.61	15.20	16.00	14.63	15.10	15.77	16.10	16.54
MnO wt %	0.08	0.09	0.02	0.11	0.10	0.09	0.08	0.07	0.10	0.07	0.04	0.01
MgO wt %	3.38	2.30	0.62	3.84	3.67	2.72	2.71	3.13	3.31	2.16	1.49	0.55
CaO wt %	2.97	2.68	1.17	5.03	4.76	3.88	3.52	2.59	2.94	4.60	2.75	1.71
Na_2O wt %	3.99	4.89	4.06	3.39	3.58	4.35	4.05	4.16	3.76	4.11	5.31	3.77
K_2O wt %	2.38	3.56	4.83	2.25	2.12	2.89	3.83	1.83	1.77	1.49	2.40	6.00
TiO_2 wt %	0.57	0.59	0.13	0.73	0.70	0.72	0.57	0.66	0.64	0.58	0.49	0.14
P_2O_5 wt %	0.17	0.27	0.06	0.21	0.19	0.24	0.30	0.13	0.11	n.a.	0.22	0.13
Fe_2O_3 wt %	6.35	6.02	1.72	8.15	7.58	0.47	6.29	6.39	11.21	n.a.	3.28	1.61
LOI wt %	2.21	1.46	0.85	2.77	1.30	0.78	1.34	1.83	2.93	1.47	1.66	0.97
Total	99.40	99.16	99.88	97.75	97.53	99.85	99.78	99.77	99.60	98.93	99.90	99.80
Ba ppm	782.14	1295.00	3170.00	664.46	593.21	1078.69	1721.46	741.42	497.05	587.50	1134.00	2454.00
Ce ppm	98.96	91.10	61.10	71.74	66.47	77.25	62.31	80.55	86.44	66.24	97.39	119.67
Co ppm	27.72	19.00	4.00	33.68	26.63	20.13	14.79	n.a.	n.a.	n.a.	7.00	n.d.
Cr ppm	126.29	50.00	20.00	115.29	115.09	107.94	196.55	198.25	158.39	n.a.	35.00	3.00
Cs ppm	1.09	0.28	0.22	2.03	2.40	0.40	0.45	n.a.	n.a.	0.39	0.29	0.36
Cu ppm	229.26	117.00	29.00	208.70	119.90	387.31	529.39	43.06	5947.32	22.34	63.00	11.00
Dy ppm	2.38	2.61	0.79	3.65	3.63	2.86	2.43	2.57	1.88	2.55	n.a.	n.a.
Er ppm	1.15	1.30	0.30	2.05	2.08	1.31	1.14	1.52	0.96	1.32	0.56	0.30
Eu ppm	1.39	1.56	1.19	1.42	1.33	1.56	1.44	1.37	1.18	1.44	1.68	1.73
Gd ppm	4.33	4.26	1.61	5.27	4.97	4.26	3.89	3.82	3.61	4.31	3.84	3.16
Hf ppm	4.61	6.30	3.05	3.72	3.81	4.10	5.18	4.79	4.73	1.66	n.a.	n.a.
Ho ppm	0.43	0.46	0.12	0.71	0.71	0.52	0.45	0.51	0.35	0.48	0.25	0.15
La ppm	49.69	46.70	33.00	35.50	32.29	38.25	35.73	41.14	42.76	32.03	50.44	66.82
Lu ppm	0.16	0.16	0.03	0.28	0.29	0.19	0.14	0.41	0.12	0.16	0.06	0.04
Nb ppm	6.84	5.40	2.35	7.98	8.23	5.76	5.78	9.54	10.55	6.00	4.15	1.28
Nd ppm	39.09	37.70	21.35	33.15	30.74	34.13	31.31	31.76	34.15	30.85	40.82	41.56

	MTBX P	MTBX WH	Clast	IQD P	QD P	FWBX W	MTBX W	MTBX WP	MBX WP	FLG	FWGN W	FWMD W
Ni ppm	309.79	175.00	19.50	209.84	107.70	231.88	122.16	54.39	1844.40	31.03	23.00	6.00
Pr ppm	11.05	10.05	6.33	8.90	8.25	9.10	8.40	9.02	9.77	8.07	11.41	13.47
Rb ppm	64.79	68.80	61.05	68.55	64.86	53.00	35.12	45.82	72.61	22.41	47.30	126.30
Sc ppm	11.69	11.00	2.50	18.72	17.55	12.95	9.86	11.32	7.29	n.a.	4.19	1.71
Sm ppm	6.11	6.46	2.96	5.85	5.51	5.90	5.41	5.28	5.51	5.22	5.90	5.14
Sr ppm	354.93	404.00	330.00	409.75	362.57	552.56	440.87	341.08	355.93	566.25	961.00	760.00
Ta ppm	0.31	0.10	0.05	0.48	0.52	0.23	0.20	0.63	0.31	0.28	0.16	n.d.
Tb ppm	0.51	0.53	0.18	0.70	0.68	0.56	0.49	0.52	0.42	0.52	0.43	0.33
Th ppm	14.38	6.04	10.84	7.67	7.59	4.02	3.25	15.11	15.12	2.15	4.85	15.43
Tm ppm	0.16	0.13	0.05	0.28	0.29	0.19	0.16	0.21	0.14	0.18	0.06	0.04
U ppm	1.18	0.56	0.32	1.44	1.68	0.48	0.33	2.22	0.79	0.28	0.34	0.35
V ppm	97.86	89.00	21.00	137.14	128.64	105.69	n.a.	107.78	87.34	81.25	48.00	17.00
Y ppm	11.39	12.30	3.50	18.65	18.62	15.37	11.25	12.56	7.95	12.34	5.80	3.60
Yb ppm	1.04	1.03	0.22	1.83	1.89	1.21	0.97	1.34	0.76	1.10	0.38	0.21
Zn ppm	76.64	54.00	38.00	77.28	66.27	76.38	71.57	42.64	89.20	n.a.	56.00	32.00
Zr ppm	176.04	236.00	117.50	144.83	142.57	187.00	n.d.	251.99	178.41	45.26	147.00	175.00

MTBX P = MTBX Parkin (this study), MTBX WH = MTBX Whistle (this study), IQD P = IQD Parkin (this study), QD P = QD Parkin (this study), FWBX W = FWBX Whistle (Carter et al. 2009), MTBX W = MTBX Whistle (Bygnes 2011), MTBX WP = MTBX Whistle-Parkin (Murphy and Spray 2002), MBX WP = Mafic Breccia Whistle-Parkin (Murphy and Spray 2002), FLG = Felsic Levack Gneiss (Péntek et al. 2011), FWGN = footwall gneiss (Lightfoot et al. 1997c), FWMD = footwall monzodiorite (Lightfoot et al. 1997c), LOI = Loss of ignition, n = number of analyses, n.a. = not analyzed.

The High-Field-Strength-Elements (HFSE) Zr, Hf, Ta and Nb are insoluble and very immobile during weathering and metamorphism and, thus, might represent the original composition of the parent rock. MTBX and FWBX (Fig. 3.5b) strongly correlate in the trace element pattern and absolute abundances with respect to the HFSE. They differ from QD and IQD (Fig. 3.5a), which show absolute abundances very similar to the Felsic Norite of the SIC. Figure 3.5c shows a comparison of the trace elements of MTBX from the Parkin and Whistle Dyke. Apart from the pronounced positive Th anomaly observed in MTBX from Parkin, whereas MTBX from Whistle show a slight negative anomaly in Th, the overall patterns are similar, even though some absolute values differ.

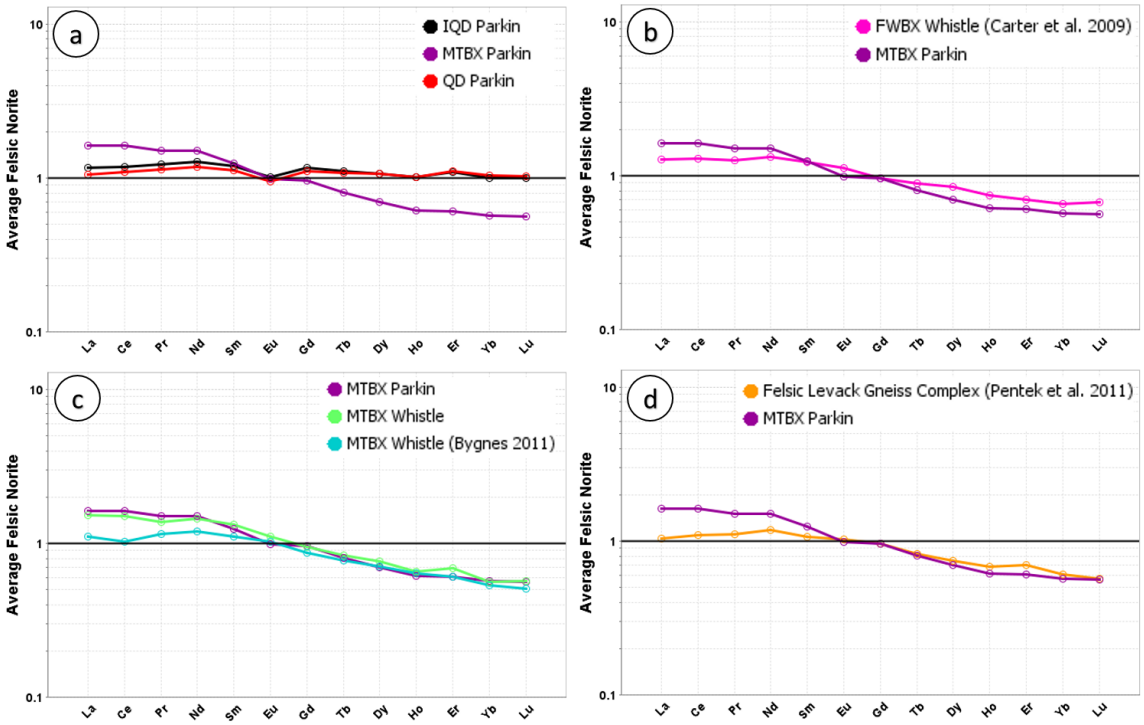

Figure 3.6. REE spider diagrams normalized to the Felsic Norite (Lightfoot et al. 1997b) showing a) IQD and QD in comparison to MTBX (this study). b) The similarities of MTBX (this study) and FWBX (Carter et al. 2009). c) MTBX (this study) from Parkin and Whistle (Bygnes 2011). d) MTBX (this study) and Felsic Levack Gneiss (Péntek et al. 2011).

The Th anomaly in MTBX from the Parkin Dyke has also been observed in two felsic clasts within MTBX from Parkin (Fig. 3.5d) and might be the source of Th enrichment within the Parkin MTBX. The Felsic Levack Gneiss (Péntek et al. 2011) (Fig. 3.4e) also displays a negative Th anomaly, similar to those of MTBX from Whistle. More importantly, it is accompanied by a pronounced negative anomaly in Zr and Hf, which can be attributed to a mafic component in the Levack Gneiss samples and is consistent with mafic clasts within the MTBX analyzed in this study. Rare Earth Element (REE) Spider plots of IQD, QD and MTBX normalized to the average Felsic Norite of the SIC (Lightfoot et al. 1997c) are shown in Figure 3.6a.

IQD and QD are markedly similar and close to the Felsic Norite of the SIC. While IQD and QD show a relatively flat pattern with no significant differences in Light REE (LREE) and Heavy REE (HREE), MTBX is enriched in LREE and depleted in HREE. This specific REE pattern corresponds to the pattern of FWBX (Fig. 3.6b) (Carter et al. 2009) and MTBX from the Whistle Offset Dyke (Fig. 3.6c) (Bygnes 2011) but is also consistent with the general trend of the Felsic Levack Gneiss Complex from the North Range (Péntek et al. 2011). The La vs. Sm plot in Figure 3.8 after Lightfoot et al. (1997a) shows QD and IQD plot nicely within an array of the SIC main mass. MTBX and FWBX samples certainly overlap with the QD and IQD fields; however, the majority of MTBX plot outside the QD and IQD fields, and even outside the main mass array. MTBX is more scattered displaying a wide variety of MTBX La/Sm compositions.

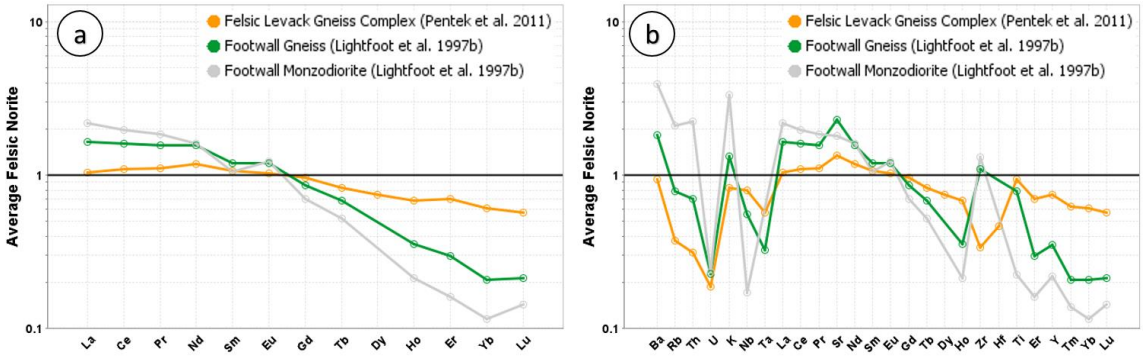

Figure 3.7. a) REE spider diagram and b) Trace element spider diagram of Felsic Levack Gneiss from Windy Lake (Péntek et al. 2011) in comparison to footwall gneiss and footwall monzodiorite from the Whistle embayment (Lightfoot et al. 1997b).

Felsic country rocks behave similarly in that they are scattered and do not plot within the array or the QD/IQD fields. Those elements are highly soluble in aqueous solutions, thus, mobile during weathering and their compositions might have been modified during alteration in those lithologies.

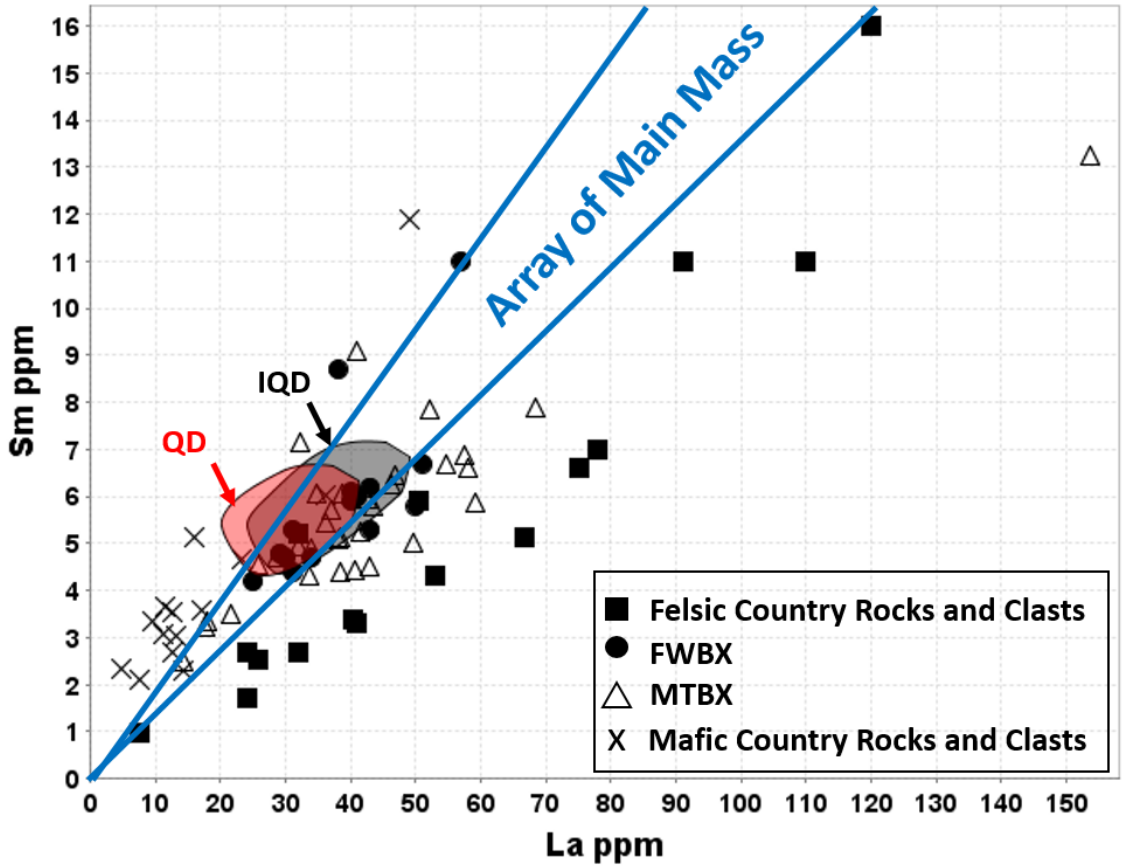

Figure 3.8. La vs. Sm illustrating the array of the main mass (Lightfoot et al. 1997a) and fields for QD (red) and IQD (black) from the Parkin Offset Dyke. The diagram shows the variations of MTBX, FWBX and numerous country rocks. QD and IQD Parkin (this study), felsic country rocks: Felsic Levack Gneiss (Péntek et al. 2011), footwall gneiss (Lightfoot et al. 1997c), footwall monzodiorite (Lightfoot et al. 1997c), felsic MTBX clasts (this study), Archean granite and Archean migmatite (Chai and Eckstrand 1994), Cartier Batholith and Levack Gneiss (Meldrum et al. 1997), felsic gneiss (Bygnes 2011); MTBX: MTBX Parkin and Whistle (this study), MTBX Whistle (Bygnes 2011), Radial and Mafic Breccia Whistle-Parkin (Murphy and Spray 2002); FWBX Whistle (Carter et al. 2009); mafic county rocks and clasts: mafic gneiss (Bygnes 2011), mafic MTBX clasts (this study).

3.7 Discussion

MTBX is an aphanitic, polymict, heterolithic, clast- to matrix-supported breccia, characterized by a meta-igneous texture, with severe signs of thermal overprint, extensive dynamic recrystallization and locally partial melting. IQD and QD show an igneous matrix crystallized from a melt with only minor occurrences of low grade recrystallization, while all three processes of dynamic recrystallization are characteristic for MTBX. With increasing temperature and decreasing stress these are: bulging (Baily and Hirsch 1962; Drury et al. 1985), subgrain rotation (Hobbs 1968; White 1976; Guillopé and Poirier 1979), and high temperature grain boundary migration recrystallization (Urai et al. 1986; Hirth and Tullis 1992; Dunlap et al. 1997; Stipp et al. 2002b). The primary, presumably igneous fabric of MTBX, has been completely replaced by a secondary fine-grained mosaic of new recrystallized grains with a wide range of grain sizes. The irregular to amoeboid, serrated grains with dark rims (Fig. 3.3b) are a result of high temperature grain boundary migration, which describes the movement of grain boundaries to remove dislocations that were caused by increased temperature and strain (Guillopé and Poirier 1979; Urai et al. 1986; Stipp et al. 2002a). Grain boundary migration is the dominant recrystallization mechanism at high temperatures of 500 to 700°C (Jessell 1987; Stipp et al. 2002b).

New smaller grains (Fig. 3.3c) are formed due to bulging, which is a characteristic feature of low temperature (300–400°C) and high strain recrystallization (Stipp et al. 2002b). The boundary of a grain with low dislocation density bulges into the neighbour grain with high dislocation density (Baily and Hirsch 1962; Drury et al. 1985; Shigematsu 1999; Stipp et al. 2002a). The bulge gets eventually pinched off by dissection (Tullis and Yund 1985) or fracturing (Stünitz et al. 2003) and included into the neighbour grain as a subgrain with original orientation (Blenkinsop 2002). Alternatively, the bulge can form an independent new grain by subsequent subgrain rotation and dissection from the host grain (Means 1981; Tungatt and Humphreys 1984; Drury et al. 1985). Subgrain rotation (Fig. 3.3d) occurs when a subgrain experiences increased crystallographic defects leading to a progressed missorientation, compared to the rest of the host grain or adjacent subgrains, and can eventually develop into new grains (Passchier and Trouw 2005). Subgrain rotation is very

common at medium temperatures of 400–500°C and medium strain rates (Lloyd and Freeman 1994; Stipp et al. 2002b).

The strain-free appearance and lack of ductile deformation features, such as preferred grain orientation, elongated or ribbon-shaped minerals, within the matrix of MTBX point to low strain rates and temperatures of more than 700°C (Blumenfeld et al. 1986; Mainprice et al. 1986), which is consistent with dynamic recrystallization. Undulose extinction and fractures in quartz grains correspond to very low-grade conditions below 300 °C. Embayed and indented quartz xenocrysts (Fig. 3.3a) distributed within the MTBX matrix represent relicts of the coarser-grained primary fabric. Undulose extinction and grain boundary migration observed in biotite grains in the MTBX matrix (Fig. 3.3f) refer to medium to high grade recrystallization (Bell 1998). Feldspar within MTBX characterized by brittle fracturing, cataclastic flow, undulose extinction and subgrains with diffuse boundaries corresponds to low grade metamorphism below 400°C (Tullis and Yund 1987; Passchier and Trouw 2005). Flame-perthite in K-feldspar and feldspathic micrographic intergrowth, observed with the MTBX matrix, is common at high temperatures over 600°C (Simpson 1985; Simpson and Wintsch 1989; Pryer 1993). Necklace structures (Fig. 3.4c) detected at the grain boundaries within quartzitic clasts formed by bulging and grain boundary migration (Ponge and Gottstein 1998). Core-and mantle features (Fig. 3.4e) represent relicts of old grains or aggregates that are surrounded by sheets of recrystallized grains, that form under conditions of low temperature and low strain (Gifkins 1976; White 1976; Shigematsu 1999). Chessboard textures observed in MTBX clasts (Fig. 3.4b) are composed of polygonal subgrains with different orientations and indicative of temperatures above 700°C (Blumenfeld et al. 1986; Mainprice et al. 1986; Stipp et al. 2002b). The recrystallization is present throughout MTBX samples from different locations and there appears to be no relationship between intensity of recrystallization and metasomatized or alteration-affected zones. This suggests that the recrystallization is not a result of post-impact hydrothermal alteration, although hydrothermal alteration certainly affected MTBX after the impact to some extent. Secondary minerals chlorite, epidote and calcite are associated with mafic minerals within MTBX and are a result of hydrothermal alteration, which is in accordance to previous observations (Bygnes 2011).

An important observation is that MTBX is present as inclusions within QD and as pods intermingling with QD indicating that MTBX already existed when the Parkin Offset Dyke was emplaced. There are no chilled or baked contacts between QD/IQD and MTBX suggesting that MTBX was hot enough to not dramatically cool down the dyke melts or cause reactions between MTBX and the hot dyke melts. The light-coloured, grey-white-pink FWBX (Fig. 3.10a) is also composed of mainly quartz and feldspar, is usually coarser-grained than MTBX, and shows diffuse matrix-clast contacts making it difficult to differentiate between clasts and matrix. The matrix is characterized by poikilitic to poikiloblastic texture, i.e. large, irregular-shaped grains of quartz containing inclusions of plagioclase (Fig. 3.10b), which coincides with previous studies (Pattison 1979; Deutsch et al. 1989). This is very similar to the poikilitic texture locally observed in MTBX (Fig. 3.3e), which points to textural similarities between MTBX and FWBX. Signs of partial melting and local recrystallization features are also detected within the matrix of FWBX. Planar deformation features (Fig. 3.4d) detected within clasts of MTBX have been reported from FWBX (Lakomy 1990) but, so far, not from QD or IQD.

Geochemical data suggests that MTBX is not genetically related to QD or IQD; although the differences between MTBX and QD/IQD are not distinctive and only detectable in detail. However, both lithologies, even though they formed under different conditions and due to completely different processes, originated from the same basement rocks, and thus, share signatures of those basement rocks. MTBX and FWBX show only limited variations of trace element abundances and have a specific pattern in common that also corresponds to basement rocks. The spider plots of country lithologies representative for the area have markedly similar patterns to MTBX and FWBX, but their differing absolute values also reflect a wide range of compositions and heterogeneity in the country rocks, which likely explains why MTBX and FWBX from Parkin and Whistle also vary in composition.

Large-Ion-Lithophile-Elements (LILE) such as K, Rb, Sr and Ba are similar in MTBX and QD/IQD. While FWBX (Fig. 3.5b) does not show any pronounced anomaly in Sr and a positive anomaly in Th, MTBX displays a negative Sr, a negative Th and a more pronounced negative U anomaly. Otherwise, the trace element patterns and the absolute values of MTBX and FWBX are markedly similar. The small negative Sr and Eu anomalies

found in QD/IQD (Fig. 3.5a) and to a lesser extend in MTBX suggests that both rocks did not or only less plagioclase feldspar. Alternatively, post-impact alteration could have also decreased the abundances of Eu. The K anomaly in QD/IQD, also characteristic for MTBX (Fig 3.5a), is most likely related to post-impact alteration and K-metasomatism (Carter et al. 2009). The depletion of HREE, as detected in MTBX, usually points to the fractionation of garnet and was most likely inherited from FWBX (Fig. 3.5b) and its precursor Archean country rocks (Fig. 3.5e). While MTBX shows a positive Th anomaly, FWBX is characterized by a negative Th anomaly (Fig. 3.5b), which was possibly caused by enrichment of Th in MTBX due to anatexis and thermal metamorphism of FWBX. The trace element similarities of QD/IQD and the Felsic Norite (Fig. 3.5a) reflect a possible relationship between both units and could suggest that the original composition of the Offset Dyke melt was close to the present composition of the Felsic Norite.

The La vs. Sm plot (Fig. 3.8) shows the main mass array defined by Lightfoot et al. (1997a). These authors explained the tight linear array formed by the main mass lithologies by a fractionation process, where the ratio of La/Sm remained constant. The majority of QD and IQD fall into this array, which led Lightfoot et al. (1997a) to suggest that both dyke lithologies originated from the main mass of the SIC. Geochemical data QD/IQD from Parkin also corresponds to those results by Lightfoot et al. (1997a), indicating a genetic relationship between the main mass of the SIC and the Offset Dykes.

The overlap of some MTBX and FWBX with the QD and IQD fields (Fig. 3.9) can be attributed to the same precursor country rocks. A mix of Archean crustal rocks and Huronian sediments is the main source of the proto-SIC (Gibbins and McNutt 1975; Hurst and Farhat 1977; Kuo and Crocket 1979; Faggart et al. 1985; Walker et al. 1991; Dickin et al. 1992, 1996, 1999; Golightly 1994; Grieve 1994; Ostermann et al. 1996; Morgan et al. 2002), and consequently also of the Offset Dykes. Archean basement rocks also represent the precursor rocks for FWBX and MTBX, which would explain why the Offset Dykes and MTBX show some similarities, despite their different formation process.

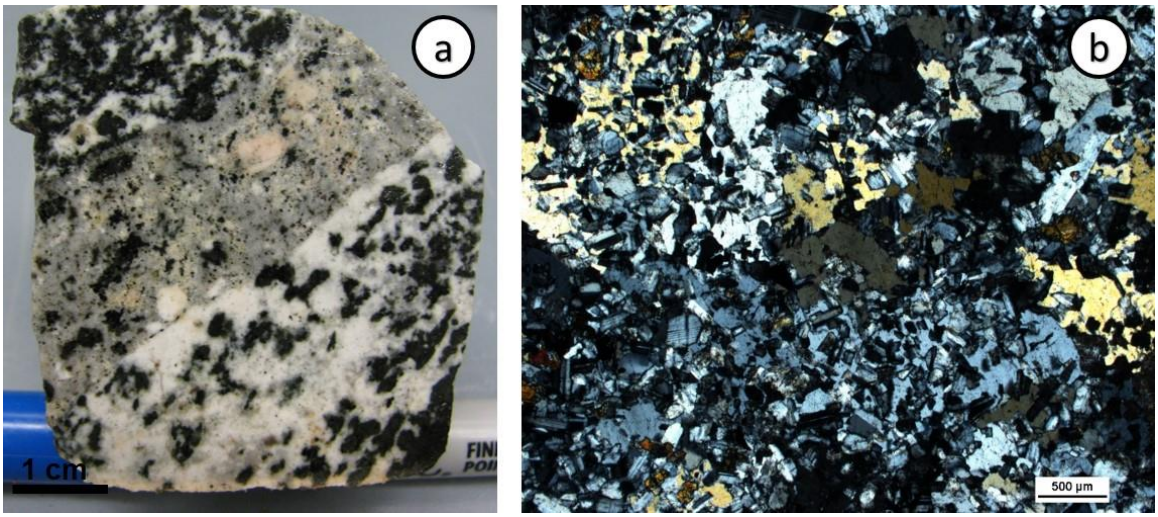

Figure 3.9. a) Photograph of a MTBX hand sample. b) Photomicrograph displaying the typical poikilitic texture within FWBX, which is similar to the poikilitic texture locally observed in MTBX (compare Fig. 3.3e).

Based on the petrographic and geochemical observations of this study, FWBX can be considered as the closest analogue to MTBX and it seems more likely that MTBX is, in fact, metamorphosed and thermally overprinted FWBX, as originally proposed by Farrow and Lightfoot (2002). FWBX formed as a result of shattering and crushing of basement rock material and subsequent partial melting by the SIC in the North Range of the Sudbury structure (Lakomy 1990; Lightfoot et al. 1997b; McCormick 2002). It extends gradationally up to 100 m into the footwall rocks (McCormick 2002). We propose that FWBX was ripped off and mobilized during the emplacement of the Offset Dykes and incorporated into the melt as partially molten "clasts". Subsequent thermal overprint by the heat of the cooling Offset Dykes led to further recrystallization and partial melting of FWBX resulting in the formation of MTBX. The initial temperature of the SIC has been estimated in the range of 1700°C (Ivanov and Deutsch 1999; Zieg and Marsh 2005) to 2000°C and higher (Grieve 1977, 1994). Assuming an initial temperature of at least 1800°C and a cooling process involving conductive and convective heat transfer, the melt sheet cooled down to the liquidus within about 10,000 years and complete solidification took approximately 56,000 to 75,000 years (Prevec and Cawthorn 2002; Zieg and Marsh 2005). Consequently, FWBX was subjected to temperatures above 1000°C (Lakomy 1990) and

even the contact aureole up to 1 km from the SIC showed temperatures of more than 600°C (Prevec and Cawthorn 2002), which provides an explanation for sharp contacts and the lack of chilled or baked rims between MTBX and QD/IQD. After crushing and shattering, FWBX was affected by batch partial melting and complete melting and to a lesser extent by recrystallization. MTBX, in contrast was mainly subject to dynamic recrystallization, which is the result of elevated temperatures caused by the dyke melt and the SIC.

MTBX and FWBX present a trace element and REE pattern similar to that of various country rocks, with a LREE enrichment and HREE depletion, although variations in absolute values exist. QD and IQD show a strong correlation in trace elements and REEs, but differ from MTBX, FWBX and country rocks. Element compositions in MTBX samples vary based on different factors:

i. The original composition of the FWBX, which in turn depends on the composition of the precursor country rock. The Levack Gneiss Complex, the precursor of the Whistle FWBX, is composed of a wide variety of different rock types ranging from tonalitic orthogneiss, diorite and granodiorite, biotite paragneiss to mafic gneiss, gabbro, and pyroxenite, which are intruded by Matachewan Diabase and Cartier Batholith (Card 1994).
ii. The type (batch, fractional or collection melting) and, more importantly, the degree of partial melting, leading to the modification in compatible and incompatible trace elements in FWBX. Fractional partial melting of footwall rocks and subsequent remobilization led to the formation of small dioritic veins throughout the FWBX (Lightfoot et al. 1997c) and, thus, to modification of the composition of the restite solid rock. This resulted in a wide variety of FWBX compositions.
iii. Temperature and stress conditions during the formation of MTBX, which depend on the original temperature of the Offset Dyke melts, the distance from the SIC as a long term heat source and the emplacement mechanism;
iv. Low degree partial melting might have locally continued in MTBX after the emplacement of the dykes. Estimated temperatures of the dyke melts range from 1450°C (Hecht et al. 2008) to 1700°C (Ostermann et al. 1996). Dynamic

recrystallization did not contribute to compositional changes in the MTBX, but only alters textural and microstructural features.

All impact lithologies, including QD and IQD, which are assumed to have formed from melts of the SIC, originate from a mix of target rocks, and thus, will all show geochemical signatures similar to those of the target rocks. Small varieties in composition exist between MTBX from Whistle and Parkin and it seems that Whistle MTBX shows a stronger correlation to the FWBX observed in the Whistle embayment. The Whistle Offset Dyke is located closer to the SIC than the Parkin Offset Dyke and, thus, would have been subjected to higher temperatures from the contact aureole of the SIC, leading to higher degrees of partial melting. Incompatible element concentrations in the solid rock will decrease with increasing degree of partial melting. Inclusions of MTBX within the Offset Dykes indicate that at least part of the MTBX/FWBX already existed when the dykes were emplaced. The cross cutting relationships of FWBX and other impact lithologies are controversial and complex. Clasts of pseudotachylytic Sudbury Breccia (SDBX) within the FWBX have been reported (Lakomy 1990), indicating that the formation of SDBX was already in progress when FWBX started to form. On the other hand, Sudbury Breccia has also been observed to intrude FWBX (Dressler 1984b); although this has not been confirmed since. The timing of the formation of both breccia lithologies may have overlapped and both FWBX and Sudbury Breccia formed early in the development of the Sudbury impact structure (Dressler 1984b). FWBX also contains Sublayer inclusion (Lightfoot et al. 1997c) suggesting that FWBX is younger than the Sublayer, or was emplaced during the solidification of the Sublayer (Pattison 1979; McCormick 2002). Considering that FWBX was included in the Offset Dyke melts, this would place the earliest timing of emplacement of the Offset Dykes during or after the solidification of the Sublayer. MTBX is only existent in the proximal part of the Parkin Offset Dyke; the distal Parkin Offset Dyke beyond Milnet Mine only contains small mm to cm sized inclusions (Coulter 2016), can be attributed to the dyke melt losing energy with increasing distance from the SIC, so that large MTBX clasts could not be transported to the northern part of the dyke.

MTBX is mainly present in the North Range of the Sudbury impact structure and has been reported from the Southern Parkin, Whistle, Trill and Foy Offset Dykes, and possibly exists

at the historical Victoria mine of the Worthington Offset Dyke in the South Range (personal communication with Wallbridge Mining Company). This coincides with the fact that FWBX is much less common in the South Range and mainly exists in the North Range of the Sudbury impact structure (Grant and Bite 1984; Deutsch et al. 1995).

3.8 Summary and conclusions

Field observations, petrographic, and geochemical investigations carried out in this study do not support a genetic relationship between QD/IQD and MTBX and, thus, the hypothesis of a similar formation processes for MTBX and QD/IQD, as proposed by Murphy and Spray (2002) and Lafrance et al. (2014). Based on the observations of this study, FWBX can be considered as the closest analogue to MTBX and it seems more likely that MTBX is, in fact, metamorphosed and thermally overprinted FWBX, as originally proposed by Farrow and Lightfoot (2002). It is proposed FWBX was ripped off when the dyke melt was injected into fractures within the country rock and was recrystallized by the heat of the Offset Dykes, forming MTBX. MTBX has only been detected in the North Range, however, it seems likely that more MTBX, which has yet to be identified, exist around the Sudbury structure. Based on the higher post-impact deformation processes in the South Range, it might be more difficult to identify MTBX. MTBX and IQD are very often indistinguishable in the field, and many researchers are not aware of the existence of MTBX after all, which might have led to the misidentification of MTBX as IQD. This is aggravated by the fact that the words FWBX, leucocratic breccia (Lightfoot et al. 1997c), Granite Breccia, Late Granite Breccia and anatexite are used interchangeably throughout the literature by researchers and mining companies to describe MTBX leading to confusion in the terminology. It is suggested that further studies on these MTBX-like lithologies be carried out.

3.9 References

Anders, D., Osinski, G.R., Grieve, R.A.F., Brillinger, D.T.M., 2015. The Basal Onaping Intrusion in the North Range: Roof rocks of the Sudbury Igneous Complex. Meteorit. Planet. Sci. 50, 1577–1594.

Baily, J.E., Hirsch, P.B., 1962. The recrystallization process in some polycrystalline metals. Proc. R. Soc. London 11–30.

Bell, T.H., 1998. Recrystallization of biotite by subgrain rotation, in: Snoke, A., Tullis, J., Todd, V.R. (Eds.), Fault Related Rocks – a Photographic Atlas. Princeton University Press, New Jersey, pp. 272–273.

Blenkinsop, T., 2002. Deformation microstructures and mechanisms in minerals and rocks.

Blumenfeld, P., Mainprice, D., Bouchez, J.L., 1986. C-slip in quartz from subsolidus deformed granite. Tectonophysics 127, 97–115.

Brocoum, S.T., Dalziel, I.W.D., 1974. The Sudbury Basin, the Southern Province, the Grenville Front, and the Penokean Orogeny. Geol. Soc. Am. Bull. 85, 1571–1850.

Bygnes, L.C., 2011. Emplacement of metabreccia and Cu-PGE-rich sulfide veins along the Whistle offset of the Sudbury impact structure. Laurentian University.

Card, K.D., 1994. Geology of the Levack gneiss complex, the northern footwall of the Sudbury structure, Ontario. Geol. Surv. Canada Curr. Res. 1994-C, 269–278.

Card, K.D., Gupta, V.K., McGrath, P.H., Grant, F.S., 1984. The Sudbury Structure: Its Regional Geological and Geophysical Setting, in: Pye, E.G., Naldrett, A.J., Giblin, P.E. (Eds.), The Geology and Ore Deposits of the Sudbury Structure. pp. 25–44.

Carter, W.M., Watkinson, D.H., Ames, D.E., Jones, P.C., 2009. Quartz Diorite Magmas and Cu-(Ni)-PGE Mineralization, Podolsky Deposit, Whistle Offset Structures, Sudbury, Ontario. Geol. Surv. Canada Open File 6134, 58 pp.

Chai, G., Eckstrand, R., 1994. Rare-earth element characteristics and origin of the Sudbury Igneous Complex, Ontario, Canada. Chem. Geol. 113, 221–244.

Coulter, A.B., 2016. Recent Discoveries in the Ni-Cu-PGE bearing Trill and Parkin Offset dykes, Sudbury impact structure, Canada. M.Sc. Thesis, West. Univ. Dep. Earth Sci. Electron. Thesis Diss. Repos. Paper 3473.

Deutsch, A., 1994. Isotope systematics support the impact origin of the Sudbury Structure (Ontario, Canada), in: Dressler, B.O., Grieve, R.A.F., Sharpton, V.L. (Eds.), Large Meteorite Impacts and Planetary Evolution I, GSA Special Paper 293. pp. 289–302.

Deutsch, A., Grieve, R.A.F., 1994. The Sudbury Structure: Constraints on its genesis from Lithoprobe results. Geophys. Res. Lett. 21, 963–966.

Deutsch, A., Grieve, R.A.F., Avermann, M., Bischoff, L., Brockmeyer, P., Buhl, D., Lakomy, R., Müller-Mohr, V., Ostermann, M., Stöffler, D., 1995. The Sudbury Structure (Ontario, Canada): a tectonically deformed multi-ring impact basin. Geol. Rundschau 84, 697–709.

Deutsch, A., Lakomy, R., Buhl, D., 1989. Strontium-and neodymium-isotopic characteristics of a heterolithic breccia in the basement of the Sudbury impact structure, Canada. Earth Planet. Sci. Lett. 93, 359–370.

Dickin, A.P., Artan, M.A., Crocket, J.H., 1996. Isotopic evidence for distinct crustal sources of North and South Range ores, Sudbury Igneous Complex. Geochim. Cosmochim. Acta 60, 1605 – 1613.

Dickin, A.P., Nguyen, T., Crocket, J.H., 1999. Isotopic evidence for a single impact melting origin of the Sudbury Igneous Complex, in: Dressler, B.O., Sharpton, V.L. (Eds.), Large Meteorite Impacts and Planetary Evolution II, GSA Special Paper 339. pp. 361–371.

Dickin, A.P., Richardson, J.M., Crocket, J.H., McNutt, R.H., Peredery, W. V., 1992. Osmium isotope evidence for a crustal origin of platinum group elements in the Sudbury nickel ore, Ontario, Canada. Geochim. Cosmochim. Acta 56, 3531 – 3537.

Dressler, B.O., 1984. The effects of the Sudbury event and the intrusion of the Sudbury Igneous Complex on the footwall rocks of the Sudbury structure, in: Pye, E.G., Naldrett, A.J., Giblin, P.E. (Eds.), The Geology and Ore Deposits of the Sudbury Structure. pp. 97–138.

Dressler, B.O., Peredery, W. V., Muir, T.L., 1992. Geology and Mineral Deposits of the

Sudbury Structure. Ontario Geological Survey Guidebook 8.

Drury, M.R., Humphreys, F.J., White, S.H., 1985. Large strain deformation studies using polycrystalline magnesium as a rock analogue. Part II: dynamic recrystallization mechanisms at high temperatures. Phys. Earth Planet. Inter. 40, 208–222.

Dunlap, W.J., Hirth, G., Teyssier, C., 1997. Thermomechanical evolution of a ductile duplex. Tectonics 16, 983.

Faggart, B.E., Basu, A.R., Tatsumoto, M., 1985. Origin of the Sudbury complex by meteoritic impact: Neodymium isotopic evidence. Science (80-.). 230, 436–439.

Farrow, C.E.G., Everest, J.O., King, D.M., Jolette, C., 2005. Sudbury Cu-(Ni)-PGE-Systems: Refining the classification: Using McCreedy West Mine, and Podolski project case studies, in: Mungall, J.E. (Ed.), Exploration for Platinum- Group Elements Deposits. Mineralogical Association of Canada, Short Course Series Volume 35, pp. 163–180.

Farrow, C.E.G., Lightfoot, P.C., 2002. Sudbury PGE Revisited: Towards an Integrated Model, in: Cabri, L.J. (Ed.), Geology, Geochemistry, Mineralogy and Mineral Beneficiation of Platinum-Group Elements. Canadian Institute of Mining, Metallurgy and Petroleum, Special Volume 54, pp. 273–297.

Gibbins, W.A., McNutt, R.H., 1975. The Age of the Sudbury Nickel Irruptive and the Murray Granite. Can. J. Earth Sci. 12, 1970–1989.

Gifkins, R.C., 1976. Grain-boundary sliding and its accommodation during creep and superplasticity. Metall. Trans. 7, 1225–1232.

Golightly, J.P., 1994. The Sudbury Igneous Complex as an impact melt: evolution and ore genesis, in: Lightfoot, P.C., Naldrett, A.J. (Eds.), Proceedings of the Sudbury-Noril'sk Symposium. Ontario Geological Survey Special Volume 5, pp. 105–118.

Grant, R.W., Bite, A., 1984. Sudbury Quartz Diorite Offset Dikes, in: Pye, E.G., Naldrett, A.J., Giblin, P.E. (Eds.), The Geology and Ore Deposits of the Sudbury Structure. pp.

275–300.

Grieve, R.A.F., 1977. Cratering processes-As interpreted from the occurrence of impact melts, in: Roddy, D.J., Pepin, R.O., Merrill, R.B. (Eds.), Impact and Explosion Cratering. Pergamon Press, New York, pp. 791–814.

Grieve, R.A.F., 1991. Terrestrial impact: The record in the rocks. Meteoritics 26, 175–194.

Grieve, R.A.F., 1994. An Impact Model of the Sudbury Structure, in: Lightfoot, P.C., Naldrett, A.J. (Eds.), Proceedings of the Sudbury-Noril'sk Symposium. Ontario Geological Survey Special Volume 5, pp. 119–132.

Guillopé, M., Poirier, J.P., 1979. Dynamic recrystallization during creep of single-crystalline halite: an experimental study. J. Geophys. Res. 84, 5557–5567.

Heaman, L.M., 1997. Global mafic magmatism at 2.45 Ga: remnants of an ancient large igneous province? Geology 25, 299.

Hecht, L., Wittek, A., Riller, U., Mohr, T., Schmitt, R.T., Grieve, R.A.F., 2008. Differentiation and emplacement of the Worthington Offset Dike of the Sudbury impact structure, Ontario. Meteorit. Planet. Sci. 43, 1659–1679.

Hirth, G., Tullis, J., 1992. Dislocation creep regimes in quartz aggregates. J. Struct. Geol. 14, 145–159.

Hobbs, B.E., 1968. Recrystallization of single crystals of quartz. Tectonophysics 6, 353–401.

Hurst, R.W., Farhat, J., 1977. Geochronologic investigations of the Sudbury Nickel Irruptive and the Superior Province granites north of Sudbury. Geochim. Cosmochim. Acta 41, 1803–1815.

Ivanov, B.A., Deutsch, A., 1999. Sudbury impact event: Cratering mechanics and thermal history, in: Dressler, B.O., Sharpton, V.L. (Eds.), Large Meteorite Impacts and Planetary Evolution II, GSA Special Paper 339. pp. 389–398.

Jessell, M.W., 1987. Grain-boundary migration microstructures in a naturally deformed quartzite. J. Struct. Geol. 9, 1007–1014.

Krogh, T.E., Davis, D.W., Corfu, F., 1984. Precise U–Pb zircon and baddeleyite ages for the Sudbury area, in: Pye, E.G., Naldrett, A.J., Giblin, P.E. (Eds.), The Geology and Ore Deposits of the Sudbury Structure. pp. 431–447.

Kuo, H.Y., Crocket, J.H., 1979. Rare earth elements in the Sudbury Nickel Irruptive; comparison with layered gabbros and implications for nickel irruptive petrogenesis. Econ. Geol. 74, 590–605.

Lafrance, B., Bygnes, L.C., 2014. Emplacement of metabreccia along the Whistle offset dike, Sudbury: implications for post-impact modification of the Sudbury impact structure. Can. J. Earth Sci. 19, 1–19.

Lakomy, R., 1990. Implications for cratering mechanics from a study of the Footwall Breccia of the Sudbury impact structure, Canada. Meteorit. Planet. Sci. 25, 195–207.

Lightfoot, P.C., Doherty, W., Farrell, K.P., Keays, R.R., Pedeski, D., 1997a. Geochemistry of the main mass, sublayer, offset dikes, and inclusions from the Sudbury Igneous Complex. Ontario Geol. Surv. Open File 5959, 231 pp.

Lightfoot, P.C., Farrow, C.E.G., 2002. Geology, geochemistry, and mineralogy of the Worthington offset dike: A genetic model for offset dike mineralization in the Sudbury Igneous Complex. Econ. Geol. 97, 1419–1446.

Lightfoot, P.C., Keays, R.R., Morrison, G.G., Bite, A., Farrell, K.P., 1997b. Geochemical relationships in the Sudbury igneous complex; origin of the main mass and offset dikes. Econ. Geol. 92, 289–307.

Lightfoot, P.C., Keays, R.R., Morrison, G.G., Bite, A., Farrell, K.P., 1997c. Geologic and geochemical relationships between the contact sublayer, inclusions, and the main mass of the sudbury igneous complex: A Case study of the whistle mine embayment. Econ. Geol. 92, 647–673.

Lightfoot, P.C., Naldrett, A.J., Morrison, G.G., 1997d. Sublayer and offset dikes of the Sudbury Igneous Complex: An introduction and field guide. Ontario Geol. Surv. Open File 5965, 50 pp.

Lloyd, G.E., Freeman, B., 1994. Dynamic recrystallisation of quartz and quartzites. J. Struct. Geol. Geol 16, 867–881.

Mainprice, D., Bouchez, J.L., Blumenfeld, P., Tubia, J.M., 1986. Dominant c-slip in naturally deformed quartz: implications for dramatic plastic softening at high temperature. Geology 14, 819–822.

McCormick, K.A., 2002. A textural, mineralogical, and statistical study of the footwall breccia within the Strathcona embayment of the Sudbury structure. Econ. Geol. 97, 125–143.

Means, W.D., 1981. The concept of steady-state foliation. Tectonophysics 78, 179–200.

Meldrum, A., Abdel-Rahman, A.F.M., Martin, R.F., Wodicka, N., 1997. The nature, age and petrogenesis of the Cartier Batholith, northern flank of the Sudbury Structure, Ontario, Canada. Precambrian Res. 82, 265–285.

Morgan, J.W., Walker, R.J., Horan, M.F., Beary, E.S., Naldrett, A.J., 2002. 190Pt – 186Os and 187Re – 187Os systematics of the Sudbury Igneous Complex, Ontario. Geochim. Cosmochim. Acta 66, 273–290.

Murphy, A.J., Spray, J.G., 2002. Geology, mineralization and emplacement of the Whistle–Parkin offset dike, Sudbury impact structure. Econ. Geol. 97, 1369–1389.

Ostermann, M., Schärer, U., Deutsch, A., 1996. Impact melt dikes in the Sudbury multi-ring basin (Canada): Implications from uranium-lead geochronology on the Foy Offset Dike. Meteorit. Planet. Sci. 31, 494–501.

Passchier, C.W., Trouw, R.A.J., 2005. Microtectonics, 2nd, Revis. ed. Springer-Verlag Berlin.

Pattison, E.F., 1979. The Sudbury Sublayer. Can. Mineral. 17, 257–274.

Péntek, A., Molnár, F., Watkinson, D.H., Jones, P.C., Aberra, M., 2011. Partial melting and melt segregation in footwall units within the contact aureole of the Sudbury Igneous Complex (North and East Ranges, Sudbury structure), with implications for their relationship to footwall Cu–Ni–PGE mineralization. Int. Geol. Rev. 53, 291–325.

Ponge, D., Gottstein, G., 1998. Necklace formation during dynamic recrystallization: mechanisms and impact on flow behavior. Acta Mater. 46, 69 – 80.

Prevec, S.A., Cawthorn, R.G., 2002. Thermal evolution and interaction between impact melt sheet and footwall: A genetic model for the contact sublayer of the Sudbury Igneous Complex, Canada. J. Geophys. Res. 107, 1–14.

Pryer, L.L., 1993. Microstructures in feldspars from a major crustal thrust zone: the Grenville Front, Ontario, Canada. J. Struct. Geol. 15, 21–36.

Shigematsu, N., 1999. Dynamic recrystallization in deformed plagioclase during progressive shear deformation. Tectonophysics 305, 437–452.

Simpson, C., 1985. Deformation of granitic rocks across the brittle-ductile transition. J. Struct. Geol. 7, 503–511.

Simpson, C., Wintsch, R.P., 1989. Evidence for deformation-induced K-feldspar replacement by myrmekite. J. Metamorph. Geol. 7, 261–275.

Sims, P.K., Van Schmus, W.R. V., Schulz, K.J., Peterman, Z.E., 1989. Tectono-stratigraphic evolution of the Early Proterozoic Wisconsin magmatic terranes of the Penokean Orogen. Can. J. Earth Sci. 26, 2145–2158.

Souch, B.E., Podolsky, T., Staff, G., 1969. The sulfide ores of Sudbury: their particular relationship to a distinctive inclusion-bearing species of the Nickel Irruptive., in: Wilson, H.D.B. (Ed.), Magmatic Ore Deposits - A Symposium. Economic Geology Monogaph 4, p. 366.

Spray, J.G., Butler, H.R., Thompson, L.M., 2004. Tectonic influences on the morphometry of the Sudbury impact structure: Implications for terrestrial cratering and modeling. Meteorit. Planet. Sci. 39, 287–301.

Stipp, M., Stunitz, H., Heilbronner, R., Schmid, S.M., 2002a. Dynamic recrystallization of quartz: correlation between natural and experimental conditions. Geol. Soc. London, Spec. Publ. 200, 171–190.

Stipp, M., Stünitz, H., Heilbronner, R., Schmid, S.M., 2002b. The eastern Tonale fault zone: a "natural laboratory" for crystal plastic deformation of quartz over a temperature range from 250 to 700 °C. J. Struct. Geol. 24, 1861–1884.

Stöffler, D., Deutsch, A., Avermann, M., Bischoff, L., Brockmeyer, P., Buhl, D., Lakomy, R., Müller-Mohr, V., 1992. The formation of the Sudbury structure, Canada, Toward a unified impact model. Geol. Soc. Am. Spec. Pap. 293, 303–318.

Stünitz, H., Fitz Gerald, J.D., Tullis, J., 2003. Dislocation generation, Slip Systems, and dynamic recrystallization in experimentally deformed plagioclase single crystals. Tectonophysics 372, 215–233.

Therriault, A.M., Fowler, A.D., Grieve, R.A.F., 2002. The Sudbury Igneous Complex: A differentiated impact melt sheet. Econ. Geol. 97, 1521–1540.

Tullis, J., Yund, R.A., 1985. Dynamic recrystallization of feldspar — a mechanism for ductile shear zone formation. Geology 13, 238–241.

Tullis, J., Yund, R.A., 1987. Transition from cataclastic flow to dislocation creep of feldspar: mechanisms and microstructures. Geology 15, 606–609.

Tungatt, P.D., Humphreys, F.J., 1984. The plastic deformation and dynamic recrystallisation of polycrystalline sodium nitrate. Acta Metall. 32, 1625 – 1635.

Urai, J.L., Means, W.D., Lister, G.S., 1986. Dynamic recrystallization of minerals, in: Mineral and Rock Deformation: Laboratory Studies, the Paterson Volume Geophys Monogr 36. American Geophysical Union, Washington DC, pp. 161–200.

Walker, R.J., Morgan, J.W., Naldrett, A.J., 1991. Re-Os isotope systematics of Ni-Cu sulfide ores, Sudbury Igneous Complex, Ontario: evidence for a major crustal component. Earth Planet. Sci. Lett. 105, 416–429.

White, S.H., 1976. The role of dislocation processes during tectonic deformation with special reference to quartz, in: Strens, R.J. (Ed.), The Physics and Chemistry of Minerals and Rocks. Wiley, London, pp. 75–91.

Zieg, M.J., Marsh, B.D., 2005. The Sudbury Igneous Complex: Viscous emulsion differentiation of a superheated impact melt sheet. Geol. Soc. Am. Bull. 117, 1427–1450.

4 Formation and Emplacement of Metabreccia – Evidence from the Trill and Foy Offset Dykes[3]

Denise Anders, Gordon R. Osinski, and Richard A. F. Grieve

4.1 Introduction

The 1.85 Ga (Krogh et al. 1984) Sudbury impact structure (Fig. 4.1) is generally considered to be a remnant of a peak ring or multi-ring impact basin (Stöffler et al. 1989, 1992; Deutsch and Grieve 1994; Deutsch et al. 1995; Spray and Thompson 1995). With an estimated original diameter ranging approximately between 150–200 km (Stöffler et al. 1992; Deutsch and Grieve 1994; Grieve 1994; Deutsch et al. 1995; Grieve et al. 2008), it is one of the largest impact structures on Earth. The Sudbury Basin comprises an extensively differentiated impact melt sheet (Faggart et al. 1985; Grieve 1991; Dickin et al. 1992, 1996; Deutsch 1994; Lightfoot et al. 1997a, 1997b), composed from bottom to top of the so-called Sublayer, Norite, Transition Zone Quartz Gabbro, Granophyre (Dressler et al. 1992; Therriault et al. 2002) and Upper Contact Unit (former Basal Member or Onaping Intrusion) (Anders et al. 2015). The so-called radial Offset Dykes emanate from embayments of the SIC (Grant and Bite 1984) and are composed of two major granodioritic lithologies: the mineralized so-called 'Inclusion-rich Quartz Diorite' (IQD), and the coarser-grained 'Quartz Diorite' (QD), which usually contains less clasts and mineralization (Lightfoot et al. 1997a, 1997c; Lightfoot and Farrow 2002; Hecht et al. 2008). A third dyke phase, the so-called Metabreccia (MTBX), is mainly associated with the North Range Offset Dykes. It has been reported from the Parkin (Murphy and Spray 2002) and Whistle Offset Dykes (Lafrance and Bygnes 2014); and in the embayments of Ministic and Foy Offset Dykes (Grant and Bite 1984). It has been described as an intensely brecciated and melted crustal rock within the North Range Offset Dykes (Souch et al. 1969) and was later interpreted as siliceous, recrystallized Footwall Breccia (FWBX) (Grant and Bite 1984). According to its suggested origin as a result of thermal metamorphism of FWBX during the cooling of the SIC and/or the Offset Dykes, it was named Metabreccia

[3] This chapter will be submitted to the Canadian Journal of Earth Sciences.

(Farrow et al. 2005). More recent studies, however, proceeded on the assumption that it was formed, similar to the formation of QD and IQD, by injection of a melt originating from the proto-SIC into offset faults around the Sudbury structure during excavation and modification stage (Lightfoot et al. 1997c; Murphy and Spray 2002; Giroux and Benn 2005; Lafrance and Bygnes 2014). MTBX is an important host for Platinum-Group-Element (PGE) mineralization and, in particular, known for its sulfide deposits at the Whistle and Podolsky Mine of the Whistle Offset Dyke. Despite its economic importance, its origin remains debated. Understanding the formation of MTBX and, thus, the Offset Dykes is a crucial detail in understanding the process of crater formation at Sudbury. In Chapter 3, the results of a field, petrographic, and geochemical study of MTBX from the Parkin Offset Dyke were presented. These results suggest that MTBX is recrystallized FWBX. Here, the results of a detailed investigation of MTBX from the Foy and Trill Offset Dykes are presented.

4.2 Regional Geology

The radial Foy Offset Dyke, located in the North Range of the Sudbury structure (Fig. 4.1), emanates from an embayment of the SIC and extends into gneissic, magmatic and granitic rocks of the Levack Gneiss Complex (~2.71 Ga, Krogh et al. 1984), the Cartier Batholith (2.64 Ga, Meldrum et al. 1997) and the Benny Greenstone Belt (~2.71 Ga, Krogh et al. 1984). With a width of 50 to 400 m and a total length of more than 30 km (Tuchscherer and Spray 2002) it represents the longest and widest of all the radial Sudbury Offset Dykes. Over the first 5 km the Foy Offset Dyke strikes roughly east to west, then northwest for another 10 km, connects to the concentric Hess Offset Dyke and follows a northeastern strike for the last 15 km.

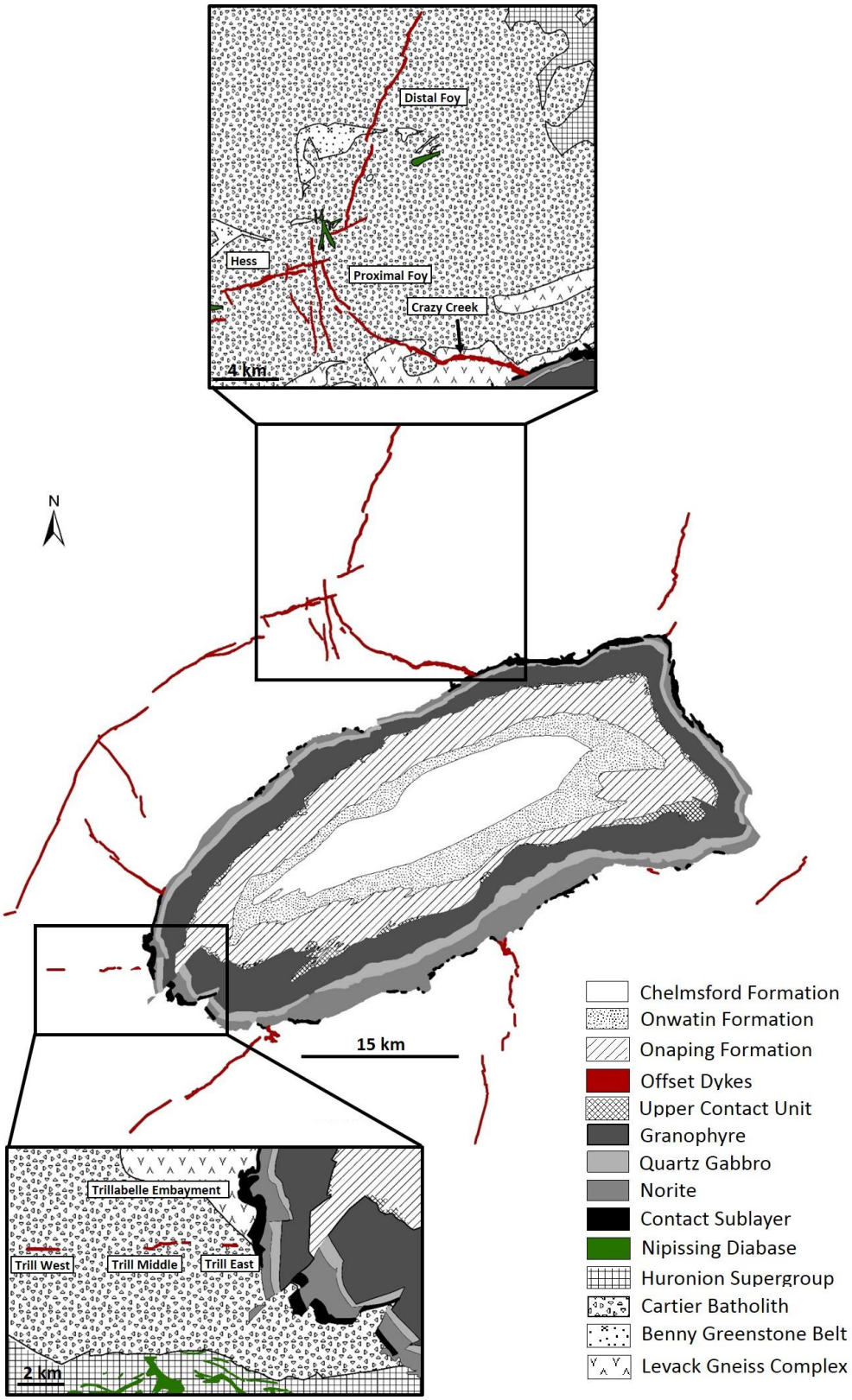

Figure 4.1. Simplified geological map of the Sudbury impact structure (modified after Ames and Gibson (2004)) with insets showing the Foy and Trill Offset Dykes.

The Foy Offset Dyke is mainly composed of QD and IQD (Tuchscherer and Spray 2002; Pilles et al. 2014a, 2014b); however, and according to several reports by Wallbridge Mining Company Limited and KGHM International Ltd., the dyke also appeared to contain MTBX.

The radial Trill Offset Dyke (Fig. 4.1), located west of the Sudbury Basin, was identified by Wallbridge Mining Company Limited in June 2005 when a 65 m long and 5 m wide Ni-Cu-PGE sulfide lens was discovered approximately ~4 km away from the SIC, today known as the Middle Trill (Coulter 2016). In September 2013, the detection of IQD east of the Middle Trill trench led to mechanical stripping of the area and to the discovery of the new Trill east showing and another part of the dyke ~500 m west of the SIC. In 2015, further IQD was identified ~8 km west of the SIC and resulted in trenching of the Trill west showing (Coulter 2016). To date the east-west trending dyke has been traced for approximately 9.5 km (Coulter 2016); however, no connection to the SIC or an embayment structure have been discovered to date. An embayment structure ~2 km north of the dyke, the so-called Trillabelle embayment might be associated to the Trill Offset Dyke. The dyke is relatively unexplored, having only been examined by Klimesch et al. (2008), Klimesch (2009), Coulter (2016), Klimesch et al. (2016) in coordination with Wallbridge Mining Company Limited. The Trill Offset Dyke is hosted by magmatic and metamorphic rocks of the ~2.71 Ga Levack Gneiss Complex (Krogh et al. 1984) and the 2.64 Ga Cartier Batholith (Meldrum et al. 1997), intruded by Matachewan Diabase dykes (2.45 Ga, Card 1994).

4.3 Methods and Samples

Fieldwork at the Trill Offset Dyke was carried out in the summer of 2014 at the middle and eastern Trill with the main focus being the study and sampling of MTBX from the Trill east showing. The Crazy Creek trenches at the proximal Foy Offset Dyke were investigated, sampled and mapped in the summer of 2015. Mapping of the trenches was carried out using a Trimble Juno Series Handheld mapping device with accurate positioning within 5 m. Polished thin sections of samples collected from the Trill and Foy Offset Dykes were examined by optical microscopy, in order to characterize mineralogy, microstructures and textures. Whole rock analyses of powdered samples were carried out

by the ALS laboratory in Sudbury. Major oxide were analyzed by inductively coupled plasma atomic emission spectroscopy (ICP-AES). Lithium borate fusion inductively coupled plasma mass spectrometry (ICP-MS) provided trace element analyses, with the exception of base metals, which were analyzed by 4-acid digestion ICP-AES. Clasts within IQD and MTBX were avoided during crushing and pulverizing, in order to ascertain the matrix composition.

4.4 Field Observations

4.4.1 Foy Offset Dyke

The studied area, called Crazy Creek (Fig. 4.1), is located ~4 km northwest of the Foy-SIC embayment and consists of several interconnected trenches containing MTBX in contact with country rocks. The Foy Offset Dyke trends approximately east-west in this area (Fig. 4.1). The studied trenches are free of QD and IQD but these lithologies have been mapped in the surrounding area up to a distance of approximately 2 km to the east and west of the trenches (Pilles et al. 2016). Thus, contact relationships MTBX between QD/IQD could not be established. MTBX is dominant in the trenches one to four, while trench 5, which is on a steep hill, is composed of country rocks and Sudbury Breccia (SDBX) (Fig 4.2). Based on the exposure of MTBX within the trenches, the dyke displays a width of approximately 130 m (Fig. 4.2). The country rocks of the Crazy Creek trenches are mainly composed of mafic gneiss of the Levack Gneiss Complex. The embayment and the first several kilometres of the dyke are hosted by Levack Gneiss; whereas Cartier Batholith is the dominant country rock of the more distant parts of the dyke (4.1). The Levack Gneiss at Crazy Creek is characterized by typical gneissic banding of white plagioclase-rich layers alternating with green to black mafic layers, with local flow structures and schlieren. Other country rocks include Nipissing Diabase throughout the trenches 1 to 5 and Matachewan Diabase in trench 2 intruding the Levack Gneiss and the dyke (Fig. 4.2). On weathered surfaces MTBX displays a light grey matrix, sometimes with a blueish-green tint, and contains clasts of different size, shape and composition (Fig. 4.3a).

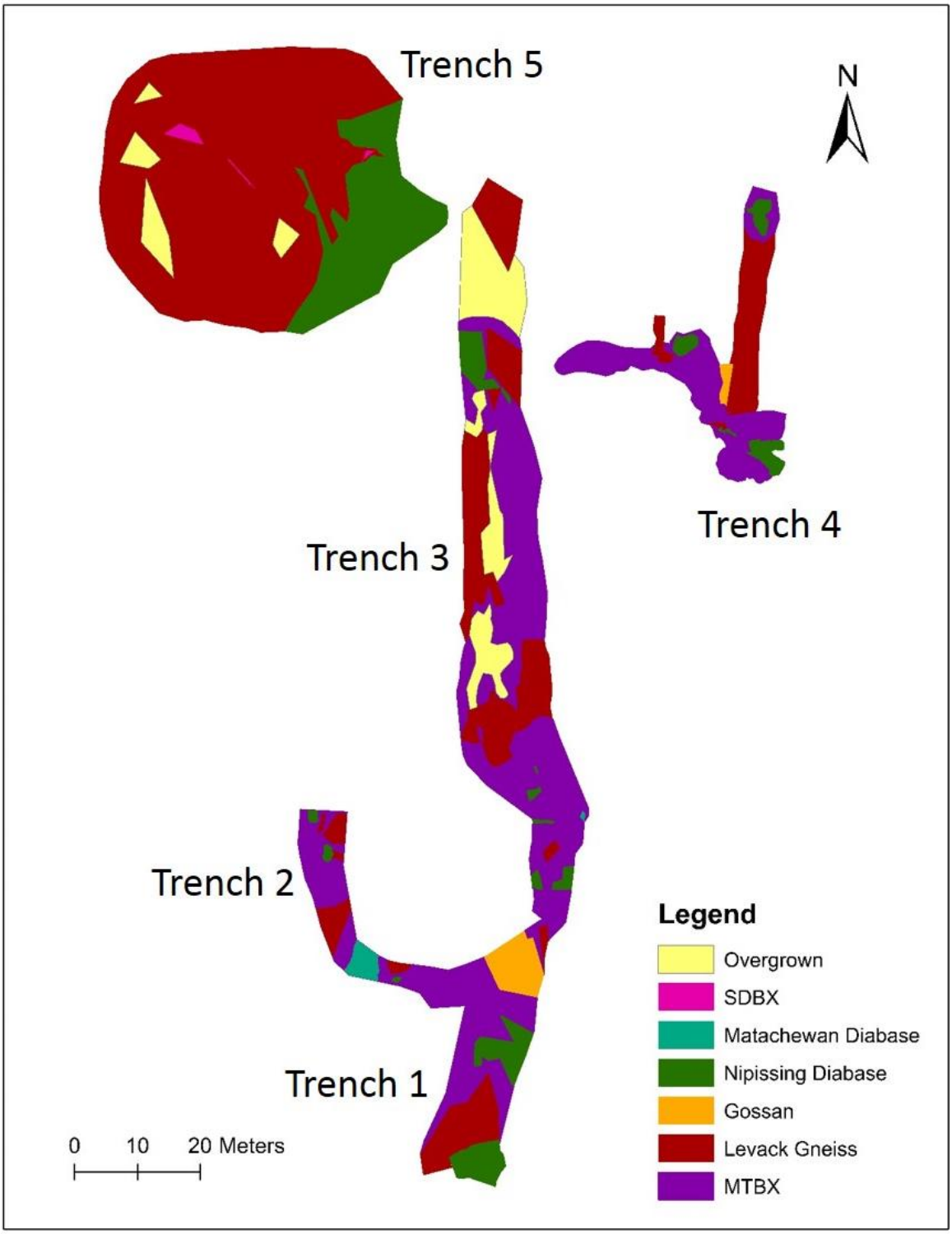

Figure 4.2. Simplified geological map of the Crazy Creek trenches.

It typically contains 50 to 75% clasts, which are usually cm-sized (Fig. 4.3a) and sometimes merge into the matrix, creating diffuse and gradational contacts. The dominant clast population are white, plagioclase-rich clasts, followed by green to black mafic clasts and rarely red to pink alkali-feldspar mineral clasts. Larger pods of country rocks have been detected on the margins of the trenches and it is sometimes difficult to establish if those are m-sized country rock inclusions within MTBX or parts host lithologies (see trench 3 in Fig. 4.2). The fresh surface of MTBX is fine-grained to aphanitic, black-grey, and milky and shows a felsic composition of mainly quartz and feldspar. Mineralization and gossanized areas are not common at the Crazy Creek trenches; however, where they occur, they are associated with MTBX. Locally, the rocks are altered by alkali-metasomatism, resulting in a reddish surface appearance.

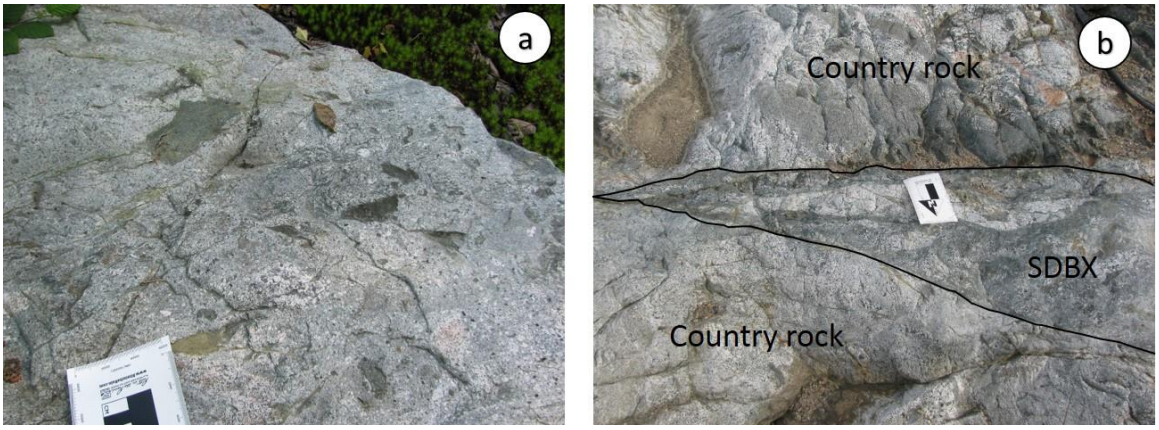

Figure 4.3. Field photographs of Foy Offset Dyke. a) MTBX, a heterolithic, clast-supported breccia (8 cm wide card for scale). b) SDBX vein cutting through country rocks (15 cm long card for scale).

SDBX (Fig. 4.5b) has been observed as up to 30 cm sized dykelets within the country rocks in trench 5 (Fig. 4.2) and is usually associated with fractures in the country rocks. The matrix of SDBX is black, dark green, aphanitic, shows locally schlieren, and includes small clasts derived from the adjacent country rocks. SDBX was not observed in contact with MTBX.

4.4.2 Trill Offset Dyke

The Trill east showing is a ~60 m long and ~10 to 40 m cliff-like outcrop comprised of the Offset Dyke in contact with mafic gneiss and porphyroblastic granitic country rocks of the Cartier Batholith, which are cut by SDBX (Fig. 4.4). The contact between dyke and host rocks is only visible on the northern side of the trench, thus, it is difficult to establish a correct thickness of the east-west trending dyke in that location.

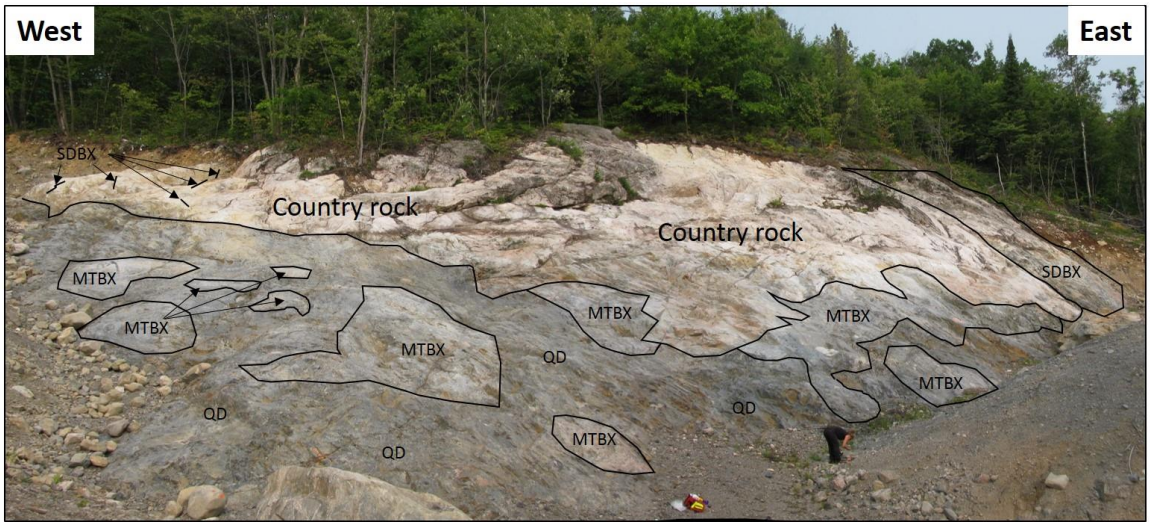

Figure 4.4. Panoramic field image of the Trill east showing, with marked lithologies (person for scale in foreground).

On a weathered surface, MTBX appears light grey (Fig. 4.5a) and locally shows reddish discolouration as a result of alkali-metasomatism. The fresh surface of MTBX shows a black-white, milky surface with the for quartz rich rocks typical flaky fracture. The fine-grained MTBX matrix contains dominantly mm to cm-sized white plagioclase-quartz clasts, followed by red alkali-feldspar-rich and mafic clasts (Fig. 4.5a). The clasts are usually in sharp contact with the matrix; however, they can also be seen merging into the matrix creating diffuse contacts, which is often associated to a higher amount of alkali-rich clasts (Fig. 4.5b). MTBX is generally located in the centre of the dyke, but also occupies marginal areas of the dyke in places (Fig. 4.4).

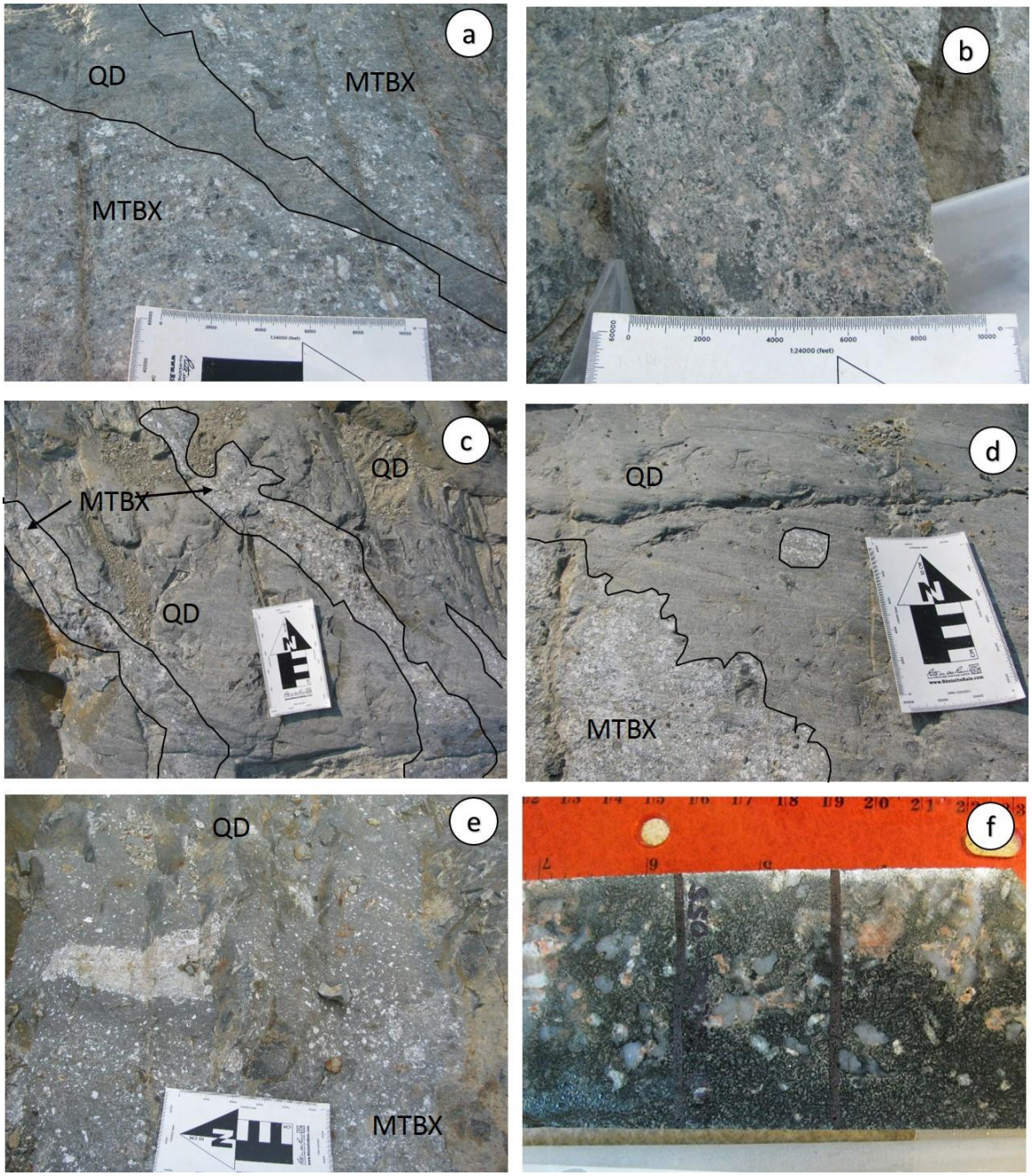

Figure 4.5. Field photographs from the Trill Offset Dyke. a) MTBX, a heterolithic, clast-supported breccia, intruded by fine-grained QD with sharp contact (15 cm long card for scale). b) MTBX showing diffuse matrix-clast contacts (15 cm long card for scale). c) Intermingling relationship of MTBX and QD with sharp contacts (15 cm long card for scale). d) MTBX in contact with QD. The clast within QD seems to be originated from MTBX (15 cm long card for scale). e) Gradational contact between MTBX and QD (15 cm long card for scale). f) IQD within a Trill core sample from Wallbridge Mining (scale on the ruler in centimetres).

It occurs as pods and intermingling inclusions within QD (Fig. 4.4) and in some locations QD observed intruding into MTBX (Figs. 4.5a and c). The contacts between the two phases are typically distinct and sharp; however, very often they are irregular-shaped and embayed (Figs. 4.5a, c and d).

Occasionally, single clasts within QD are detected in close vicinity to the sharp MTBX-QD contact that seem to be very similar in appearance to MTBX (Fig. 4.5d). Rarely, MTBX-QD contacts that are gradational over several centimetres have been detected and are characterized by a decrease in clast amount from MTBX to QD (Fig. 4.5e).

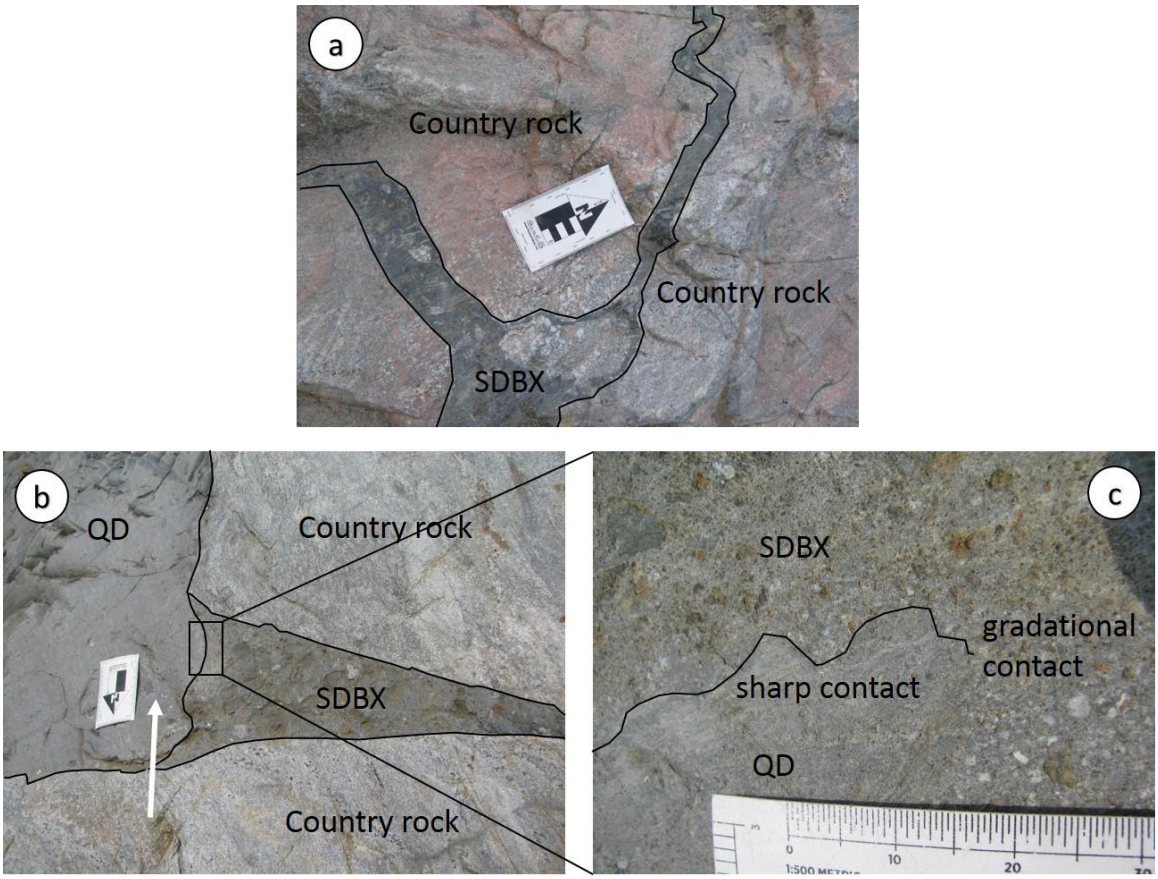

Figure 4.6. Field relationships of SDBX from the Trill Offset Dyke (15 cm long card for scale). a) SDBX vein cutting through granitic country rocks (15 cm long card for scale). b) SDBX-QD contact with locally dissolved SDBX clast within QD matrix marked with a white arrow (15 cm long card for scale). c) Close-up of the contact relationship (scale on the card in centimetres).

The inclusion-free phase is the dominant QD lithology. While IQD is not present in the outcrop (Fig. 4.4), it has been detected in several cores from the area. The QD phase in the trench is somewhat unusual compared to typical QD phases. It is characterized by a dark, fine-grained to aphanitic texture, similar to the marginal chilled phases of QD reported from other dykes (Figs. 4.5a, c and d). SDBX occurs as cm-wide interconnected dykes and veinlets cutting through the country rocks (Fig. 4.6a), with sharp and distinctive contacts. Its macroscopic appearance seems to depend on the host rock. SDBX within alkali-feldspar-rich, granitic county rocks is characterized by a dark black, aphanitic assemblage, with local schlieren, and mainly contains red alkali-feldspar clasts (Fig. 4.6a). However, when hosted within more mafic and plagioclase-rich country rocks, the matrix displays an aphanitic, mafic, dark green matrix with dominant mafic clasts, followed by white plagioclase inclusions (Fig. 4.6b). On rare occasions, marginal QD is in contact with SDBX cutting through country rocks (Figs. 4.6b and c). The contact is sharp, however, on closer examination, SDBX seems to have been partially molten and digested, and clasts included within QD, thus, showing locally a gradational contact (Fig. 4.6c).

Compared to MTBX, SDBX has a darker, finer-grained matrix, breaks into angular and sharp pieces and does not show the white-flaky quartz fracture observed in MTBX. No crosscutting or contact relationships between SDBX and MTBX have been observed at the Trill Dyke. Gossanized and mineralized areas within the trench are rare and if existent, are associated to MTBX.

4.5 Petrography

MTBX from the Foy and Trill Offset Dykes display similar features and textures. The matrix is characterized by a fine-grained intergrowth of quartz and feldspar with diffuse, merging and interlocking grain boundaries, and shows features indicative of intensive recrystallization (Fig. 4.7). Minor minerals within the matrix include biotite and amphiboles, which are altered and replaced by chlorite, iron oxides and epidote. New quartz and feldspar grains replace the original fabric and display irregular, interlobate, merging to amoeboid grain boundaries with dark rims (Fig. 4.7a). The grain boundaries are often characterized by bulges that emerge into adjacent grains.

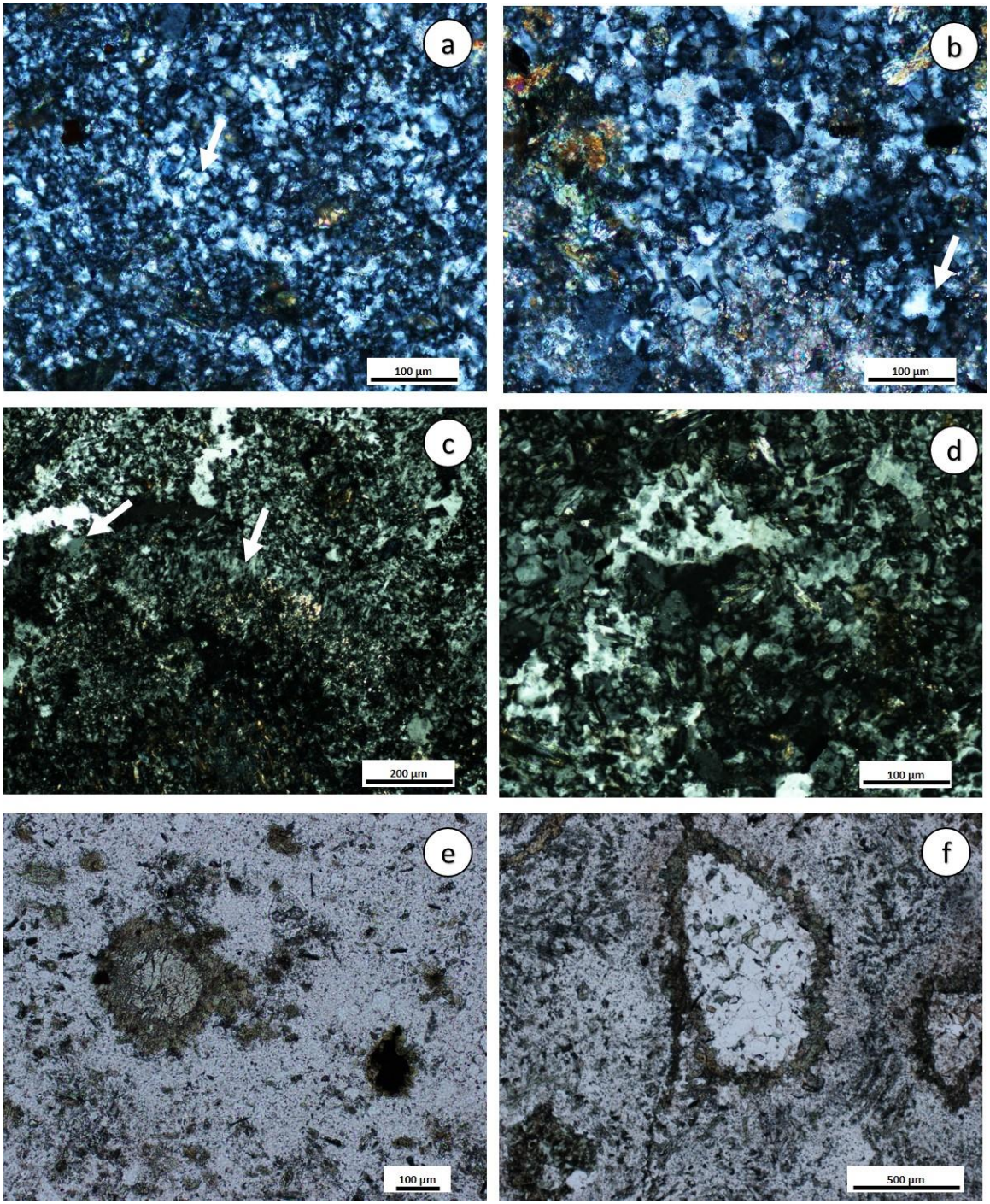

Figure 4.7. Photomicrographs of a) Recrystallized texture of MTBX (SUD-DA-Foy-014, XPL). Amoeboid grain boundaries with dark rims are marked by the white arrow. b) Small subgrain within another grain (white arrow) (SUD-DA-FOY-002, XPL). c) Subgrains showing different orientation from the host grain (white arrow) (SUD-DA-TR-018, XPL). d) Relicts of poikiloblastic texture (SUD-DA-TR-018, XPL). e) Amphibole core-and-mantle feature with a rim of small recrystallized amphiboles

(SUD-DA-FOY-002, PPL). f) Quartzitic clast surrounded by a mafic rim (SUD-DA-FOY-015, PPL).

Subgrains, sections of grains which display progressed missorientation compared to the other parts of the same grain, are common within the matrix (Fig. 4.7c). Locally, MTBX shows relicts of a poikiloblastic texture, i.e. larger grains of quartz include small feldspar laths (Fig. 4.7d). MTBX appears strain free and ductile deformation features, such as preferred grain orientation, elongated or ribbon-shaped minerals, have not been detected. Embayed and indented quartz xenocrysts are distributed within the MTBX matrix and show undulose extinction. Other minerals also display signs of recrystallization, for example, the amphibole grain pictured in Figure 4.7e, which displays a core-and-mantle structure with a rim of fine-grained, recrystallized amphibole.

Clasts within MTBX are usually rounded to subrounded and display signs of partial melting and digestion. Some quartzitic clasts, usually associated with subgrain recrystallization features, have developed partial or discontinuous rims of mafic minerals (Fig. 4.7f). Similar reaction rims have been detected around clasts from the Parkin Offset Dyke (Chapter 3); and are also present within large granitic country rock fragments and blocks where aggregates of matrix quartz are surrounded by a layer of mafic minerals. The dominant clast types are pure quartz aggregates, followed by clasts composed of quartz and feldspar, and mafic clasts that usually are altered to chlorite and epidote. Planar deformation features have not been detected in the quartzitic clasts within MTBX samples examined from Trill and Foy, as has been detected within MTBX from Parkin (Chapter 3).

SDBX from Trill and Foy is a matrix to clast-supported breccia characterized by a brown to black, very fine-grained, clastic, pulverized (Fig. 4.8a) or devitrified groundmass (Fig. 4.8b). Fragments within SDBX are brecciated, crushed and fractured, subrounded to angular, do not show reaction rims or do not show signs of partial melting and digestion but sharp contacts (e.g., Fig. 4.8a). Locally, flow structures and banding are developed in the matrix. QD and IQD from the Trill Offset Dyke differ from SDBX and MTBX in that they display an igneous textured groundmass (Figs. 4.8c and d).

QD is characterized by a spherulitic assemblage of acicular amphiboles (Fig. 4.8c) while IQD is composed of a coarse-grained assemblage of euhedral quartz, feldspar and mafic minerals, usually tabular amphibole, rarely biotite (Fig. 4.8d). Clasts with reaction rims have not been detected within IQD from Trill; however, have locally been observed in IQD thin sections from the Parkin Offset Dyke.

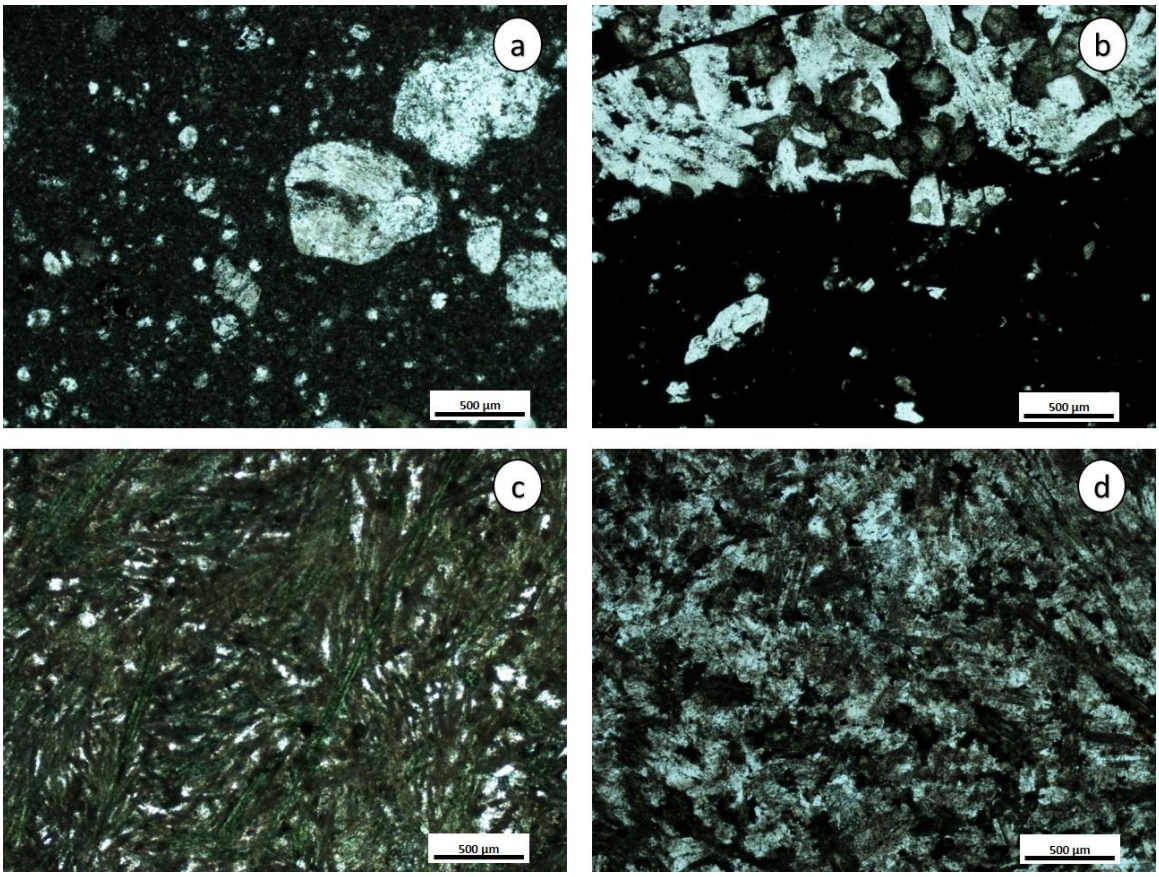

Figure 4.8. Photomicrographs of a) Aphanitic, cataclastic assemblage of SDBX matrix including clasts of different sizes (SUDCore-036, PPL). b) Glassy SDBX matrix (SUDCore-034, PPL). c) Spherulitic texture of QD (SUDCore-054, PPL). d) Igneous texture of IQD (SUDCore-055, PPL).

4.6 Geochemistry

Figure 4.9a shows Rare Earth Element (REE) spider plots normalized to the SIC Felsic Norite (Lightfoot et al. 1997a) of MTBX samples from the Foy Crazy Creek trenches and the Trill Offset Dyke in comparison to MTBX from Parkin. The plot confirms that all

samples, even though they slightly differ in absolute values, show a similar pattern with an enrichment in Light REE (LREE) and a depletion in Heavy REE (HREE) compared to the Felsic Norite of the SIC. Those observations correspond to the results reported from MTBX from the Parkin Offset Dyke (Chapter 3). Moreover, the plot demonstrates that MTBX from Trill and Foy are almost identical in absolute values. MTBX from Trill shows a slightly negative Eu anomaly, which is less pronounced in the REE pattern of the MTBX samples from Foy and Parkin. Trill and Foy MTBX exhibit slightly lower LREE than MTBX from Parkin. The REE pattern of Cartier Batholith granite (Meldrum et al. 1997) and Quartz Monzonite, which represent host rocks from the Trill Offset Dyke, are displayed in Figure 4.9b. The overall REE pattern of the granitic rocks of the Cartier Batholith correspond to the pattern of Trill MTBX. Both country rocks are characterized by a negative Eu anomaly, even though it is more pronounced than the Eu anomaly in MTBX from Trill. Furthermore, they are characterized by a higher abundance of LREEs compared to MTBX from Trill. Figure 4.9c displays the REE pattern of MTBX from Crazy Creek compared to host rocks of the Levack Gneiss Complex (Péntek et al. 2011) and Cartier Batholith granite (Meldrum et al. 1997), and it demonstrates that all three lithologies show little geochemical variation. However, the pattern of MTBX from Foy displays more similarities, including resembling absolute values, to Levack Gneiss than to Cartier Batholith. The comparison of FWBX from Hess (Wood and Spray 1998) and Whistle (Carter et al. 2009) to MTBX from Trill and Foy (Fig. 4.9d) shows, that those rock types display a very close compositional relationship with a similar trace element pattern and resembling absolute abundances.

4.7 Discussion and Interpretations

4.7.1 Formation and Origin of MTBX

The overall macroscopic and microscopic appearance of MTBX from the Foy and Trill Offset Dykes is identical to MTBX from the Parkin Offset Dyke (Fig. 4.9). At all three locations, MTBX is characterized by an intensively recrystallized assemblage formed by the three main processes of dynamic recrystallization: grain boundary migration, subgrain formation, and subgrain rotation. This results in the development of a secondary texture characterized by a mosaic of new grains with decreased grain size and amoeboid grain

boundaries (Fig. 4.7). Grain boundary migration (Fig. 4.7a), a high temperature–low strain process starting at temperatures of 500–700°C (Jessell 1987; Stipp et al. 2002b) dominates the texture of MTBX. Grain boundary migration describes the movement of existing grain boundaries to remove dislocations that were caused by increased temperature and strain (Guillopé and Poirier 1979; Urai et al. 1986; Stipp et al. 2002a).

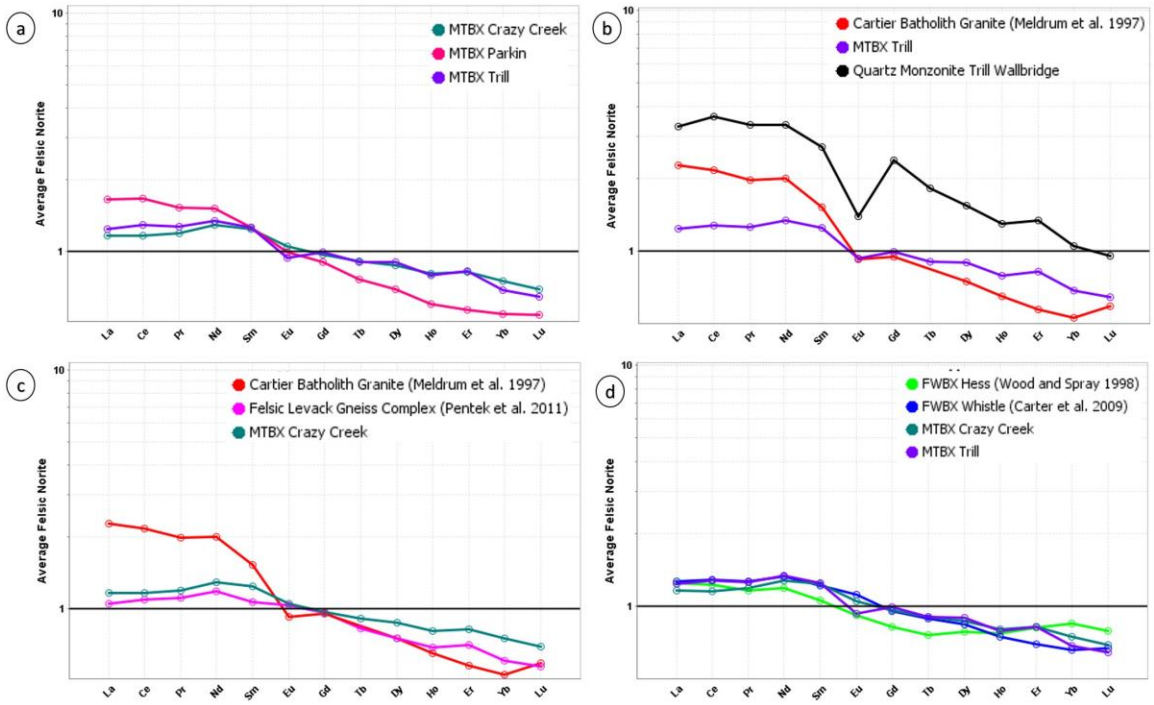

Figure 4.9. Rare Earth Element plots normalized to the main mass Felsic Norite (Lightfoot et al. 1997a) of a) MTBX from Trill and Foy (this study) compared to the Parkin Offset Dyke (Chapter 3). b) MTBX from Trill (this study), quartz monzonite (Wallbridge Mining) and host rocks of the Cartier Batholith (Meldrum et al. 1997). c) MTBX from Crazy Creek (this study), rocks of the Cartier Batholith (Meldrum et al. 1997) and the Felsic Levack Gneiss Complex (Péntek et al. 2011). d) FWBX from Hess (Wood and Spray 1998) and Whistle (Carter et al. 2009), in comparison to MTBX from Trill and Foy (this study).

New grains (Fig. 4.7b) are formed due to bulging, which is a process where the grain boundary of a grain with low dislocation density bulges into the neighbour grain with high

dislocation density. It gets eventually pinched off by dissection (Tullis and Yund 1985) or fracturing (Stünitz et al. 2003) and included into the neighbour grain as a subgrain (Baily and Hirsch 1962; Drury et al. 1985; Shigematsu 1999; Stipp et al. 2002a), or develops a new grain by subsequent subgrain rotation (Means 1981; Tungatt and Humphreys 1984; Drury et al. 1985). Bulging is a characteristic feature of low temperature of 300-400°C and high strain rates (Stipp et al. 2002b). Subgrain rotation (Fig. 4.7c) occurs at medium temperatures of 400–500°C and medium strain rates (Lloyd and Freeman 1994; Stipp et al. 2002b) and is a progressed missorientation of subgrains caused by increased crystallographic defects (Passchier and Trouw 2005). In the matrix distributed, embayed and indented quartz xenocrysts are relicts of the coarser-grained primary fabric. The core- and mantle features (Fig. 4.7e) are interpreted as relicts of old grains or aggregates that are surrounded by sheets of recrystallized grains, that form under conditions of low temperature and low strain (Gifkins 1976; White 1976; Shigematsu 1999). While MTBX is characterized by a fine-grained meta-igneous texture, QD and IQD show a primary igneous groundmass as a result of crystallization from a melt (Figs. 4.8c and d). The lack of QD and IQD at the Crazy Creek trenches prevented an investigation of contact relationships with MTBX; however, field observations from the Parkin (Chapter 3) and Trill Offset Dykes show an intermingling of MTBX and QD where fingers of QD intrude MTBX (Figs. 4.5a and c) and also there are inclusions of MTBX within QD (Fig. 4.4).

Figure 4.10. Comparative view of MTBX from a) Parkin (12 cm long pencil for scale), b) Foy (15 cm long card for scale), and c) Trill (15 cm long card for scale).

A genetic relationship of MTBX to SDBX can also be excluded. MTBX occurs as pods (at Foy and Trill), and irregularly-shaped inclusions intermingling with QD (at Parkin and

Trill), while SDBX is characterized by dykelets with straight forms and lines associated with country rocks. SDBX has not been observed in contact with MTBX. A difference in clast content is particularly clear at the Foy Offset Dyke, where the inclusions within SDBX originated from adjacent country rock, while MTBX contains clasts that do not represent adjacent or local country rocks. This is also emphasized by the fact that SDBX shows different appearances dependent on the host rocks (Fig. 4.6). SDBX is composed of a very fine-grained groundmass and rock fragments, formed by milling, cataclasis, comminution, and/or frictional melting (Dietz and Butler 1964; Card 1978; Dressler 1984b; Lakomy 1990; Spray 1992, 1997; Müller-Mohr 1992; Spray and Thompson 1995; Thompson and Spray 1996; Scott and Spray 2000; Scott and Benn 2002; Legault et al. 2003; Rousell et al. 2003; Riller 2005; Lafrance et al. 2008).

In terms of clast and groundmass textures, MTBX has more in common with FWBX than QD/IQD or SDBX. Locally, MTBX shows relicts of a poikiloblastic texture, which is characteristic for FWBX (Pattison 1979; Deutsch et al. 1989). This is also supported by geochemistry where MTBX of the Foy and Trill Offset Dykes show similarities with FWBX and country rocks (Fig 4.9). This has also been demonstrated at the Parkin Offset Dyke (Chapter 3). When taken together, these results strongly suggest that MTBX from Parkin, Trill and Foy have been formed by the same mechanism: metamorphic overprint of FWBX by the Offset Dykes. This results in a simple model for MTBX formation whereby fragments of FWBX are ripped off and included into the dyke causing intensive recrystallization of FWBX. FWBX forms discontinuous kilometre-long layers of up to 200 m thick underlying the SIC (Coats and Snajdr 1984; Dressler 1984b; Lakomy 1990; Dressler and Reimold 2004), and locally extending up to 250 m into the footwall rocks (McCormick 2002; Dressler and Reimold 2004). Clasts included within the matrix are up to several metres in size (McCormick 2002; Naldrett 2004), angular to subrounded and originate from adjacent country rocks (Dressler and Reimold 2004), main mass Norite, SDBX (Dressler 1984b; Lakomy 1990; Dressler and Reimold 2004), and rarely exotic fragments (Dressler and Reimold 2004). FWBX was formed by crushing and brecciation of crater floor rocks at shock pressures exceeding 10 GPa (Lakomy 1990), during the first stages of the impact event (Deutsch et al. 1989; Lakomy 1990; Lightfoot et al. 1997b; Farrow and Lightfoot 2002; McCormick 2002; Dressler and Reimold 2004; Carter et al.

2009) and subsequent thermal metamorphism and partial melting (Dressler 1984b; Deutsch et al. 1995) by the SIC at temperatures above 1000°C (Deutsch et al. 1989; Lakomy 1990; Prevec and Cawthorn 2002).

The geochemical variations seen between MTBX and FWBX from the different dykes are attributed to the compositional heterogeneity in the basement rocks. MTBX from Trill shows a slightly more pronounced negative Eu anomaly than MTBX from Parkin and Foy. In contrast to the Parkin Offset Dyke and the Crazy Creek area, the Trill Offset Dyke is mainly hosted by Cartier Batholith, which, thus, played a more important role in the geochemical composition of the Trill MTBX. The rocks of the Cartier Batholith also show a negative Eu anomaly, which could have resulted in the negative Eu anomaly in the Trill MTBX. Rounded to subrounded clasts within MTBX locally show mafic reaction rims, which usually are the result of melt-clast interactions and common in igneous and impact melt rocks (Taylor and Dence 1969; Fudali 1974; Grieve 1975; Floran and Grieve 1978). The mafic rims around clasts observed within MTBX are discontinuous and limited to small, up to 1 cm sized, quartzitic clasts often associated with recrystallization features or chessboard textures. However, they are not present in every sample. Those reaction rims have also been detected around quartz grains and aggregates of larger fragments and blocks of granitic basement rocks within MTBX. Mafic reaction corona around quartz xenoliths and phenocrysts within igneous rocks have been associated to magmatic contamination, i.e., the intrusion of a mafic into a silicic magma, and form as a result of diffusion of Mg, Fe, and Ca from the mafic magma into silicic melt surrounding the xenoliths (Nixon, 1988).

Sublayer inclusions have been detected within FWBX (Lightfoot et al. 1997c) indicating an interaction of FWBX and Sublayer. It is possible that, during its formation, FWBX was locally intruded by Sublayer melt, which could have represented a mafic magma that contaminated the partial melt of the silicic FWBX. Where quartz xenolith and grains within FWBX surrounded by a layer of partial melt, came in contact with Sublayer melt, the formation of those mafic reaction rims would be possible. It is, thus, likely that those reaction rims could be relicts of the original FWBX texture that survived the recrystallization processes during the MTBX formation.

Based on the above mentioned results the following process of MTBX formation is proposed:

i. The formation of FWBX happened within the early stages of the impact cratering process. It may have begun simultaneously with, or shortly after the formation of SDBX had started. The timing of formation of the two units could have overlapped; however, SDBX clasts (Pattison 1979; Lakomy 1990; Moore and Nikolic 1994) within FWBX indicate that SDBX already existed in places when FWBX formed.
ii. During the crater excavation stage, before the emplacement of the proto-SIC, brecciation and crushing of the crater floor rocks led to the formation of a clastic breccia, the precursor to the FWBX.
iii. The emplacement and subsequent cooling of the proto-SIC led to thermal metamorphism and partial to full melting of the crater floor rocks and the clastic breccia, resulting in the meta-igneous texture of the FWBX.
iv. Proto-SIC and then also Sublayer melt intruded the still evolving proto-FWBX resulting in mixing of felsic partial melt with impact melt. At this point the breccia also incorporated Sublayer inclusions.
v. During the emplacement of the Offset Dykes blocks and fragments FWBX were ripped off and transported with dyke melt.
vi. The temperature of the Offset Dykes led to further recrystallization of the FWBX forming MTBX.
vii. Locally, FWBX fragments could have been assimilated and digested by the dyke melt and contributed to the clast population within QD/IQD.

4.7.2 Implications for Offset Dyke emplacement

If these interpretations above are correct, then MTBX within the studied dykes originates from FWBX, which, in turn, formed by brecciation and partial melting of basement rocks below the SIC and the embayments. Because MTBX exists as clasts with the Parkin, Foy and Trill Offset Dykes, this suggests the radial outward transport of FWBX within the dyke melt during the injection of the dykes into fractures of the country rocks. The dyke melt moved from the embayments outwards, transporting and thermally overprinting the ripped off blocks and fragments of FWBX, and producing MTBX. FWBX formed early in the

development of the Sudbury impact structure (Dressler 1984b). FWBX contains Sublayer inclusions (Lightfoot et al. 1997c) suggesting that it is younger than the Sublayer, or that it was emplaced during the solidification of the Sublayer (Pattison 1979; McCormick 2002). Given FWBX was entrained in the Offset Dyke melts, this would place the earliest timing of emplacement of the Parkin, Foy and Trill Offset Dykes during or after the solidification of the Sublayer.

The injection of the radial Offset Dykes occurred into fractures within the crater floor and surrounding footwall rocks, that were possibly generated by the impact event (Grant and Bite 1984; Wood and Spray 1998; Scott and Spray 1999; Lightfoot and Farrow 2002; Murphy and Spray 2002; Scott and Benn 2002; Tuchscherer and Spray 2002). At the Trill and Foy Offset Dykes SDBX is part of the host rock lithologies, which may have further weakened the host rock, resulting in an decrease of its resistance and, thus, facilitating the emplacement of the melt (Brown et al. 2007). Considering that large m-sized clasts have been mobilized and transported over long distances by the dyke melt (see Figs. 4.2 and 4.3), a forceful injection of the melt originating from the SIC is possible, as had already been suggested by Murphy and Spray (2002). Pre-existing fractures in the host rocks caused by the impact could have locally reduced the stiffness of the host-rock, reducing the required magma driving pressure (Barton and Choubey 1977; Rubin 1995) further supporting the transport of large blocks. MTBX has only been detected in the proximal part of the Foy Offset Dyke; the distal Foy Offset Dyke only contains QD and IQD (Pilles et al. 2016), which can be attributed to the dyke melt losing energy with increasing distance from the SIC, so that large MTBX fragments could not be transported to the distant part of the dyke, and are, thus, limited to the proximal dyke. This is in accordance with the observations from the Parkin Offset Dyke (Coulter 2016).

4.8 Conclusions

MTBX from the Trill or Foy Offset Dykes, here reported and described for the first time, share many similarities with MTBX from the Parkin Offset Dyke. It is a heterolithic, clast-supported breccia and displays features of an intensive recrystallized matrix. Subgrain rotation, bulging and grain boundary migration provide petrologic evidence for dynamic recrystallization at high temperatures of at least 500 to 700°C and low strain rates. As

proposed in Chapter 3, MTBX displays a close geochemical relationship to FWBX and to host rocks of the Levack Gneiss Complex and the Cartier Batholith, which is also the case for MTBX from the Foy and Trill Offset Dykes. The observations made in this study suggest that MTBX represents metamorphosed and recrystallized FWBX, as has been suggested for MTBX from Parkin (see Chapter 3). It is proposed that MTBX was emplaced as fragments within the Offset Dykes by injecting melt derived from the SIC at some point after the solidification of the Sublayer into pre-existing fractures and breccia zones. Based on field relationships, it is possible that the interaction of melt and fragments of MTBX could have contributed to the clast content within QD and IQD. While the observations for the Foy, Parkin and Trill Offset Dykes are self-consistent, it remains to be determined if these results can be translated around the Sudbury Basin. While the basic mechanisms may be similar for the emplacement of all radial Sudbury Offset Dykes, the details of injection and emplacement may differ from North to South Range, from dyke to dyke and even from proximal to distal parts of the same dyke. Identifying the mechanism at one location does not automatically imply similar processes at another dykes.

4.9 References

Ames, D.E., Gibson, H.L., 2004. Geology, alteration and mineralization of the Onaping Formation, Morgan Township, Sudbury Structure, Ontario. Geol. Surv. Canada Open File 3717, 2 maps.

Anders, D., Osinski, G.R., Grieve, R.A.F., Brillinger, D.T.M., 2015. The Basal Onaping Intrusion in the North Range: Roof rocks of the Sudbury Igneous Complex. Meteorit. Planet. Sci. 50, 1577–1594.

Baily, J.E., Hirsch, P.B., 1962. The recrystallization process in some polycrystalline metals. Proc. R. Soc. London 11–30.

Barton, N., Choubey, V., 1977. The shear strength of rock joints in theory and practice. Rock Mech. Rock Eng. 10, 1–54.

Brown, R.J., Kavanagh, J.L., Sparks, R.S.J., Tait, M., Field, M., 2007. Mechanically disrupted and chemically weakened zones in segmented dike systems cause vent

localization: Evidence from kimberlite volcanic systems. Geology 35, 815–818.

Card, K.D., 1978. Metamorphism of the middle Precambrian (Aphebian) rocks of the Eastern Southern Province, in: Fraser, J.A., Heywood, W.W. (Eds.), Metamorphism in the Canadian Shield, Geological Survey of Canada, 78, 10. pp. 269–282.

Card, K.D., 1994. Geology of the Levack gneiss complex, the northern footwall of the Sudbury structure, Ontario. Geol. Surv. Canada Curr. Res. 1994-C, 269–278.

Carter, W.M., Watkinson, D.H., Ames, D.E., Jones, P.C., 2009. Quartz Diorite Magmas and Cu-(Ni)-PGE Mineralization, Podolsky Deposit, Whistle Offset Structures, Sudbury, Ontario. Geol. Surv. Canada Open File 6134, 58 pp.

Coats, C.J.A., Snajdr, P., 1984. Ore deposits of the North Range, Onaping–Levack area, Sudbury, in: Pye, E.G., Naldrett, A.J., Giblin, P.E. (Eds.), The Geology and Ore Deposits of the Sudbury Structure. pp. 327–346.

Coulter, A.B., 2016. Recent Discoveries in the Ni-Cu-PGE bearing Trill and Parkin Offset dykes, Sudbury impact structure, Canada. M.Sc. Thesis, West. Univ. Dep. Earth Sci. Electron. Thesis Diss. Repos. Paper 3473.

Deutsch, A., 1994. Isotope systematics support the impact origin of the Sudbury Structure (Ontario, Canada), in: Dressler, B.O., Grieve, R.A.F., Sharpton, V.L. (Eds.), Large Meteorite Impacts and Planetary Evolution I, GSA Special Paper 293. pp. 289–302.

Deutsch, A., Grieve, R.A.F., 1994. The Sudbury Structure: Constraints on its genesis from Lithoprobe results. Geophys. Res. Lett. 21, 963–966.

Deutsch, A., Grieve, R.A.F., Avermann, M., Bischoff, L., Brockmeyer, P., Buhl, D., Lakomy, R., Müller-Mohr, V., Ostermann, M., Stöffler, D., 1995. The Sudbury Structure (Ontario, Canada): a tectonically deformed multi-ring impact basin. Geol. Rundschau 84, 697–709.

Deutsch, A., Lakomy, R., Buhl, D., 1989. Strontium-and neodymium-isotopic characteristics of a heterolithic breccia in the basement of the Sudbury impact

structure, Canada. Earth Planet. Sci. Lett. 93, 359–370.

Dickin, A.P., Artan, M.A., Crocket, J.H., 1996. Isotopic evidence for distinct crustal sources of North and South Range ores, Sudbury Igneous Complex. Geochim. Cosmochim. Acta 60, 1605 – 1613.

Dickin, A.P., Richardson, J.M., Crocket, J.H., McNutt, R.H., Peredery, W. V., 1992. Osmium isotope evidence for a crustal origin of platinum group elements in the Sudbury nickel ore, Ontario, Canada. Geochim. Cosmochim. Acta 56, 3531 – 3537.

Dietz, R.S., Butler, L.W., 1964. Shatter-cone orientation at Sudbury Canada. Nature 204, 280–281.

Dressler, B.O., 1984. The effects of the Sudbury event and the intrusion of the Sudbury Igneous Complex on the footwall rocks of the Sudbury structure, in: Pye, E.G., Naldrett, A.J., Giblin, P.E. (Eds.), The Geology and Ore Deposits of the Sudbury Structure. pp. 97–138.

Dressler, B.O., Peredery, W. V., Muir, T.L., 1992. Geology and Mineral Deposits of the Sudbury Structure. Ontario Geological Survey Guidebook 8.

Dressler, B.O., Reimold, W.U., 2004. Order or chaos? Origin and mode of emplacement of breccias in floors of large impact structures. Earth-Science Rev. 67, 1–54.

Drury, M.R., Humphreys, F.J., White, S.H., 1985. Large strain deformation studies using polycrystalline magnesium as a rock analogue. Part II: dynamic recrystallization mechanisms at high temperatures. Phys. Earth Planet. Inter. 40, 208–222.

Faggart, B.E., Basu, A.R., Tatsumoto, M., 1985. Origin of the Sudbury complex by meteoritic impact: Neodymium isotopic evidence. Science (80-.). 230, 436–439.

Farrow, C.E.G., Everest, J.O., King, D.M., Jolette, C., 2005. Sudbury Cu-(Ni)-PGE-Systems: Refining the classification: Using McCreedy West Mine, and Podolski project case studies, in: Mungall, J.E. (Ed.), Exploration for Platinum- Group Elements Deposits. Mineralogical Association of Canada, Short Course Series

Volume 35, pp. 163–180.

Farrow, C.E.G., Lightfoot, P.C., 2002. Sudbury PGE Revisited: Towards an Integrated Model, in: Cabri, L.J. (Ed.), Geology, Geochemistry, Mineralogy and Mineral Beneficiation of Platinum-Group Elements. Canadian Institute of Mining, Metallurgy and Petroleum, Special Volume 54, pp. 273–297.

Floran, R.J., Grieve, R.A.F., 1978. Manicouagan impact melt, Quebec, 1, Stratigraphy, petrology, and chemistry. J. Geophys. Res. 83, 2737–2758.

Fudali, R.F., 1974. Genesis of the melt rocks at Tenoumer crater, Mauritania. J. Geophys. Res. 79, 2115–2121.

Gifkins, R.C., 1976. Grain-boundary sliding and its accommodation during creep and superplasticity. Metall. Trans. 7, 1225–1232.

Giroux, L.A., Benn, K., 2005. Emplacement of the Whistle dike, the Whistle embayment and hosted sulfides, Sudbury Impact Structure, based on anisotropies of magnetic susceptibility and. Econ. Geol. 100, 1207–1227.

Grant, R.W., Bite, A., 1984. Sudbury Quartz Diorite Offset Dikes, in: Pye, E.G., Naldrett, A.J., Giblin, P.E. (Eds.), The Geology and Ore Deposits of the Sudbury Structure. pp. 275–300.

Grieve, R.A.F., 1975. Petrology and chemistry of the impact melt at Mistastin Lake crater, Labrador. Geol. Soc. Am. Bull. 86, 1617–1629.

Grieve, R.A.F., 1991. Terrestrial impact: The record in the rocks. Meteoritics 26, 175–194.

Grieve, R.A.F., 1994. An Impact Model of the Sudbury Structure, in: Lightfoot, P.C., Naldrett, A.J. (Eds.), Proceedings of the Sudbury-Noril'sk Symposium. Ontario Geological Survey Special Volume 5, pp. 119–132.

Grieve, R.A.F., Reimold, W.U., Morgan, J., Riller, U., Pilkington, M., 2008. Observations and interpretations at Vredefort, Sudbury, and Chicxulub; towards an empirical model

of terrestrial impact basin formation. Meteorit. Planet. Sci. 43, 855–882.

Guillopé, M., Poirier, J.P., 1979. Dynamic recrystallization during creep of single-crystalline halite: an experimental study. J. Geophys. Res. 84, 5557–5567.

Hecht, L., Wittek, A., Riller, U., Mohr, T., Schmitt, R.T., Grieve, R.A.F., 2008. Differentiation and emplacement of the Worthington Offset Dike of the Sudbury impact structure, Ontario. Meteorit. Planet. Sci. 43, 1659–1679.

Jessell, M.W., 1987. Grain-boundary migration microstructures in a naturally deformed quartzite. J. Struct. Geol. 9, 1007–1014.

Klimesch, L., 2009. Mapping Project: Creighton Pluton at Graham Fault, Sudbury, Canada. and Emplacement, Differentiation and Mineralisation of the Trill Offset Dike, Sudbury, Canada. Freie Universität Berlin.

Klimesch, L., Hecht, L., Riller, U., 2008. Petrology of the Trill Offset Dike, Sudbury, Canada, in: 86th Annual Meeting of the German Mineralogical Society. p. abstract # 545.

Klimesch, L.-M., Hecht, L., Riller, U., 2016. Geology, geochemistry and mineralization of the Trill Offset Dike, Sudbury, Canada. Econ. Geol. Pap. Revis.

Krogh, T.E., Davis, D.W., Corfu, F., 1984. Precise U–Pb zircon and baddeleyite ages for the Sudbury area, in: Pye, E.G., Naldrett, A.J., Giblin, P.E. (Eds.), The Geology and Ore Deposits of the Sudbury Structure. pp. 431–447.

Lafrance, B., Bygnes, L.C., 2014. Emplacement of metabreccia along the Whistle offset dike, Sudbury: implications for post-impact modification of the Sudbury impact structure. Can. J. Earth Sci. 19, 1–19.

Lafrance, B., Legault, D., Ames, D.E., 2008. The formation of the Sudbury breccia in the North Range of the Sudbury impact structure. Precambrian Res. 165, 107–119.

Lakomy, R., 1990. Implications for cratering mechanics from a study of the Footwall

Breccia of the Sudbury impact structure, Canada. Meteorit. Planet. Sci. 25, 195–207.

Legault, D., Lafrance, B., Ames, D.E., 2003. Structural study of Sudbury breccia and sulphide veins, Levack embayment, North Range of the Sudbury structure, Ontario. Geol. Surv. Canada Curr. Res. 2003-C1, 11 pp.

Lightfoot, P.C., Doherty, W., Farrell, K.P., Keays, R.R., Pedeski, D., 1997a. Geochemistry of the main mass, sublayer, offset dikes, and inclusions from the Sudbury Igneous Complex. Ontario Geol. Surv. Open File 5959, 231 pp.

Lightfoot, P.C., Farrow, C.E.G., 2002. Geology, geochemistry, and mineralogy of the Worthington offset dike: A genetic model for offset dike mineralization in the Sudbury Igneous Complex. Econ. Geol. 97, 1419–1446.

Lightfoot, P.C., Keays, R.R., Morrison, G.G., Bite, A., Farrell, K.P., 1997b. Geochemical relationships in the Sudbury igneous complex; origin of the main mass and offset dikes. Econ. Geol. 92, 289–307.

Lightfoot, P.C., Keays, R.R., Morrison, G.G., Bite, A., Farrell, K.P., 1997c. Geologic and geochemical relationships between the contact sublayer, inclusions, and the main mass of the sudbury igneous complex: A Case study of the whistle mine embayment. Econ. Geol. 92, 647–673.

Lloyd, G.E., Freeman, B., 1994. Dynamic recrystallisation of quartz and quartzites. J. Struct. Geol. Geol 16, 867–881.

McCormick, K.A., 2002. A textural, mineralogical, and statistical study of the footwall breccia within the Strathcona embayment of the Sudbury structure. Econ. Geol. 97, 125–143.

Means, W.D., 1981. The concept of steady-state foliation. Tectonophysics 78, 179–200.

Meldrum, A., Abdel-Rahman, A.F.M., Martin, R.F., Wodicka, N., 1997. The nature, age and petrogenesis of the Cartier Batholith, northern flank of the Sudbury Structure, Ontario, Canada. Precambrian Res. 82, 265–285.

Moore, C.M., Nikolic, S., 1994. The Craig Deposit, Sudbury, Ontario, in: Proceedings of the Sudbury-Noril'sk Symposium. pp. 77–90.

Müller-Mohr, V., 1992. Breccias in the basement of a deeply eroded impact structure, Sudbury, Canada. Tectonophysics 216, 219–226.

Murphy, A.J., Spray, J.G., 2002. Geology, mineralization and emplacement of the Whistle–Parkin offset dike, Sudbury impact structure. Econ. Geol. 97, 1369–1389.

Naldrett, A.J., 2004. Magmatic Sulfide Deposits: Geology, Geochemistry and Exploration. Springer Verlag, Heidelberg, Berlin.

Passchier, C.W., Trouw, R.A.J., 2005. Microtectonics, 2nd, Revis. ed. Springer-Verlag Berlin.

Pattison, E.F., 1979. The Sudbury Sublayer. Can. Mineral. 17, 257–274.

Péntek, A., Molnár, F., Watkinson, D.H., Jones, P.C., Aberra, M., 2011. Partial melting and melt segregation in footwall units within the contact aureole of the Sudbury Igneous Complex (North and East Ranges, Sudbury structure), with implications for their relationship to footwall Cu–Ni–PGE mineralization. Int. Geol. Rev. 53, 291–325.

Pilles, E., 2016. Emplacement of the Foy, Hess and Pele Offset Dykes at the Sudbury impact structure, Canada. PhD. Thesis, Dep. Earth Sci. Univ. West. Ontario in work.

Pilles, E., Osinski, G.R., Bailey, J., Smith, D., 2014a. Outward Emplacement of the FoyOffset Dyke at the Sudbury Impact Structure, Canada – Evidence from the Variation in Inclusions Along Strike. GSA Annu. Meet. Vancouver, Bitish Colomb. Paper No.

Pilles, E., Osinski, G.R., Bailey, J., Smith, D., 2014b. Emplacement of the Foy Offset Dyke at the Sudbury Impact Structure, Canada. 45th Lunar Planet. Sci. Conf. Houston, Texas abstract #.

Pilles, E., Osinski, G.R., Grieve, R.A.F., Smith, D., Bailey, J., 2016. Variations and genetic relationships between the Hess and the Foy Offset Dikes at the Sudbury Impact Structure. Meteorit. Planet. Sci. submitted.

Prevec, S.A., Cawthorn, R.G., 2002. Thermal evolution and interaction between impact melt sheet and footwall: A genetic model for the contact sublayer of the Sudbury Igneous Complex, Canada. J. Geophys. Res. 107, 1–14.

Riller, U., 2005. Structural characteristics of the Sudbury impact structure, Canada: Impact-induced versus orogenic deformation-A review. Meteorit. Planet. Sci. 40, 1723–1740.

Rousell, D.H., Fedorowich, J.S., Dressler, B.O., 2003. Sudbury Breccia (Canada): a product of the 1850 Ma Sudbury Event and host to footwall Cu–Ni–PGE deposits. Earth-Science Rev. 60, 147–174.

Rubin, A.M., 1995. Propagation of magma-filled cracks. Annu. Rev. Earth Planet. Sci. 23, 287–336.

Scott, R.G., Benn, K., 2002. Emplacement of Sulfide Deposits in the Copper Cliff Offset Dike during Collapse of the Sudbury Crater Rim: Evidence from Magnetic Fabric Studies. Econ. Geol. 97, 1447–1458.

Scott, R.G., Spray, J.G., 1999. Magnetic fabric constraints on friction melt flow regimes and ore emplacement direction within the South Range Breccia Belt, Sudbury Impact Structure. Tectonophysics 307, 163–189.

Scott, R.G., Spray, J.G., 2000. The South Range Breccia Belt of the Sudbury Impact Structure : Meteorit. Planet. Sci. 505–520.

Shigematsu, N., 1999. Dynamic recrystallization in deformed plagioclase during progressive shear deformation. Tectonophysics 305, 437–452.

Souch, B.E., Podolsky, T., Staff, G., 1969. The sulfide ores of Sudbury: their particular relationship to a distinctive inclusion-bearing species of the Nickel Irruptive., in:

Wilson, H.D.B. (Ed.), Magmatic Ore Deposits - A Symposium. Economic Geology Monogaph 4, p. 366.

Spray, J.G., 1992. A physical basis for the frictional melting of some rock-forming minerals. Tectonophysics 204, 205–221.

Spray, J.G., 1997. Superfaults. Geology 25, 579–582.

Spray, J.G., Thompson, L.M., 1995. Friction melt distribution in a multi-ring impact basin. Nature 373, 130–132.

Stipp, M., Stunitz, H., Heilbronner, R., Schmid, S.M., 2002a. Dynamic recrystallization of quartz: correlation between natural and experimental conditions. Geol. Soc. London, Spec. Publ. 200, 171–190.

Stipp, M., Stünitz, H., Heilbronner, R., Schmid, S.M., 2002b. The eastern Tonale fault zone: a "natural laboratory" for crystal plastic deformation of quartz over a temperature range from 250 to 700 °C. J. Struct. Geol. 24, 1861–1884.

Stöffler, D., Avermann, M., Bischoff, L., Brockmeyer, P., Deutsch, A., Dressler, B.O., Lakomy, R., Müller-Mohr, V., 1989. Sudbury, Canada: Remnant of the only multi-ring (?) impact basin on Earth. Meteoritics 24, 328.

Stöffler, D., Deutsch, A., Avermann, M., Bischoff, L., Brockmeyer, P., Buhl, D., Lakomy, R., Müller-Mohr, V., 1992. The formation of the Sudbury structure, Canada, Toward a unified impact model. Geol. Soc. Am. Spec. Pap. 293, 303–318.

Stünitz, H., Fitz Gerald, J.D., Tullis, J., 2003. Dislocation generation, Slip Systems, and dynamic recrystallization in experimentally deformed plagioclase single crystals. Tectonophysics 372, 215–233.

Taylor, F.C., Dence, M.R., 1969. A probable meteorite origin for Mistastin Lake. Can. J. Earth Sci. 6, 39 – 45.

Therriault, A.M., Fowler, A.D., Grieve, R.A.F., 2002. The Sudbury Igneous Complex: A

differentiated impact melt sheet. Econ. Geol. 97, 1521–1540.

Thompson, L.M., Spray, J.G., 1996. Pseudotachylyte petrogenesis: constraints from the Sudbury impact structure. Contrib. to Mineral. Petrol. 125, 359–374.

Tuchscherer, M.G., Spray, J.G., 2002. Geology, mineralization, and emplacement of the Foy Offset Dike, Sudbury impact structure. Econ. Geol. 97, 1377–1397.

Tullis, J., Yund, R.A., 1985. Dynamic recrystallization of feldspar — a mechanism for ductile shear zone formation. Geology 13, 238–241.

Tungatt, P.D., Humphreys, F.J., 1984. The plastic deformation and dynamic recrystallisation of polycrystalline sodium nitrate. Acta Metall. 32, 1625 – 1635.

Urai, J.L., Means, W.D., Lister, G.S., 1986. Dynamic recrystallization of minerals, in: Mineral and Rock Deformation: Laboratory Studies, the Paterson Volume Geophys Monogr 36. American Geophysical Union, Washington DC, pp. 161–200.

White, S.H., 1976. The role of dislocation processes during tectonic deformation with special reference to quartz, in: Strens, R.J. (Ed.), The Physics and Chemistry of Minerals and Rocks. Wiley, London, pp. 75–91.

Wood, C.R., Spray, J.G., 1998. Origin and emplacement of Offset Dykes in the Sudbury impact structure: Constraints from Hess. Meteorit. Planet. Sci. 33, 337–347.

5 Sulfide Mineralization within Metabreccia

Denise Anders, Gordon R. Osinski, Richard A. F. Grieve

5.1 Introduction

The Sudbury Ni-Cu-platinum-group element (Ni-Cu-PGE) deposits are unique and are the only known such deposits in the world that originated from an impact melt sheet (Naldrett 2004). The first Ni-Cu deposit was discovered in 1883 (Giblin 1984) and, since then, Sudbury has grown to be one of the world's largest and most productive mining camps (Ames et al. 2008). The pre-mining resource is estimated at more than 1,648 million tons at ~1.2 % Ni and ~1.0 % Cu (Naldrett and Lightfoot 1993). The sulfide deposits are believed to be of both magmatic and hydrothermal origin (Farrow and Lightfoot 2002; Naldrett 2004; Ames and Farrow 2007; Ames et al. 2008; Carter et al. 2009). The Ni-Cu-PGE deposits from the Sudbury structure are divided into: i) Contact deposits within the Sublayer and Footwall Breccia, ii) Offset-type deposits iii) deposits within the South Range Breccia Belt, and iii) footwall-type deposits hosted by footwall rocks up to 1000 m below the SIC (Keays and Lightfoot 2004; Ames and Farrow 2007; Ames et al. 2008). Approximately 25% of the Sudbury resources are hosted within the Offset-type deposits (Ames et al. 2008), which, together with the contact deposits, formed by sulfide segregation during cooling of the Sudbury Igneous Complex (SIC) (Hawley 1962; Keays and Crocket 1970; Naldrett et al. 1979; Naldrett 1984b; Farrow and Watkinson 1997; Farrow and Lightfoot 2002).

The Offset dykes are composed of two main phases, the so-called inclusion-rich (IQD) and inclusion-poor Quartz Diorite (QD), of which the inclusion-rich phase is usually the sulfide-bearing lithology. Metabreccia (MTBX), a third dyke phase has, so far, only been detected at the Whistle (Lafrance and Bygnes 2014), Parkin (Murphy and Spray 2002, Chapter 3), Foy (Chapter 4) and Trill Offset Dykes (Chapter 4) in the North Range. It had been suggested, that MTBX was a dyke lithology like QD and IQD and emplaced by the injection of a melt derived from the SIC into fractures of the country rocks. Recent studies from Offset Dykes in the North Range, however, provided evidence that MTBX originated from Footwall Breccia (FWBX) and was included into the Offset Dykes, when those were

emplaced (Chapter 3 and 4). MTBX is a major host rock of Ni-Cu-PGE sulfides at the Podolsky and Whistle Mine (Farrow and Lightfoot 2002; Farrow et al. 2005), where it has been classified as a footwall-type deposit. Here, we present a study of some sulfide occurrences within MTBX from the radial Parkin, Trill and Foy Offset Dykes of the North Range compared to IQD.

5.2 Geological Setting

The 9.5 km long Parkin Offset Dyke (Fig. 5.1) is located ~3 km north of the northeastern corner of the SIC. The southern part of the dyke is hosted by metavolcanic rocks of the Cartier Batholith (2.64 Ga, Meldrum et al. 1997) and Benny Greenstone Belt (~2.71 Ga, Krogh et al. 1984), while the northern part of the dyke intrudes Huronian sediments (2.40–2.20 Ga, Young et al. 2001). The dyke contains the ore deposits of the Milnet 1500 zone; discovered in 2009, and the historical Milnet Mine, which was active from 1952 to 1954 (Wallbridge report 2013).

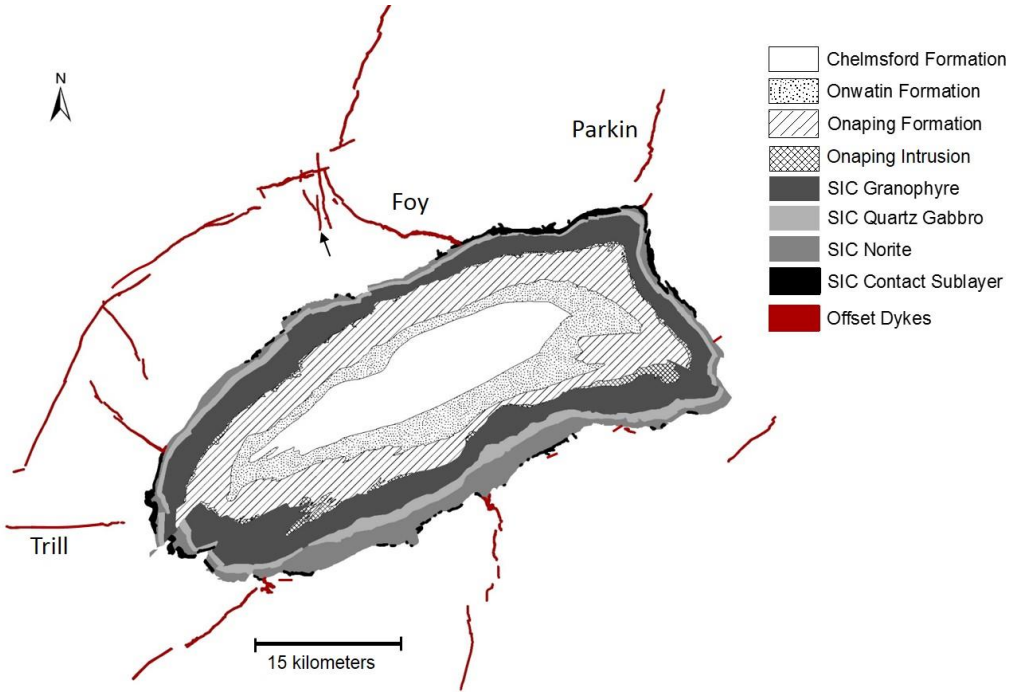

Figure 5.1. Simplified map of the Sudbury impact structure showing the location of the Parkin, Trill and Foy Offset Dykes.

The Foy Offset Dyke (Fig. 5.1) emanates from an embayment of the SIC and extends as well into rocks of the Levack Gneiss Complex, the Cartier Batholith, and the Benny Greenstone Belt. The dyke mainly contains QD and IQD (Tuchscherer and Spray 2002; Pilles et al. 2014a, 2014b); however, MTBX has previously been detected an described in detail (Chapter 4). The east-west trending Trill Offset Dyke (Fig. 4.1) west of the Sudbury Basin, was identified by Wallbridge Mining Company Limited in June 2005, and since then, has been traced for approximately 9.5 km to west (Coulter 2016). The host rocks are composed of Levack Gneiss and Cartier Batholith, intruded by Matachewan Diabase dykes (2.45 Ga, Card 1994).

5.3 Methodology

Polished thin sections of sulfide bearing IQD, MTBX, FWBX and Sudbury Breccia (SDBX) samples were collected from the Parkin, Trill and Foy Offset Dykes, during summer fieldwork in 2013, 2014 and 2015. The thin sections were examined by optical microscopy using transmitted and reflected light, in order to characterize mineralogy, microstructures and textures of sulfide minerals. Selected thin sections were carbon coated and analyzed by a JEOL JXA-8530F field-emission electron microprobe (EPMA Laboratory, University of Western Ontario). Wavelength dispersive spectrometry (WDS) provided quantitative point analyses of sulfides and Platinum-Group-minerals (PGMs), while energy dispersive spectrometry (EDS) was used to conduct semi-quantitative point measurements. For all analyses, the beam diameter was 1 μm. The used standards are for WDS and EDS analyses are listed in Table 5.1. Back-scattered electron images (BSE images) and point analyses of sulfides were created using an acceleration voltage of 20.00 keV. Element mapping of zoned pyrites with pixel sizes ranging from 1-8 μm were accomplished by WDS for As, Co, Fe, Ni, and Se and EDS for Cu and S. The acceleration voltage was 20.00 keV, the dwell time 10 ms, and the beam current ranged from 50-100 nA.

Table 5.1. Standards used during point analyses.

Element	Standard for Pyrite/ Pyrrhotite	Standard for Pentlandite	Standard for Chalcopyrite	Standard for PGM
Fe (EDS)	Pyrite	Pentlandite	Chalcopyrite	Chalcopyrite
S (EDS)	Pyrite	Pentlandite	Chalcopyrite	
Ni (EDS)	Pentlandite	Pentlandite	Chalcopyrite	
Cu (EDS)			Chalcopyrite	Chalcopyrite
Ag				Silver
As	Gallium Arsenide	Gallium Arsenide	Gallium Arsenide	Gallium Arsenide
Bi				Bismuth
Co	Cobalt	Cobalt	Cobalt	
Ir	Iridium	Iridium	Iridium	
Ni				Nickel
Os	Osmium	Osmium	Osmium	
Pb	Lead	Lead	Lead	Lead
Pd	Palladium	Palladium	Palladium	Palladium
Pt	Platinum	Platinum	Platinum	Platinum
Rh	Rhodium	Rhodium	Rhodium	
Ru	Ruthenium	Ruthenium	Ruthenium	
S				Millerite
Sb				Antimony
Se	Selenium	Selenium	Selenium	Selenium
Sn				Tin
Te				Tellurium

5.4 Observations

Sulfides within MTBX, IQD and QD from the Parkin, Foy and Trill Offset Dykes occur mainly as blebby to disseminated aggregates within the matrix. Locally small pods of massive sulfides up to one metre in size were observed within MTBX at Parkin (Figs. 5.2a-c). The middle trench at the Trill Offset Dykes hosts a large, several metres wide sulfide lens within IQD (Fig. 5.2c). The Crazy Creek trenches of the Foy Offset Dyke do not contain sulfide pods but rather disseminated and blebby sulfides distributed within the matrix of MTBX. Sulfides are commonly associated with mafic clasts (Fig. 5.2a). Sulfide occurrences are generally oxidized and gossanized, resulting in a characteristic red-brown surface weathering (Figs. 5.2b and d). Sulfide mineralization within MTBX consists mainly of chalcopyrite and pyrite, with minor pyrrhotite and pentlandite, while pyrrhotite

is the dominant sulfide mineral within IQD followed by pentlandite, chalcopyrite, and pyrite. The examined FWBX did not contain much mineralization and is mainly composed of some individual pyrite grains.

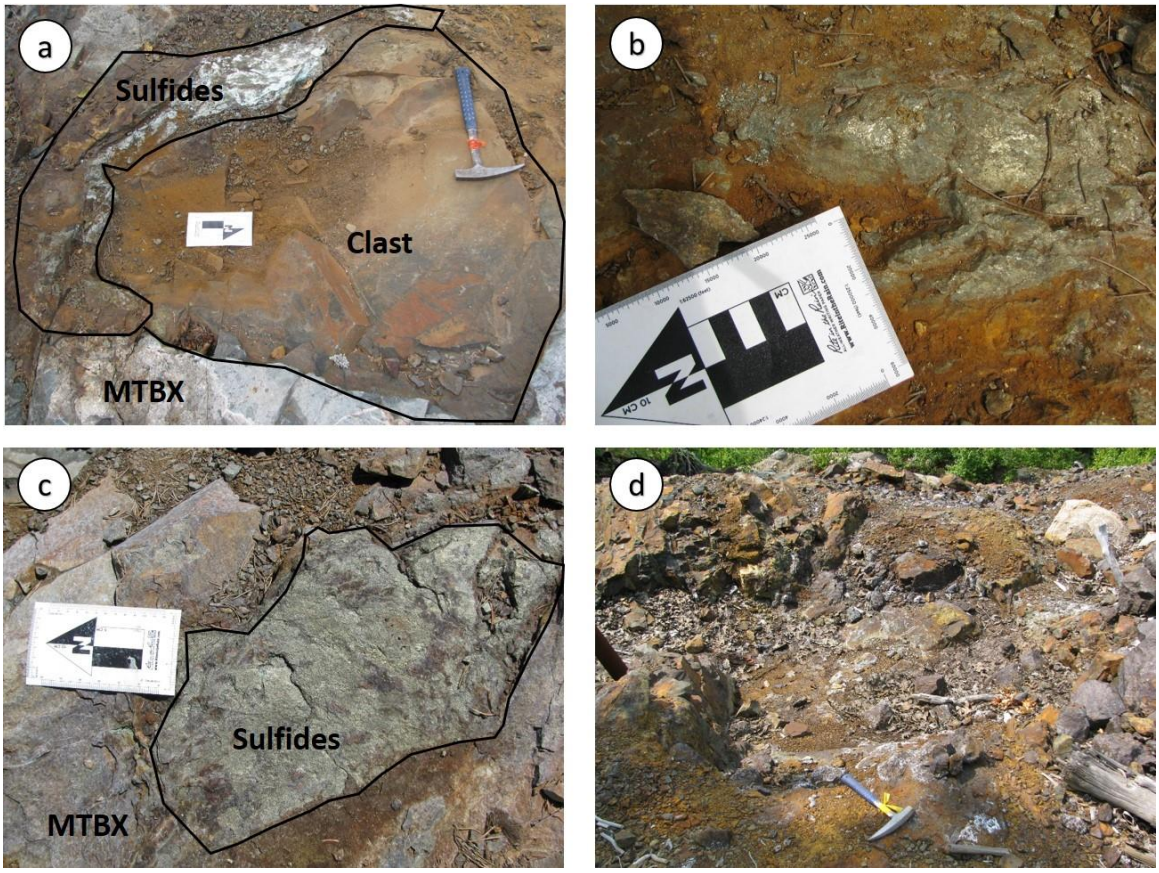

Figure 5.2. Field photographs of a) Mafic clast partially surrounded by sulfides within MTBX from Parkin (Trench 3, SUD-DA-086, 32 cm long hammer for scale). b) Massive sulfide pod of ~20 cm in size from the Parkin Offset Dyke (Brady trench, SUD-DA2014-050, 15 cm long card for scale) c) Massive sulfide pod of ~50 cm in size from the Parkin Offset Dyke (Brady trench SUD-DA2014-028, 15 cm long card for scale). d) Large, m-sized pod of massive sulfides from the Trill (middle trench, SUD-DA-TR-005, 32 cm long hammer for scale).

5.4.1 PGE traces in sulfide minerals

Chalcopyrite, pentlandite, pyrite and pyrrhotite within MTBX, IQD and FWBX contain traces of PGEs (<0.03 wt %) and the variations of Iridium-group PGEs (Ru, Ir, Os) and PGEs (Pt, Pd, Rh) are illustrated in Figures 5.1 and 5.2. The majority of chalcopyrites

contain traces of Os and some Ir; however, with the exception of two chalcopyrites within MTBX, Ru is below detection (Fig. 5.1a).

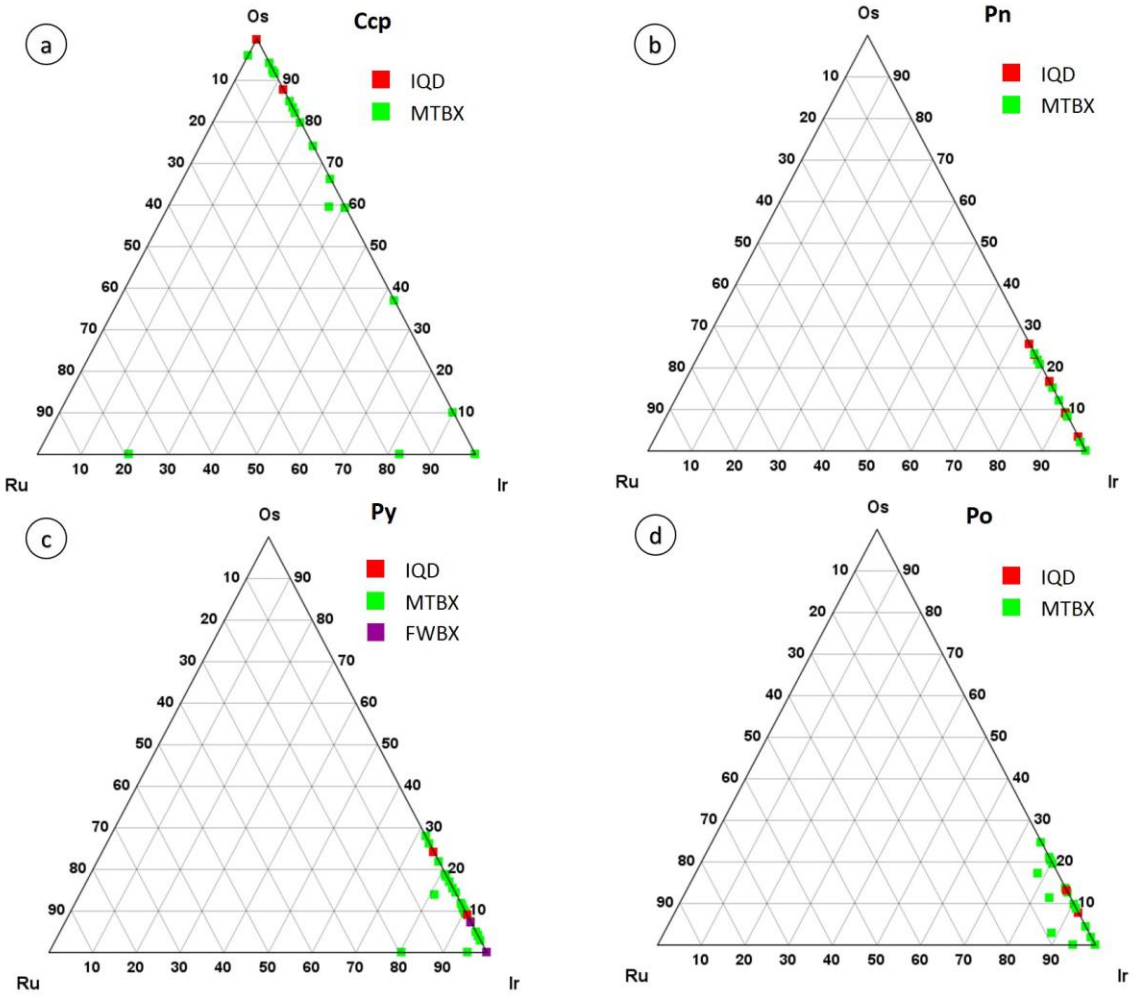

Figure 5.3. Ternary plots showing the enrichments of IPGEs of a) Chalcopyrite b) Pentlandite c) Pyrite and d) Pyrrhotite within samples of IQD (red), MTBX (green) and FWBX (purple).

Pentlandites, pyrites and pyrrhotites include traces of Ir and to a lesser extent Os (Figs. 5.1b-d). Rh is the main trace PGE detected in chalcopyrite (Fig. 5.1a), but has not been observed in the other sulfide minerals, which only contain traces of Ir (Figs. 5.1b-d).

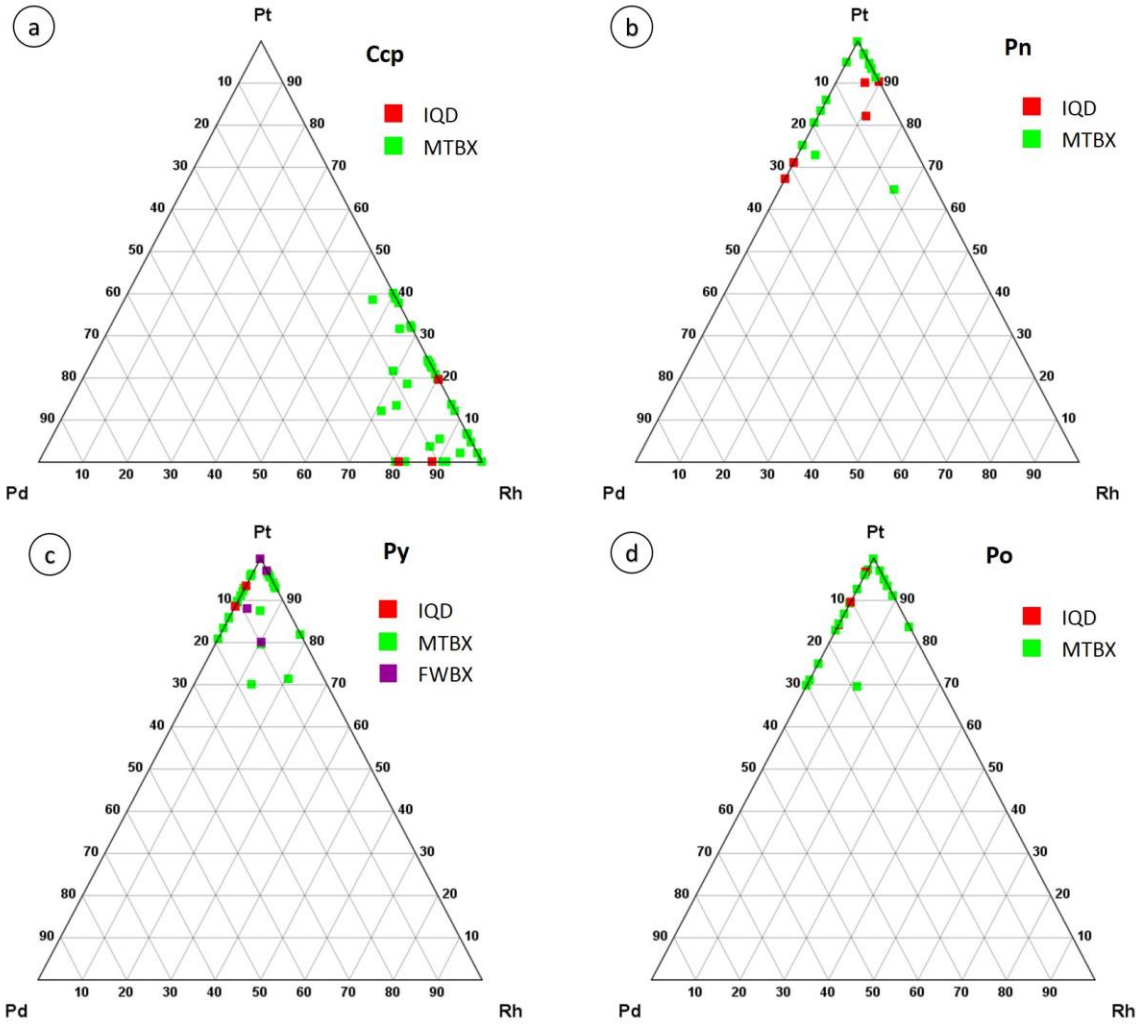

Figure 5.4. Ternary plots showing the enrichment of PGEs of a) Chalcopyrite b) Pentlandite c) Pyrite and d) Pyrrhotite within samples of IQD (red), MTBX (green) and FWBX (purple).

5.4.2 Zoning of pyrites

Pyrite grains within MTBX appear optically homogeneous and unzoned; however, elemental mapping reveals an oscillatory distributions of trace elements, as illustrated in Figures 5.5, 5.6 and 5.7 (also see Appendix 3).

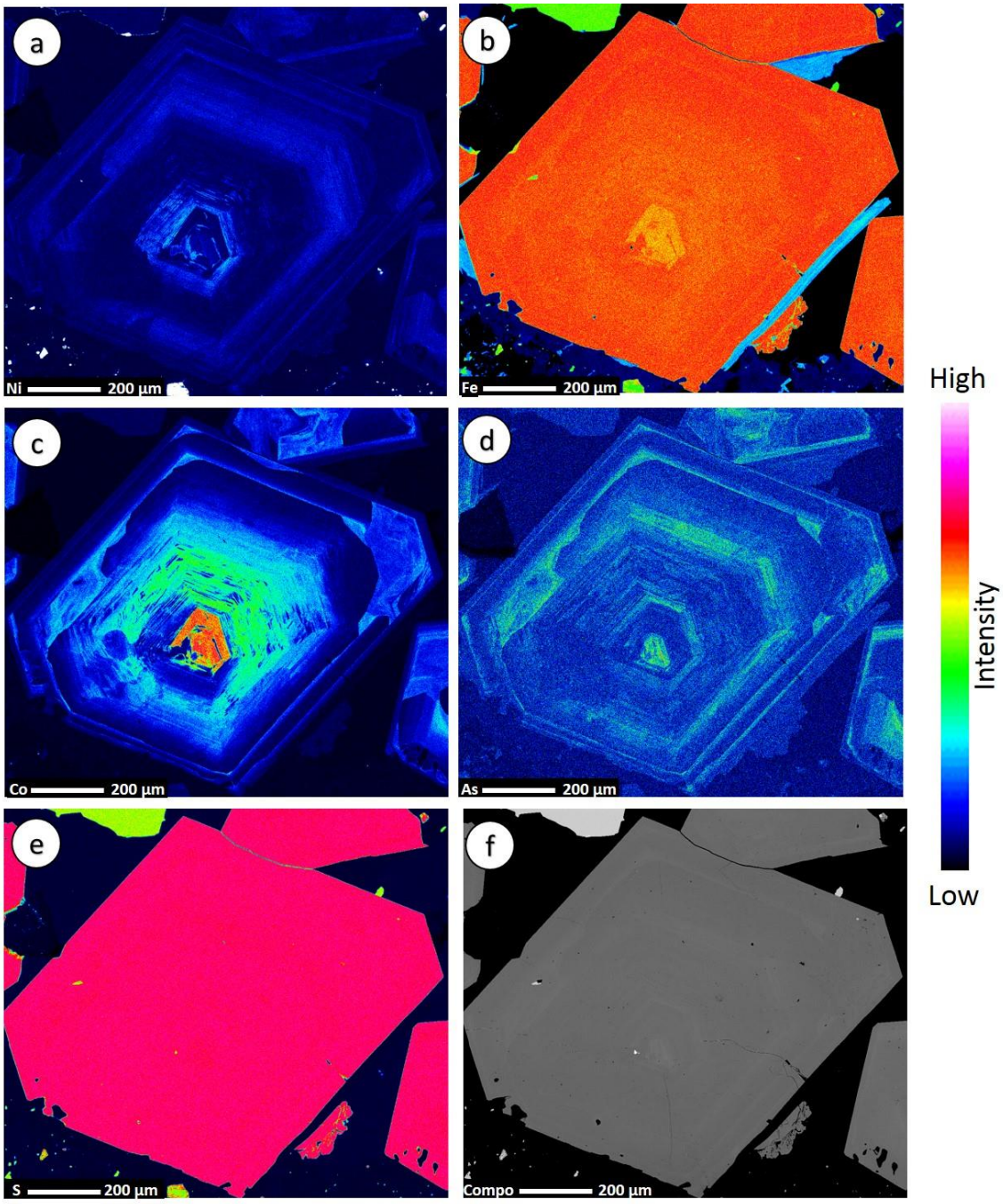

Figure 5.5. Microprobe semi-quantitative element maps showing a typical zoned, octahedral pyrite grain (SUD-DA-003, Parkin Trench 3). a) Ni only shows several weakly zoned layers. b) Fe is slightly enriched in the centre of the grain and gradually increases outwards. c) The zoning starts with a Co-rich core, which gradually decreases outwards. d) As correlates with Co, however, the zoning is less pronounced. e) S does not display zoning. f) Backscattered Electron image (BSE image) of the mapped pyrite.

Oscillatory zoning has been observed within MTBX samples from the Parkin and Whistle Offset Dykes and is usually associated with individual grains of idiomorphous, octahedral crystal habit (Fig. 5.5). Massive sulfide samples do not contain euhedral pyrite grains and no zoning. Zoned pyrites are limited to MTBX from Parkin and Whistle and have not been detected within MTBX samples from the Foy and Trill Offset Dykes, or within IQD, SDBX or FWBX. The zoning is generally parallel to crystallographic planes and involves mainly the elements Co and As, to a lesser extent Ni and Fe, while Cu, S and Se are evenly distributed within the pyrite grains. While some pyrites show extensive zoning (Fig. 5.5), others are characterized by a less pronounced distribution pattern and only slight changes in trace element composition (see Appendix 3).

Two types of pyrites have been identified: pyrites characterized by a Co-rich euhedral-shaped core (Fig. 5.5c) and pyrites with a Co-depleted centre of irregular shape surrounded by a euhedral Co-rich layer (Fig. 5.6c). Figure 5.3 shows element maps of a pyrite grain with a Co- and As-rich centre. The concentration of Co decreases gradually outwards (Fig. 5.5c), while As only shows small changes in concentration resulting in slightly zoned layers (Fig. 5.5d). It follows a zone of Co depletion, associated with decreased As which correlates with a weak increase in Ni (Fig. 5.5a). The zoning is asymmetrical and irregular, with one side showing thicker compositional layers than the opposite side (Fig. 5.5c). In contrast, the pyrite in Figure 5.6 is characterized by a Co-depleted irregular-shaped centre surrounded by a zone enriched in Co, As (Figs. 5.6c and d) and slightly in S (Fig. 5.6e). The outer layer is depleted in Co (Fig. 5.6c) but weakly enriched in Ni (Fig. 5.6d). The grain depicted in Figure 5.7 contains two small Co and As-enriched pyrites (Figs. 5.7c and d) surrounded by an irregular-shaped chalcopyrite and an asymmetrical distributed layer of Co and As pyrite with an outer rim depleted in As and Co (Figs. 5.7c and d) but slightly enriched in Ni (Fig. 5.7a). The resulting pyrite is embayed but shows the outline of a euhedral-shaped pyrite crystal. The distribution of Co correlates with As; however, the layers of As are usually thinner than the Co layers (Figs. 5.7c and d).

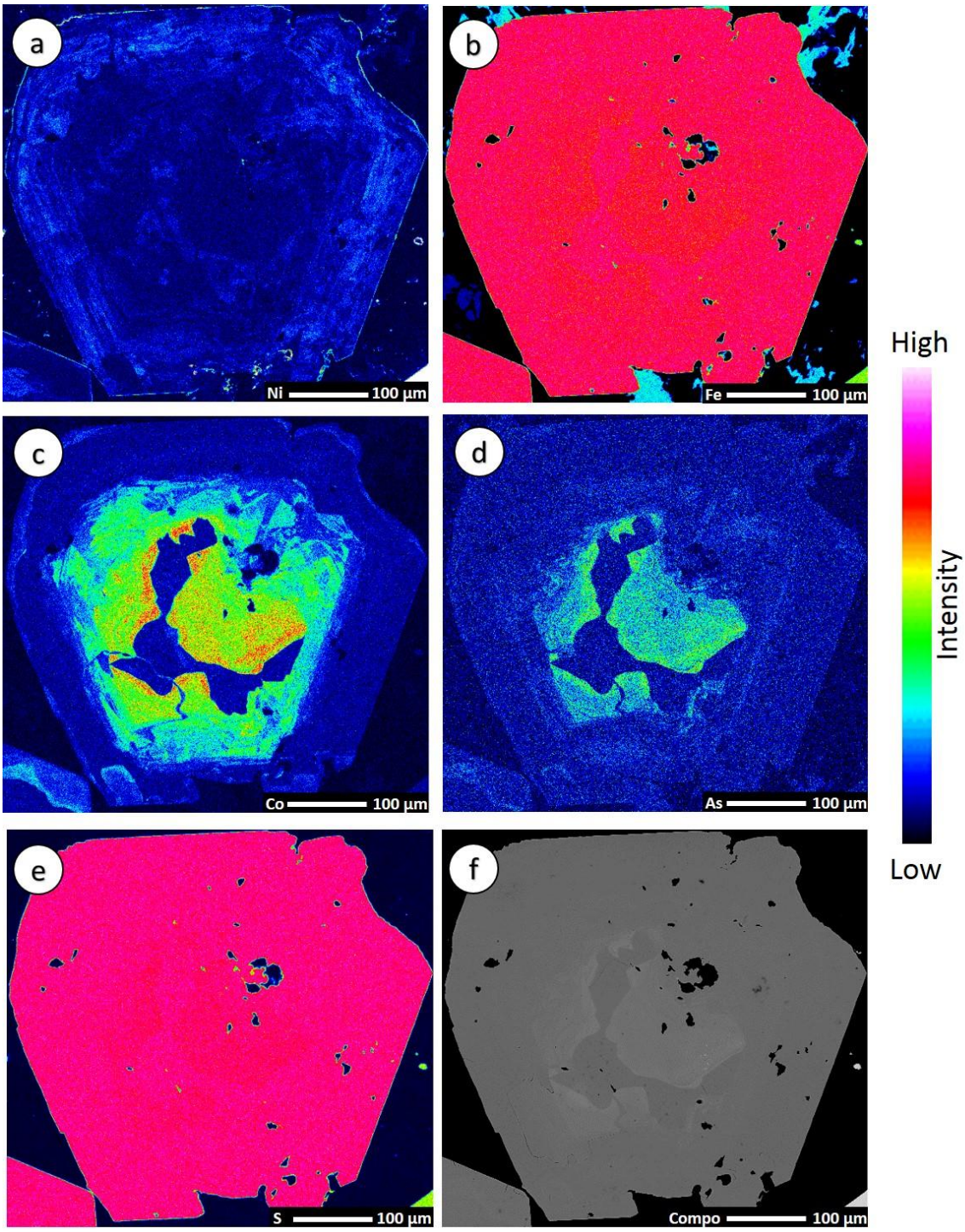

Figure 5.6. Microprobe semi-quantitative element maps showing less intensive zoning within a pyrite grain (SUD-DA-013 map, Parkin Trench 3). a) Ni showing slight zoning in the outer parts of the grain. b) Slight Fe zoning correlated to Co. c) Co is depleted in the irregular-shaped core and increases outwards. The outer zone is again Co-depleted. d) As correlated with the zoning of Co. e) Slight zoning of S. f) Backscattered Electron image (BSE image).

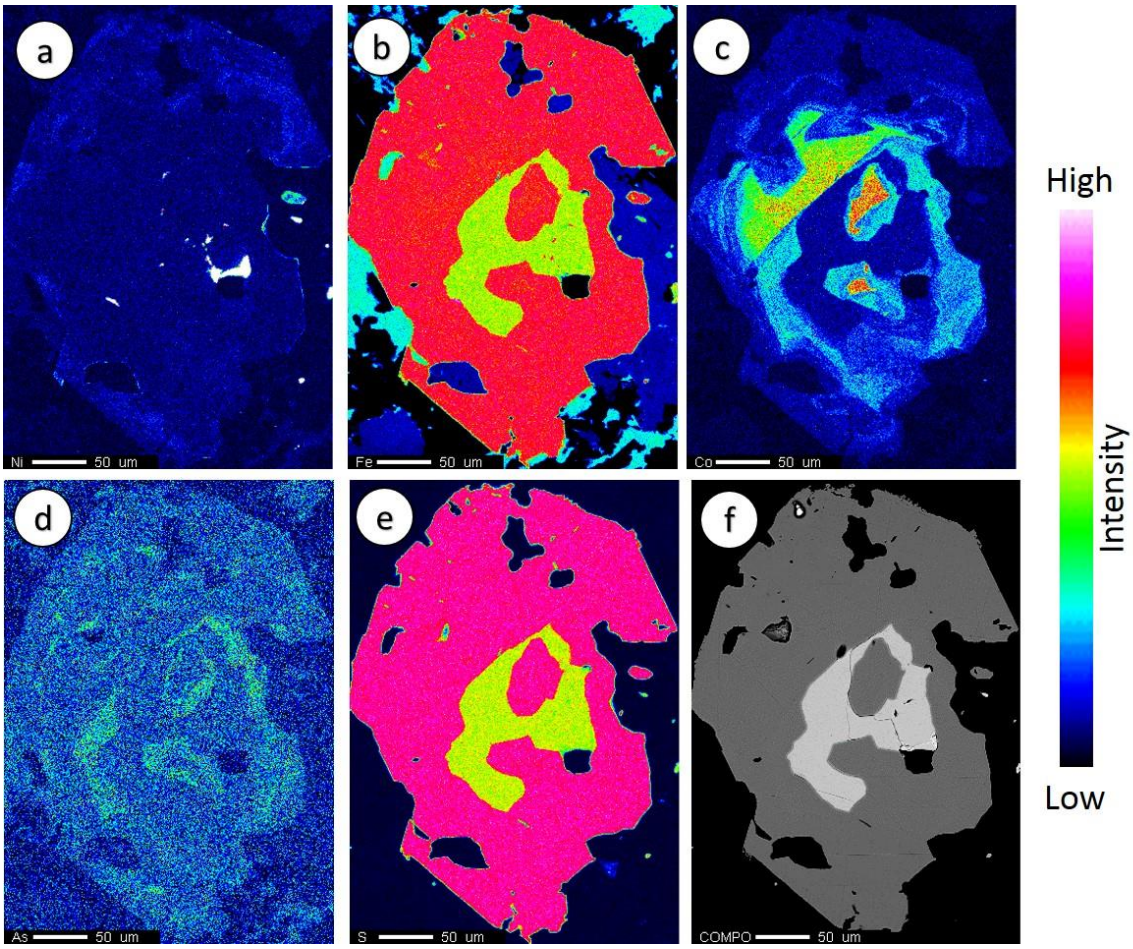

Figure 5.7. Microprobe semi-quantitative element maps of a small centred zoned pyrite grains within chalcopyrite, which is surrounded by compositionally zoned pyrite (SUD-DA-003, Parkin Trench 3). a) Only slight visible zoning in Ni. b) No Fe zoning within the pyrite grain. c) Co shows intensive asymmetrical zoning and correlates d) with As. e) No zoning in S. f) Backscattered Electron image (BSE image).

5.4.3 Platinum-Group Minerals

Platinum-Group minerals have been observed within samples of MTBX, IQD and SDBX. The FWBX sample examined in this study did not contain PGMs; however, the investigated sample from the Coleman mine was generally poor in sulfide mineralization.

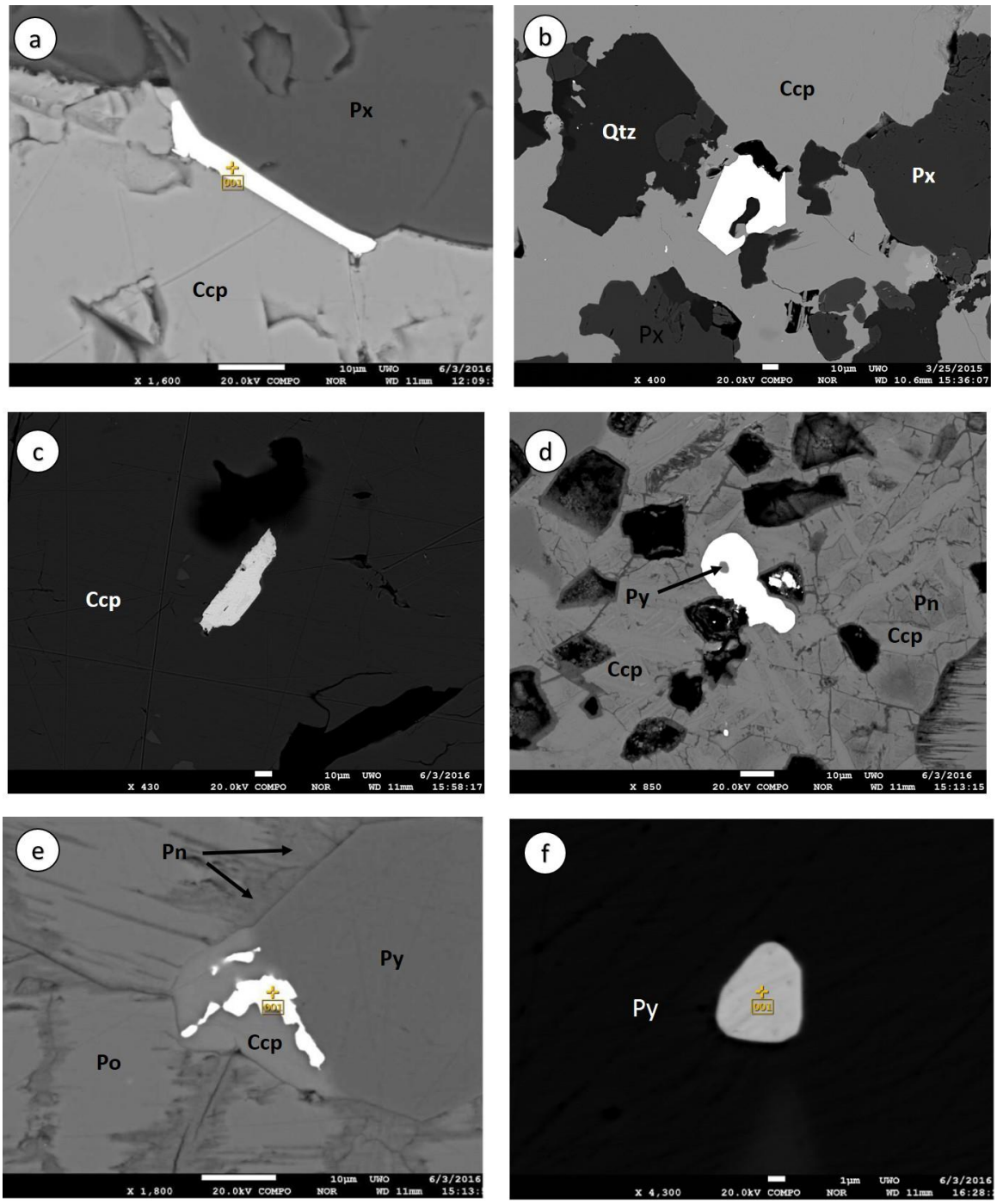

Figure 5.8. Backscattered electron images (BSE) of PGMs. a) Moncheite (white) in MTBX from Foy (SUD-DA-FOY-007) located at the grain boundary between Chalcopyrite (Ccp) and pyroxene (Px). b) Sperrylite in MTBX from Parkin (SUD-DA-086B). c) Bismutho-telluride with only traces of PGEs in MTBX from Parkin (SUD-DA-2014-028). d) Merenskyite with a pyrite inclusion within IQD from Trill (SUD-DA-TR-005). d) Niggliite in IQD from Trill (SUD-DA-TR-005). f) Kotulskite within SDBX from Trill (SUD-NB-113).

PGMs in MTBX occur as minute, rounded to droplet-shaped particles of several μm in size and rarely as elongated laths up to a length of 30 μm (Fig. 5.8a). They are predominantly hosted within chalcopyrite and in some occasions at grain boundaries between sulfides and silicates (Fig. 5.8a), or within the silicate matrix itself. The majority of the PGMs detected in MTBX belong to the moncheite group $(PtPd)(TeBi)_2$, predominantely bismuthotellurides with dominant Pt and Te over Pd and Bi (Fig. 5.8a). Some minor occurrences of sperrylite ($PtAs_2$) (Fig. 5.8b) and bismuthotellurides with only traces of PGEs (Fig. 5.8c) have also been detected.

In contrast, the PGM assemblage in IQD, mainly hosted in pyrrhotite, but also pentlandite and is mainly composed of Pd- and Te-rich bismuthotellurides of the merenskyite group $(PdPt)(TeBi)_2$ (Fig. 5.8d) and locally niggliite (PtSn) (Fig. 5.8e). Kotulskite (PdTe) (Fig. 5.8f), hosted in pyrite, is the main PGM observed within SDBX from the Trill Offset Dyke. Moncheite and merenskyite form a complete solid solution with melonite ($NiTe_2$), and to some extent with insizwaite ($PtBi_2$), froodite ($PdBi_2$) and geversite ($PtSb_2$), and can also incorporate other trace elements (Cabri 2002), which creates a wide range of various Pd-Pt-bismuthotellurides compositions (Fig. 5.9).

The composition of the PGE minerals is shown in the ternary merenskyite-moncheite-melonite diagram in Figure 5.8a. PGMs within MTBX plot, with the exception of one, in the moncheite field, but show a wide range of Pt-Pd composition. PGMs in IQD fall within the field of the Pd-mineral merenskyite. The PGMs contain significant, but varying amounts of Cu, Fe and Ag (Fig. 5.8b), which substitute for Pt and Pd. Merenskyite and kotulskite incorporated mainly Fe (up to 2.9 wt %); whereas, moncheites are characterized by a higher amount of Cu (up to 5.8wt %). Silver only exists in traces within all PGMs (<1 wt %). Traces of Se have been detected in all moncheites, however, none of the merenskyites in IQD contains Se. All PGMs contain dominantly Te over Bi, however, merenskyites and kotulskite within IQD and SDBX display a slightly higher amount of Bi than moncheites within MTBX (Fig. 5.8c). Bismutho-tellurides in MTBX, with only traces of Pd and Pt, are characterized by increased amounts of Bi with lower Te contents.

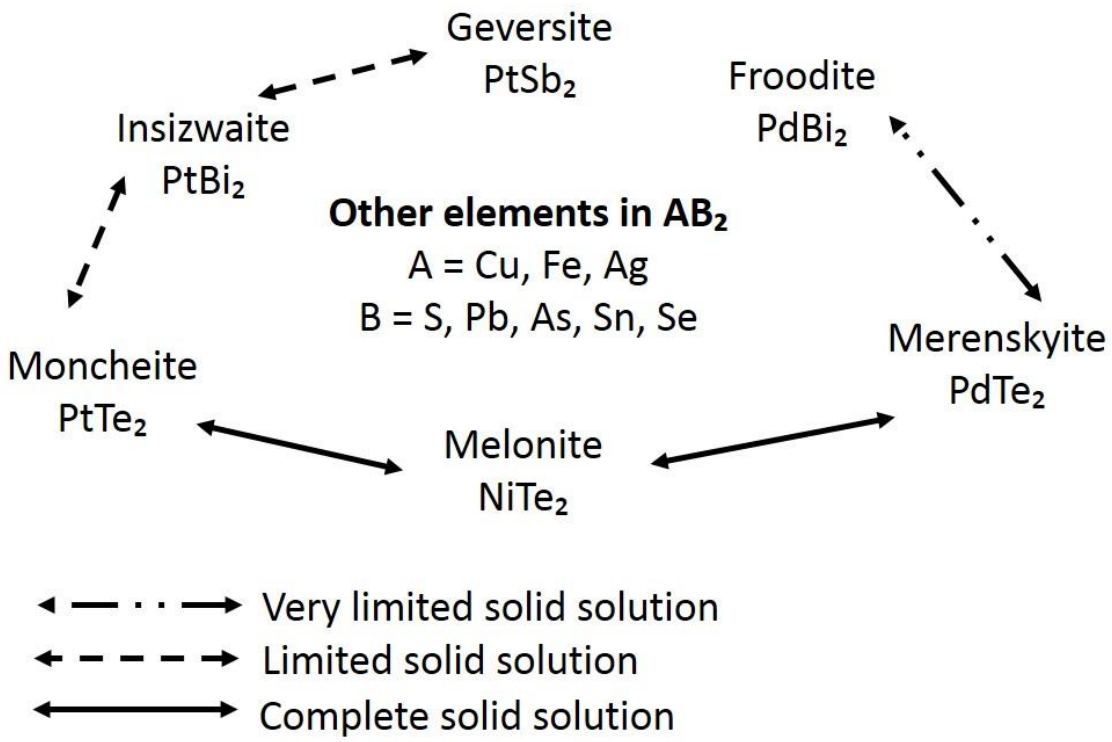

Figure 5.9. Overview of the composition of PGE-bismuthotellurides. An intensive solid solution has been observed within the endmembers moncheite, melonite and merenskyite.

5.5 Discussion

Sulfide minerals in IQD consist predominantly of pyrrhotite, which is in accordance to previous studies of Offset-type deposits (Grant and Bite 1984; Farrow and Lightfoot 2002; Farrow et al. 2005). In contrast, sulfide mineralization within MTBX is composed of mainly chalcopyrite and pyrite, which corresponds to the style of footwall-type deposits (Farrow et al. 2005). Mineralization within MTBX has not been studied in detail and has only been reported from the Podolsky and Whistle Mines at the Whistle Offset Dyke, where MTBX is host to economically important Ni-Cu-PGE ore deposits (Lightfoot and Farrow 2002; Farrow et al. 2005). The origin of Cu-rich footwall-type deposits has been reported to be the result of a Cu-rich residuum after the fractionation of the Ni-bearing Fe monosulfide solid-solution that formed the contact ores (Li et al. 1992, 1993; Ebel and Naldrett 1996).

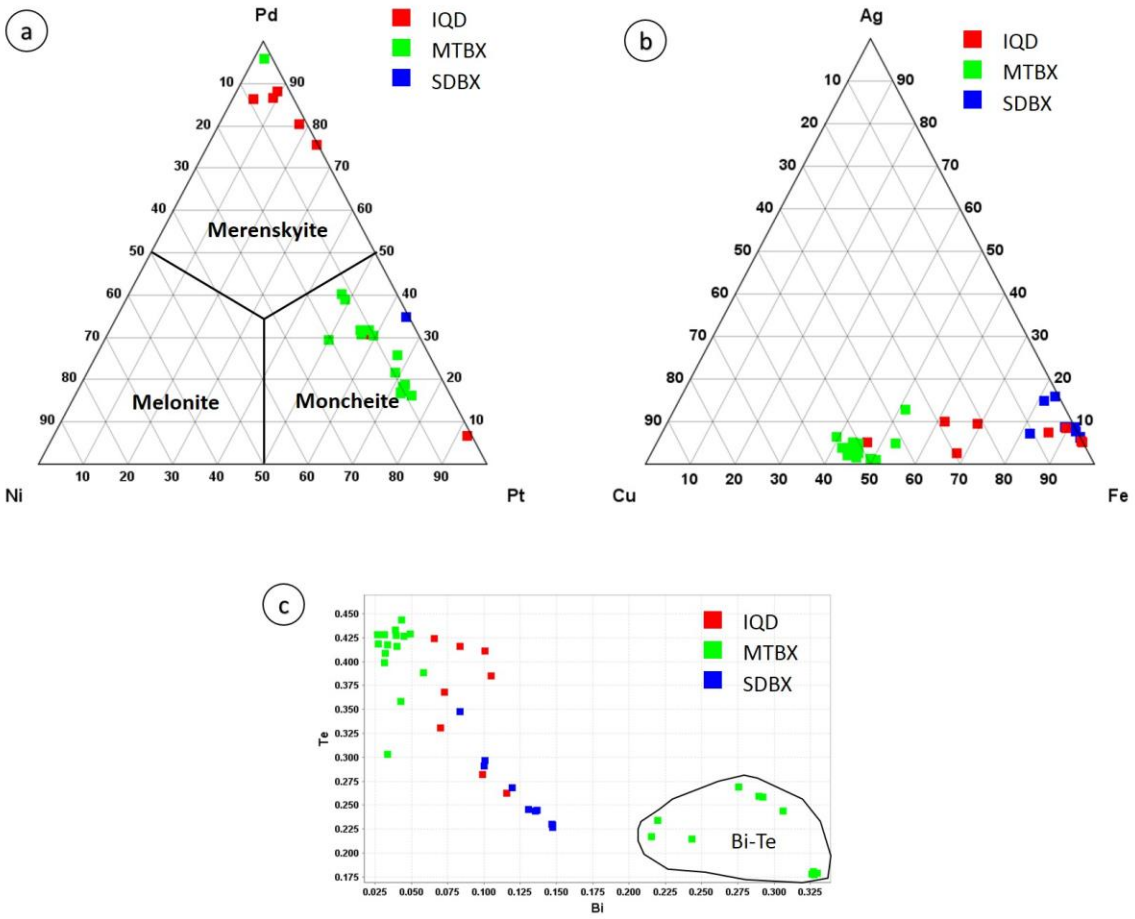

Figure 5.10. Geochemical variations of the PGMs detected within MTBX, IQD and SDBX (in atomic proportions). a) Merenskyite-moncheite-melonite ternary diagram showing the composition of PGMs. b) Ternary diagram illustrating the extent of incorporation of races of Cu, Ag and Fe within PGMs.

The Cu-rich sulfide fractionated from the sulfide liquid within the SIC, migrated into the footwall and host rocks and solidified there at ~900°C (Barnes and Lightfoot 2005). With respect to PGEs in sulfide minerals, it is interesting that chalcopyrite shows a different trace element signature than pyrite, pyrrhotite and pentlandite. Chalcopyrite in MTBX is characterized by higher amounts of Os and Rh, whereas, pyrite, pentlandite and pyrrhotite do not contain traces of those elements but rather traces of Ir and Pt. Rhenium and Pd were absent in all sulfide minerals. These results are at odds with the assumption that during

fractionation at temperatures of 1180–950°C, the Cu-rich sulfide liquid gets enriched in Pt, Pd and Au, whereas Os, Ir, Ru and Rh fractionate into the Fe-rich monosulfide solid solution (Barnes and Lightfoot 2005; Dare et al. 2011).Geochemical zoning in pyrites (Figs. 5.3, 5.4 and 5.5) has only been detected within MTBX and is usually associated with euhedral pyrites, while massive pyrites or irregular-shaped grains do not show zoning. The crystals grew from the centre outward and the element distribution pattern reflects the geochemical variations of the parental fluid from which the mineral crystallized. Cobalt, and to a lesser extent As, were apparently enriched in the early stages of pyrite growth and decreased gradually over time (Figs. 5.3c and d). In some cases, however, the initial fluid was Co-As-depleted and increased after growth of the pyrite had already started leading to the development of a Co-As-depleted core with a Co-As-rich middle layer (Figs. 5.4c and d). This indicates that the fluid composition was not identical an all locations. As and Ni show less intensive zoning, however the composition of those elements in the parental fluid seem to have changed several times, resulting in smaller concentric layers with only slight variations in the amount. The elements are apparently not always evenly distributed in the fluids around the grain, resulting in an irregular growth, with one side of the grain showing higher element concentration than the other side. This is very distinctive with respect to Co and might be related to varying diffusion rates. Enriched Co zoned usually correlate with increased concentrations of As and decreased amounts of Ni, indicating that the parental fluid was either enriched in Co and As and depleted in Ni, or was low in Co and As and slightly enriched in Ni. Similar zoning has been reported from the McCreedy East deposit (Dare et al. 2011) and the Craig Mine (Craig and Solberg 1999) and had been identified as primary pyrites formed from a magmatic fluid with varying composition. The sulfides investigated in those studies are hosted within FWBX and are, so far, the only reported occurrences of zoned pyrites around the Sudbury structure. This indicates that there might exist a genetic relationship between sulfides within FWBX and MTBX. As already established in Chapter 3 and 4, FWBX seem to be the closest proxy to the MTBX. FWBX and MTBX show similarities in texture and geochemical composition and it is very likely that MTBX, in fact, originated from FWBX. Thus, it is also likely that both lithologies share similar sulfide composition and origins.

The majority of the Pd and Pt occur as bismuthotelluride minerals of the moncheite-merenskyite group, which is in accordance to previous studies in North Range (Cabri and Laflamme 1976; Naldrett 2004; Farrow et al. 2005). However, with the significant incorporation of Fe and Cu, they show somewhat unusual composition, although traces of those elements have been reported within PGMs (Cabri 2002). PGMs within MTBX consist of moncheite, a Pt enriched bismuthotellurides, whereas IQD mainly contains the Pd-bismuthotelluride merenskyite. Moncheite has been reported as more common in the North Range than the South and is associated to footwall-type deposits (Farrow and Lightfoot 2002; Farrow et al. 2005). Increased amounts of Pt within PGMs have been ascribed to higher crystallization temperatures than Pd enriched PGMs (Helmy et al. 2010), which might indicate that the PGMs within MTBX formed at elevated temperatures, and thus, earlier than the PGMs within IQD. The incorporation of Fe and Cu into PGMs might reflect the composition of the parental fluid they crystallized from. Moncheites in MTBX contain significant amounts of Cu, while merenskyites in IQD and kotulskite within pyrites of SDBX show higher amounts of iron. It seems that the parental fluid from which the PGMs within MTBX originated was enriched in Cu, which is in accordance to the Cu-rich residuum that formed the Cu-rich footwall-type deposits (Li et al. 1992, 1993; Ebel and Naldrett 1996; Barnes and Lightfoot 2005). As MTBX originated from FWBX, which was ripped off and transported with the dyke melt when the Offset Dykes were emplaced, the Cu-rich residuum must have already penetrated the footwall and accumulated within the footwall rocks, when the Offset Dykes were emplaced. The fact that IQD does only contain minor pyrite, without zoning, might indicate that the formation of sulfides in MTBX and IQD occurred under different conditions and within a different time frame. MTBX originated from FWBX and was mobilized and included into the dyke phases when they were emplaced as Offset Dykes into fractures of country rocks. FWBX was formed as a clastic breccia due to brecciation of the crater floor. During and after the emplacement of the proto-impact melt sheet, melt intruded into fractures of the brecciated footwall rocks and resulted into partial and fully melting, and the formation of FWBX. Over the course of the formation of FWBX, it was in interaction with the proto-impact melt sheet, which could have caused the accumulation of sulfides from the melt sheet. During the injection of a melt from the melt sheet into fractures of the country rocks, FWBX fragments, together

with the accumulated sulfides within the FWBX, were mobilized and included into dyke. The dyke melt was hot enough to thermally overprint and metamorphose the FWBX fragments, resulting in the formation of MTBX. The included Cu-rich sulfide liquid cooled and crystallized to form a sulfide assemblage of mainly composed chalcopyrite. Alternatively, the observed sulfide pods within MTBX could also be interpreted as fragments that originated from a pre-existing source. Such sulfide fragments are already known from FWBX (Pattison 1979) and could have been inherited and incorporated into MTBX during the dyke emplacement.

5.6 Conclusions

The results of this study indicate that the sulfides within MTBX and IQD do not share many similarities and, thus, formed most likely from different parental fluids. The increased Cu contents within MTBX mineralization points to an origin from the Cu-enriched residuum after the fractionation of the Ni-bearing Fe monosulfide solid-solution, which is not the case for sulfides in IQD. If MTBX and IQD were genetically related and both formed by injection of a melt from the SIC as Offset Dykes, they would most likely both inherit similar sulfide composition. The sulfide composition and assemblage in MTBX seems to be more similar to contact- and footwall-type deposits than Offset Dyke deposits, and thus, points to a genetic relationship between the FWBX and MTBX.

5.7 References

Ames, D.E., Davidson, A., Wodicka, N., 2008. Geology of the giant Sudbury polymetallic mining camp, Ontario, Canada. Econ. Geol. 103, 1057–1077.

Ames, D.E., Farrow, C.E.G., 2007. Metallogeny of the Sudbury mining camp, Ontario, in: Goodfellow, W.D. (Ed.), Mineral Deposits of Canada: A Synthesis of Major Deposit-Types, District Metallogeny, the Evolution of Geological Provinces, and Exploration Methods. Geological Association of Canada, Mineral Deposits Division, Special Publication 5. pp. 329–350.

Barnes, S.-J., Lightfoot, P.C., 2005. Formation of magmatic nickel-sulfide ore deposits and processses affecting their copper and platinum-group element contents. Econ. Geol.

100, 179–213.

Cabri, L.J., 2002. The Platinum-Group Minerals, in: Cabri, L.J. (Ed.), Geology, Geochemistry, Mineralogy and Mineral Beneficiation of Platinum-Group Elements. Canadian Institute of Mining, Metallurgy and Petroleum, Special Volume 54, pp. 13–129.

Cabri, L.J., Laflamme, J.H.G., 1976. The mineralogy of the platinum-group elements from some copper-nickel deposits of the Sudbury area, Ontario. Econ. Geol. 71, 1159–1195.

Card, K.D., 1994. Geology of the Levack gneiss complex, the northern footwall of the Sudbury structure, Ontario. Geol. Surv. Canada Curr. Res. 1994-C, 269–278.

Carter, W.M., Watkinson, D.H., Ames, D.E., Jones, P.C., 2009. Quartz Diorite Magmas and Cu-(Ni)-PGE Mineralization, Podolsky Deposit, Whistle Offset Structures, Sudbury, Ontario. Geol. Surv. Canada Open File 6134, 58 pp.

Coulter, A.B., 2016. Recent Discoveries in the Ni-Cu-PGE bearing Trill and Parkin Offset dykes, Sudbury impact structure, Canada. M.Sc. Thesis, West. Univ. Dep. Earth Sci. Electron. Thesis Diss. Repos. Paper 3473.

Craig, J.R., Solberg, T.N., 1999. Compositional zoning in ore minerals at the Craig mine, Sudbury, Ontario, Canada. Can. Mineral. 37, 1163–1176.

Dare, S.A.S., Barnes, S.-J., Prichard, H.M., Fisher, P.C., 2011. Chalcophile and platinum-group element (PGE) concentrations in the sulfide minerals from the McCreedy East deposit, Sudbury, Canada, and the origin of PGE in pyrite. Miner. Depos. 46, 381–407.

Ebel, D.S., Naldrett, A.J., 1996. Fractional crystallization of sulfide ore liquids at high temperature. Econ. Geol. 91, 607–621.

Farrow, C.E.G., Everest, J.O., King, D.M., Jolette, C., 2005. Sudbury Cu-(Ni)-PGE-Systems: Refining the classification: Using McCreedy West Mine, and Podolski

project case studies, in: Mungall, J.E. (Ed.), Exploration for Platinum- Group Elements Deposits. Mineralogical Association of Canada, Short Course Series Volume 35, pp. 163–180.

Farrow, C.E.G., Lightfoot, P.C., 2002. Sudbury PGE Revisited: Towards an Integrated Model, in: Cabri, L.J. (Ed.), Geology, Geochemistry, Mineralogy and Mineral Beneficiation of Platinum-Group Elements. Canadian Institute of Mining, Metallurgy and Petroleum, Special Volume 54, pp. 273–297.

Farrow, C.E.G., Watkinson, D.H., 1997. Diversity of precious-metal mineralization in footwall Cu-Ni-PGE deposits, Sudbury, Ontario; implications for hydrothermal models of formation. Can. Mineral. 35, 817–839.

Giblin, P.E., 1984. History of Exploration and Development, of Geological Studies and Development of Geological Concepts, in: Pye, E.G., Naldrett, A.J., Giblin, P.E. (Eds.), The Geology and Ore Deposits of the Sudbury Structure. pp. 3–23.

Grant, R.W., Bite, A., 1984. Sudbury Quartz Diorite Offset Dikes, in: Pye, E.G., Naldrett, A.J., Giblin, P.E. (Eds.), The Geology and Ore Deposits of the Sudbury Structure. pp. 275–300.

Hawley, J.E., 1962. The Sudbury ores, their mineralogy and origin; Part 3, Interpretations; The history and origin of the Sudbury ores. Can. Mineral. 7, 146–207.

Helmy, H.M., Ballhaus, C., Wohlgemuth-Ueberwasser, C., Fonseca, R.O.C., Laurenz, V., 2010. Partitioning of Se, As, Sb, Te and Bi between monosulfide solid solution and sulfide melt – Application to magmatic sulfide deposits. Geochim. Cosmochim. Acta 74, 6174–6179.

Keays, R.R., Crocket, J.H., 1970. A study of precious metals in the Sudbury nickel irruptive ores. Econ. Geol. 65, 438–450.

Keays, R.R., Lightfoot, P.C., 2004. Formation of Ni–Cu–Platinum Group Element sulfide mineralization in the Sudbury Impact Melt Sheet. Mineral. Petrol. 82, 217 – 258.

Krogh, T.E., Davis, D.W., Corfu, F., 1984. Precise U–Pb zircon and baddeleyite ages for the Sudbury area, in: Pye, E.G., Naldrett, A.J., Giblin, P.E. (Eds.), The Geology and Ore Deposits of the Sudbury Structure. pp. 431–447.

Lafrance, B., Bygnes, L.C., 2014. Emplacement of metabreccia along the Whistle offset dike, Sudbury: implications for post-impact modification of the Sudbury impact structure. Can. J. Earth Sci. 19, 1–19.

Li, C., Naldrett, A.J., Coats, C.J.A., Johannessen, P., 1992. Platinum, palladium, gold, copper-rich stringers at the Strathcona Mine, Sudbury; their enrichment by fractionation of a sulfide liquid. Econ. Geol. 87, 1584–1598.

Li, C., Naldrett, A.J., Rucklidge, J.C., Kilius, L.R., 1993. Concentrations of Platinum-Group Elements and gold in sulfides from the Strathcona deposit, Sudbury, Ontario. Can. Mineral. 30, 523–531.

Lightfoot, P.C., Farrow, C.E.G., 2002. Geology, geochemistry, and mineralogy of the Worthington offset dike: A genetic model for offset dike mineralization in the Sudbury Igneous Complex. Econ. Geol. 97, 1419–1446.

Meldrum, A., Abdel-Rahman, A.F.M., Martin, R.F., Wodicka, N., 1997. The nature, age and petrogenesis of the Cartier Batholith, northern flank of the Sudbury Structure, Ontario, Canada. Precambrian Res. 82, 265–285.

Murphy, A.J., Spray, J.G., 2002. Geology, mineralization and emplacement of the Whistle–Parkin offset dike, Sudbury impact structure. Econ. Geol. 97, 1369–1389.

Naldrett, A.J., 1984. Ni–Cu ores of the Sudbury Igneous Complex –Introduction, in: Pye, E.G., Naldrett, A.J., Giblin, P.E. (Eds.), The Geology and Ore Deposits of the Sudbury Structure. pp. 302–307.

Naldrett, A.J., 2004. Magmatic Sulfide Deposits: Geology, Geochemistry and Exploration. Springer Verlag, Heidelberg, Berlin.

Naldrett, A.J., Hoffman, E.L., Green, A.H., Chou, C., Naldrett, S.R., 1979. The

composition of Ni-Sulfide ores, with particular reference to their content of PGE and Au. Can. Mineral. 17, 403–415.

Naldrett, A.J., Lightfoot, P.C., 1993. Ni-Cu-PGE ores of the Noril'sk region Siberia: A model for giant magmatic ore deposits associated with flood basalt. Soc. Econ. Geol. Spec. Publ. 2, 81–123.

Pattison, E.F., 1979. The Sudbury Sublayer. Can. Mineral. 17, 257–274.

Pilles, E., Osinski, G.R., Bailey, J., Smith, D., 2014a. Outward Emplacement of the FoyOffset Dyke at the Sudbury Impact Structure, Canada – Evidence from the Variation in Inclusions Along Strike. GSA Annu. Meet. Vancouver, Bitish Colomb. Paper No.

Pilles, E., Osinski, G.R., Bailey, J., Smith, D., 2014b. Emplacement of the Foy Offset Dyke at the Sudbury Impact Structure, Canada. 45th Lunar Planet. Sci. Conf. Houston, Texas abstract #.

Tuchscherer, M.G., Spray, J.G., 2002. Geology, mineralization, and emplacement of the Foy Offset Dike, Sudbury impact structure. Econ. Geol. 97, 1377–1397.

Young, G.M., Long, D.G.F., Fedo, C.M., Nesbitt, H.W., 2001. Paleoproterozoic Huronian basin: product of a Wilson cycle punctuated by glaciations and a meteorite impact. Sediment. Geol. 141-142, 233–254.

6 Discussion and conclusions

The Sudbury basin is outlined by the elliptical Sudbury Igneous Complex (SIC), a differentiated impact melt sheet composed from bottom to top of the so-called Sublayer, Norite, Quartz Gabbro, and Granophyre (Dressler et al. 1992). Until the 1960s, SIC was assumed to have been formed during an intrusive, magmatic process after the formation of the Onaping Formation and the deposition of post-impact sediments (Burrows and Rickaby 1930; Stevenson 1960, 1963). Today, an impact origin is widely accepted. The SIC is the result of fractional crystallization and differentiation of a single superheated melt sheet (Grieve et al. 1991; Grieve 1994; Deutsch et al. 1995; Ostermann et al. 1996; Warner et al. 1998; Dickin et al. 1999; Therriault et al. 2002), that was formed by impact melting of a mix of crustal target rocks of the Superior Province and Huronian metasedimentary rocks (Gibbins and McNutt 1975; Hurst and Farhat 1977; Kuo and Crocket 1979; Faggart et al. 1985; Walker et al. 1991; Dickin et al. 1992, 1996, 1999; Golightly 1994; Grieve 1994; Ostermann et al. 1996; Morgan et al. 2002). The goal of this thesis was to investigate other melt products of the Sudbury impact event that have been less well studied and/or remain debated despite many decades of study.

The first part of this thesis focused on the origin of the so-called “Basal Onaping Intrusion” in the North Range (Chapter 2). The observations indicate an igneous nature of the groundmass of the Basal Onaping Intrusion, which is composed of a skeletal intergrowth of feldspar and quartz suggesting simultaneous cooling of those minerals. Based on the presence of PDFs the Basal Onaping Intrusion can be classified as an impact melt rock. Rims around clasts are a result of interaction processes between liquid melt and target rock clasts. Increasing grain size, decreasing amounts of clasts with increasing depth and a transitional contact between Granophyre of the SIC and the Basal Onaping Intrusion are consistent with general features of roof rocks at coherent impact melt sheets. It is concluded that the “Basal Onaping Intrusion” are the roof rocks of the SIC, and, thus, should be no longer considered part of the complex breccia series of the Onaping Formation. As part of the SIC, the new name “Upper Contact Unit” is suggested.

This has important implications as the roof rocks on top of the SIC would have been the first to crystallize and, thus, should represent the bulk composition of the proto-SIC before differentiation. Previous studies have suggested that the marginal chilled phases of the Offset Dykes show compositions close to the initial composition of the proto-SIC (Lightfoot et al. 1997a; Lavrenchuk et al. 2010), which requires the emplacement of the dykes, or part of dykes, before differentiation of the SIC. However, the timing relationships of the emplacement of the Offset Dykes have not yet been established in detail and are still topic of intensive research and discussion (Coulter 2016; Pilles 2016: see also Chapter 3 and 4). It is, thus, recommended that the Upper Contact Unit be considered the closest proxy to the initial bulk composition of the proto-SIC, rather than the granodiorite phases of the Offset Dykes. The Onaping Formation, and thus, the Upper Contact Unit are characterized by, locally intensive, hydrothermal alteration attributed to the development of a post-impact hydrothermal system on top of the SIC (Ames et al. 1998), which might have caused significant compositional modification within the rocks. This needs to be considered when working with the Upper Contact Unit as a proxy for the bulk composition of the SIC. Based on geochemical data, it has been suggested that the Basal Onaping Intrusion is similar in composition to the least altered Onaping Formation and to the Offset Dyke phases (Carter et al. 2009). Investigating those geochemical signatures could determine any genetic relationships between the Upper Contact Unit and the Offset Dykes and might provide further information with respect to the timing of the emplacement of the dykes.

The second part of the research project focused on the origin and formation of metabreccia (MTBX) from the Parkin, Trill and Foy Offset Dykes in the North Range. Fieldwork, petrographic investigations and geochemical analyses were carried out to characterize MTBX, the inclusion-rich (IQD) and inclusion-poor (QD) dyke phases, Sudbury Breccia (SDBX) and Footwall Breccia (FWBX) in order to determine origin and genetic relationships of MTBX. The main characteristics of MTBX, FWBX, SDBX, QD and IQD are listed in Table 6.1. MTBX from all three the dykes clearly display significant similarities in field relationships, petrography and geochemical composition.

Table 6.1. Overview of features and characteristics of QD, IQD, MTBX, SDBX, FWBX.

	QD	IQD	MTBX	SDBX	FWBX
Partial Melting	no	no	+	+ to ++	+++
Recrystallization	no	no	+++	+	++
Sulfides	+	+++	++ to +++	+++	+++
Granophyric Intergrowth	++	++	(+)	no	+
Texture	Igneous	Igneous	Metamorphic, recrystallized	Cataclastic, metamorphic	Igneous-metamorphic
Dykes	Whistle, Parkin, Foy, Trill	Whistle, Parkin, Foy, Trill	Whistle, Parkin Foy, Trill,	Trill, Foy	
Location	Within the dyke	Within the dyke	Within the dyke	Within country rocks	Crater floor and wall rocks
Grainsize	Fine-, medium-, coarse-grained, spherulitic, chilled	Fine- to medium-grained	Aphanitic to fine-grained	Aphanitic	Fine- to medium-grained
Clast Amount	None to +	+ to ++	+++	+++	+++
Clast Population	SIC wall rocks	SIC wall rocks	SIC wall rocks	Adjacent country rocks	Crater floor rocks
Origin	Injected melt from the SIC	Injected melt from the SIC	Metamorphosed FWBX	Friction melting, cataclasis	Brecciated, partially/fully molten crater floor rocks

The most important feature is the intensive recrystallization of matrix and clasts, caused by the three main processes of dynamic recrystallization bulging, grain-boundary migration and subgrain rotation, indicating thermal metamorphism and overprint. Thus, MTBX did not form by crystallization from a melt phase from the proto-SIC injected into fractures of the country rocks, as it had been suggested in previous studies (Murphy and Spray 2002; Lafrance and Bygnes 2014). This study provides first documentation of the presence of MTBX from the Foy and Trill Offset Dykes. Given how common it is in these dykes, this suggests that MTBX could represent a more frequent lithology around the Sudbury structure than previously assumed. Currently, MTBX is not well-known, and very often an overlooked factor in the Offset Dyke research; however, based on the results from the

Parkin, Trill and Foy Offset Dykes, it may have played a more important role in the Offset Dyke emplacement than previously assumed. Acknowledging the existence of MTBX, and including it as an important factor into future studies might help to provide solutions for currently unanswered questions in the Offset Dyke research.

Previous research on the Trill Offset Dyke resulted in the conclusion that the emplacement of the Offset Dykes occurred in three different injection phases emplacing an initial glassy dyke phase first, followed by IQD and QD (Klimesch et al. 2008, 2016; Klimesch 2009). Similar emplacement mechanism have also been suggested for other Offset Dykes around the Sudbury structure, which is also based on the reported observation that the inclusion- and sulfide poor QD is usually detected at the margins of the dyke while the sulfide- and inclusion rich IQD is located in the centre (Morris and Pay 1981; Lightfoot et al. 1997b; Lightfoot and Farrow 2002; Murphy and Spray 2002; Hecht et al. 2008; Lafrance and Bygnes 2014). However, the results of the studies on the Parkin and Trill Offset Dykes, suggest that the arrangement of QD and IQD is not always consistent with the theory of a marginal QD and inner IQD phase. Both, QD and IQD contain inclusions and sulfides (Pilles 2016), the grain size and texture of both phases vary from chilled, aphanitic and glassy to spherulitic, and medium- to coarse-grained. QD usually contains less inclusions than IQD; however, a uniform and consistent classification scheme for QD and IQD does not exist. Thus, the distinction between QD and IQD is solely based on objective features and can vary from scientist to scientist. The existence of MTBX is not yet widely accepted and known, possibly leading to misidentification of MTBX for IQD. Furthermore, the words leucocratic breccia (Lightfoot et al. 1997c), Granite Breccia, Late Granite Breccia and anatexite are used interchangeably throughout the literature by researchers and mining companies to describe MTBX and FWBX leading to confusion in the terminology. To avoid misunderstanding and misusage it is suggested to differentiate between the terms MTBX and FWBX based on their location: FWBX is strictly located immediately within the crater floor below the SIC or in the surroundings of the embayments, whereas MTBX is included within the dykes.

The strong textural and compositional relationship between MTBX and FWBX suggests that MTBX originated from FWBX. As described in Chapter 2 and 3, it is suggested that

fragments of FWBX were ripped off the crater floor below the SIC, incorporated into and transported within the dyke melt and subsequently metamorphosed and thermally overprinted, creating MTBX. This suggests an outward emplacement of the radial Offset Dykes. Field relationships confirm that MTBX is strongly associated to the inclusion-poor dyke phase. It has been observed as fragments and m-sized blocks within QD at the Parkin and Trill Offset Dykes (see Chapter 3 Figure 3.2a and Chapter 4 Figure 4.4). In case of a two-pulse dyke emplacement, MTBX would have been emplaced together with the first inclusion-poor QD. Transporting m-sized FWBX blocks over a long distance requires a significant amount of energy and might indicate a forceful injection of the melt phases into country rock fractures. With increasing distance from the SIC, the dyke melt loses energy, which could explain that fact that the distal parts of the Offset Dykes usually only contain small cm-sized inclusions, but no large blocks of MTBX.

Depending on the timing of the injection, the Offset Dyke melt most likely contained crystalline load, volatiles and fragments of country rocks which increase the resistance of the melt to shear stress. This would have caused the melt to behave as a Bingham fluid rather than a Newtonian fluid (Sparks et al. 1977; Yamato et al. 2012). In contrast to Newtonian fluids, which deform as soon as shear stress is applied, the shear stress applied on Bingham fluids needs to reach a certain amount before any deformation (flow) (Malin 1997). This could also be indicative of a forceful injection of the dyke melt. The incorporation of fragments and inclusions led to changes in density and, thus, the dynamics of the melt during the emplacement. Large blocks of MTBX of varying size and irregular shape within the dykes might have destabilized the magma flow. The present exposed dykes show complex shapes and thickness and direction of the dykes vary over the course of the dyke length, leading to variations in velocity. Those constantly changing parameters during the dyke emplacement might indicate a turbulent, rather than a laminar flow. Laminar flow is characterized by a higher velocity in the centre of the dyke and a lower velocity on the walls leading to a typical velocity profile (Yamato et al. 2012), which could result in flow differentiation (Pilles 2016). In contrast, turbulent flow show chaotic streamlines and irregular changes in pressure and velocity throughout the dyke, however, the outer layer in contact with the wall, always behaves laminar. Generally the emplacement of the Offset Dykes was a highly complex process, and even though, the

basic processes were similar around the Sudbury structure, the details may have varied from dyke to dyke and between North and South Range.

MTBX and FWBX show only limited variations of trace element abundances and have a distinct REE pattern in common, with an enrichment in LREE and depletion in HREE that also corresponds to basement rocks of the Levack Gneiss Complex and Cartier Batholith. Geochemical differences within MTBX and FWBX can be associated to compositional inhomogeneities within the country rocks. The Levack Gneiss Complex is composed of a wide variety of different rock types ranging from tonalitic orthogneiss, diorite and granodiorite, biotite paragneiss to mafic gneiss, gabbro, and pyroxenite, which are intruded by Matachewan Diabase and Cartier Batholith (Card 1994). A multicomponent rock system like the Levack Gneiss Complex that melts over a range of temperatures below the SIC leads to various degrees of partial melting and produces a wide variety of liquid compositions within FWBX. Low degree partial melting might have locally continued in MTBX after the emplacement of the dykes, further modifying the composition of MTBX.

IQD and QD from one Offset Dyke, and even between different dykes from the North Range, show a strong correlation in composition and trace element and REEs pattern, but differ from MTBX, FWBX and country rocks. This might suggest that the source for both lithologies, QD and IQD, could have been very similar and time-wise close. The major differences in composition of IQD and QD, in fact, occur between the Offset Dykes from the North Range and the South Range.

MTBX mineralization shows similarities to the Cu-rich footwall-type deposits and, thus, could be considered as a possible, economically important host lithology of Ni-Cu-PGE mineralization. The increased Cu contents within MTBX mineralization indicate the formation of the sulfides from the Cu-enriched residuum after the fractionation of the Ni-bearing Fe monosulfide solid-solution, which is not the case for sulfides in IQD. If MTBX and IQD were genetically related and both formed by injection of a melt from the SIC as Offset Dykes, they would most likely both inherit similar sulfide composition. MTBX shows similarities to the Cu-rich footwall-type deposits and, thus, should be considered as a possible, economically important host lithology of Ni-Cu-PGE mineralization.

Based on the presented observations an approximate time line can be created. The majority of those processes, however, took place simultaneously and over a prolonged time.

1. Brecciation and crushing of the crater floor at shock pressures exceeding 10 GPa (Lakomy 1990) resulted in the formation of a clastic breccia during crater and excavation stage, and possibly continued well into the modification stage (Fig. 6.1a). Formation of SDBX and FWBX was most likely simultaneously; however, SDBX clasts within FWBX (Pattison 1979; Lakomy 1990; Moore and Nikolic 1994) indicate that SDBX already in parts existed when the FWBX formed.

2. Overlapping with the brecciation process, the proto-SIC was emplaced due to the melting of a large volume of crustal target rocks (Fig. 6.1a). The initial temperatures of the SIC have been estimated at ~1800°C or higher (Ivanov and Deutsch 1999; Zieg and Marsh 2005). Proto-impact melt intruded fractures and cavities within the crater floor and the clastic breccia, reacted with the solid rock fragments and initiated partial and fully melting (Fig. 6.1b).

3. Deposition of ~200 m (Grieve et al. 2010) fallback material on top of the proto-SIC and incorporation of cold clasts into the top of proto-SIC resulted in faster cooling and crystallization of the upper part of the proto-SIC and the formation of the Upper Contact Unit, potentially preserving the initial bulk composition of the SIC (Fig. 6.1c).

4. During cooling of the SIC, the clastic breccia below the cavity was further heated to temperatures of up to 1000°C (Lakomy 1990; Zieg and Marsh 2005) and metamorphosed, partially and fully molten the rocks to a depth of about 500 m below the SIC (Prevec and Cawthorn 2002) leading to the formation of FWBX with an igneous-metamorphosed texture. Sublayer melt intruded into the still evolving FWBX resulting in the formation of the mafic Sublayer and the felsic melt of the FWBX. This led to reaction rims, relicts of which are still observable within MTBX.

5. Sea water flowing into the crater depression (Fig. 6.2a) interacts with the hot, undifferentiated melt of the proto-SIC leading to melt-fuel-coolant interaction explosions in the upper parts of the proto-SIC (Fig. 6.2b) (Grieve et al. 2010) and

resulting in the deposition of the complex breccias of the Onaping Formation (Fig. 6.2c). Where the proto-SIC was not breached, the Upper Contact Unit remains at the present day.

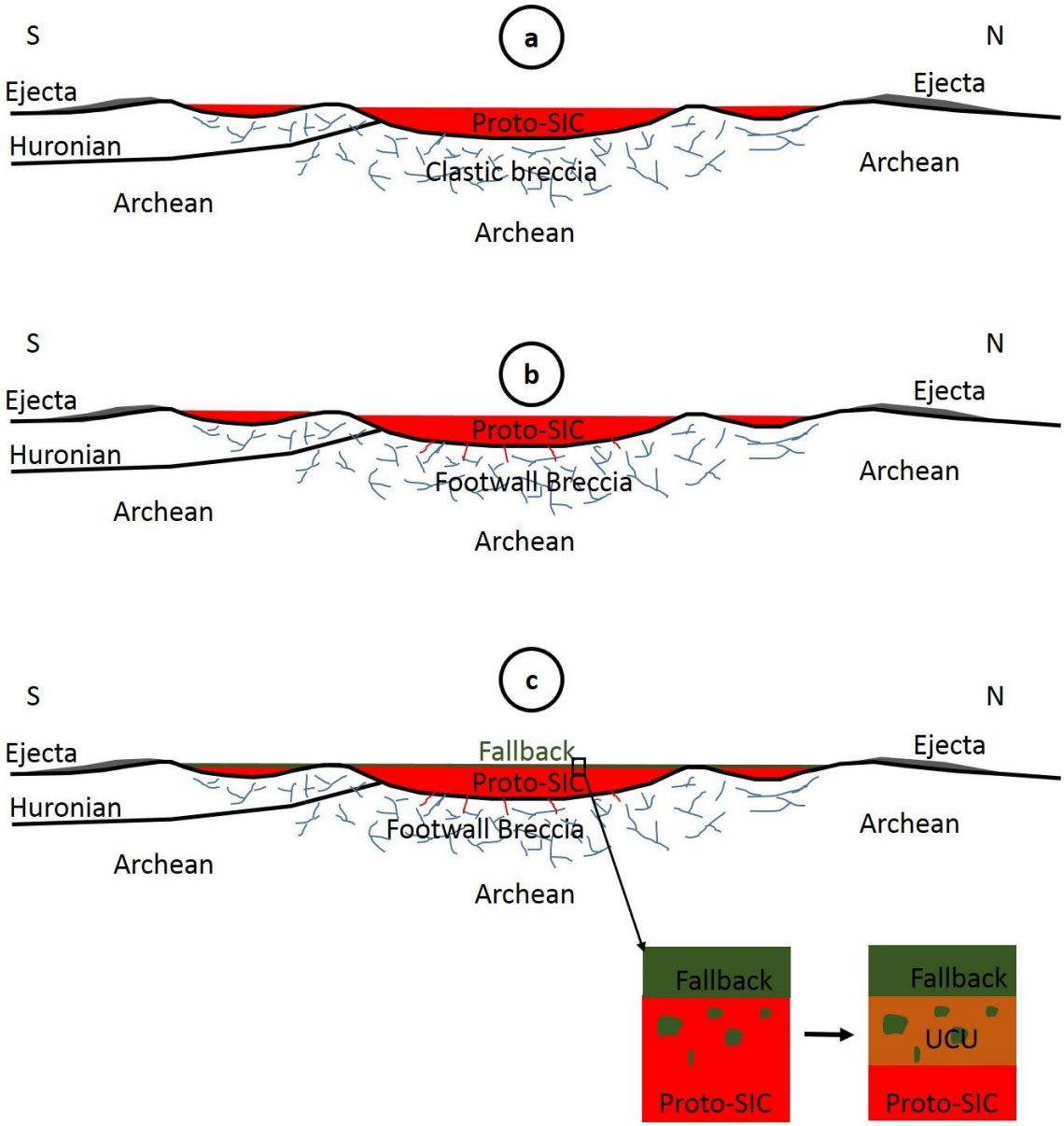

Figure 6.1. Schematic illustrations displaying the approximate formation processes of the Sudbury impact structure. a) Formation of a clastic breccia below the crater floor. b) Partial and fully melting of the clastic breccia due to the intrusion of melt of the proto-SIC into the crater floor and the cooling of the SIC leading to the formation FWBX. c) Deposition of 200 m fallback material on top of the proto-SIC.

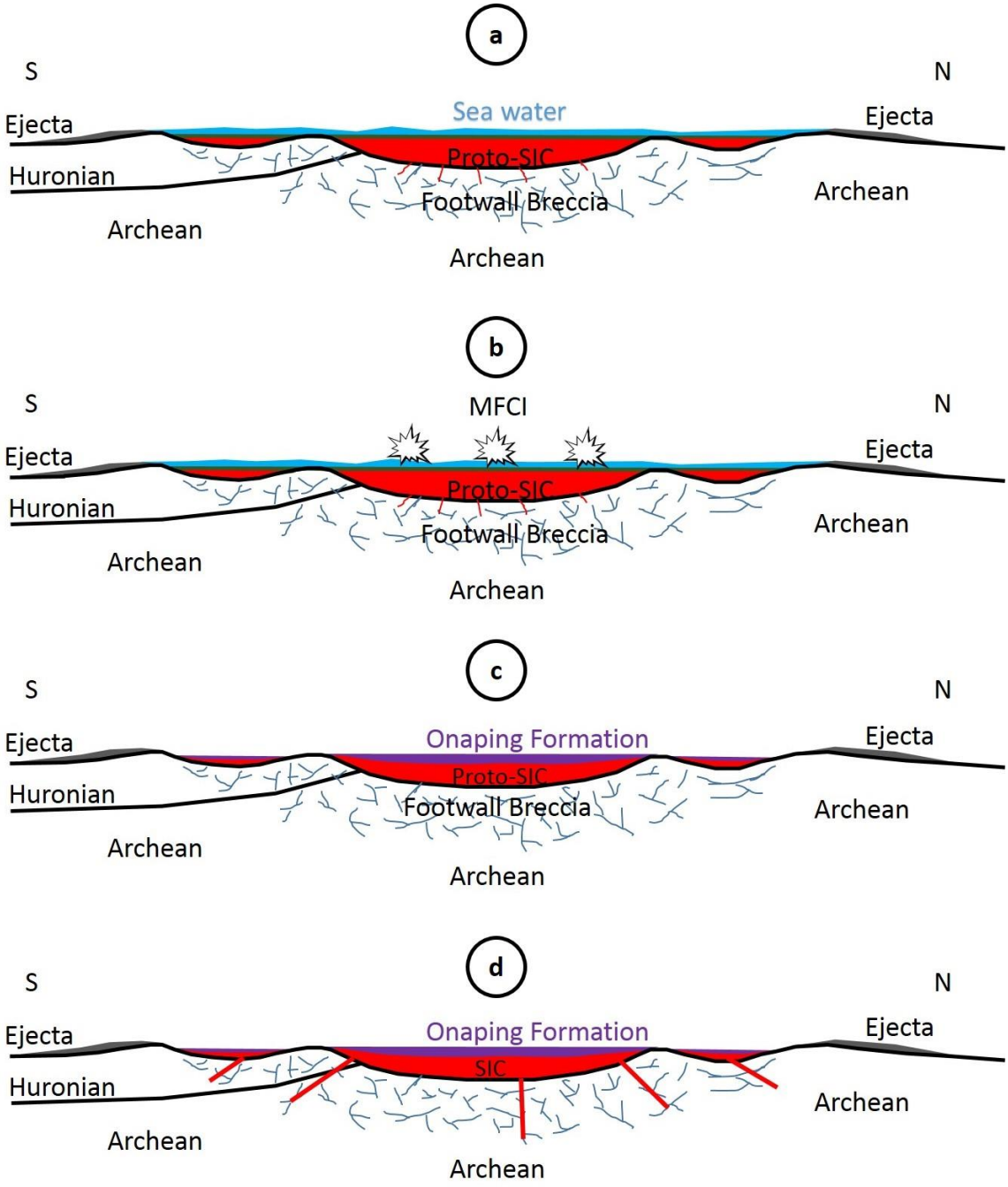

Figure 6.2. Schematic illustrations showing further development and modification of the Sudbury impact structure. a) Sea water flows back into the cater depression interacting with the hot proto impact melt sheet. b) This leads to melt-fuel-coolant-interaction explosions and to the deposition of c) the Onaping Formation on top pf the proto-SIC. d) Emplacement of the Offset Dykes during differentiation of the SIC and formation of MTBX.

6. Melt derived from the proto-SIC was forcefully injected into fractures within the country rocks forming the Offset Dykes (Fig. 6.2d). The timing of the emplacement is not yet completely clear but possibly occurred within the first stages of differentiation. It has been suggested that the dykes derived from the proto-SIC before differentiation (Pattison 1979; Grant and Bite 1984; Dressler et al. 1996; Lightfoot et al. 1997a; Ames et al. 2002; Tuchscherer and Spray 2002), or from intermediate stages of fractional crystallization of the main mass (Chai and Eckstrand 1993, 1994; Wood and Spray 1998; Prevec 2000; Therriault et al. 2002). Considering a cooling model for the SIC that involves conductive and convective cooling (Prevec and Cawthorn 2002), that would place the timing of the emplacement of the Offset Dykes within the first 1000 years of the formation of the SIC.

7. FWBX was ripped off and mobilized when the dykes where emplaced. The incorporated FWBX blocks and fragments were transported from the embayments radial outwards within an inclusion-free or poor melt phase.

8. The high temperatures of the Offset Dyke melt, which could have been between 1450°C (Hecht et al. 2008) and 1700°C (Ostermann et al. 1996), led to recrystallization of the FWBX, and thus, forming MTBX. Depending on the initial temperature of the FWBX fragments and the temperature of the dyke melt, low degree partial melting might have occurred, in particular close to the dyke embayments. Locally, FWBX fragments could have been assimilated and digested by the dyke melt and contributed to the clast population within QD/IQD.

9. Further cooling, differentiation and crystallization of the melt sheet to finally form the present SIC. With an initial temperature of at least 1800°C and assuming a cooling process that involved conductive and convective heat transfer, the melt sheet cooled down to the liquidus within approximately 10,000 years and complete solidification took approximately 56,000 to 75,000 years (Prevec and Cawthorn 2002; Zieg and Marsh 2005).

To summarize, the following contributions were made in this study:

i. We identified the Basal Onaping Intrusion as the roof rocks of the SIC and suggested the new name ‘Upper Contact Unit’.
ii. We identified MTBX as metamorphosed and recrystallized FWBX and thus contributed to the understanding of the emplacement of the Offset Dykes which was most likely forcefully and away from the SIC.
iii. We first reported and described MTBX from the Foy and the Trill Offset Dykes.
iv. We provided the first analyses of sulfides and PGMs within MTBX in comparison to the sulfides in IQD and concluded that the sulfide formation within MTBX differs from the sulfide formation within IQD. This might have important application for the search for economically important ore deposits and exploration.
v. We provided new information and knowledge that takes us a step further to understanding the process of crater formation at the Sudbury impact structure.

6.1 References

Ames, D.E., Golightly, J.P., Lightfoot, P.C., Gibson, R.L., 2002. Vitric compositions in the Onaping Formation and their relationship to the Sudbury Igneous Complex, Sudbury structure. Econ. Geol. 97, 1541–1562.

Ames, D.E., Watkinson, D.H., Parrish, R.R., 1998. Dating of a regional hydrothermal system induced by the 1850 Ma Sudbury impact event. Geology 26, 447–450.

Burrows, A.G., Rickaby, H.C., 1930. Sudbury Basin Area. Ontario Dep. Mines Annu. Rep. 38, 55 pp.

Card, K.D., 1994. Geology of the Levack gneiss complex, the northern footwall of the Sudbury structure, Ontario. Geol. Surv. Canada Curr. Res. 1994-C, 269–278.

Carter, W.M., Watkinson, D.H., Ames, D.E., Jones, P.C., 2009. Quartz Diorite Magmas and Cu-(Ni)-PGE Mineralization, Podolsky Deposit, Whistle Offset Structures, Sudbury, Ontario. Geol. Surv. Canada Open File 6134, 58 pp.

Chai, G., Eckstrand, R., 1993. Origin of the Sudbury Igneous Complex, Ontario -

differentiate of two separate magmas. Geol. Surv. Canada Open File 93-1E, 219–230.

Chai, G., Eckstrand, R., 1994. Rare-earth element characteristics and origin of the Sudbury Igneous Complex, Ontario, Canada. Chem. Geol. 113, 221–244.

Coulter, A.B., 2016. Recent Discoveries in the Ni-Cu-PGE bearing Trill and Parkin Offset dykes, Sudbury impact structure, Canada. M.Sc. Thesis, West. Univ. Dep. Earth Sci. Electron. Thesis Diss. Repos. Paper 3473.

Deutsch, A., Grieve, R.A.F., Avermann, M., Bischoff, L., Brockmeyer, P., Buhl, D., Lakomy, R., Müller-Mohr, V., Ostermann, M., Stöffler, D., 1995. The Sudbury Structure (Ontario, Canada): a tectonically deformed multi-ring impact basin. Geol. Rundschau 84, 697–709.

Dickin, A.P., Artan, M.A., Crocket, J.H., 1996. Isotopic evidence for distinct crustal sources of North and South Range ores, Sudbury Igneous Complex. Geochim. Cosmochim. Acta 60, 1605 – 1613.

Dickin, A.P., Nguyen, T., Crocket, J.H., 1999. Isotopic evidence for a single impact melting origin of the Sudbury Igneous Complex, in: Dressler, B.O., Sharpton, V.L. (Eds.), Large Meteorite Impacts and Planetary Evolution II, GSA Special Paper 339. pp. 361–371.

Dickin, A.P., Richardson, J.M., Crocket, J.H., McNutt, R.H., Peredery, W. V., 1992. Osmium isotope evidence for a crustal origin of platinum group elements in the Sudbury nickel ore, Ontario, Canada. Geochim. Cosmochim. Acta 56, 3531 – 3537.

Dressler, B.O., Peredery, W. V., Muir, T.L., 1992. Geology and Mineral Deposits of the Sudbury Structure. Ontario Geological Survey Guidebook 8.

Dressler, B.O., Weiser, T., Brockmeyer, P., 1996. Recrystallized impact glasses of the Onaping formation and the Sudbury igneous Complex, Sudbury Structure, Ontario, Canada. Geochim. Cosmochim. Acta 60, 2019 – 2036.

Faggart, B.E., Basu, A.R., Tatsumoto, M., 1985. Origin of the Sudbury complex by

meteoritic impact: Neodymium isotopic evidence. Science (80-.). 230, 436–439.

Gibbins, W.A., McNutt, R.H., 1975. The Age of the Sudbury Nickel Irruptive and the Murray Granite. Can. J. Earth Sci. 12, 1970–1989.

Golightly, J.P., 1994. The Sudbury Igneous Complex as an impact melt: evolution and ore genesis, in: Lightfoot, P.C., Naldrett, A.J. (Eds.), Proceedings of the Sudbury-Noril'sk Symposium. Ontario Geological Survey Special Volume 5, pp. 105–118.

Grant, R.W., Bite, A., 1984. Sudbury Quartz Diorite Offset Dikes, in: Pye, E.G., Naldrett, A.J., Giblin, P.E. (Eds.), The Geology and Ore Deposits of the Sudbury Structure. pp. 275–300.

Grieve, R.A.F., 1994. An Impact Model of the Sudbury Structure, in: Lightfoot, P.C., Naldrett, A.J. (Eds.), Proceedings of the Sudbury-Noril'sk Symposium. Ontario Geological Survey Special Volume 5, pp. 119–132.

Grieve, R.A.F., Ames, D.E., Morgan, J. V., Artemieva, N.A., 2010. The evolution of the Onaping Formation at the Sudbury impact structure. Meteorit. Planet. Sci. 45, 759–782.

Grieve, R.A.F., Stöffler, D., Deutsch, A., 1991. The Sudbury structure: Controversial or misunderstood? J. Geophys. Res. 96, 753–764.

Hecht, L., Wittek, A., Riller, U., Mohr, T., Schmitt, R.T., Grieve, R.A.F., 2008. Differentiation and emplacement of the Worthington Offset Dike of the Sudbury impact structure, Ontario. Meteorit. Planet. Sci. 43, 1659–1679.

Hurst, R.W., Farhat, J., 1977. Geochronologic investigations of the Sudbury Nickel Irruptive and the Superior Province granites north of Sudbury. Geochim. Cosmochim. Acta 41, 1803–1815.

Ivanov, B.A., Deutsch, A., 1999. Sudbury impact event: Cratering mechanics and thermal history, in: Dressler, B.O., Sharpton, V.L. (Eds.), Large Meteorite Impacts and Planetary Evolution II, GSA Special Paper 339. pp. 389–398.

Klimesch, L., 2009. Mapping Project: Creighton Pluton at Graham Fault, Sudbury, Canada. and Emplacement, Differentiation and Mineralisation of the Trill Offset Dike, Sudbury, Canada. Freie Universität Berlin.

Klimesch, L., Hecht, L., Riller, U., 2008. Petrology of the Trill Offset Dike, Sudbury, Canada, in: 86th Annual Meeting of the German Mineralogical Society. p. abstract # 545.

Klimesch, L.-M., Hecht, L., Riller, U., 2016. Geology, geochemistry and mineralization of the Trill Offset Dike, Sudbury, Canada. Econ. Geol. Pap. Revis.

Kuo, H.Y., Crocket, J.H., 1979. Rare earth elements in the Sudbury Nickel Irruptive; comparison with layered gabbros and implications for nickel irruptive petrogenesis. Econ. Geol. 74, 590–605.

Lafrance, B., Bygnes, L.C., 2014. Emplacement of metabreccia along the Whistle offset dike, Sudbury: implications for post-impact modification of the Sudbury impact structure. Can. J. Earth Sci. 19, 1–19.

Lakomy, R., 1990. Implications for cratering mechanics from a study of the Footwall Breccia of the Sudbury impact structure, Canada. Meteorit. Planet. Sci. 25, 195–207.

Lavrenchuk, A., Latypov, R., Lightfoot, P.C., 2010. The Sudbury Igneous Complex, Canada: Numerical Modeling Confirms Fractionation of a Single Parental Magma, in: 11th International Platinum Symposium. Ontario Geological Survey.

Lightfoot, P.C., Doherty, W., Farrell, K.P., Keays, R.R., Pedeski, D., 1997a. Geochemistry of the main mass, sublayer, offset dikes, and inclusions from the Sudbury Igneous Complex. Ontario Geol. Surv. Open File 5959, 231 pp.

Lightfoot, P.C., Farrow, C.E.G., 2002. Geology, geochemistry, and mineralogy of the Worthington offset dike: A genetic model for offset dike mineralization in the Sudbury Igneous Complex. Econ. Geol. 97, 1419–1446.

Lightfoot, P.C., Keays, R.R., Morrison, G.G., Bite, A., Farrell, K.P., 1997b. Geochemical

relationships in the Sudbury igneous complex; origin of the main mass and offset dikes. Econ. Geol. 92, 289–307.

Lightfoot, P.C., Keays, R.R., Morrison, G.G., Bite, A., Farrell, K.P., 1997c. Geologic and geochemical relationships between the contact sublayer, inclusions, and the main mass of the sudbury igneous complex: A Case study of the whistle mine embayment. Econ. Geol. 92, 647–673.

Malin, M.R., 1997. The turbulent flow of Binham plastic fluids in smooth circular tubes. Int. Commun. Heat Mass Transf. 24, 739–804.

Moore, C.M., Nikolic, S., 1994. The Craig Deposit, Sudbury, Ontario, in: Proceedings of the Sudbury-Noril'sk Symposium. pp. 77–90.

Morgan, J.W., Walker, R.J., Horan, M.F., Beary, E.S., Naldrett, A.J., 2002. 190Pt – 186Os and 187Re – 187Os systematics of the Sudbury Igneous Complex, Ontario. Geochim. Cosmochim. Acta 66, 273–290.

Morris, W.A., Pay, R., 1981. Genesis of the Foy (?) offset and its sulfide ores; the paleomagnetic evidence from a study in Hess Township, Sudbury, Ontario. Econ. Geol. 76, 1895–1905.

Murphy, A.J., Spray, J.G., 2002. Geology, mineralization and emplacement of the Whistle–Parkin offset dike, Sudbury impact structure. Econ. Geol. 97, 1369–1389.

Ostermann, M., Schärer, U., Deutsch, A., 1996. Impact melt dikes in the Sudbury multi-ring basin (Canada): Implications from uranium-lead geochronology on the Foy Offset Dike. Meteorit. Planet. Sci. 31, 494–501.

Pattison, E.F., 1979. The Sudbury Sublayer. Can. Mineral. 17, 257–274.

Pilles, E., 2016. Emplacement of the Foy, Hess and Pele Offset Dykes at the Sudbury impact structure, Canada. PhD. Thesis, Dep. Earth Sci. Univ. West. Ontario in work.

Prevec, S.A., 2000. An examination of modal variation mechanisms in the contact sublayer

of the Sudbury Igneous Complex, Canada. Mineral. Petrol. 68, 141–157.

Prevec, S.A., Cawthorn, R.G., 2002. Thermal evolution and interaction between impact melt sheet and footwall: A genetic model for the contact sublayer of the Sudbury Igneous Complex, Canada. J. Geophys. Res. 107, 1–14.

Sparks, R.S.J., Pinkerton, H., MacDonald, R., 1977. The transport of xenoliths in magmas. Earth Planet. Sci. Lett. 35, 234–238.

Stevenson, J.S., 1960. Origin of quartzite at the base of the Whitewater series, Sudbury basin, Ontario. Internat. Geol. Congr. 21st Sess. Nord. 32–41.

Stevenson, J.S., 1963. The upper contact phase of the Sudbury micropegmatite. Can. Mineral. 7, 413–419.

Therriault, A.M., Fowler, A.D., Grieve, R.A.F., 2002. The Sudbury Igneous Complex: A differentiated impact melt sheet. Econ. Geol. 97, 1521–1540.

Tuchscherer, M.G., Spray, J.G., 2002. Geology, mineralization, and emplacement of the Foy Offset Dike, Sudbury impact structure. Econ. Geol. 97, 1377–1397.

Walker, R.J., Morgan, J.W., Naldrett, A.J., 1991. Re-Os isotope systematics of Ni-Cu sulfide ores, Sudbury Igneous Complex, Ontario: evidence for a major crustal component. Earth Planet. Sci. Lett. 105, 416–429.

Warner, S., Martin, R.F., Abdel-Rahman, A.F.M., Doig, R., 1998. Apatite as a monitor of fractionation, degassing, and metamorphism in the Sudbury igneous complex, Ontario. Can. Mineral. 36, 981–999.

Wood, C.R., Spray, J.G., 1998. Origin and emplacement of Offset Dykes in the Sudbury impact structure: Constraints from Hess. Meteorit. Planet. Sci. 33, 337–347.

Yamato, P., Tartese, R., Duretz, T., May, D.A., 2012. Numerical modelling of magma transport in dykes. Tectonophysics 526-529, 97–109.

Zieg, M.J., Marsh, B.D., 2005. The Sudbury Igneous Complex: Viscous emulsion

differentiation of a superheated impact melt sheet. Geol. Soc. Am. Bull. 117, 1427–1450.

7 Future Work

In this study, the Upper Contact Unit has only been examined from one location in the North Range, however, it would interesting to investigate other occurrences around the Sudbury impact structure. So-called melt bodies intruding the Onaping Formation have been reported from the Onaping Falls area in the North Range (Muir and Peredery 1984). Those melt phases have not been examined in detail and an investigation would give information about their origin and relationship to the Upper Contact Unit. Andesitic aphanitic dykes and sills, located within the lower 500 m of the Sandcherry Member and in contact with the Upper Contact Unit also require investigation to determine their origin and their relationship to the Upper Contact Unit. Representing the roof rocks of the SIC, the Upper Contact Unit should display a composition close to the original bulk composition of the proto-SIC. Numerical modelling using an average composition of the Upper Contact Unit might give important information about the crystallization history of the SIC and, furthermore, could provide an estimate for the timing of the Offset Dyke emplacement.

As mentioned before, MTBX has, only been detected in the North Range. It is important to determine whether MTBX in the South Range exist and to what extent. Based on personal communication with Wallbridge Mining Limited, there might be some occurrence at the closed Victoria Mine at the Worthington Offset Dyke. The South Range was objected to more intensive post-impact deformation than the North Range, and it might be difficult to identify MTBX. FWBX has been reported within the Hess Offset Dyke and it is important to detect if this is, in fact, FWBX or possible MTBX, as this would be the first occurrence of MTBX within the concentric Offset Dykes. The transport of large blocks of FWBX within the dyke melt, compared to small inclusions, requires high energy level. This fact complicates the understanding of the dyke emplacement. It might, thus, be of use to investigate the dyke emplacement by numerical modelling and fluid mechanics to determine kinetic and energetic factors of the dyke formation and whether the dykes were emplaced laminar or turbulent. Furthermore, a more detailed study of the sulfide mineralization within the MTBX should be carried out to determine if MTBX is of economic importance.

Appendices

Appendix A: Sample locations Parkin and Whistle

Sample ID	Easting NAD83	Northing NAD83	Location	Rock Type
SUD-DA-001	509189	5183219	Parkin trench 3	Felsic volcanic
SUD-DA-002	509190	5183221	Parkin trench 3	QD
SUD-DA-003	509189	5183226	Parkin trench 3	Contact MTBX-mafic clast
SUD-DA-004	509191	5183229	Parkin trench 3	Contact MTBX-felsic clast
SUD-DA-005	509192	5183228	Parkin trench 3	MTBX
SUD-DA-006	509184	5183235	Parkin trench 3	MTBX
SUD-DA-007	509192	5183240	Parkin trench 3	MTBX
SUD-DA-008	509191	5183238	Parkin trench 3	MTBX
SUD-DA-009	509190	5183232	Parkin trench 3	IQD
SUD-DA-010	509190	5183220	Parkin trench 3	Felsic volcanic
SUD-DA-011	509187	5183224	Parkin trench 3	QD
SUD-DA-012	509188	5183228	Parkin trench 3	IQD
SUD-DA-013	509191	5183230	Parkin trench 3	MTBX
SUD-DA-014	509191	5183227	Parkin trench 3	MTBX
SUD-DA-015	509194	5183230	Parkin trench 3	MTBX
SUD-DA-016	509191	5183235	Parkin trench 3	MTBX
SUD-DA-017	509192	5183235	Parkin trench 3	Felsic gneiss
SUD-DA-018	509195	5183234	Parkin trench 3	QD
SUD-DA-019	509199	5183234	Parkin trench 3	IQD
SUD-DA-020	509198	5183239	Parkin trench 3	MTBX
SUD-DA-021 Matrix	509118	5183105	Parkin trench 4	Contact MTBX-felsic clast
SUD-DA-022	509116	5183109	Parkin trench 4	Mafic Volcanic
SUD-DA-023	509117	5183102	Parkin trench 4	Mafic Volcanic
SUD-DA-024	509118	5183102	Parkin trench 4	Mafic Volcanic
SUD-DA-025A	509119	5183112	Parkin trench 4	MTBX
SUD-DA-025B	509119	5183112	Parkin trench 4	MTBX
SUD-DA-026	509106	5183121	Parkin trench 4	QD
SUD-DA-027	509115	5183105	Parkin trench 4	MTBX
SUD-DA-028	509117	5183107	Parkin trench 4	Mafic Volcanic
SUD-DA-029	509113	5183116	Parkin trench 4	Mafic Volcanic
SUD-DA-032A	509941	5184486	Parkin Brady trench	Felsic volcanic
SUD-DA-032B	509941	5184486	Parkin Brady trench	MTBX
SUD-DA-033	509927	5184485	Parkin Brady trench	Felsic Volcanic

SUD-DA-034	509939	5184482	Parkin Brady trench	Felsic volcanic
SUD-DA-035	509944	5184479	Parkin Brady trench	MTBX
SUD-DA-036	509942	5184480	Parkin Brady trench	QD
SUD-DA-037A	509938	5184468	Parkin Brady trench	Mafic Volcanic
SUD-DA-037B	509938	5184468	Parkin Brady trench	MTBX
SUD-DA-038	509926	5184470	Parkin Brady trench	Mafic Volcanic
SUD-DA-039	509921	5184467	Parkin Brady trench	MTBX
SUD-DA-040	509929	5184465	Parkin Brady trench	Mafic volcanic
SUD-DA-041	509928	5184454	Parkin Brady trench	MTBX
SUD-DA-042	509924	5184456	Parkin Brady trench	IQD
SUD-DA-043	509924	5184455	Parkin Brady trench	IQD
SUD-DA-044	509923	5184453	Parkin Brady trench	QD
SUD-DA-045	509914	5184444	Parkin Brady trench	Mafic Volcanic
SUD-DA-046	509917	5184444	Parkin Brady trench	Mafic Volcanic
SUD-DA-047	509935	5184469	Parkin Brady trench	Mafic Volcanic
SUD-DA-048	509938	5184471	Parkin Brady trench	QD
SUD-DA-049	509940	5184469	Parkin Brady trench	MTBX
SUD-DA-050Dr	509938	5184470	Parkin Brady trench	Dykelet
SUD-DA-051Dr	509936	5184466	Parkin Brady trench	MTBX
SUD-DA-052Dr	509937	5184465	Parkin Brady trench	MTBX
SUD-DA-053Dr	509931	5184460	Parkin Brady trench	QD
SUD-DA-054	509931	5184457	Parkin Brady trench	Mafic Volcanic
SUD-DA-055Dr	509935	5184454	Parkin Brady trench	MTBX
SUD-DA-057Ss A	509948	5184464	Parkin Brady trench	MTBX
SUD-DA-057Ss B	509948	5184464	Parkin Brady trench	IQD

SUD-DA-057Ss C	509948	5184464	Parkin Brady trench	MTBX
SUD-DA-058Ss A	509930	5184460	Parkin Brady trench	Mafic Volcanic
SUD-DA-058Ss B	509930	5184460	Parkin Brady trench	Mafic Volcanic
SUD-DA-058Ss C	509930	5184460	Parkin Brady trench	MTBX
SUD-DA-059	509915	5184443	Parkin Brady trench	Mafic Volcanic
SUD-DA-060Ss A	509921	5184451	Parkin Brady trench	Amphibolite
SUD-DA-060Ss B	509921	5184451	Parkin Brady trench	IQD
SUD-DA-061Ss A	509916	5184448	Parkin Brady trench	IQD
SUD-DA-061Ss B	509916	5184448	Parkin Brady trench	IQD
SUD-DA-061Ss C	509916	5184448	Parkin Brady trench	MTBX
SUD-DA-061Ss D	509916	5184448	Parkin Brady trench	MTBX
SUD-DA-061Ss E	509916	5184448	Parkin Brady trench	MTBX
SUD-DA-062-Ss A	509911	5184448	Parkin Brady trench	Mafic Volcanic
SUD-DA-062-Ss B	509911	5184448	Parkin Brady trench	Contact MTBX-mafic clast
SUD-DA-062-Ss C	509911	5184448	Parkin Brady trench	MTBX
SUD-DA-062-Ss D	509911	5184448	Parkin Brady trench	Contact MTBX-QD
SUD-DA-062-Ss E	509911	5184448	Parkin Brady trench	QD
SUD-DA-062-Ss F	509911	5184448	Parkin Brady trench	QD
SUD-DA-062-Ss G	509911	5184448	Parkin Brady trench	QD
SUD-DA-063Ss A	509915	5184445	Parkin Brady trench	Mafic Volcanic
SUD-DA-063Ss B	509915	5184445	Parkin Brady trench	Mafic Volcanic
SUD-DA-063Ss C	509915	5184445	Parkin Brady trench	Mafic Volcanic
SUD-DA-064Ss A	509915	5184444	Parkin Brady trench	Contact MTBX-Matachewan
SUD-DA-064Ss B	509915	5184444	Parkin Brady trench	MTBX
SUD-DA-065Ss Matrix	509915	5184447	Parkin Brady trench	Contact MTBX-felsic clast

SUD-DA-066Ss	509911	5184446	Parkin Brady trench	Mafic gneiss
SUD-DA-067Ss	509908	5184412	Parkin Brady trench	Mafic Volcanic
SUD-DA-068	509894	5184418	Parkin Brady trench	QD
SUD-DA-069	509895	5184418	Parkin Brady trench	QD
SUD-DA-070	509894	5184416	Parkin Brady trench	QD
SUD-DA-071	509894	5184422	Parkin Brady trench	QD
SUD-DA-073	509894	5184417	Parkin Brady trench	Mafic gneiss
SUD-DA-075	509898	5184416	Parkin Brady trench	Contact MTBX-mafic clast
SUD-DA-076Ss	509899	5184416	Parkin Brady trench	Mafic gneiss
SUD-DA-077Ss	509898	5184414	Parkin Brady trench	Contact MTBX-mafic gneiss
SUD-DA-078	509901	5184415	Parkin Brady trench	Mafic Volcanic
SUD-DA-079	509900	5184413	Parkin Brady trench	MTBX
SUD-DA-080Ss A	509926	5184452	Parkin Brady trench	Mafic Volcanic
SUD-DA-080Ss B	509926	5184452	Parkin Brady trench	Mafic Volcanic
SUD-DA-080Ss C	509926	5184452	Parkin Brady trench	Mafic Volcanic
SUD-DA-080Ss D	509926	5184452	Parkin Brady trench	MTBX
SUD-DA-081Ss	509928	5184452	Parkin Brady trench	QD
SUD-DA-082	509926	5184451	Parkin Brady trench	IQD
SUD-DA-083Ss A	509923	5184439	Parkin Brady trench	Mafic Gneiss
SUD-DA-083Ss B	509923	5184439	Parkin Brady trench	Mafic Gneiss
SUD-DA-084	509930	5184441	Parkin Brady trench	Felsic gneiss
SUD-DA-085Ss I	509914	5184447	Parkin Brady trench	Mafic Volcanic
SUD-DA-085Ss II	509914	5184447	Parkin Brady trench	MTBX
SUD-DA-086Ss A	509185	5183246	Parkin trench 3	Sulfides in MTBX
SUD-DA-086Ss B	509185	5183246	Parkin trench 3	Sulfides and mafic clast in MTBX

SUD-DA-086Ss C	509185	5183246	Parkin trench 3	Sulfides and mafic clast in MTBX
SUD-DA-086Ss D	509185	5183246	Parkin trench 3	Sulfides and mafic clast in MTBX
SUD-DA2014-003	509952	5184427	Parkin Brady trench	Felsic volcanic
SUD-DA2014-006	509952	5184436	Parkin Brady trench	MTBX
SUD-DA2014-008	509396	5183730	Parkin trench 1	IQD
SUD-DA2014-009	509399	5183734	Parkin trench 1	QD
SUD-DA2014-010	509388	5183737	Parkin trench 1	QD
SUD-DA2014-011	509386	5183737	Parkin trench 1	Amphibolite
SUD-DA2014-014	509395	5183728	Parkin trench 1	IQD
SUD-DA2014-015	509949	5184468	Parkin Brady trench	Felsic volcanic
SUD-DA2014-016Ss	509947	5184474	Parkin Brady trench	Gneiss
SUD-DA2014-017Ss	509947	5184478	Parkin Brady trench	MTBX
SUD-DA2014-018	509940	5184472	Parkin Brady trench	IQD
SUD-DA2014-019Ss	509943	5184474	Parkin Brady trench	MTBX
SUD-DA2014-020	509941	5184472	Parkin Brady trench	MTBX
SUD-DA2014-021	509944	5184476	Parkin Brady trench	QD
SUD-DA2014-022Ss	509929	5184439	Parkin Brady trench	MTBX
SUD-DA2014-023Ss	509923	5184453	Parkin Brady trench	MTBX
SUD-DA2014-025	509922	5184469	Parkin Brady trench	MTBX
SUD-DA2014-026	509934	5184459	Parkin Brady trench	MTBX
SUD-DA2014-027	509934	5184461	Parkin Brady trench	Sulfides in MTBX
SUD-DA2014-028Dr	509934	5184460	Parkin Brady trench	Sulfides in MTBX
SUD-DA2014-029	509931	5184461	Parkin Brady trench	QD
SUD-DA2014-030	509930	5184458	Parkin Brady trench	MTBX
SUD-DA2014-031	509928	5184461	Parkin Brady trench	QD
SUD-DA2014-032Ss	509929	5184453	Parkin Brady trench	MTBX
SUD-DA2014-033Ss	509923	5184448	Parkin Brady trench	MTBX

SUD-DA2014-034	509928	5184454	Parkin Brady trench	MTBX
SUD-DA2014-035	509925	5184454	Parkin Brady trench	IQD
SUD-DA2014-036	509923	5184453	Parkin Brady trench	MTBX
SUD-DA2014-037	509925	5184455	Parkin Brady trench	IQD
SUD-DA2014-038Ss	509928	5184452	Parkin Brady trench	MTBX
SUD-DA2014-039Ss	509919	5184447	Parkin Brady trench	Contact MTBX-QD
SUD-DA2014-040	509903	5184426	Parkin Brady trench	Mafic Volcanic
SUD-DA2014-041	509908	5184425	Parkin Brady trench	MTBX
SUD-DA2014-042	509905	5184425	Parkin Brady trench	MTBX
SUD-DA2014-043	509903	5184424	Parkin Brady trench	Mafic volcanic
SUD-DA2014-044	509912	5184433	Parkin Brady trench	MTBX
SUD-DA2014-045	509912	5184433	Parkin Brady trench	MTBX
SUD-DA2014-046	509912	5184418	Parkin Brady trench	MTBX
SUD-DA2014-048Ss	509185	5183245	Parkin Brady trench	Mafic Volcanic
SUD-DA2014-049	509190	5183244	Parkin trench 3	Contact MTBX-QD
SUD-DA2014-050Dr	509185	5183243	Parkin trench 3	MTBX
SUD-DA2014-051Dr	509185	5183244	Parkin trench 3	Mafic Volcanic
SUD-DA2014-053	509186	5183254	Parkin trench 3	MTBX
SUD-DA2014-054	509188	5183256	Parkin trench 3	MTBX
SUD-DA2014-055	509187	5183255	Parkin trench 3	MTBX
SUD-DA2014-056	509187	5183260	Parkin trench 3	Felsic volcanic
SUD-DA2014-057	509188	5183257	Parkin trench 3	Contact of MTBX-Matachewan
SUD-DA2014-058	509189	5183245	Parkin trench 3	QD
SUD-DA2014-059	509190	5183243	Parkin trench 3	IQD
SUD-DA2014-060	509188	5183255	Parkin trench 3	MTBX
SUD-DA2014-062	509189	5183253	Parkin trench 3	Felsic volcanic
SUD-DA2014-063	509188	5183252	Parkin trench 3	MTBX
SUD-DA2014-064	509191	5183253	Parkin trench 3	Mafic volcanic
SUD-DA2014-065	509106	5183129	Parkin trench 4	MTBX
SUD-DA2014-066	509109	5183125	Parkin trench 4	IQD
SUD-DA2014-067	509108	5183126	Parkin trench 4	QD
SUD-DA2014-068	509110	5183127	Parkin trench 4	IQD

SUD-DA2014-069	509110	5183125	Parkin trench 4	QD
SUD-DA2014-070	509107	5183119	Parkin trench 4	IQD
SUD-DA2014-071	509109	5183118	Parkin trench 4	MTBX
SUD-DA2014-072	509107	5183117	Parkin trench 4	MTBX
SUD-DA2014-073	509107	5183117	Parkin trench 4	IQD
SUD-DA2014-074	509105	5183120	Parkin trench 4	MTBX
SUD-DA2014-075	509108	5183117	Parkin trench 6	IQD
SUD-DA2014-076	509066	5183029	Parkin trench 6	IQD
SUD-DA2014-077	509067	5183038	Parkin trench 6	QD
SUD-DA2014-078	509066	5183035	Parkin trench 6	Contact QD-felsic volcanic
SUD-DA2014-079	509056	5183039	Parkin trench 6	Mafic volcanic
SUD-DA2014-080	509067	5183034	Parkin trench 6	QD
SUD-DA2014-081	509068	5183025	Parkin trench 6	MTBX
SUD-DA2014-082	509069	5183031	Parkin trench 6	IQD
SUD-DA2014-083	509157	5183209	Parkin trench 6	MTBX
SUD-DA2014-084	509160	5183215	Parkin trench 6	MTBX
SUD-DA2014-085	509156	5183209	Parkin trench 6	QD
SUD-DA2014-086	509158	5183211	Parkin trench 6	MTBX
SUD-DA2014-087	509159	5183219	Parkin trench 6	MTBX
SUD-DA2014-088Ss	509084	5183020	Parkin trench 6	IQD
SUD-DA2014-089	509071	5183028	Parkin trench 6	IQD
SUD-DA2014-090	509089	5183014	Parkin trench 6	MTBX
SUD-DA2014-091	509080	5183022	Parkin Milnet	MTBX
SUD-DA2014-092Ss	510333	5185370	Parkin Milnet	QD
SUD-DA2014-093	510335	5185372	Parkin Milnet	MTBX
SUD-DA2014-094	510399	5185304	Parkin Milnet	IQD
SUD-DA2014-095	510377	5185311	Parkin Milnet	QD
SUD-DA2014-096	510378	5185310	Parkin Milnet	QD
SUD-DA2014-097	510090	5185440	Parkin Milnet	Felsic gneiss
SUD-DA2014-098	510433	5185861	Parkin Milnet north	IQD
SUD-DA2014-099	510478	5185848	Parkin Milnet north	MTBX
SUD-DA2015-001	509043	5182948	New Parkin trenches	MTBX
SUD-DA2015-002	509043	5182951	New Parkin trenches	MTBX
SUD-DA2015-003	509046	5182948	New Parkin trenches	MTBX
SUD-DA2015-004	509082	5183036	New Parkin trenches	MTBX
SUD-DA2015-005	509084	5183035	New Parkin trenches	Felsic Volcanic
SUD-DA2015-006	509068	5183024	New Parkin trenches	IQD

SUD-DA2015-007	509341	5183504	New Parkin trenches	MTBX
SUD-DA2015-008	509338	5183502	New Parkin trenches	MTBX
SUD-DA2015-009	509182	5183242	New Parkin trenches	MTBX
SUD-DA2015-010	509175	5183236	New Parkin trenches	MTBX
SUD-DA2015-011	509172	5183236	New Parkin trenches	Felsic Volcanic
SUD-DA2015-012	509141	5183187	New Parkin trenches	MTBX
SUD-DA2015-014	509139	5183190	New Parkin trenches	MTBX
SUD-DA2015-015	509127	5183119	New Parkin trenches	IQD
SUD-DA2015-016	509126	5183120	New Parkin trenches	MTBX
SUD-DA2015-017	509069	5183007	New Parkin trenches	IQD
SUD-DA2015-019	509061	5183000	New Parkin trenches	MTBX
SUD-NB-052	509079	518079	Parkin trench 6	Sulfides in MTBX
SUD-WH-001	510302	5181364	Whistle	MTBX
SUD-WH-002	510294	5181361	Whistle	MTBX
SUD-WH-003	510285	5181370	Whistle	IQD
SUD-WH-004	510292	5181347	Whistle	MTBX
SUD-WH-005	510283	5181340	Whistle	Contact MTBX-mafic clast
SUD-WH-006	510290	5181343	Whistle	Contact MTBX-mafic clast
SUD-WH-008	510289	5181334	Whistle	QD
SUD-WH-009	510292	5181337	Whistle	Contact MTBX-QD
SUD-WH-011	510293	5181337	Whistle	IQD
SUD-WH-012	510289	5181341	Whistle	Mafic volcanic
SUD-WH-013	510290	5181347	Whistle	Gneiss

Appendix B: Sample locations Foy and Trill

Sample ID	Easting NAD83	Northing NAD83	Location	Rock Type
SUD-DA-FOY-001	485927	5177537	Foy trench 5	Felsic volcanic
SUD-DA-FOY-002	485928	5177532	Foy trench 5	MTBX
SUD-DA-FOY-003	485937	5177528	Foy trench 5	SDBX
SUD-DA-FOY-004	485936	5177528	Foy trench 5	SDBX
SUD-DA-FOY-005	485937	5177526	Foy trench 5	MTBX
SUD-DA-FOY-006	485936	5177527	Foy trench 5	MTBX
SUD-DA-FOY-007	485942	5177518	Foy trench 5	MTBX
SUD-DA-FOY-008	485940	5177518	Foy trench 5	contact MTBX-felsic gneiss
SUD-DA-FOY-009	485939	5177523	Foy trench 5	MTBX
SUD-DA-FOY-010	485944	5177524	Foy trench 5	SDBX
SUD-DA-FOY-011	485941	5177520	Foy trench 5	SDBX
SUD-DA-FOY-012	485947	5177512	Foy trench 5	MTBX
SUD-DA-FOY-013	485943	5177509	Foy trench 5	Mafic volcanic
SUD-DA-FOY-014	485928	5177510	Foy trench 5	Felsic volcanic
SUD-DA-FOY-015	486004	5177498	Foy trench 4	Felsic volcanic
SUD-DA-FOY-016	486006	5177497	Foy trench 4	MTBX
SUD-DA-FOY-017	486014	5177483	Foy trench 4	Contact MTBX-mafic clast
SUD-DA-FOY-018	486017	5177488	Foy trench 4	MTBX
SUD-DA-FOY-019	486001	5177493	Foy trench 4	MTBX
SUD-DA-FOY-020	485979	5177433	Foy trench 3	MTBX
SUD-DA-FOY-021	485980	5177405	Foy trench 4	MTBX
SUD-DA-FOY-022	485970	5177371	Foy trench 1	MTBX
SUD-DA-FOY-023	485971	5177402	Foy trench 2	MTBX
SUD-DA-TR-001	454840	5147274	Trill middle	QD
SUD-DA-TR-002	454844	5147274	Trill middle	QD
SUD-DA-TR-003	454847	5147271	Trill middle	QD
SUD-DA-TR-004	454858	5147273	Trill middle	IQD
SUD-DA-TR-005	454857	5147275	Trill middle	Sulfides in IQD
SUD-DA-TR-006	458344	5146933	Trill east	SDBX
SUD-DA-TR-007	458341	5146932	Trill east	Felsic gneiss
SUD-DA-TR-008	458341	5146936	Trill east	Contact SDBX-felsic gneiss
SUD-DA-TR-009	458347	5146936	Trill east	Felsic gneiss
SUD-DA-TR-010	458347	5146928	Trill east	SDBX
SUD-DA-TR-011	458346	5146937	Trill east	Contact SDBX-felsic gneiss
SUD-DA-TR-012	458354	5146936	Trill east	Contact SDBX-felsic gneiss
SUD-DA-TR-013	458367	5146930	Trill east	MTBX
SUD-DA-TR-014	458367	5146934	Trill east	MTBX

SUD-DA-TR-015	458370	5146928	Trill east	MTBX
SUD-DA-TR-016	458370	5146924	Trill east	Contact MTBX-QD
SUD-DA-TR-017	458373	5146921	Trill east	QD
SUD-DA-TR-018	458372	5146928	Trill east	Contact MTBX-QD
SUD-DA-TR-019	458368	5146928	Trill east	MTBX
SUD-DA-TR-020	458369	5146925	Trill east	MTBX
SUD-DA-TR-021	458371	5146927	Trill east	Contact MTBX-QD
SUD-DA-TR-022	458373	5146926	Trill east	MTBX
SUD-DA-TR-023	458378	5146925	Trill east	MTBX
SUD-DA-TR-024	458379	5146927	Trill east	MTBX
SUD-DA-TR-025	458378	5146931	Trill east	MTBX
SUD-DA-TR-026	458377	5146929	Trill east	MTBX
SUD-DA-TR-027	458376	5146931	Trill east	MTBX
SUD-DA-TR-028	458375	5146933	Trill east	MTBX
SUD-DA-TR-029	458365	5146936	Trill east	MTBX
SUD-DA-TR-030	458371	5146940	Trill east	Contact MTBX-felsic clast
SUD-DA-TR-031	458373	5146940	Trill east	Felsic gneiss
SUD-DA-TR-032	458382	5146945	Trill east	MTBX
SUD-DA-TR-033	458380	5146952	Trill east	MTBX
SUD-DA-TR-034	458377	5146954	Trill east	MTBX
SUD-DA-TR-035	458381	5146961	Trill east	MTBX
SUD-DA-TR-036	458376	5146965	Trill east	SDBX
SUD-DA-TR-037	458376	5146967	Trill east	SDBX
SUD-DA-TR-038	458225	5146877	Trill east	MTBX
SUD-NB-103	458357	5146939	Trill east	SDBX

Appendix C: Wallbridge core samples

Sample ID	Core	Easting	Northing	Location	Depth m	Rock Type
SUDCore-DA-001A	WMP-009	509237	5182995	Southern Parkin	10.89-11.05	MTBX
SUDCore-DA-001B	WMP-009	509237	5182995	Southern Parkin	10.89-11.05	MTBX
SUDCore-DA-002	WMP-009	509237	5182995	Southern Parkin	20.75-20.9	MTBX
SUDCore-DA-003	WMP-009	509237	5182995	Southern Parkin	21.03-21.13	MTBX
SUDCore-DA-004	WMP-009	509237	5182995	Southern Parkin	38.16-38.27	MTBX
SUDCore-DA-005	WMP-009	509237	5182995	Southern Parkin	46.86-47.04	Contact MTBX-QD
SUDCore-DA-006	WMP-009	509237	5182995	Southern Parkin	47.96-48.26	MTBX
SUDCore-DA-007	WMP-009	509237	5182995	Southern Parkin	48.67-48.82	Contact MTBX-QD
SUDCore-DA-012	WCB-003	509977	5184278	Brady	846.12-846.24	IQD
SUDCore-DA-014	WMM-003	510371	5185123	Milnet	535.22-535.41	IQD
SUDCore-DA-017	WTR-51	5146800	458354	Trill	45.77-45.88	SDBX
SUDCore-DA-018	WTR-51	5146800	458354	Trill	48.19-48.29	SDBX
SUDCore-DA-019	WTR-51	5146800	458354	Trill	48.52-48.63	SDBX
SUDCore-DA-020	WTR-51	5146800	458354	Trill	285.20-285.35	SDBX
SUDCore-DA-023	WTR-51	5146800	458354	Trill	361.66-361.72	SDBX
SUDCore-DA-026	WTR-51	5146800	458354	Trill	192.12-192.26	SDBX
SUDCore-DA-028	WTR-49			Trill	91.85-91.99	IQQ
SUDCore-DA-029	WTR-49			Trill	92.89-93.01	MTBX
SUDCore-DA-030	WTR-49			Trill	97.68-97.92	MTBX
SUDCore-DA-031	WTR-49			Trill	100.27-100.53	SDBX
SUDCore-DA-034	WTR-50			Trill	8.85-9.07	SDBX

SUDCore-DA-035	WTR-50			Trill	16.16-16.42	SDBX
SUDCore-DA-036	WTR-50			Trill	16.82-17.04	SDBX
SUDCore-DA-037	WTR-50			Trill	140.22-140.44	SDBX
SUDCore-DA-040	WTR-50			Trill	243.55-243.74	MTBX
SUDCore-DA-041	WTR-50			Trill	245.05-245.27	MTBX
SUDCore-DA-042	WTR-50			Trill	249.36-249.47	IQD
SUDCore-DA-043	WTR-50			Trill	267.76-267.92	SDBX
SUDCore-DA-044	WTR-50			Trill	270.23-270.42	SDBX
SUDCore-DA-045	WTR-57			Trill	38.15-38.35	SDBX
SUDCore-DA-046	WTR-57			Trill	39.27-39.55	SDBX
SUDCore-DA-047	WTR-57			Trill	69.25-69.45	SDBX
SUDCore-DA-050	WTR-56			Trill	73.87-74.09	SDBX
SUDCore-DA-051	WTR-56			Trill	74.84-75.14	SDBX
SUDCore-DA-052	WTR-56			Trill	289.62-289.75	SDBX
SUDCore-DA-053	WTR-55			Trill	402.1-402.24	SDBX
SUDCore-DA-054	WTR-55			Trill	403.00-403.3	IQD
SUDCore-DA-055	WTR-55			Trill	404.62-404.76	MTBX
SUDCore-DA-057	WTR-53			Trill	91.85-92.00	MTBX
SUDCore-DA-058	WTR-53			Trill	92.16-92.33	MTBX
SUDCore-DA-059	WTR-53			Trill	101.72-101.82	MTBX
SUDCore-DA-060	WTR-53			Trill	102.46-102.62	MTBX
SUDCore-DA-062	WMP-48	509168	5182980	Southern Parkin	63.21-63.44	MTBX
SUDCore-DA-063	WMP-016	509105	5182847	Southern Parkin	16.09-16.23	MTBX
SUDCore-DA-064	WMP-016	509105	5182847	Southern Parkin	17.3-17.43	MTBX

SUDCore-DA-065	WMP-016	509105	5182847	Southern Parkin	32.01-32.16	IQD

Appendix D: Whole rock geochemical analyses

Sample		FWBXIII	SUD-DA-021 Clast	SUD-DA-065Ss Clast	SUD-DA-042	SUD-DA-060Ss B
Description		FWBX	GrCl in MTBX	GrCl in MTBX	IQD	IQD
Location		Coleman	Parkin	Parkin	Parkin	Parkin
SiO_2	wt %	15.45	71.1	72.5	59.7	65.3
Al_2O_3	wt %	3.43	14.35	14.15	14.65	13.2
Fe_2O_3	wt %	40.9	1.62	1.81	7.82	6.81
CaO	wt %	1.34	0.81	1.53	5.07	2.17
MgO	wt %	0.47	0.72	0.51	3.86	5.03
Na_2O	wt %	1.05	3.51	4.6	2.99	3.65
K_2O	wt %	0.44	5.75	3.91	2.37	0.92
Cr_2O_3	wt %	<0.01			0.02	0.03
TiO_2	wt %	0.17	0.1	0.16	0.73	0.62
MnO	wt %	0.03	0.02	0.02	0.11	0.1
P_2O_5	wt %	0.04	0.03	0.09	0.2	0.16
SrO	wt %	0.02	0.04	0.04	0.05	0.02
BaO	wt %	0.01	0.38	0.32	0.07	0.02
LOI	wt %	9.34	0.93	0.76	1.49	2.78
Total	wt %	72.69	99.36	100.4	99.13	100.81
C	wt %	0.01	0.05	0.09	0.04	0.06
S	wt %	27.6	0.01	0.01	0.12	0.01
Ba	ppm	123.5	3400	2940	617	206
Ce	ppm	33.7	74.6	47.6	73.7	55.1
Cr	ppm	20	30	10	160	230
Cs	ppm	0.2	0.25	0.18	2.31	0.19
Dy	ppm	0.77	0.65	0.92	3.74	2.99
Er	ppm	0.43	0.23	0.37	1.89	1.51
Eu	ppm	0.42	1.48	0.9	1.46	0.86
Ga	ppm	5.6	15.2	12.8	18.2	14
Gd	ppm	1.12	1.74	1.47	4.34	3.17
Ge	ppm	<5				
Hf	ppm	1.1	2.2	3.9	4.2	4
Ho	ppm	0.14	0.1	0.14	0.72	0.56
La	ppm	17.5	40.3	25.7	36.2	27.2
Lu	ppm	0.06	0.03	0.03	0.3	0.27
Nb	ppm	2.9	1.9	2.8	8	7.1
Nd	ppm	12	25.1	17.6	31.5	22.8
Pr	ppm	3.58	7.59	5.07	8.45	6.28
Rb	ppm	9.8	68.8	53.3	90.1	24
Sm	ppm	1.76	3.39	2.53	5.89	4.22

Sn	ppm	3	1	1	1	1
Sr	ppm	148	351	309	435	171.5
Ta	ppm	0.1	0.1		0.5	0.5
Tb	ppm	0.13	0.17	0.19	0.67	0.5
Th	ppm	4.2	15.1	6.58	7.62	7.53
Tm	ppm	0.08	0.04	0.05	0.29	0.26
U	ppm	0.4	0.36	0.27	1.66	1.46
V	ppm	35	21	21	146	118
W	ppm	<1				
Y	ppm	3.7	2.9	4.1	19.8	15.4
Yb	ppm	0.33	0.19	0.24	1.94	1.64
Zr	ppm	52	72	163	173	156
As	ppm	0.5	1.7	1.3	1.8	7.6
Bi	ppm	2.62	0.03	0.07	0.08	0.09
Hg	ppm	0.006	0.009	0.016	0.011	0.014
In	ppm	0.065				
Re	ppm	0.109				
Sb	ppm	0.08	0.12	0.22	0.08	0.07
Se	ppm	63.7	0.2	0.2	0.5	0.3
Te	ppm	2.89	0.01	0.01	0.03	0.02
Tl	ppm	0.88	0.02	0.02	0.56	0.02
Ag	ppm	1.4				
Cd	ppm	0.8				
Co	ppm	1060	4	4	33	28
Cu	ppm	2800	40	18	179	118
Cu	wt %	0.28				
Li	ppm	10			20	10
Mo	ppm	1				
Pb	ppm	14	25	27	10	9
Sc	ppm	2	3	2	16	13
Zn	ppm	58	33	43	74	80
Ni	ppm	51000	22	17	187	283
Ni	wt %	5.11				
Au	ppm	0.017				
Pt	ppm	1.17				
Pd	ppm	0.429				

GrCl = Granite clast

Sample		SUD-DA-061Ss A	SUD-DA-061Ss B	SUD-DA-TR-004	SUD-DA-WH-003	SUD-DA-WH-011
Description		IQD	IQD	IQD	IQD	IQD
Location		Parkin	Parkin	Trill	Whistle	Whistle
SiO_2	wt %	55.3	56.5	57.6	53.5	59.7
Al_2O_3	wt %	13.9	13	13.7	15	14.65
Fe_2O_3	wt %	9.61	11.2	11.1	11.25	7.09
CaO	wt %	4.51	4.19	4.84	3.84	3.31
MgO	wt %	4.64	5.46	3.4	4.37	3.53
Na_2O	wt %	4.25	3.82	3.32	4.69	6.22
K_2O	wt %	1.18	1.18	1.61	1.12	2.33
Cr_2O_3	wt %	0.04	0.05	0.02	0.02	0.02
TiO_2	wt %	0.71	0.6	0.72	1.18	0.8
MnO	wt %	0.12	0.13	0.15	0.16	0.13
P_2O_5	wt %	0.2	0.16	0.17	0.21	0.2
SrO	wt %	0.04	0.03	0.04	0.04	0.01
BaO	wt %	0.04	0.05	0.07	0.04	0.04
LOI	wt %	3.94	2.87	1.8	3.06	1.04
Total	wt %	98.48	99.24	98.54	98.48	99.07
C	wt %	0.07	0.03	<0.01	0.08	0.02
S	wt %	0.52	1.61	1.4	1.18	0.07
Ba	ppm	392	395	597	348	379
Ce	ppm	63.1	53.6	69.2	47.6	74
Cr	ppm	270	320	120	110	120
Cs	ppm	0.41	0.37	0.78	0.4	0.29
Dy	ppm	3.35	2.71	3.64	3.71	3.76
Er	ppm	1.73	1.52	1.93	2.23	2.18
Eu	ppm	1.17	0.87	1.22	0.91	1.04
Ga	ppm	17.5	13.8	16.3	18.5	17.6
Gd	ppm	4.27	3.44	4.33	4.24	4.79
Ge	ppm			<5	5	5
Hf	ppm	4.4	3	4.5	3.8	5.1
Ho	ppm	0.65	0.53	0.71	0.75	0.76
La	ppm	30.9	26	33.9	22.4	35
Lu	ppm	0.25	0.24	0.29	0.35	0.28
Nb	ppm	7.6	6.6	7.5	6.2	7.8
Nd	ppm	26.7	23.2	29.5	23	31.5
Pr	ppm	7.26	6.38	7.71	5.65	8.5
Rb	ppm	38.9	33.4	40.5	38.6	49.2
Sm	ppm	5.16	4.44	5.1	4.92	6.55

Sn	ppm	2	1	3	2	2
Sr	ppm	323	240	315	354	117.5
Ta	ppm	0.4	0.3	0.4	0.2	0.4
Tb	ppm	0.58	0.52	0.58	0.64	0.68
Th	ppm	9.73	5.57	7.15	2.74	7.79
Tm	ppm	0.27	0.21	0.26	0.31	0.28
U	ppm	1.76	1.1	1.55	0.42	1.59
V	ppm	152	113	130	188	124
W	ppm					
Y	ppm	17.2	14.2	18	18.9	19.5
Yb	ppm	1.76	1.39	1.7	2.23	2.02
Zr	ppm	180	126	158	145	180
As	ppm	14.1	7	0.4	20.4	3.2
Bi	ppm	0.54	0.48	2.17	0.28	0.2
Hg	ppm	0.058	0.036	0.012	0.006	0.006
In	ppm			0.039	0.022	0.016
Re	ppm			0.006	0.001	0.001
Sb	ppm	0.45	0.15	0.2	0.23	0.3
Se	ppm	3.6	3.4	5	0.9	0.5
Te	ppm	0.21	0.21	1.88	0.07	0.07
Tl	ppm	0.83	0.42	0.24	0.15	0.08
Ag	ppm	2.2		2.9		
Cd	ppm			0.8		
Co	ppm	42	136	79	88	23
Cu	ppm	853	1090	4810	95	43
Cu	wt %					
Li	ppm			20	20	10
Mo	ppm	2	1	1		1
Pb	ppm	127	12	138	2	2
Sc	ppm	18	16	16	28	16
Zn	ppm	92	109	119	110	61
Ni	ppm	358	2010	2010	160	195
Ni	wt %					
Au	ppm					
Pt	ppm					
Pd	ppm					

Sample		SUD-DA-FOY-001	SUD-DA-FOY-005	SUD-DA-FOY-006	SUD-DA-FOY-016	SUD-DA-FOY-017
Description		MTBX	MTBX	MTBX	MTBX	MTBX
Location		Foy	Foy	Foy	Foy	Foy
SiO_2	wt %	67.9	66.5	62.4	62.1	61.5
Al_2O_3	wt %	15.65	15.75	14.75	14.8	15.35
Fe_2O_3	wt %	4.13	4.22	7.17	8.7	5.88
CaO	wt %	3.66	4.1	5.36	2.85	4.26
MgO	wt %	1.5	2.14	3.14	3.4	2.95
Na_2O	wt %	5.17	5.76	4.43	4.14	4.2
K_2O	wt %	1.32	0.52	0.75	1.09	1.86
Cr_2O_3	wt %	0.01	0.01	0.01	0.02	0.02
TiO_2	wt %	0.4	0.47	0.71	0.73	0.63
MnO	wt %	0.04	0.06	0.1	0.1	0.09
P_2O_5	wt %	0.12	0.19	0.2	0.19	0.2
SrO	wt %	0.07	0.08	0.06	0.04	0.07
BaO	wt %	0.09	0.06	0.04	0.06	0.11
LOI	wt %	0.34	0.89	0.98	2.36	1.35
Total	wt %	100.4	100.75	100.1	100.58	98.47
C	wt %	0.01	0.02	0.01	0.14	0.06
S	wt %	0.03	0.03	0.06	0.1	0.26
Ba	ppm	768	554	352	554	954
Ce	ppm	21.2	46	39.7	78.6	62.8
Cr	ppm	40	60	90	140	110
Cs	ppm	0.47	0.13	0.5	0.46	0.56
Dy	ppm	0.58	1.48	2.49	3.17	2.14
Er	ppm	0.4	0.68	1.44	1.92	1.04
Eu	ppm	0.76	1.14	1.2	1.36	1.29
Ga	ppm	19.5	19	18.8	18.2	18.6
Gd	ppm	1.19	2.62	3.51	4.47	3.34
Ge	ppm					
Hf	ppm	3.1	3.1	3.6	4.7	4.1
Ho	ppm	0.12	0.25	0.47	0.62	0.45
La	ppm	13	25.4	20.3	41.4	31.4
Lu	ppm	0.03	0.08	0.21	0.25	0.16
Nb	ppm	1.4	3.4	3.8	6.9	4.3
Nd	ppm	9.5	21	20.3	35.5	27.4
Pr	ppm	2.62	5.7	5.2	9.82	7.25
Rb	ppm	17.7	5.2	11.9	18.2	28.9
Sm	ppm	1.67	3.81	4.21	6.04	4.59

Sn	ppm	1	1	1	3	1
Sr	ppm	599	688	494	411	574
Ta	ppm		0.1	0.2	0.3	0.1
Tb	ppm	0.13	0.31	0.49	0.61	0.41
Th	ppm	0.35	1.05	1.1	7.4	3.99
Tm	ppm	0.04	0.11	0.24	0.3	0.15
U	ppm	0.06	0.17	0.13	0.77	0.46
V	ppm	49	69	104	126	96
W	ppm					
Y	ppm	2.9	7	13.3	16.4	10.9
Yb	ppm	0.29	0.6	1.4	1.79	0.93
Zr	ppm	129	129	155	190	147
As	ppm	0.3	0.9	0.2	0.1	0.3
Bi	ppm	0.01	0.13	0.07	0.11	0.64
Hg	ppm				0.007	0.006
In	ppm		0.006	0.006	0.046	0.01
Re	ppm				0.001	0.001
Sb	ppm	0.18	0.08	0.17	0.07	0.09
Se	ppm	0.2	0.2	0.5	0.8	0.6
Te	ppm	0.01	0.01	0.02	0.07	0.21
Tl	ppm	0.12	0.03	0.1	0.13	0.16
Ag	ppm					
Cd	ppm				0.8	0.6
Co	ppm	8	10	19	9	24
Cu	ppm	36	42	54	641	305
Cu	wt %					
Li	ppm	10	10	10	20	20
Mo	ppm	2	1	1	1	1
Pb	ppm	2	21	6	22	54
Sc	ppm	5	7	15	14	11
Zn	ppm	48	58	87	152	125
Ni	ppm	51	45	50	210	186
Ni	wt %					
Au	ppm					
Pt	ppm					
Pd	ppm					

Sample		SUD-DA-FOY-018	SUD-DA-FOY-020	SUD-DA-007	SUD-DA-015	SUD-DA-021Matrix
Description		MTBX	MTBX	MTBX	MTBX	MTBX
Location		Foy	Foy	Parkin	Parkin	Parkin
SiO_2	wt %	53.1	54.4	69.3	61.6	63
Al_2O_3	wt %	15.15	15.65	15.45	16.35	14.45
Fe_2O_3	wt %	9.81	9.13	2.57	5.91	6.43
CaO	wt %	6.8	5.81	0.95	2.73	1.94
MgO	wt %	5.01	3.98	1.45	2.93	3.25
Na_2O	wt %	3.8	3.92	4.1	4.14	3.8
K_2O	wt %	1.05	1.51	2.7	3.37	2.07
Cr_2O_3	wt %	0.02	0.01		0.02	0.03
TiO_2	wt %	0.99	1.63	0.27	0.69	0.55
MnO	wt %	0.14	0.11	0.02	0.06	0.09
P_2O_5	wt %	0.5	0.76	0.04	0.32	0.11
SrO	wt %	0.07	0.07	0.04	0.07	0.04
BaO	wt %	0.06	0.11	0.09	0.13	0.1
LOI	wt %	1.52	2.18	2.52	1.7	2.26
Total	wt %	98.02	99.27	99.5	100.02	98.12
C	wt %	0.03	0.05	0.2	0.13	0.07
S	wt %	0.25	0.63		0.1	0.02
Ba	ppm	523	972	841	1210	906
Ce	ppm	61	183	299	73.8	63.4
Cr	ppm	110	70	10	130	190
Cs	ppm	0.74	0.68	0.48	1.98	0.54
Dy	ppm	4.35	6.62	1.71	2.47	2.24
Er	ppm	2.09	3.22	0.43	0.98	1.06
Eu	ppm	1.63	2.89	2.08	1.46	1.11
Ga	ppm	20.7	22.7	18.3	20.5	17.9
Gd	ppm	5.24	10.05	5.56	4.32	2.89
Ge	ppm					
Hf	ppm	2.2	9.5	7.8	3.8	3.7
Ho	ppm	0.78	1.25	0.21	0.43	0.43
La	ppm	32.5	85.3	153.5	34.7	33.6
Lu	ppm	0.25	0.38	0.06	0.12	0.17
Nb	ppm	3.9	14.7	4.6	8.6	7.4
Nd	ppm	36.3	83.9	101.5	33.4	24.6
Pr	ppm	8.63	21.7	30.8	8.71	7.08
Rb	ppm	15.2	36.3	89.1	126.5	40
Sm	ppm	7.01	15.1	13.25	6.07	4.32

Sn	ppm	1	2	1	1	1
Sr	ppm	524	591	316	563	338
Ta	ppm	0.1	0.4	0.1	0.4	0.4
Tb	ppm	0.77	1.28	0.55	0.52	0.4
Th	ppm	0.95	3.42	39.5	7.74	8.02
Tm	ppm	0.28	0.42	0.06	0.14	0.2
U	ppm	0.11	0.46	0.84	0.66	1.09
V	ppm	175	153	25	113	101
W	ppm					
Y	ppm	19.2	31.1	5.5	11.6	11.5
Yb	ppm	1.81	2.74	0.33	0.76	1.15
Zr	ppm	88	388	306	145	146
As	ppm	0.8	0.3	0.7	1.7	1.7
Bi	ppm	0.17	0.1	0.03	0.24	0.07
Hg	ppm	0.01	0.019	0.015	0.015	0.019
In	ppm	0.01	0.016			
Re	ppm	0.001	0.001			
Sb	ppm	0.08	0.08	0.09	0.14	0.14
Se	ppm	0.9	0.9	0.2	0.4	0.2
Te	ppm	0.05	0.04	0.01	0.03	0.02
Tl	ppm	0.16	0.27	0.06	0.72	0.11
Ag	ppm					
Cd	ppm					
Co	ppm	42	41	4	16	15
Cu	ppm	159	253	11	50	37
Cu	wt %					
Li	ppm	20	20	10	10	10
Mo	ppm	1				
Pb	ppm	16	12	15	14	18
Sc	ppm	21	16	3	11	11
Zn	ppm	123	113	23	72	94
Ni	ppm	119	100	34	44	91
Ni	wt %					
Au	ppm					
Pt	ppm					
Pd	ppm					

Sample		SUD-DA-039	SUD-DA-057Ss B	SUD-DA-058Ss C	SUD-DA-061Ss C	SUD-DA-061Ss E
Description		MTBX	MTBX	MTBX	MTBX	MTBX
Location		Parkin	Parkin	Parkin	Parkin	Parkin
SiO_2	wt %	61.7	59.6	54.6	57.8	55.4
Al_2O_3	wt %	17	14.8	15.1	14	14.9
Fe_2O_3	wt %	3.15	9.11	10.5	9	10.15
CaO	wt %	3.14	2.62	2.95	4.16	4.62
MgO	wt %	2.4	3.97	8.09	4.08	5.65
Na_2O	wt %	7.08	4.21	3.1	3.77	3.36
K_2O	wt %	2.7	2.33	1.76	1.29	1.5
Cr_2O_3	wt %	0.02	0.02	0.01	0.03	0.04
TiO_2	wt %	0.52	0.67	0.73	0.67	0.68
MnO	wt %	0.07	0.11	0.15	0.1	0.12
P_2O_5	wt %	0.29	0.12	0.29	0.15	0.16
SrO	wt %	0.03	0.04	0.03	0.05	0.05
BaO	wt %	0.08	0.05	0.08	0.06	0.05
LOI	wt %	1.29	2.55	3.53	2.96	2.8
Total	wt %	99.47	100.2	100.92	98.12	99.48
C	wt %	0.13	0.3	0.06	0.03	0.02
S	wt %		0.12	0.02	0.66	0.71
Ba	ppm	713	457	694	509	484
Ce	ppm	82.1	75.8	109.5	67.7	77.3
Cr	ppm	120	150	90	220	280
Cs	ppm	0.23	1.78	1.56	0.49	1.36
Dy	ppm	2.25	2.64	3.39	2.88	2.48
Er	ppm	0.99	1.33	1.71	1.42	1.2
Eu	ppm	1.74	1.1	1.71	1.18	1.46
Ga	ppm	20.5	17.5	18.5	15.9	19.2
Gd	ppm	4.29	4	5.59	3.72	4.1
Ge	ppm					
Hf	ppm	4	3.9	6.9	5.2	4.3
Ho	ppm	0.41	0.51	0.61	0.53	0.45
La	ppm	42.5	36.2	52.2	33.8	38.2
Lu	ppm	0.15	0.2	0.24	0.22	0.15
Nb	ppm	7.2	8.1	7.1	7.8	8.9
Nd	ppm	36	32	46.4	28.1	31.9
Pr	ppm	9.36	8.87	12.75	7.82	8.71

Rb	ppm	40.7	92.2	64.3	36.9	60.6
Sm	ppm	5.93	5.45	7.85	4.91	5.1
Sn	ppm	1	1	2	1	1
Sr	ppm	306	358	239	368	414
Ta	ppm	0.5	0.4	0.3	0.4	0.3
Tb	ppm	0.47	0.52	0.66	0.56	0.49
Th	ppm	7.23	12.75	16.2	10.5	10.85
Tm	ppm	0.12	0.2	0.24	0.2	0.15
U	ppm	2.26	1.42	1.4	1.55	0.83
V	ppm	75	134	140	114	132
W	ppm					
Y	ppm	10.4	14	16.4	14.6	12.2
Yb	ppm	0.81	1.27	1.53	1.51	1.08
Zr	ppm	154	153	289	202	162
As	ppm	1.1	0.1	1.7	7.7	57.8
Bi	ppm	0.05	0.05	0.57	0.4	0.36
Hg	ppm	0.005	0.016	0.035	0.041	0.041
In	ppm					
Re	ppm					
Sb	ppm	0.29	0.06	0.08	0.22	0.12
Se	ppm	0.3	0.5	0.4	1.9	1.8
Te	ppm		0.03	0.02	0.12	0.17
Tl	ppm	0.08	0.57	0.39	0.48	0.44
Ag	ppm					0.7
Cd	ppm				0.5	0.8
Co	ppm	10	26	30	67	93
Cu	ppm	10	239	172	641	1010
Cu	wt %					
Li	ppm		10	30		10
Mo	ppm				1	
Pb	ppm	4	6	24	16	15
Sc	ppm	10	16	15	16	14
Zn	ppm	44	102	117	99	167
Ni	ppm	35	292	284	997	1435
Ni	wt %					
Au	ppm					
Pt	ppm					
Pd	ppm					

Sample		SUD-DA-062SsD	SUD-DA-065Ss Matrix	SUD-DA2015-010	SUD-DA-TR-014	SUD-DA-TR-016
Description		**MTBX**	**MTBX**	**MTBX**	**MTBX**	**MTBX**
Location		**Parkin**	**Parkin**	**Parkin**	**Trill**	**Trill**
SiO_2	wt %	60.2	67.1	75.1	63.9	62.7
Al_2O_3	wt %	14.95	14.55	13.15	15.6	13.65
Fe_2O_3	wt %	8.09	5.64	2.32	5.3	7.49
CaO	wt %	4.57	2.88	2.33	3.52	4.55
MgO	wt %	4.03	2.42	0.86	2.25	3.65
Na_2O	wt %	3.42	4.92	3.33	4.12	3.3
K_2O	wt %	2.11	0.95	2.93	2.66	1.78
Cr_2O_3	wt %	0.02	0.01		0.01	0.02
TiO_2	wt %	0.66	0.6	0.23	0.59	0.65
MnO	wt %	0.11	0.07	0.03	0.09	0.13
P_2O_5	wt %	0.13	0.12	0.07	0.24	0.15
SrO	wt %	0.05	0.05	0.05	0.07	0.05
BaO	wt %	0.08	0.03	0.11	0.11	0.07
LOI	wt %	2.22	1.84	0.65	1.82	1.81
Total	wt %	100.64	101.18	101.16	100.28	100
C	wt %	0.11	0.11	0.06	0.1	0.08
S	wt %	0.4	0.07	0.01	0.12	0.08
Ba	ppm	707	276	943	945	604
Ce	ppm	66.1	114	79.6	82.2	55.8
Cr	ppm	170	100	30	60	120
Cs	ppm	0.59	0.44	0.64	0.64	0.96
Dy	ppm	2.5	1.99	1.35	2.5	3.47
Er	ppm	1.13	0.87	0.57	1.2	1.84
Eu	ppm	1.17	1.28	1.03	1.35	1.02
Ga	ppm	18	17.9	15.1	19.1	17
Gd	ppm	3.83	3.45	2.59	3.82	4.3
Ge	ppm				<5	<5
Hf	ppm	2.8	4.5	4.6	4.2	4.3
Ho	ppm	0.47	0.34	0.24	0.47	0.66
La	ppm	31.9	59.2	40.6	42	27.2
Lu	ppm	0.16	0.13	0.07	0.14	0.28
Nb	ppm	6.2	7.9	3.2	5.5	7.3
Nd	ppm	28	42.6	29.1	34.8	27.2
Pr	ppm	7.65	12.1	8.39	9.17	6.62

Rb	ppm	56.5	29.7	55.8	72.6	58.3
Sm	ppm	4.93	5.89	4.42	5.67	5.46
Sn	ppm	1	1	1	2	1
Sr	ppm	369	360	397	569	358
Ta	ppm	0.2	0.2	0.1	0.2	0.4
Tb	ppm	0.44	0.38	0.28	0.47	0.65
Th	ppm	8.71	19.65	16.65	8.38	7.66
Tm	ppm	0.16	0.12	0.08	0.15	0.25
U	ppm	0.83	0.73	1.05	0.93	2.2
V	ppm	143	100	30	73	125
W	ppm					
Y	ppm	12.2	9.3	5.9	11.5	17.5
Yb	ppm	1.01	0.91	0.56	0.98	1.61
Zr	ppm	110	170	149	160	154
As	ppm	3.6	0.9	0.5	0.6	1.3
Bi	ppm	0.19	0.04	0.06	0.05	0.08
Hg	ppm	0.026	0.008	0.005	<0.005	<0.005
In	ppm				0.01	0.009
Re	ppm				<0.001	0.001
Sb	ppm	0.14	0.18	0.15	0.09	4.1
Se	ppm	1	0.4	0.2	0.5	0.5
Te	ppm	0.1	0.01	0.01	0.02	0.04
Tl	ppm	0.17	0.18	0.22	0.08	0.18
Ag	ppm				<0.5	<0.5
Cd	ppm				<0.5	<0.5
Co	ppm	41	15	4	14	17
Cu	ppm	540	40	30	57	44
Cu	wt %					
Li	ppm	10	10	10	10	20
Mo	ppm		1	2	2	1
Pb	ppm	11	7	25	4	3
Sc	ppm	16	11	4	8	15
Zn	ppm	100	58	27	62	53
Ni	ppm	692	53	19	38	70
Ni	wt %					
Au	ppm					
Pt	ppm					
Pd	ppm					

Sample		SUD-DA-TR-018	SUD-DA-TR-019	SUD-DA-TR-026	SUD-DA-TR-027	SUD-DA-WH-001
Description		MTBX	MTBX	MTBX	MTBX	MTBX
Location		Trill	Trill	Trill	Trill	Whistle
SiO_2	wt %	58.5	59.7	62.9	63.2	61
Al_2O_3	wt %	17.65	16.15	14.65	13.05	16.1
Fe_2O_3	wt %	6.38	5.7	5.56	7.24	6.02
CaO	wt %	3.68	3.51	3.05	4.8	2.68
MgO	wt %	2.97	3.45	2.29	3.58	2.3
Na_2O	wt %	4.53	4.03	3.55	3.2	4.89
K_2O	wt %	2.31	2.99	4.25	2.42	3.56
Cr_2O_3	wt %	0.01	0.02	0.01	0.01	0.01
TiO_2	wt %	0.4	0.45	0.75	0.57	0.59
MnO	wt %	0.09	0.09	0.08	0.15	0.09
P_2O_5	wt %	0.41	0.42	0.34	0.16	0.27
SrO	wt %	0.07	0.07	0.05	0.04	0.05
BaO	wt %	0.07	0.11	0.16	0.08	0.14
LOI	wt %	2	1.84	0.94	0.84	1.46
Total	wt %	99.07	98.53	98.58	99.34	99.16
C	wt %	0.05	0.05	0.05	0.03	0.03
S	wt %	0.19	0.02	0.02	0.27	0.13
Ba	ppm	656	1030	1520	724	1295
Ce	ppm	56.3	43.6	180	62.7	91.1
Cr	ppm	80	160	100	90	50
Cs	ppm	0.5	0.95	1.7	1.79	0.28
Dy	ppm	3.19	3.94	5.28	2.99	2.61
Er	ppm	1.49	1.98	2.68	1.63	1.3
Eu	ppm	1.27	1.17	1.8	1.1	1.56
Ga	ppm	20.7	19.1	20.7	15.5	19.3
Gd	ppm	4.3	5.05	8.15	3.88	4.26
Ge	ppm	<5	<5	<5	<5	5
Hf	ppm	2	0.8	9.8	4.1	6.3
Ho	ppm	0.55	0.65	0.92	0.6	0.46
La	ppm	26.1	19.6	87.4	31	46.7
Lu	ppm	0.17	0.2	0.25	0.22	0.16
Nb	ppm	4.4	5.8	10	6.6	5.4
Nd	ppm	26.8	27.5	74.9	28.1	37.7
Pr	ppm	6.83	6.05	20.3	7.13	10.05
Rb	ppm	62.5	88.4	136.5	80.3	68.8
Sm	ppm	5.65	6.58	12.05	5.2	6.46

Sn	ppm	1	1	3	2	2
Sr	ppm	589	604	464	334	404
Ta	ppm	0.2	0.2	0.3	0.4	0.1
Tb	ppm	0.53	0.69	1.04	0.51	0.53
Th	ppm	2.84	0.96	11.75	7.87	6.04
Tm	ppm	0.21	0.23	0.31	0.22	0.13
U	ppm	0.79	0.38	1.12	2.02	0.56
V	ppm	83	67	76	109	89
W	ppm					
Y	ppm	14.9	17.6	24.1	14.5	12.3
Yb	ppm	1.29	1.33	2	1.42	1.03
Zr	ppm	71	32	368	146	236
As	ppm	5.9	0.5	0.3	1.5	4.7
Bi	ppm	0.12	0.02	0.03	0.04	0.11
Hg	ppm	<0.005	<0.005	<0.005	<0.005	0.005
In	ppm	0.009	0.006	0.022	0.007	0.018
Re	ppm	<0.001	<0.001	<0.001	0.001	0.001
Sb	ppm	0.21	0.08	0.13	0.19	0.35
Se	ppm	0.9	0.5	0.9	0.4	0.6
Te	ppm	0.03	0.01	0.01	0.01	0.04
Tl	ppm	0.05	0.08	0.42	0.27	0.07
Ag	ppm	<0.5	<0.5	<0.5	<0.5	
Cd	ppm	<0.5	<0.5	<0.5	<0.5	
Co	ppm	19	12	12	19	19
Cu	ppm	79	12	23	77	117
Cu	wt %					
Li	ppm	20	20	10	10	10
Mo	ppm	1	1	1	3	1
Pb	ppm	<2	3	11	4	4
Sc	ppm	11	18	10	13	11
Zn	ppm	44	51	62	63	54
Ni	ppm	73	40	39	62	175
Ni	wt %					
Au	ppm					
Pt	ppm					
Pd	ppm					

Sample		SUD-DA-036	SUD-DA2014-092	SUD-DA-TR-002	SUD-DA-TR-017	SUD-DA-FOY-010
Description		QD	QD	QD	QD	SDBX
Location		Parkin	Parkin	Trill	Trill	Foy
SiO_2	wt %	59.6	63.3	60.9	61.6	52.1
Al_2O_3	wt %	14.65	15.05	14.8	13.45	16.8
Fe_2O_3	wt %	8.37	4.9	7.65	7.39	9.64
CaO	wt %	3.57	2.91	5.19	4.81	8.15
MgO	wt %	3.69	3.57	3.62	3.68	4.07
Na_2O	wt %	3.01	8.01	3.35	3.49	4.26
K_2O	wt %	3.23	0.32	2.29	1.63	0.06
Cr_2O_3	wt %	0.02	0.02	0.02	0.02	0.01
TiO_2	wt %	0.71	0.68	0.77	0.64	0.67
MnO	wt %	0.11	0.07	0.12	0.14	0.14
P_2O_5	wt %	0.18	0.15	0.18	0.16	0.24
SrO	wt %	0.04	0.01	0.05	0.04	0.06
BaO	wt %	0.16	0.01	0.08	0.06	
LOI	wt %	1.56	1.03	1.11	1.76	2.22
Total	wt %	98.9	100.03	100.13	98.87	98.42
C	wt %	0.02	0.02	0.02	0.09	0.02
S	wt %	0.01	0.04	0.04	0.12	0.02
Ba	ppm	1390	77.2	695	574	37.7
Ce	ppm	75.3	55	72.3	53.2	40.3
Cr	ppm	160	120	130	120	60
Cs	ppm	2.38	0.08	1.71	1.12	0.07
Dy	ppm	3.69	3.94	3.58	3.16	2.36
Er	ppm	1.95	2.19	2.04	1.86	1.41
Eu	ppm	1.35	1.19	1.3	1.04	1.11
Ga	ppm	18.2	14.2	17.4	16.3	22.3
Gd	ppm	4.38	4.55	4.23	4.03	3.39
Ge	ppm			<5	<5	
Hf	ppm	4.9	4.7	4.4	4.5	2.6
Ho	ppm	0.7	0.72	0.69	0.66	0.49
La	ppm	37.4	22.4	36.3	25.8	19.7
Lu	ppm	0.28	0.3	0.27	0.27	0.16
Nb	ppm	8.1	7.5	7.4	7.6	3.5
Nd	ppm	31.7	24.5	31.1	25.9	21.7
Pr	ppm	8.73	6.47	8.21	6.5	5.49
Rb	ppm	99.4	5.1	86	59.1	1
Sm	ppm	6.09	5.53	5.46	5.01	4.17

Sn	ppm	1	2	1	2	2
Sr	ppm	348	70.2	375	337	552
Ta	ppm	0.6	0.5	0.4	0.4	0.1
Tb	ppm	0.64	0.7	0.65	0.53	0.5
Th	ppm	8.71	8.02	7.26	6.85	0.24
Tm	ppm	0.31	0.31	0.28	0.26	0.23
U	ppm	1.9	1.63	1.64	2.08	0.06
V	ppm	142	94	130	122	152
W	ppm					
Y	ppm	19.6	19.3	17.6	16.3	13.1
Yb	ppm	1.81	2.04	1.85	1.69	1.2
Zr	ppm	196	164	161	150	109
As	ppm	0.7	3.1	0.7	0.6	0.2
Bi	ppm	0.07	0.1	0.06	0.04	0.24
Hg	ppm	0.006	0.009	0.01	<0.005	
In	ppm			0.017	0.007	0.024
Re	ppm			<0.001	0.001	
Sb	ppm	0.1	0.22	0.09	0.12	0.09
Se	ppm	0.3	0.6	0.6	0.3	0.3
Te	ppm	0.01	0.02	0.02	0.02	0.11
Tl	ppm	0.57	0.03	0.37	0.18	0.02
Ag	ppm			<0.5	<0.5	
Cd	ppm			<0.5	<0.5	0.6
Co	ppm	19	22	24	18	14
Cu	ppm	122	23	199	41	136
Cu	wt %					
Li	ppm	10		20	20	10
Mo	ppm			1	2	3
Pb	ppm	10	2	10	2	71
Sc	ppm	15	15	16	15	12
Zn	ppm	83	19	79	56	100
Ni	ppm	114	116	165	67	440
Ni	wt %					
Au	ppm					
Pt	ppm					
Pd	ppm					

Sample		SUD-DA-FOY-011	SUD-DA-TR-012	SUD-DA-TR-036	SUD-DA-TR-037	SUD-DA-TR-005
Description		SDBX	SDBX	SDBX	SDBX	Sulf in IQD
Location		Foy	Trill	Trill	Trill	Trill
SiO_2	wt %	64.5	69.6	58.1	57.2	0.1
Al_2O_3	wt %	14.2	14.7	14.85	14.45	0.01
Fe_2O_3	wt %	6.51	2.96	8.46	9.37	41
CaO	wt %	4.96	2.01	5.63	4.28	0.01
MgO	wt %	2.96	0.97	3.67	4.11	0.01
Na_2O	wt %	4.26	4.37	3.51	3.67	<0.01
K_2O	wt %	0.87	3.49	1.64	0.88	0.01
Cr_2O_3	wt %	0.02	<0.01	0.02	0.02	0.04
TiO_2	wt %	0.63	0.24	0.84	0.86	0.04
MnO	wt %	0.1	0.04	0.12	0.11	0.01
P_2O_5	wt %	0.14	0.06	0.27	0.27	<0.01
SrO	wt %	0.05	0.05	0.08	0.06	<0.01
BaO	wt %	0.05	0.09	0.08	0.05	<0.01
LOI	wt %	0.81	1.25	2.15	2.98	18.45
Total	wt %	100.06	99.83	99.42	98.31	59.68
C	wt %	0.03	0.12	0.13	0.14	0.02
S	wt %	0.06	0.15	0.16	0.34	39.5
Ba	ppm	416	847	716	435	0.5
Ce	ppm	51.6	37	95.2	98.6	<0.5
Cr	ppm	110	20	120	130	250
Cs	ppm	0.51	0.45	2.71	0.56	0.04
Dy	ppm	2.29	0.93	3.42	3.62	<0.05
Er	ppm	1.46	0.4	1.72	1.87	<0.03
Eu	ppm	1.02	0.75	1.77	1.91	<0.03
Ga	ppm	18	15.9	19.1	19.7	0.7
Gd	ppm	2.97	1.48	5.19	5.21	<0.05
Ge	ppm		<5	<5	<5	<5
Hf	ppm	3.9	1.8	5.4	4.4	<0.2
Ho	ppm	0.45	0.16	0.62	0.71	<0.01
La	ppm	29.2	19.8	46.2	46.9	<0.5
Lu	ppm	0.18	0.05	0.21	0.25	<0.01
Nb	ppm	3.7	5	15.3	16.5	<0.2
Nd	ppm	21.6	13.7	42.7	41.8	0.1
Pr	ppm	6.11	3.9	11.1	11.15	<0.03
Rb	ppm	13.5	84.6	72.1	20.7	<0.2
Sm	ppm	3.5	2.09	7.35	7.21	<0.03
Sn	ppm	1	1	1	2	<1
Sr	ppm	424	385	679	469	0.7

Ta	ppm	0.2	<0.1	0.3	0.3	<0.1
Tb	ppm	0.45	0.2	0.62	0.66	<0.01
Th	ppm	2.79	5.19	6.46	6.51	<0.05
Tm	ppm	0.22	0.07	0.25	0.25	<0.01
U	ppm	0.2	0.53	1	1.03	<0.05
V	ppm	113	31	157	162	56
W	ppm					<1
Y	ppm	11.9	4.7	15.8	16.9	<0.5
Yb	ppm	1.39	0.4	1.47	1.58	<0.03
Zr	ppm	155	69	203	159	<2
As	ppm	0.2	1.7	0.8	0.6	0.1
Bi	ppm	0.2	0.31	0.06	0.1	0.93
Hg	ppm		0.014	<0.005	0.005	<0.005
In	ppm	0.007	0.017	0.014	0.012	0.116
Re	ppm	0.001	0.001	0.001	0.001	0.379
Sb	ppm	0.09	0.28	0.11	0.07	<0.05
Se	ppm	0.3	0.5	0.7	0.9	44.8
Te	ppm	0.02	0.21	0.02	0.04	1.55
Tl	ppm	0.13	0.06	0.41	0.03	0.57
Ag	ppm		1.2	<0.5	<0.5	3.3
Cd	ppm		0.8	<0.5	<0.5	<0.5
Co	ppm	19	6	27	32	2450
Cu	ppm	92	466	76	128	5250
Cu	wt %					0.525
Li	ppm	10	10	20	20	<10
Mo	ppm	1	1	1	2	<1
Pb	ppm	49	132	13	8	13
Sc	ppm	15	3	17	19	<1
Zn	ppm	122	349	87	90	26
Ni	ppm	157	201	66	70	42200
Ni	wt %					4.22
Au	ppm					0.12
Pt	ppm					2.94
Pd	ppm					10.15

Sulf = sulfides

Sample		SUD-DA-007	SUD-DA-015	SUD-DA-086A	SUD-DA-086A I	SUD-DA-086B
Description		Sulf in MTBX	Sulf in MTBX	Sulf in MTBX	Sulf in MTBX	Sulf in MTBX
Location		Parkin	Parkin	Parkin	Parkin	Parkin
SiO_2	wt %	69.3	61.6	17.2	48.5	60
Al_2O_3	wt %	15.45	16.35	4.47	11.7	13.9
Fe_2O_3	wt %	2.57	5.91	29.9	17.8	9.52
CaO	wt %	0.95	2.73	1.27	3.93	3.62
MgO	wt %	1.45	2.93	0.89	2.24	2.99
Na_2O	wt %	4.1	4.14	0.4	2.56	3.57
K_2O	wt %	2.7	3.37	0.9	1.68	2.08
Cr_2O_3	wt %	0.01	0.02	0.01	0.02	0.02
TiO_2	wt %	0.27	0.69	0.14	0.59	0.69
MnO	wt %	0.02	0.06	0.05	0.09	0.11
P_2O_5	wt %	0.04	0.32	0.02	0.15	0.17
SrO	wt %	0.04	0.07	0.01	0.04	0.04
BaO	wt %	0.09	0.13	0.02	0.05	0.06
LOI	wt %	2.52	1.7	14.7	5.74	2.36
Total	wt %	99.5	100.02	69.98	95.09	99.13
C	wt %	0.2	0.13	0.05	0.06	0.03
S	wt %	0.01	0.1	23	3.71	0.55
Ba	ppm	841	1210	143	411	551
Ce	ppm	299	73.8	11	50.9	64.7
Cr	ppm	10	130	100	110	120
Cs	ppm	0.48	1.98	0.09	1.03	1.69
Dy	ppm	1.71	2.47	0.91	2.82	3.55
Er	ppm	0.43	0.98	0.69	1.59	1.99
Eu	ppm	2.08	1.46	0.44	1.08	1.2
Ga	ppm	18.3	20.5	9.3	14.8	17.3
Gd	ppm	5.56	4.32	1.01	3.86	4.35
Ge	ppm			<5	5	5
Hf	ppm	7.8	3.8	1.8	3.8	4.6
Ho	ppm	0.21	0.43	0.2	0.57	0.66
La	ppm	153.5	34.7	5.3	24	30.9
Lu	ppm	0.06	0.12	0.11	0.22	0.26
Nb	ppm	4.6	8.6	2.9	6.8	8.5
Nd	ppm	101.5	33.4	5.1	22	27.3
Pr	ppm	30.8	8.71	1.29	6.05	7.46
Rb	ppm	89.1	126.5	21.8	52.6	76.2
Sm	ppm	13.25	6.07	1.04	3.95	4.87
Sn	ppm	1	1	15	61	9

Sr	ppm	316	563	137	301	289
Ta	ppm	0.1	0.4	0.2	0.3	0.4
Tb	ppm	0.55	0.52	0.16	0.48	0.64
Th	ppm	39.5	7.74	1.65	6.79	9.16
Tm	ppm	0.06	0.14	0.11	0.2	0.28
U	ppm	0.84	0.66	0.54	1.47	2.03
V	ppm	25	113	58	115	128
W	ppm	1	1	<1	1	1
Y	ppm	5.5	11.6	5.3	14.6	18.3
Yb	ppm	0.33	0.76	0.71	1.41	1.95
Zr	ppm	306	145	83	144	187
As	ppm	0.7	1.7	5.6		
Bi	ppm	0.03	0.24	59.9	51.2	9.68
Hg	ppm	0.015	0.015	0.127	0.044	0.029
In	ppm			3.47	0.018	0.022
Re	ppm			0.126	0.001	0.001
Sb	ppm	0.09	0.14	2.26	1.18	0.33
Se	ppm	0.2	0.4	80.1	30.1	4.2
Te	ppm	0.01	0.03	55.8	35.1	3.95
Tl	ppm	0.06	0.72	0.48	1.01	0.88
Ag	ppm	0.5	0.5	121	17.3	9.9
Cd	ppm	0.5	0.5	9.6	3.6	1.9
Co	ppm	4	16	671	19	18
Cu	ppm	11	50	112000	36300	6140
Cu	wt %	0.0011	0.005	11.2	3.63	0.614
Li	ppm	10	10	10	10	20
Mo	ppm	1	1	1	1	1
Pb	ppm	15	14	95	279	77
Sc	ppm	3	11	3	13	15
Zn	ppm	23	72	308	171	103
Ni	ppm	34	44	13000	737	416
Ni	wt %	0.0034	0.0044	1.3	0.0737	0.0416
Au	ppm	0.001	0.002	175.5		
Pt	ppm	0.005	0.005	44.8		
Pd	ppm	0.001	0.001	45.6		

Sample		SUD-DA-086C	SUD-DA-086C I	SUD-DA2014-020	SUD-DA2014-027	SUD-DA2014-028
Description		Sulf in MTBX	Sulf in MTBX	Sulf in MTBX	Sulf in MTBX	Sulf in MTBX
Location		Parkin	Parkin	Parkin	Parkin	Parkin
SiO_2	wt %	32.6	51.1	52.9	1.22	1.13
Al_2O_3	wt %	7.98	13.1	12.8	0.39	0.23
Fe_2O_3	wt %	25.6	14.45	12.85	16.65	19.15
CaO	wt %	4.21	9.4	4.1	0.02	0.26
MgO	wt %	1.74	5.73	3.42	0.09	0.04
Na_2O	wt %	1.24	1.98	3.47	<0.01	<0.01
K_2O	wt %	0.78	1.16	2.08	0.22	0.01
Cr_2O_3	wt %	0.01	0.01	0.02	<0.01	<0.01
TiO_2	wt %	0.45	0.87	0.67	0.01	0.02
MnO	wt %	0.07	0.21	0.11	<0.01	0.01
P_2O_5	wt %	0.09	0.11	0.14	<0.01	<0.01
SrO	wt %	0.04	0.03	0.03	<0.01	<0.01
BaO	wt %	0.02	0.03	0.04	0.01	<0.01
LOI	wt %	10.15	1.72	3.88	14.8	14.85
Total	wt %	84.98	99.9	96.51	33.41	35.7
C	wt %	0.05	0.1	0.05	0.04	0.02
S	wt %	11.7	0.05	2.6	33.9	34.5
Ba	ppm	150.5	284	378	71.2	3.1
Ce	ppm	41.7	21	56.3	1.4	1.9
Cr	ppm	70	80	150	<10	<10
Cs	ppm	0.17	1.55	0.19	0.02	0.01
Dy	ppm	1.78	3.78	2.8	0.05	<0.05
Er	ppm	1.08	2.23	1.64	<0.03	0.04
Eu	ppm	0.76	0.98	1.03	0.03	0.03
Ga	ppm	11.4	16.6	14.7	0.9	0.6
Gd	ppm	2.6	3.42	3.35	0.06	0.07
Ge	ppm	<5	5	<5	<5	<5
Hf	ppm	1.9	2	3.4	<0.2	0.2
Ho	ppm	0.37	0.73	0.56	0.01	0.01
La	ppm	20.4	9.8	28.5	0.8	1.1
Lu	ppm	0.12	0.33	0.21	<0.01	<0.01
Nb	ppm	4.4	3.1	7.3	<0.2	<0.2
Nd	ppm	18.3	11	24.8	0.6	0.6
Pr	ppm	4.84	2.74	6.64	0.15	0.2
Rb	ppm	18.3	46.9	49.5	3.5	0.4
Sm	ppm	3.16	2.87	4.39	0.16	0.08

Sn	ppm	67	2	3	18	6
Sr	ppm	298	287	280	4.4	35
Ta	ppm	0.1	0.1	0.3	<0.1	<0.1
Tb	ppm	0.37	0.59	0.46	<0.01	<0.01
Th	ppm	4.89	1.84	7.76	0.09	0.36
Tm	ppm	0.13	0.34	0.22	<0.01	<0.01
U	ppm	0.61	0.44	1.22	<0.05	<0.05
V	ppm	93	303	143	10	<5
W	ppm	<1	1	1	<1	<1
Y	ppm	9.1	20.9	14.1	<0.5	<0.5
Yb	ppm	0.9	2.26	1.4	0.04	<0.03
Zr	ppm	83	81	137	3	12
As	ppm	3.8		5.4	1.4	0.8
Bi	ppm	50.1	2.26	1.67	144.5	41.8
Hg	ppm	0.141	0.009	0.174	3.81	8.32
In	ppm	3.21	0.016	0.143	7.44	0.905
Re	ppm	0.001	0.001	0.024	0.001	0.001
Sb	ppm	1.38	0.08	0.24	0.24	0.27
Se	ppm	55.8	0.6	10.2	124	102
Te	ppm	32.6	0.06	1.03	60.5	22.6
Tl	ppm	0.34	0.59	0.27	0.18	0.15
Ag	ppm	101	0.9	31.2	419	271
Cd	ppm	11.2	2.3	3.1	79.9	83.2
Co	ppm	51	40	21	7	39
Cu	ppm	100000	247	34300	333000	327000
Cu	wt %	10	0.0247	3.43	33.3	32.7
Li	ppm	10	10	10	<10	<10
Mo	ppm	<1	1	1	1	1
Pb	ppm	207	75	11	738	324
Sc	ppm	10	37	15	1	1
Zn	ppm	365	151	274	2440	1880
Ni	ppm	2090	80	396	468	1225
Ni	wt %	0.209	0.008	0.0396	0.0468	0.1225
Au	ppm	5.12		0.177	0.211	0.114
Pt	ppm	19.45		0.366	21.3	9.97
Pd	ppm	19.95		0.799	0.128	5.78

Sample		SUD-DA2014-050	SUD-DA-FOY-021	SUD-NB-056	SUD-WH-012	SUD-NB-113
Description		Sulf in MTBX	Sulf in MTBX	Sulf in MTBX	Sulf in MTBX	Sulf in MTBX
Location		Parkin	Foy	Parkin	Whistle	Trill
SiO_2	wt %	1.35	40.8	40.7	29.8	4.44
Al_2O_3	wt %	0.28	12.55	9.3	9.36	1.59
Fe_2O_3	wt %	18.35	20.3	24.8	32.8	32.9
CaO	wt %	0.13	9.13	3.74	1.9	1.02
MgO	wt %	0.07	2.75	3.09	3.45	0.08
Na_2O	wt %	0.03	1.39	1.98	1.4	0.01
K_2O	wt %	0.02	0.38	1.09	0.8	0.01
Cr_2O_3	wt %	<0.01	0.02	0.01	0.01	0.01
TiO_2	wt %	0.01	0.51	0.45	0.71	0.05
MnO	wt %	0.01	0.09	0.1	0.12	0.01
P_2O_5	wt %	<0.01	0.19	0.11	0.47	0.03
SrO	wt %	<0.01	0.12	0.03	0.02	0.01
BaO	wt %	<0.01	0.02	0.03	0.02	<0.01
LOI	wt %	14.6	7.36	7.3	11.6	27.9
Total	wt %	34.85	95.61	92.73	92.46	68.06
C	wt %	0.02	0.01	0.05	0.02	0.08
S	wt %	32.7	9.1	10.7	13.6	33.2
Ba	ppm	7.7	147	247	151.5	2.8
Ce	ppm	1.3	49.4	40.5	58.8	4.1
Cr	ppm	<10	110	70	50	60
Cs	ppm	0.07	0.18	0.24	0.78	0.01
Dy	ppm	0.07	1.94	2.19	2.34	0.12
Er	ppm	0.05	0.88	1.37	1.12	0.07
Eu	ppm	0.04	1.59	1.06	1.2	0.09
Ga	ppm	0.7	25	11.3	12.9	4.1
Gd	ppm	0.09	2.64	2.5	3.38	0.16
Ge	ppm	<5	<5	<5	<5	<5
Hf	ppm	<0.2	2	2.7	1.9	<0.2
Ho	ppm	0.03	0.34	0.44	0.44	0.02
La	ppm	0.7	23.8	19.4	26.9	2
Lu	ppm	0.01	0.11	0.16	0.15	<0.01
Nb	ppm	<0.2	3.1	5.3	4.8	0.6
Nd	ppm	0.5	22.7	17.9	29	1.8
Pr	ppm	0.15	5.93	4.84	7.12	0.48
Rb	ppm	0.9	10.7	25.2	37.9	<0.2
Sm	ppm	0.11	3.57	3.3	5.12	0.27

Sn	ppm	14	6	4	4	4
Sr	ppm	12.3	965	243	139	112
Ta	ppm	<0.1	<0.1	0.2	0.2	<0.1
Tb	ppm	0.01	0.34	0.38	0.44	0.01
Th	ppm	0.17	1.65	5.69	2.01	0.77
Tm	ppm	<0.01	0.13	0.17	0.15	<0.01
U	ppm	<0.05	0.29	1.16	0.46	0.36
V	ppm	<5	120	91	162	55
W	ppm	<1	<1	1	<1	<1
Y	ppm	<0.5	8.3	11.1	11.6	0.5
Yb	ppm	0.05	0.83	1.1	0.99	0.05
Zr	ppm	4	86	115	87	6
As	ppm	5.7	4.6	7.2	>250	56.4
Bi	ppm	158.5	5.31	5.76	7.4	11.8
Hg	ppm	0.346	0.011	0.095	0.035	0.012
In	ppm	8.75	0.17	0.387	0.179	0.158
Re	ppm	<0.001	0.002	0.009	0.005	0.082
Sb	ppm	1.78	0.09	0.34	0.76	0.45
Se	ppm	150	25.2	26.2	33.7	71
Te	ppm	127.5	4.63	3.63	4.33	13.3
Tl	ppm	0.18	0.08	0.35	0.19	0.02
Ag	ppm	491	24.4	9.7	5.2	14.6
Cd	ppm	69	0.7	3.5	0.5	0.6
Co	ppm	12	308	245	464	1505
Cu	ppm	321000	20900	37800	6720	27600
Cu	wt %	32.1	2.09	3.78	0.672	2.76
Li	ppm	10	20	10	20	10
Mo	ppm	<1	4	1	1	4
Pb	ppm	270	28	33	18	253
Sc	ppm	1	11	12	17	<1
Zn	ppm	1680	78	205	100	36
Ni	ppm	825	1465	8250	13150	18350
Ni	wt %	0.0825	0.1465	0.825	1.315	1.835
Au	ppm	2.49	0.57	0.067	0.966	0.948
Pt	ppm	37	0.539	1.06	0.483	4.21
Pd	ppm	53.3	0.558	0.906	1.58	11.75

Appendix E: Element Maps

SUD-DA-003-2

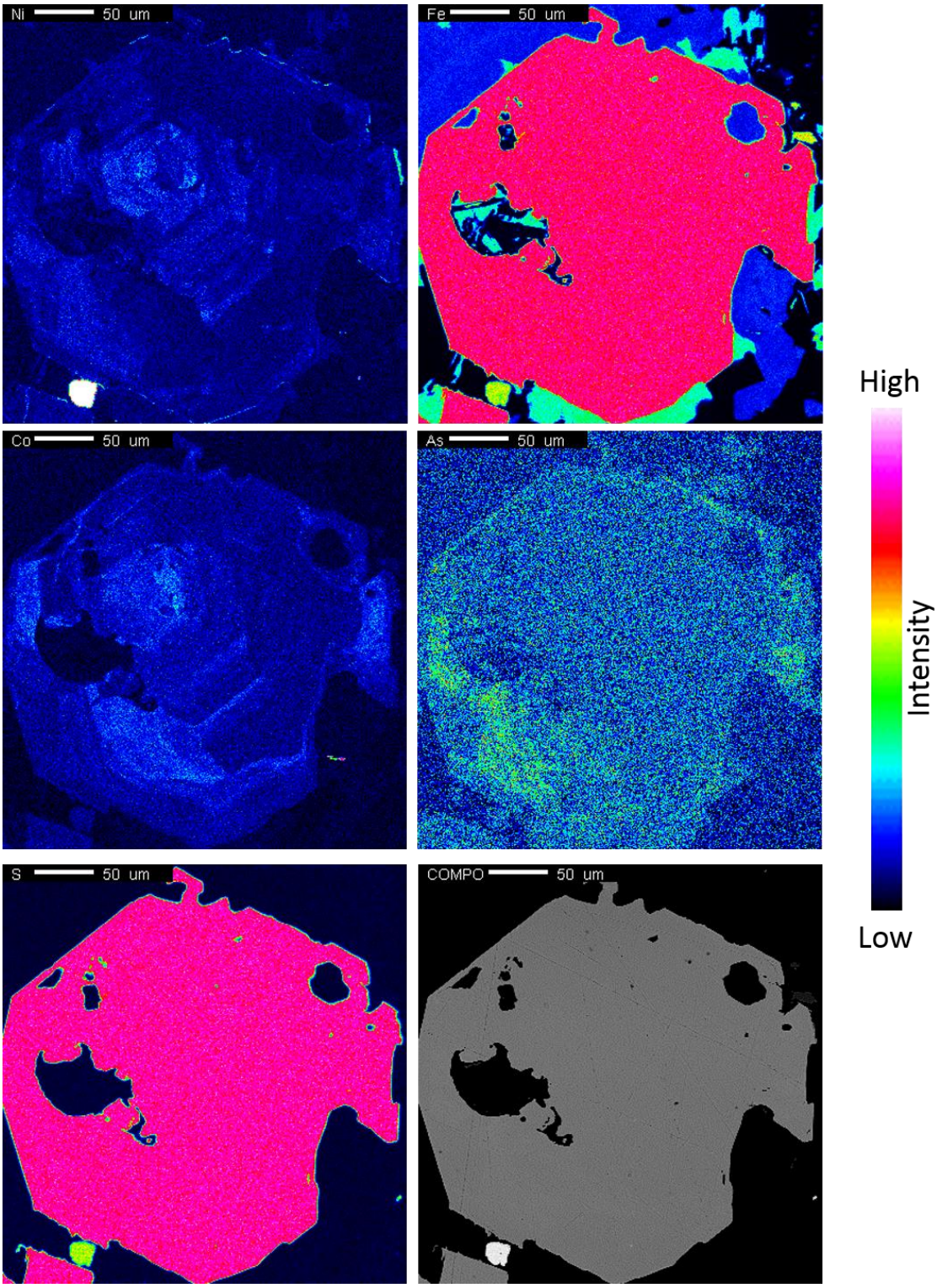

SUD-DA-013-1

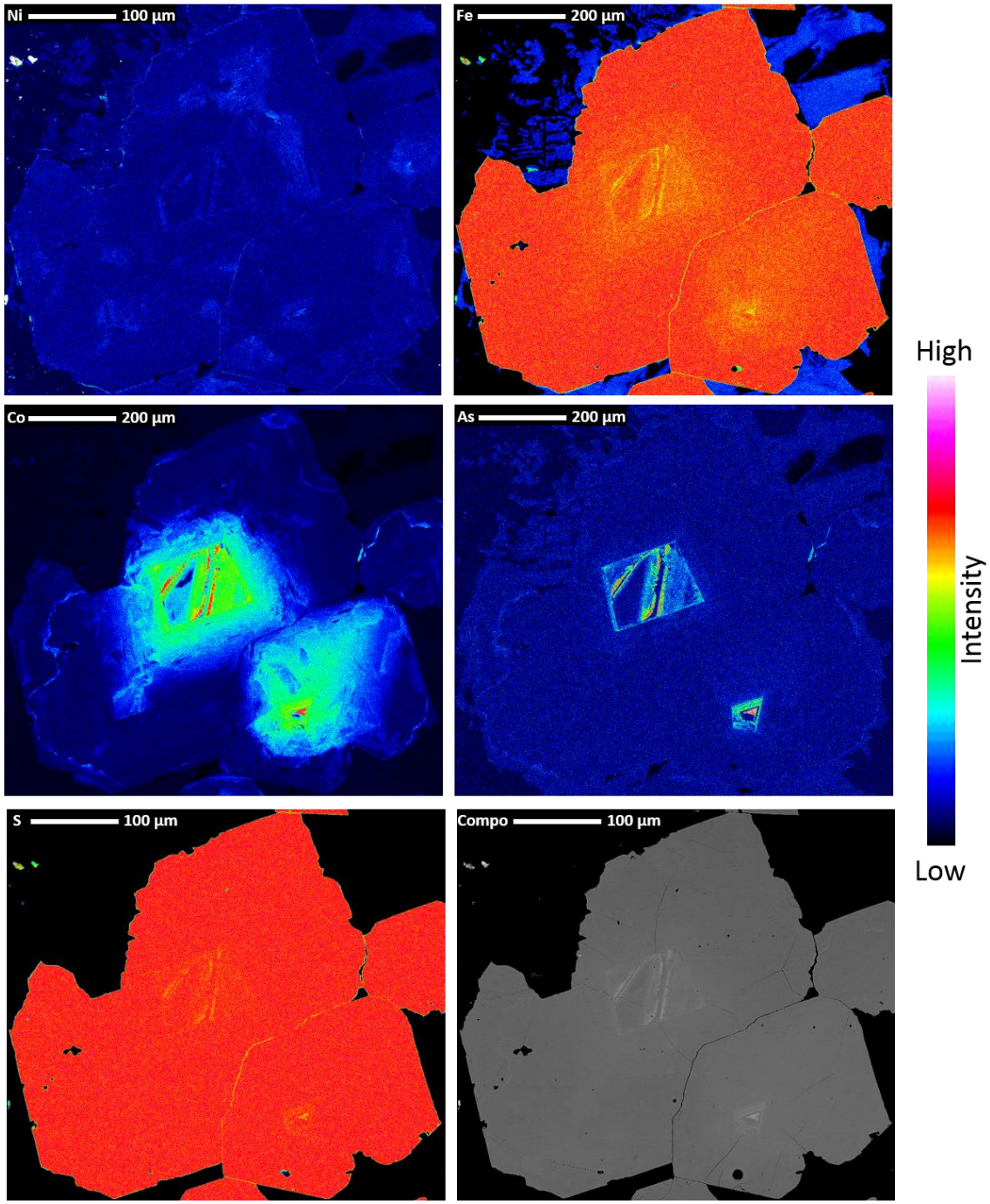
Ni 100 µm
Fe 200 µm
Co 200 µm
As 200 µm
S 100 µm
Compo 100 µm
High
Intensity
Low

SUD-DA-013-2

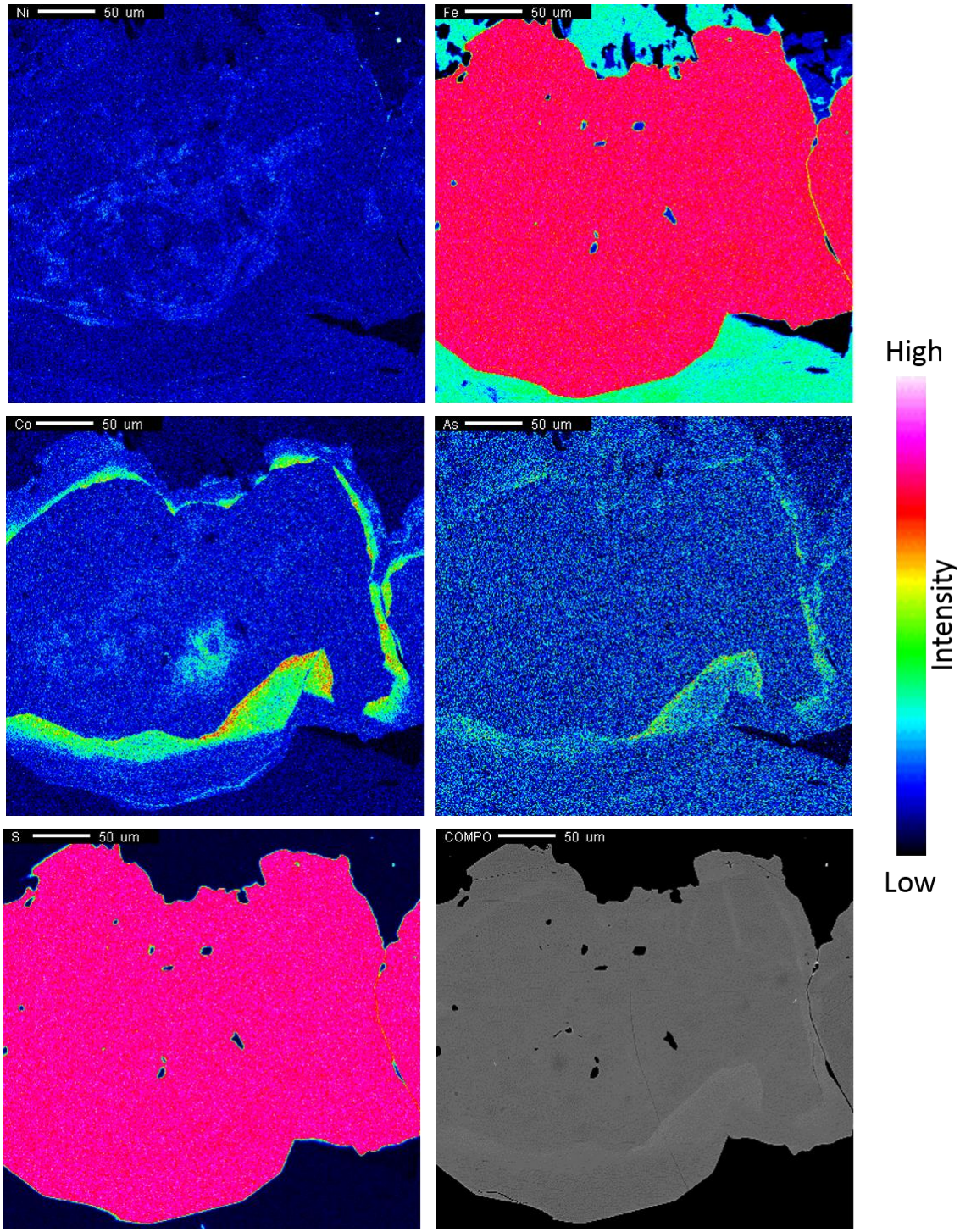
Ni 50 um
Fe 50 um
Co 50 um
As 50 um
S 50 um
COMPO 50 um
High
Intensity
Low

SUD-DA-013-4

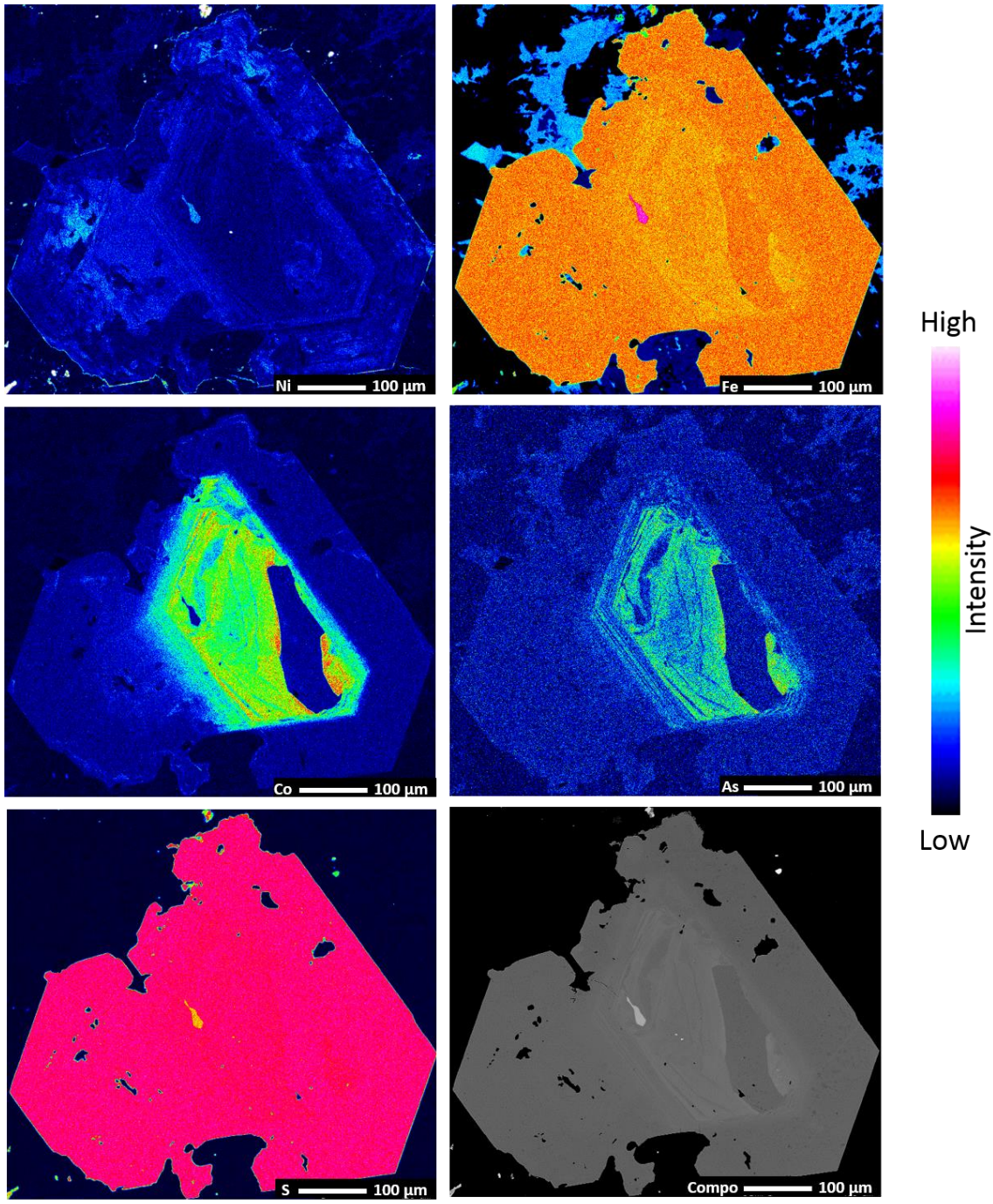
Ni 100 µm
Fe 100 µm
Co 100 µm
As 100 µm
S 100 µm
Compo 100 µm
High
Intensity
Low

SUD-DA-025B-2

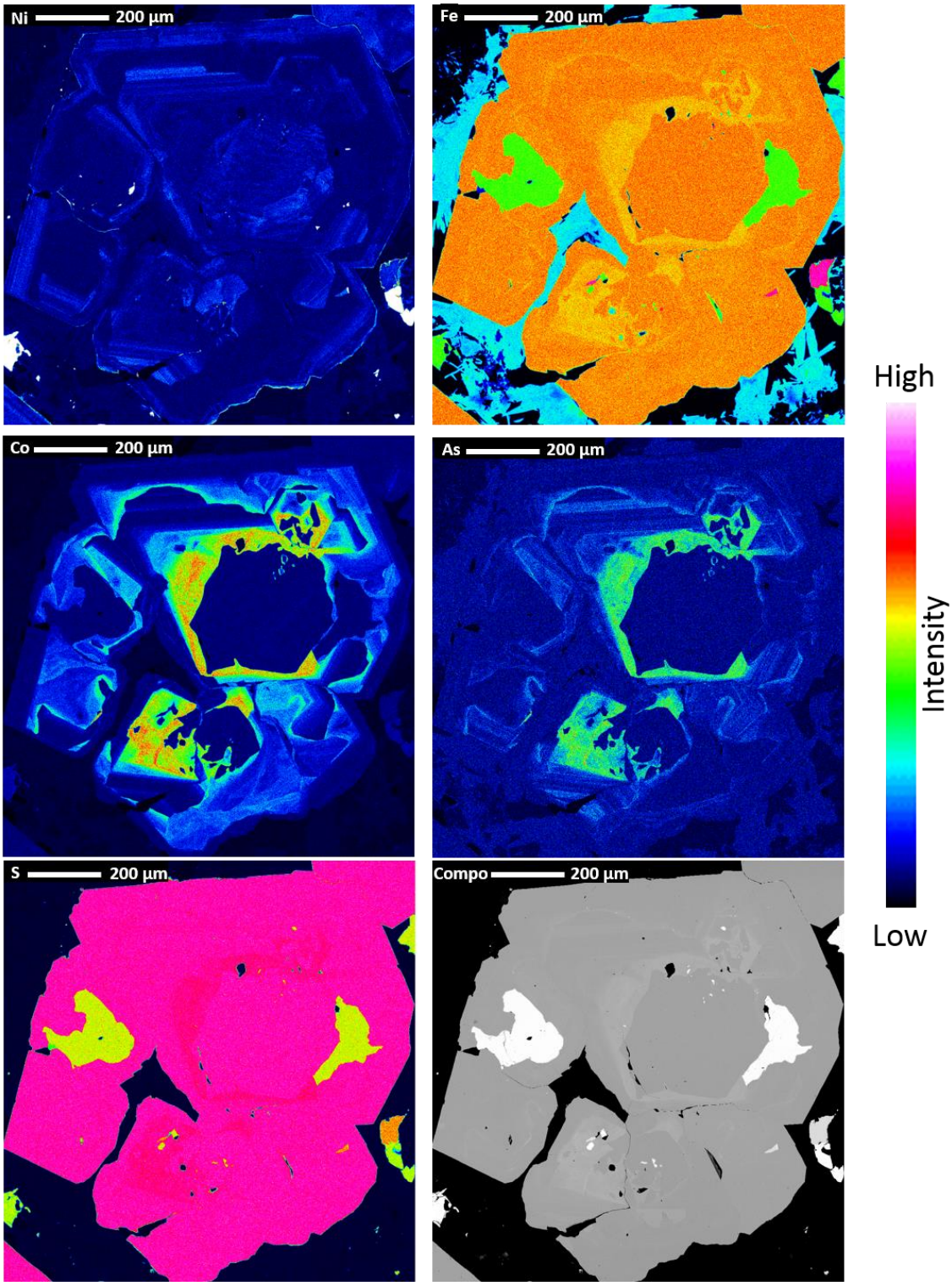
Ni 200 µm
Fe 200 µm
Co 200 µm
As 200 µm
S 200 µm
Compo 200 µm
High
Intensity
Low

SUD-DA-025B-3

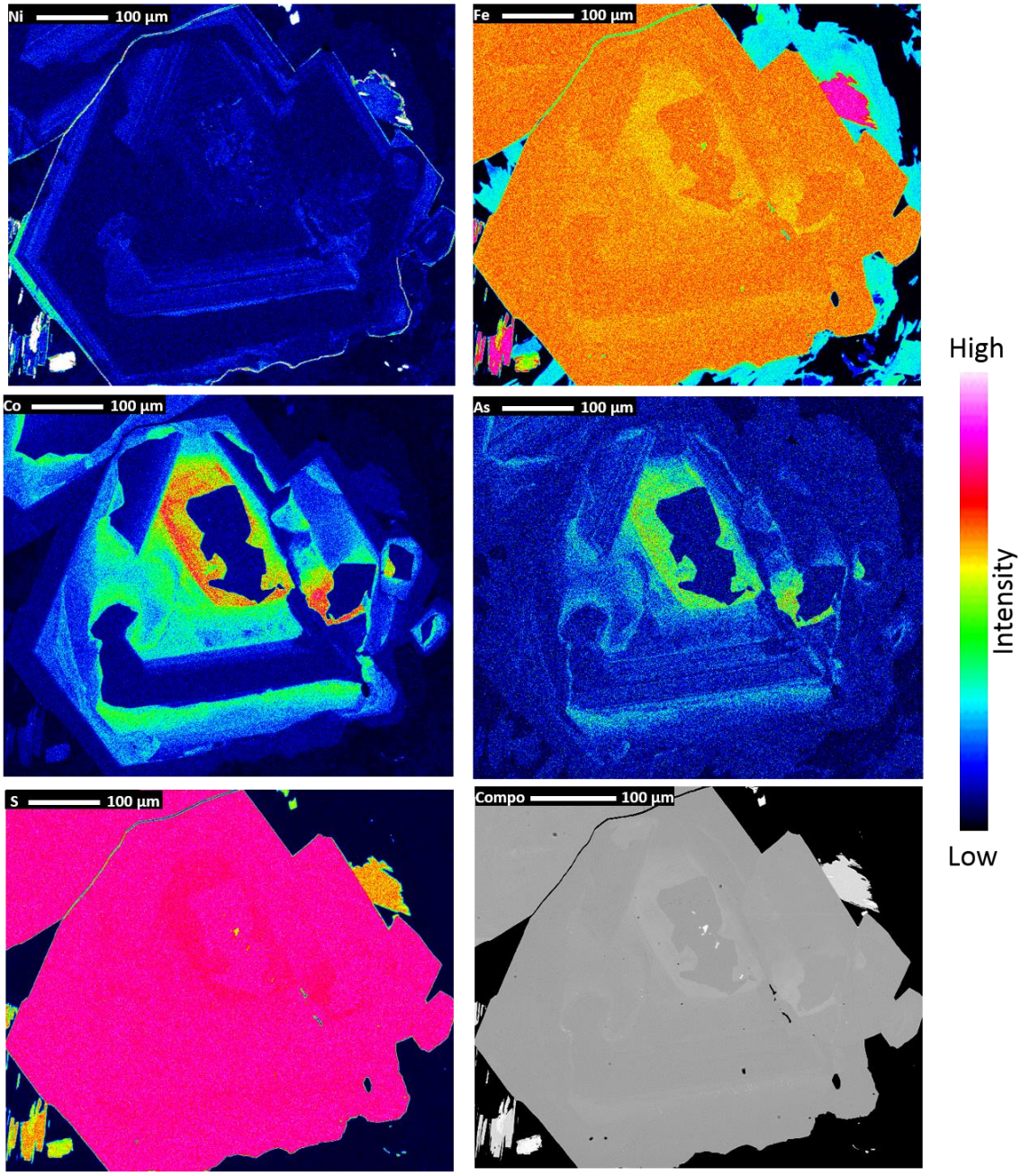
Ni 100 µm
Fe 100 µm
Co 100 µm
As 100 µm
S 100 µm
Compo 100 µm
High
Intensity
Low

SUD-NB-052-1

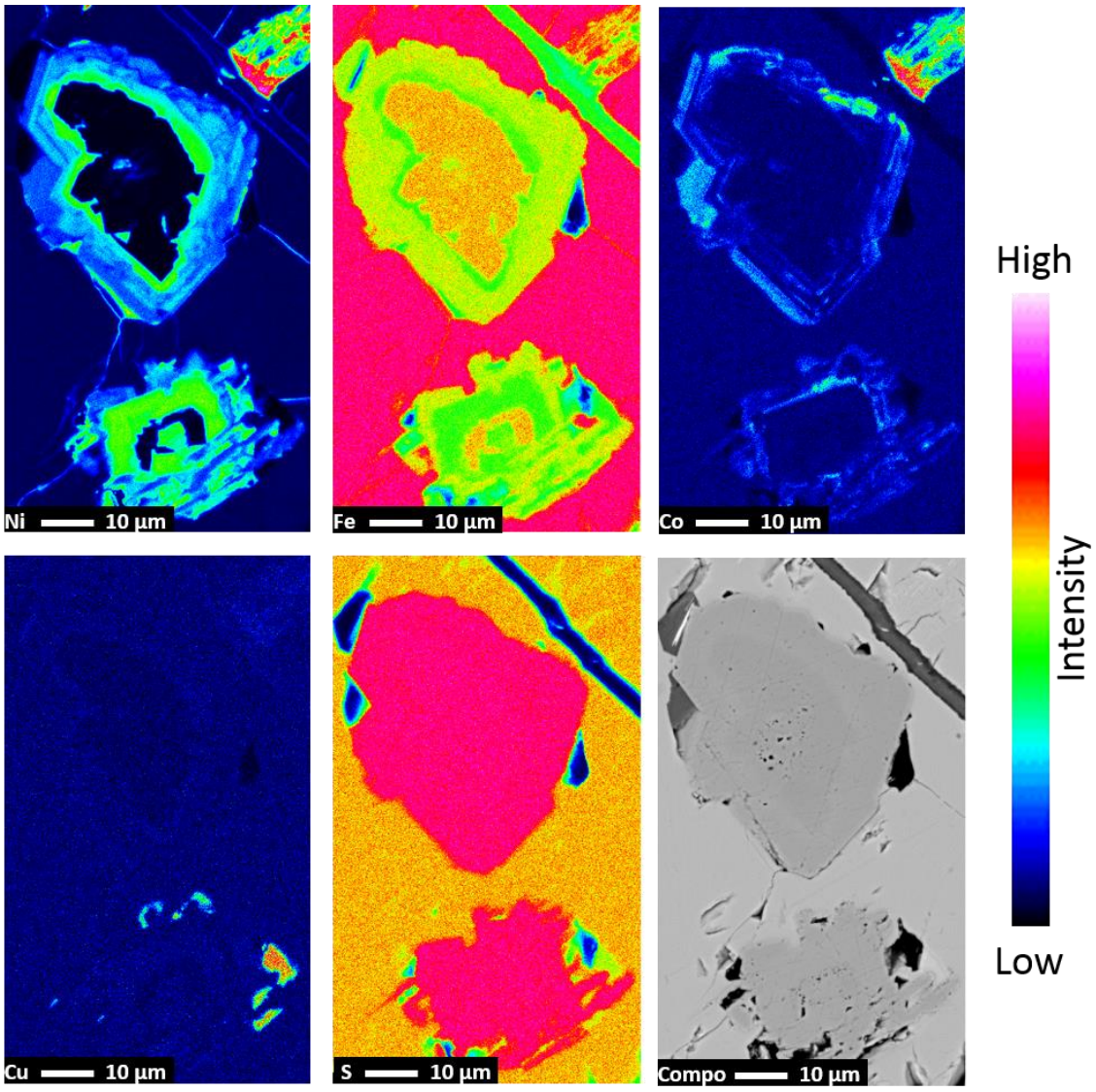
Ni 10 µm
Fe 10 µm
Co 10 µm
Cu 10 µm
S 10 µm
Compo 10 µm
High
Intensity
Low

SUD-WH-003-1

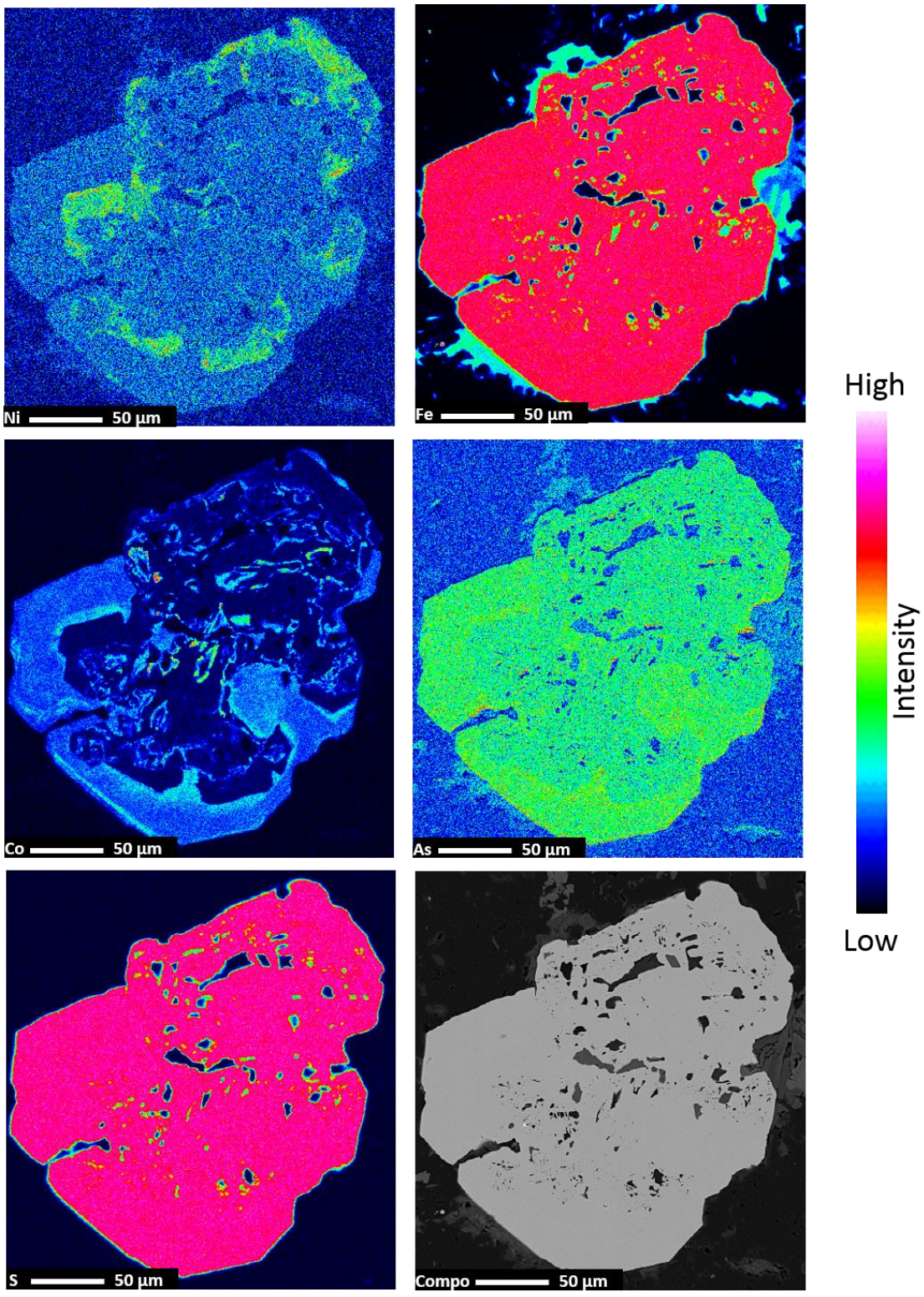
Ni 50 µm
Fe 50 µm
Co 50 µm
As 50 µm
S 50 µm
Compo 50 µm
High
Intensity
Low

SUD-WH-003-2

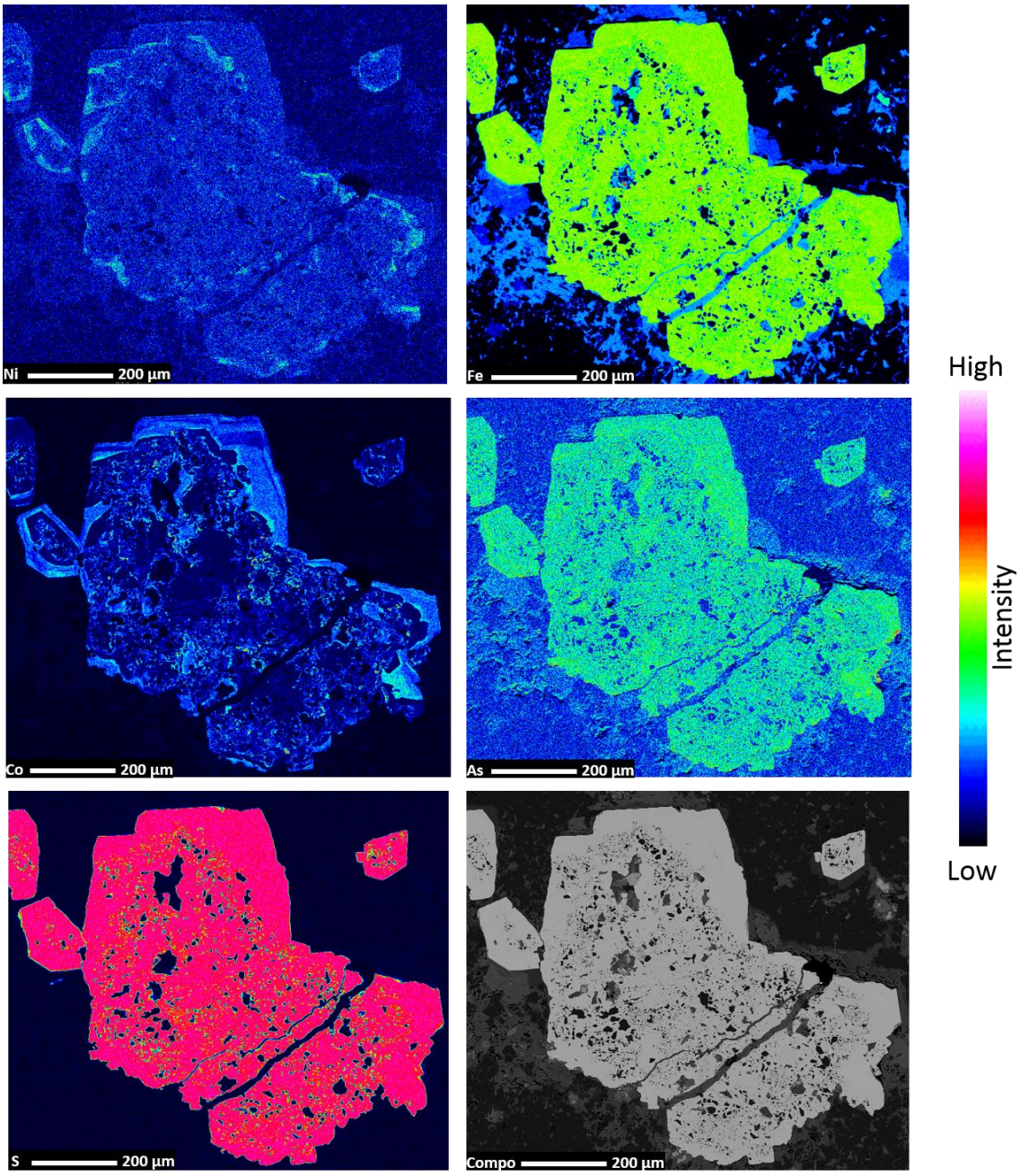
Ni 200 µm
Fe 200 µm
Co 200 µm
As 200 µm
S 200 µm
Compo 200 µm
High
Intensity
Low

SUD-WH-003-3

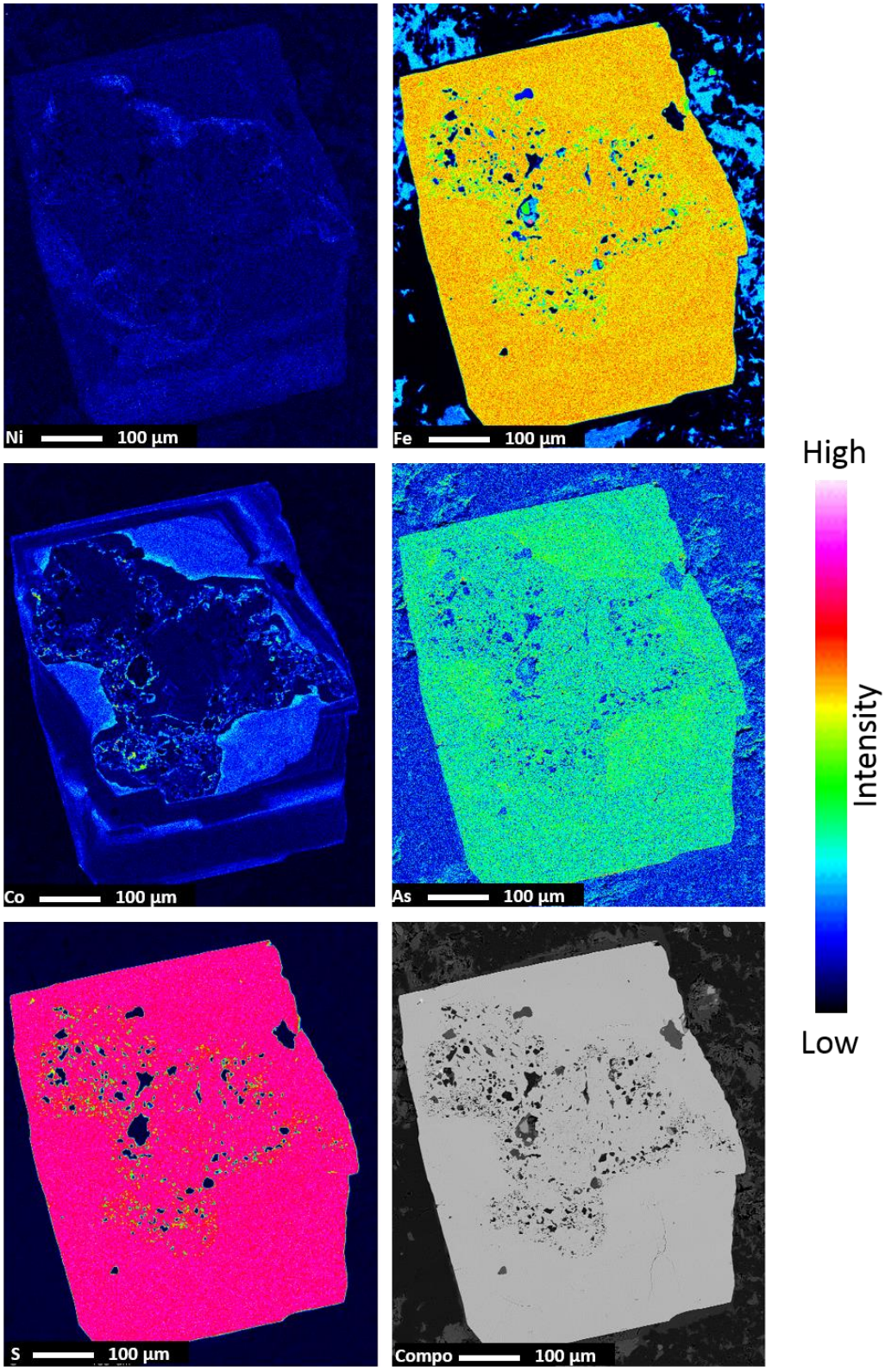
Ni 100 µm
Fe 100 µm
Co 100 µm
As 100 µm
S 100 µm
Compo 100 µm
High
Intensity
Low

SUD-WH-003-4

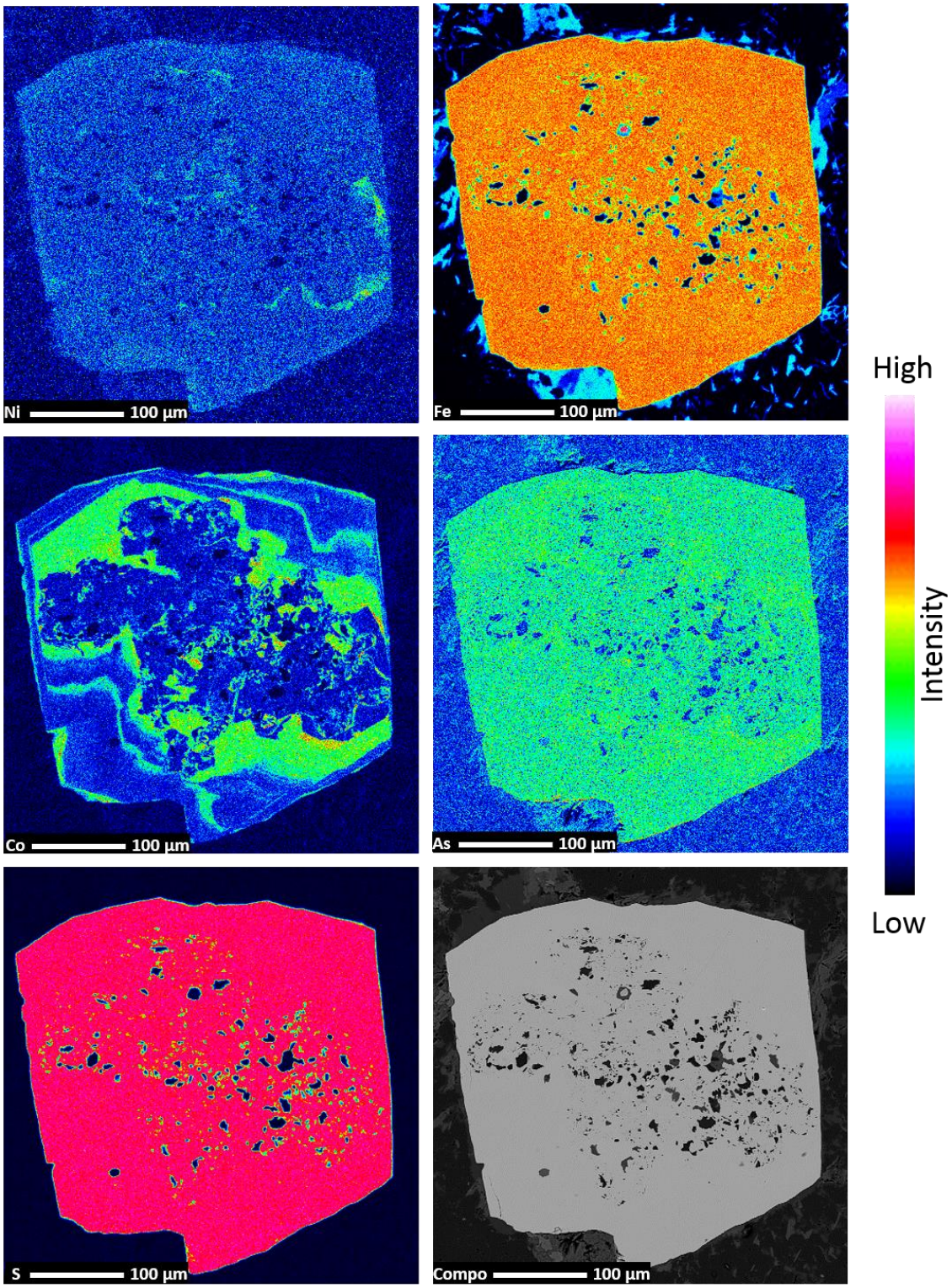
Ni
100 µm
Fe
100 µm
High
Intensity
Low
Co
100 µm
As
100 µm
S
100 µm
Compo
100 µm

SUD-WH-012-1

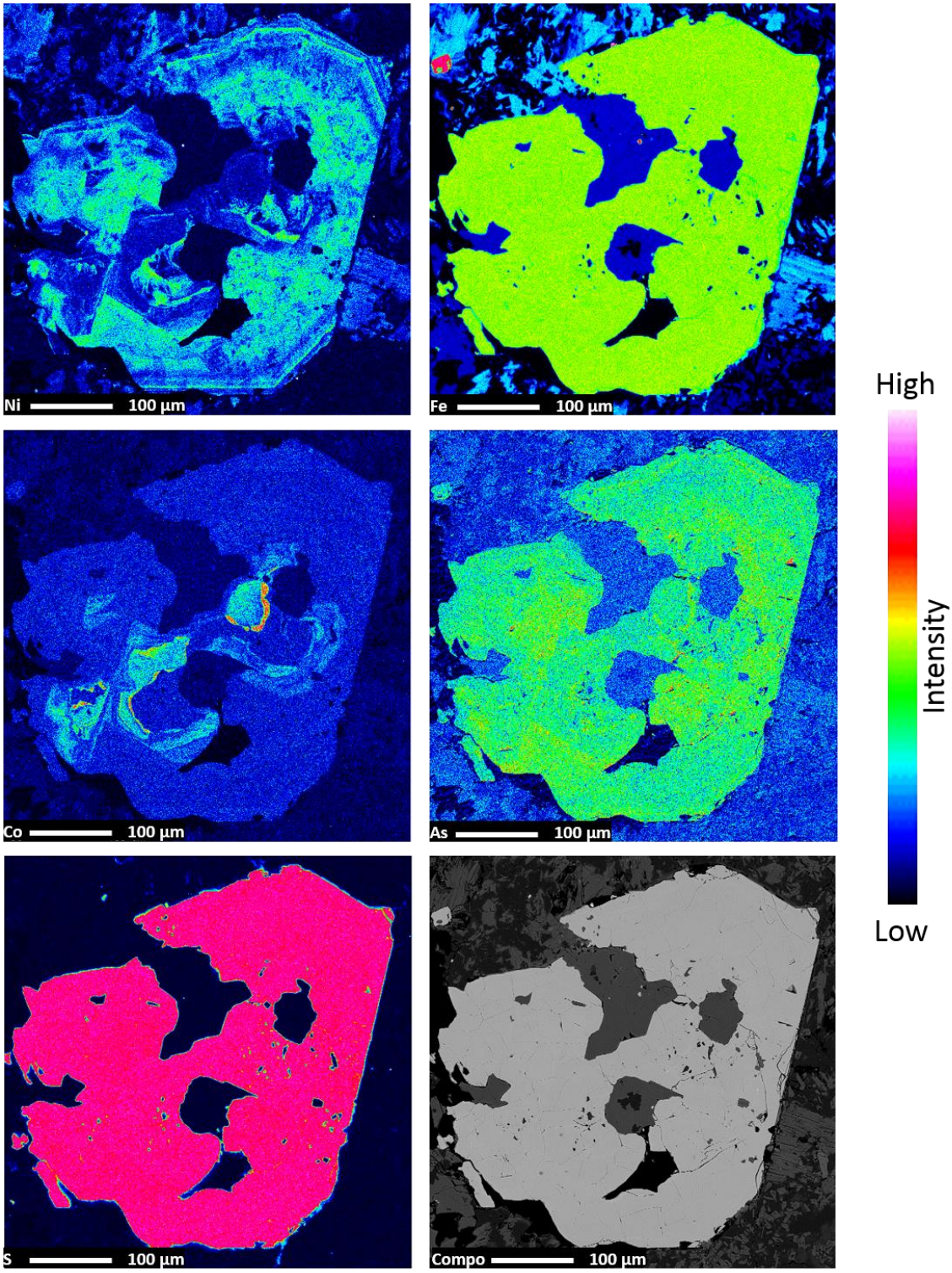
Ni 100 µm
Fe 100 µm
Co 100 µm
As 100 µm
S 100 µm
Compo 100 µm
High
Intensity
Low

SUD-WH-012-2

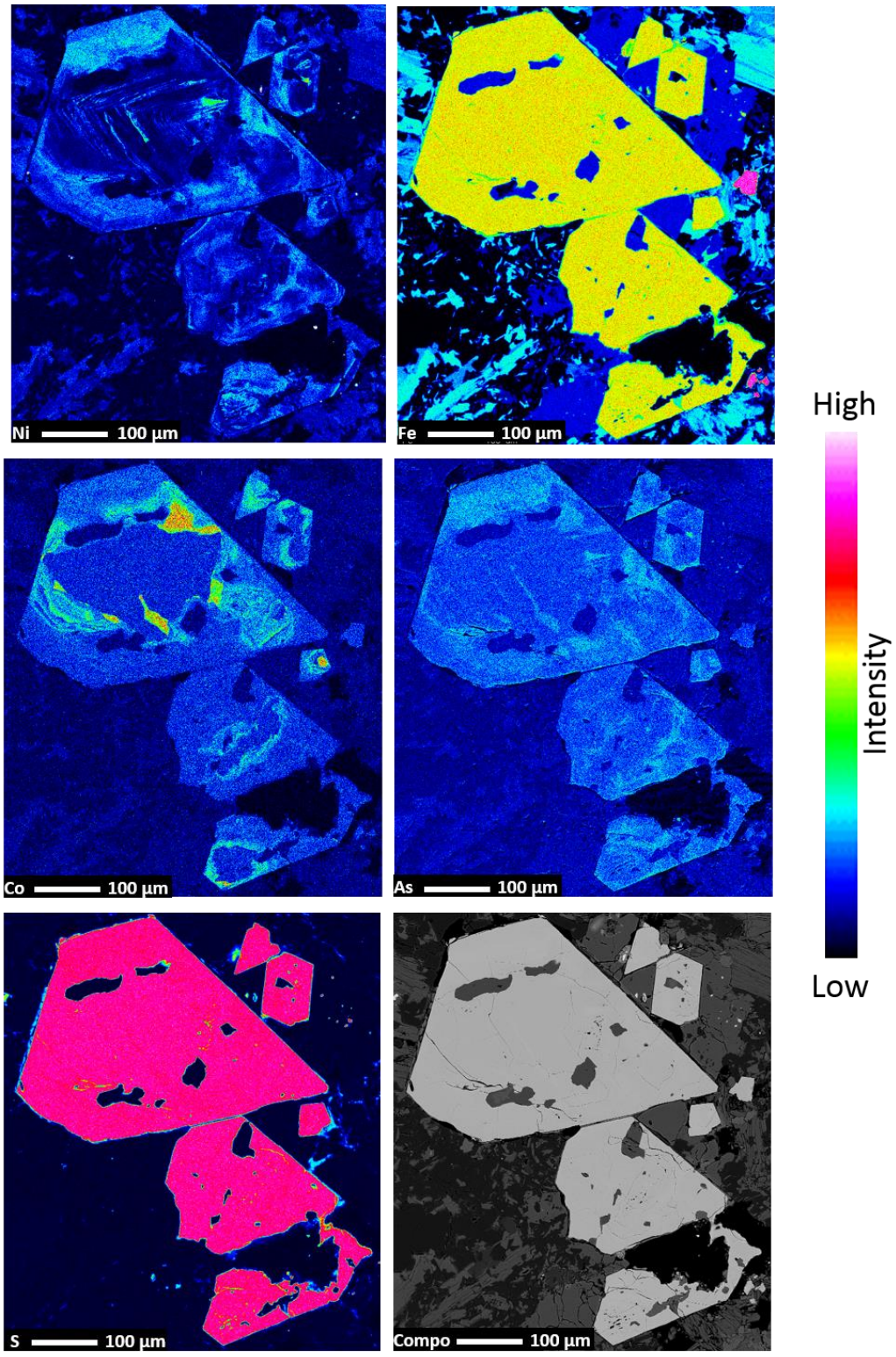
Ni 100 µm
Fe 100 µm
Co 100 µm
As 100 µm
S 100 µm
Compo 100 µm
High
Intensity
Low

SUD-WH-012-3

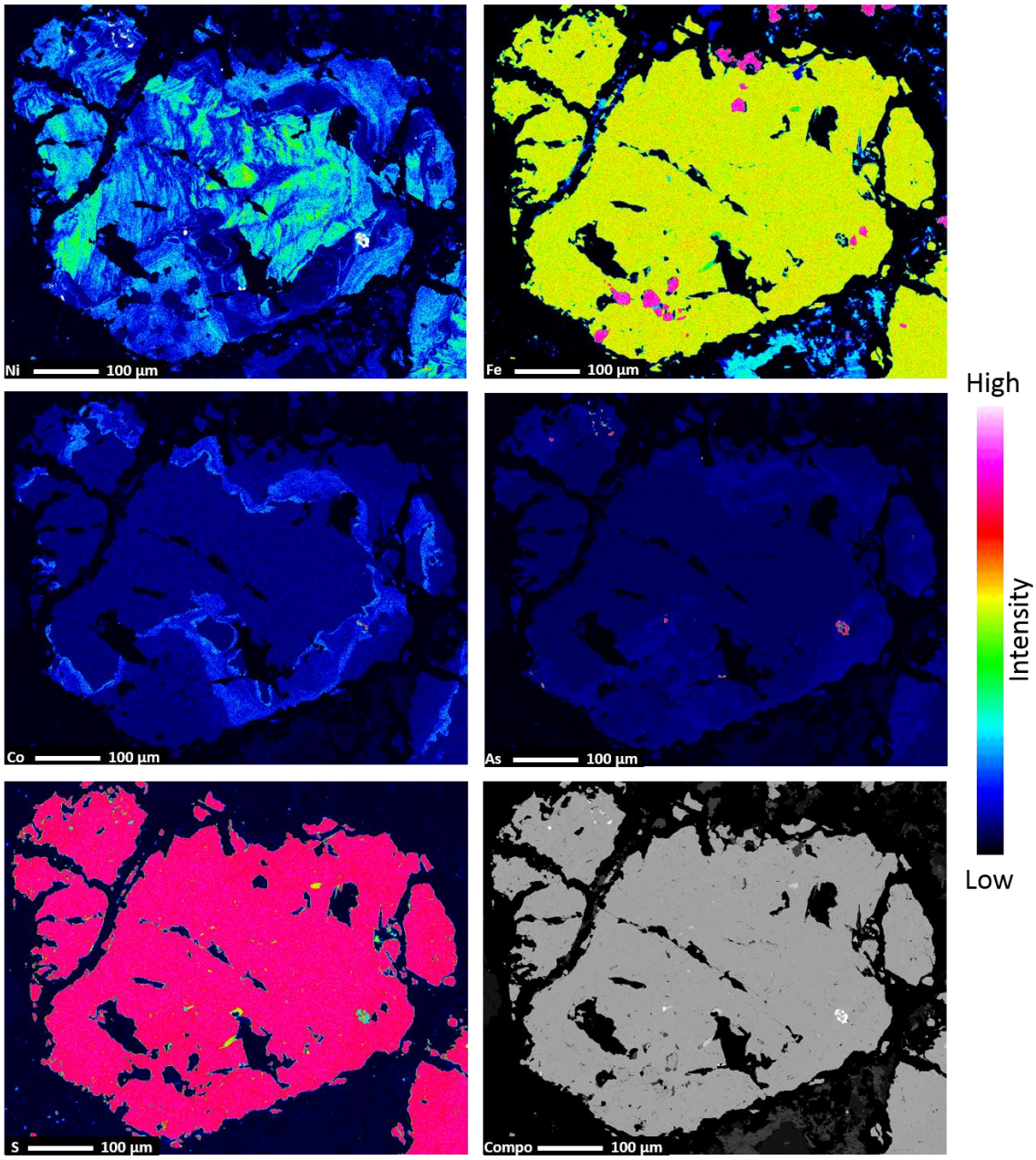
Ni 100 µm
Fe 100 µm
Co 100 µm
As 100 µm
S 100 µm
Compo 100 µm
High
Intensity
Low

SUD-WH-012-5

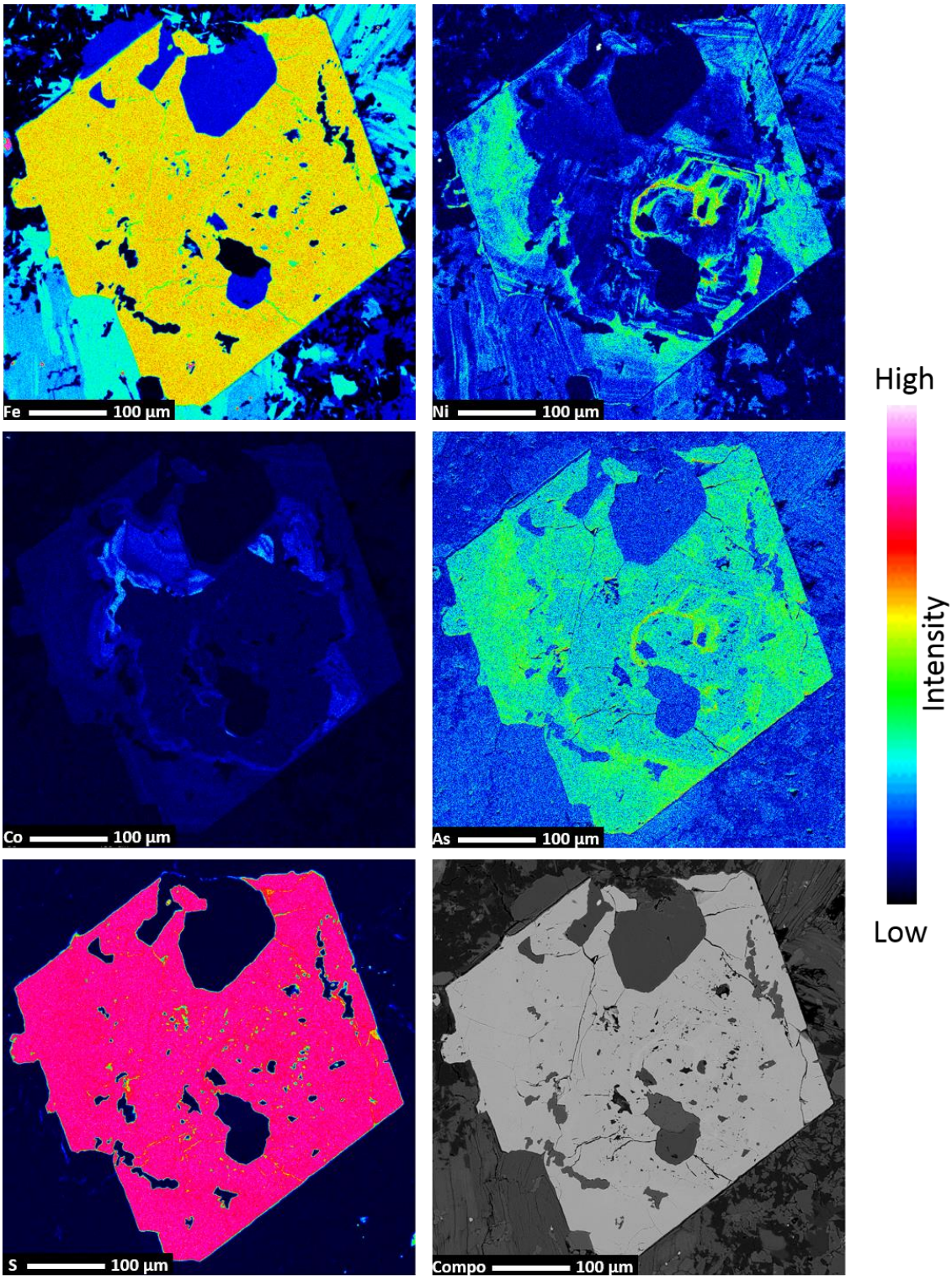
Fe 100 µm
Ni 100 µm
Co 100 µm
As 100 µm
S 100 µm
Compo 100 µm
High
Intensity
Low

SUD-WH-012-4

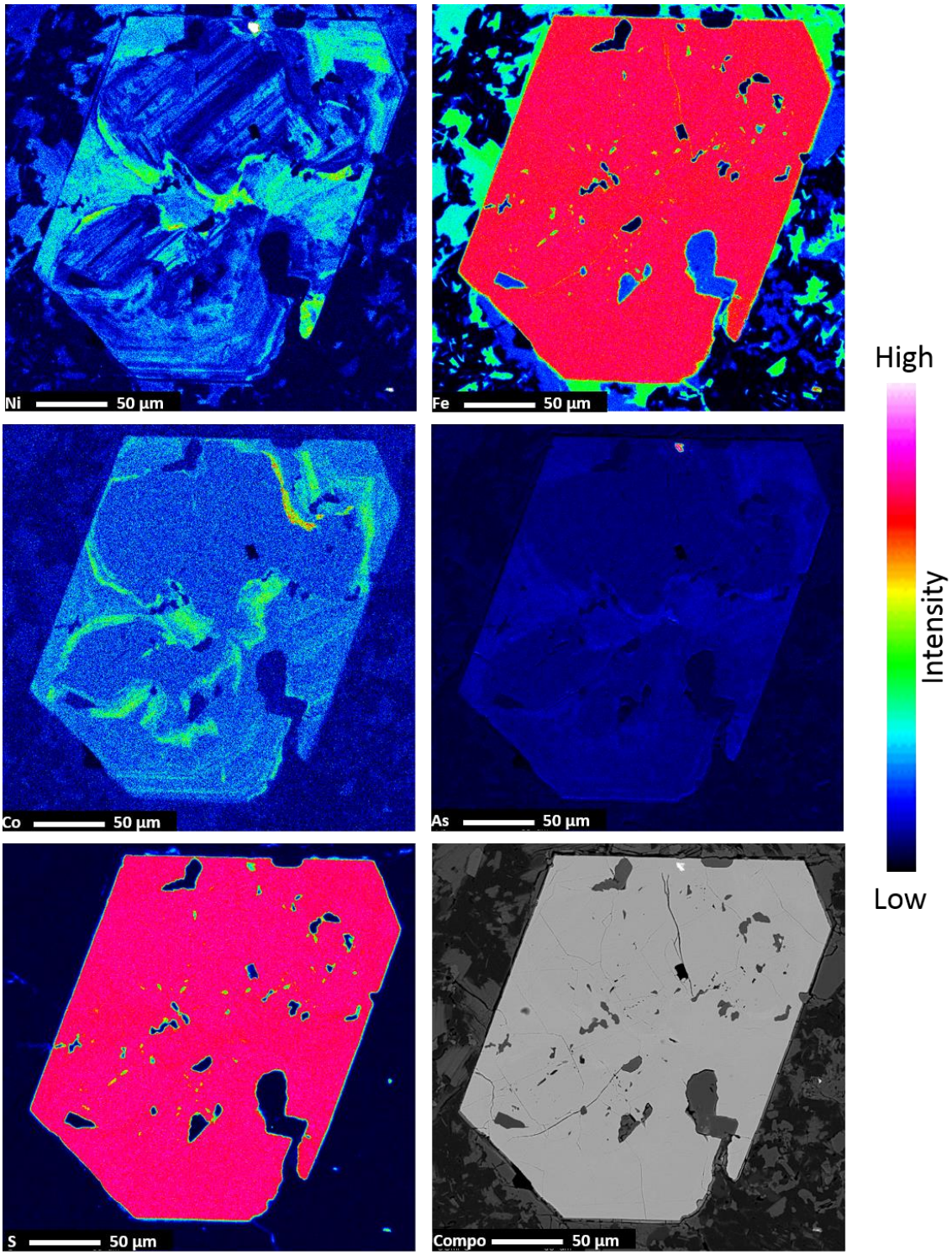
Ni 50 µm
Fe 50 µm
Co 50 µm
As 50 µm
S 50 µm
Compo 50 µm
High
Intensity
Low

Curriculum Vitae

Name: Denise Anders

Post-secondary Education and Degrees:

Christian-Albrechts-University (CAU) of Kiel
Kiel, Germany
2007-2011 B.A.

The University of Western Ontario
London, Ontario, Canada
2011-2016 Ph.D.

Honours and Awards:

Barringer Travel Award
Bridging the Gap 2015

Mitacs Accelerate Internship
2013-2014

Young Scientist's Travel Award
EGU General Assembly 2011

LPI Travel Stipend
LPSC 2010

LPI Summer Intern Stipend
2009

Related Work Experience

Teaching Assistant
The University of Western Ontario
2011-2016

Research Assistant
The University of Western Ontario
2011-2016

Research and Teaching Assistant
Christian-Albrechts-University (CAU) of Kiel
2008-2010

Summer Intern
Lunar and Planetary Institute, Houston, Texas
2009

Internship
German Aerospace Center (DLR), Berlin, Germany

2008

Publications:

Anders, D., Osinski, G.R., Grieve, R.A.F. (2015) Meteoritics & Planetary Science 50, Nr 9, 1577–1594.

Anders, D., Buchner E., Schmieder, M., Kegler, P. (2013) Varietäten von Schmelzelithologien in den Impaktiten des Steinheimer Beckens (SW-Deutschland) [Varieties of melt lithologies in the Steinheim basin (SW Germany)]. ZDGG German Journal of Geosciences 164, 491–501.

Conference abstracts:

Anders D., Osinski G.R., Grieve R.A.F. (2015). The Basal Onaping Intrusion – the missing roof rocks of the Sudbury Igneous Complex? [#1107]. Bridging the Gap III 2015. Freiburg, Germany, October 2015 (poster presentation).

Anders D., Osinski G. R., Grieve R. A. F., Péntek A. Formation and origin of Metabreccia from the Parkin Offset Dyke at the Sudbury impact structure [#1110]. Bridging the Gap III 2015. Freiburg, Germany, October 2015 (poster presentation).

Anders D., Osinski G.R., Grieve R.A.F. (2014). Southern Parkin Offset Dyke – First Results. PDAC FindMine Student Day (talk).

Anders D., Osinski G.R., Grieve R.A.F. (2013). The Onaping Intrusion, Sudbury, Canada – Impact melt and roof rocks of the Sudbury Igneous Complex? Large Meteorite Impacts and Planetary Evolution V, #3092 (talk).

Anders D., Osinski G.R., Grieve R.A.F. (2013). The Onaping Intrusion, Sudbury, Canada – An impact melt origin and relationship to the Sudbury Igneous Complex. 44th Lunar and Planetary Science Conference, #1637 (talk).

Anders D., Osinski G.R., Grieve R.A.F. (2013). Planar deformation features from the Onaping Formation of the Sudbury impact structure, Canada. 44th Lunar and Planetary Science Conference, #1651 (poster presentation).

Anders D., Osinski G.R., Grieve R.A.F., Schmieder M., Kegler P. and Buchner E (2012). Geochemical signatures of carbonate impact melts from the Steinheim impact crater, Germany. GAC-MAC conference St. John's 2012, #360 (poster presentation).

Anders D., Kegler P., Buchner E., Schmieder M. (2011). Carbonate melt lithologies from the Steinheim impact structure (Baden-Württemberg, Germany). EGU General Assembly 2011, #461 (talk).

Anders D., Kegler P., Buchner E., Schmieder M. (2011). Carbonate melt lithologies from the Steinheim impact crater (SW Germany). 42nd Lunar and Planetary Science Conference, #1997 (poster presentation).

Anders D., Kring D. A., Holzheid A. (2010). Carbonate-rich material associated with Meteor Crater impact melt. 41st Lunar and Planetary Science Conference, #1799 (poster presentation).